The University Of Sheffield.

Mathematical modelling of ignition behaviour in pulverised fuel flames

By:

Tejas Navnitlal Ashar

The report submitted in partial fulfilment of the requirements for the degree of Engineering Doctorate.

The University of Sheffield

School of Mechanical Engineering

Department of Energy 2050

July 11, 2022

Declaration

The candidate confirms that the work submitted is his own, except where work, which has formed part of jointly authored publications, has been included. The contribution of the candidate and the other authors to this work has been explicity indicated below. The candidate confirms that appropriate credit has been given within the thesis where reference has been made to the work of others.

This copy has been supplied on the understanding that it is copyright material and that no quotation from the thesis made be published without proper acknowledgement.

The right of Tejas Navnitlal Ashar to be identified as author of this work has been asserted by him in accordance with the Copyright, Designs and Patents Act 1988.

Acknowledgements

I would like to express sincere appreciation to my supervisors Prof. Mohamed Pourkashanian, Prof. Derek B. Ingham and Prof. Lin Ma for giving me the opportunity to conduct the research at Energy 2050 group. They not only showed confidence in me but also provided guidance and advice during the difficult times of my EngD.

I would also like to thank Dr Alastair for sharing his deep understanding of CFD and his tutelage at various stages of my research. He has truly been an inspiration and his expertise in this combustion have contributed at various stages of my research.

I would also like to show my gratitude to Dr Kevin Hughes who provided me with computational access during the pandemic and assembled a powerful computer without which the research conducted in the last chapter would have not been possible. I would also like to acknowledge my colleagues at the University of Sheffield and Nottingham for their support.

I would, also, like to thank the CDT for Carbon Capture and Storage and Cleaner Fossil Energy, the University of Sheffield, Doosan Babcock Ltd and the EPSRC for funding the overall EngD.

Finally, I would dedicate this work to my late Father Navnitlal Ashar. I would also like to thank my Mum and my Wife for staying interested in my discussion about combustion, providing support and believing in me. I could have not made it so far without the sacrifices they have made during this period.

Abstract

Coal is going to play an important role in meeting future energy demands but it produces carbon dioxide, which is considered to be a major contributor towards climate change. Oxyfuel technology is a promising carbon capture technology where the N_2 in the oxidiser stream is replaced with CO_2 to enhance the capture process at the exit of the power plant. The oxyfuel technology results in changing the combustion environment, which may affect the flame characteristics, fuel efficiency, the emissions and overall boiler performance. The aim of this research was to develop an ignition model, which provides further understanding of the flame characteristics due to fuel switching and changes in the combustion environment.

An investigation was conducted analysing predictions of different coal devolatilisation models. The three models analysed were CPD, FG-DVC and PC-Coal Lab where the models simulated hot wire mesh experimental conditions. The results showed that the PC-Coal Lab and CPD is able to accurately predict the devolatilisation behaviour for a broad range of coals whereas FG-DVC is less effective. The CPD model is chosen for further investigations over PC-Coal Lab as it entails a licensing cost whereas CPD is open source and proves to be less demanding.

An ignition model is developed to understand the fundamental ignition mechanisms of a single particle of a solid fuel, which are categorised as either homogeneous or heterogeneous. The model accurately couples kinetics, heat and mass transport phenomena between the interior and exterior of the particle. The study accounts for variation in ambient conditions (including oxyfuel conditions) and fuel properties where the results are validated against experimental data. On extending the ignition model to different particle size, a correlation is obtained for the ignition mechanism based on particle size and ambient oxygen concentration. The correlation developed is useful in investigating ignition in pilot/full scale boiler assisting in any design and operational changes.

Baseline CFD simulations were conducted on an IFRF and Utah furnace replicating their respective experimental flows. The simulations were repeated with integration of the correlation using the methodology developed in previous study. The results are compared against the experimental data suggesting that ignition model improves the overall predictions of the flame lift (i.e ignition zone) and thus the model can be used for further investigating novel combustion environments and fuels. The validated ignition model is applied in investigating the pilot scale burner, which indicated a small improvement in the species prediction but a further development will be required in the turbulent chemistry model.

Table of Contents

List of Figures

List of Tables

Nomenclature

Acronyms

ar	As received basis
ASU	Air separation unit
CCS	Carbon Capture & Storage
CFD	Computational Fluid Dynamics
CPD	Chemical Percolation Devolatilisation
CPDNLG	Chemical Percolation Devolatilisation Nitrogen and Light Gases
daf	Dry ash free basis
DNS	Direct Numerical Simulation
DO	Discrete Ordinates
DTF	Drop Tube Furnace
DTM	Discrete transfer method
EBM	Eddy Break-up Model
EDC	Eddy Dissipation Concept Model
EDM	Eddy Dissipation Model
FCV	Finite control volume
FFCM	Foundation flame chemistry model
FG-DVC	Functional Group–Devolatilisation, Vaporisation, Crosslinking
FRED	Finite Rate Eddy Dissipation
GHG	Greenhouse Gas
HI	Heterogeneous ignition
HO	Homogeneous ignition

HO-HI	Simultaneous ignition
HTVY	High temperature volatile yield
HTWM	High temperature wire mesh
IGCC	Integrated gasification combined cycle
LES	Large Eddy Simulation
LES	Large eddy simulation
LNG	Liquefied natural gas
MEA	Monoethanolamine
NMR	Nuclear Magnetic Resonance
RANS	Reynolds-averaged Navier–Stokes equations
RFG	Recycle flue gas
RTE	Radiation transfer equation
SEM	Scanned Electron Microscope
TG-FTIR	Thermogravimetry-Fourier Transform Infrared
TGA	Thermogravemetric analysis
UDF	User define functions
UDS	User defined scalars
UKCCSRC	United Kingdom carbon capture storage research centre
WSSG	Weighted sum of gray gas

List of Greek symbols

$\alpha_{prod,k}$	Concentration exponent for product species(reaction order)	
$\alpha_{react,k}$	Concentration exponent for reactant species(reaction order)	
ς_{k_l}	Characteristic length	Å
μ	Dynamic viscosity	kg/(m·s)
Ω_D	Diffusion collision integral	-
ρ	Density	kg/m^3

ρ_g	Density of the gas	kg/m^3
ρ_{ox}	Density of the oxidant	kg/m^3
ϵ	Emissivity of the particle	-
η	Effectiveness factor	-
ϖ_{k_l}	Energy parameter	k
Φ	Generic scalar field quantity	-
ρ_{p0}	Initial particle density	kg/m^3
ε_0	Initial porosity	-
δ_{ij}	Kronecker delta	-
ρ_a	Particle ash density	kg/m^3
ρ_c	Particle char density	kg/m^3
ρ_m	Particle moisture density	kg/m^3
ρ_p	Particle density	kg/m^3
ρ_v	Particle volatiles density	kg/m^3
σ_h	Prandtl number = $\frac{c_p \mu}{k_{th}}$ i^{th} direction	m/s^2
ε	Porosity	-
ν'_{prod}	Stoichiometric coefficient for product species	-
ν'_{react}	Stoichiometric coefficient for reactant species	-
Ω	Stoichiometric coefficient of the char reaction's	-
σ	Stefan-Boltzmann constant	W/m^2·K^4
τ_{ij}	Stress tensor	kg/m-s^2
β	Temperature exponent	-
ϕ	Thiele modulus	-
ρ_{true}	True density of the particle	kg/m^3
τ	Tortousity	1/m

List of Roman symbols

ΔH_c	Enthalpy of formation due to char reaction	kJ/kg
ΔH_{latent}	Latent heat of evaporation	kJ/kg

ΔH_{vol}	Latent heat of evaporation of the volatiles	kJ/kg
$\dot{m}_{p_{char}}$	Mass loss rate due to char combustion	kg/s
$\dot{m}_{p_{vol}}$	Mass loss rate due to devolatilisation	kg/s
$\dot{r}_C$	Particle mass loss rate due to char combustion	kg/(m^3·s)
$\dot{r}_M$	Particle mass loss rate due to drying	kg/(m^3·s)
$\dot{r}_V$	Particle mass loss rate due to volatile loss	kg/(m^3·s)
$\dot{r}_{Ci}$	Reaction rate of char combustion for the i^{th} reaction-	
A	Area	m^2
A_k	Pre exponential factor	1/s
A_p	Surface area of the particle	m^2
A_{Ci}	Pre exponential factor for the i^{th} char reaction	1/s
A_v	Pre exponential factor for devolatilisation	1/s
C_2	Inertial resistance factor	1/m^3
C_D	Drag coefficient	-
c_p	Specific heat at constant pressure	J/(kg·K)
C_{diff}	Diffusion constant	m^3/K$^{0.75}$
CT	Volumetric concentration of species	kmol/m^3
D	Molecular diffusivity	m^2/s
D_e	Effective diffusion coefficient	m^2/s
D_k	Diffusion coefficient for the k^{th} specie	m^2/s
D_o	Bulk molecular diffusion rate	m^2/s
d_p	Particle diameter	m
D_{kl}	Diffusion coefficient in binary mixture	m^2/s
D_{km}	Diffusion coefficient of specie k in mixture m	m^2/s
D_{Kn}	Knudsen diffusion coefficient	m^2/s
d_{pore}	Local pore diameter	m
E	Specific energy	J/kg
E_k	Activation energy	J/kmol

E_{Ci}	Activation energy for the i^{th} char reaction	J/kmol
E_v	Activation energy for devolatilisation	J/kmol
F_D	Drag Force	N
g_i	Gravity component in the i^{th} direction	m/s^2
H	Enthalpy per unit mass	J/kg
h	Convective heat transfer coefficient	W/(m^2·K)
H_g	Enthalpy of the gas	J/kg
H_p	Enthalpy of the particle	J/kg
K	Permeability	m^2
k_{eff_g}	Effective thermal conductivity of gas phase	W/(m·K)
k_{eff_p}	Effective thermal conductivity of the particle	W/(m·K)
k_{eff}	Effective thermal conductivity	W/(m·K)
K_{th}	Thermal conductivity	W/(m·K)
m	Mass	kg
m_k	Mass of specie k	kg
m_p	Mass of the particle	kg
m_{total}	Total mass of mixture k	kg
MW_k	Molecular weight of k^{th} specie	g/mol
$MWox$	Molecular weight of oxidant	g/mol
Nu	Nusselt number	-
p	Pressure	Pa
P_{O_2}	Partial pressure of O_2	Pa
P_{abs}	Absolute pressure	Pa
Q_G	Heat gain curve	W/m
Q_L	Heat loss curve	W/m
Q_n	Net heat supply	W/m
Q_{vol}	High temperature volatile yield	-
R	Universal gas constant=8314.7	J/(kmol·K)

$R_{k,r}$	Net reaction rate to produce specie k	mol/m^3
$R_{s,c}$	Chemical reaction rate	m^2/s
Re	Reynolds number	-
S_m	Mass source term	kg/(m^3·s)
S_p	Particle net mass loss rate	kg/(m^3·s)
S_Φ	Source term	-
S_{char}	Specific internal surface area	m^2/m^3
S_{rad}	Source term for the radiation	W/m^3
S_{rxn}	Source term for the reaction	W/m^3
S_{Y_k}	Source term for the k^{th} specie	kg/(m^3·s)
T	Temperature	K
t	time	s
T_p	Particle temperature	K
T_{wall}	Wall temperature	K
u_g	Gas velocity	m/s
u_j	Velocity component in j^{th} direction	m/s
u_p	Particle velocity	m/s
V	Volume	m^3
V_t	Particle terminal velocity	m/s
X_k	Mole fraction of specie k	-
Y_k	Mass fraction for the k^{th} specie	-

1 Introduction

There has been an increase in energy consumption in the last two decades, which is mainly due to economic growth in developing countries [1]. A broad energy mix has been achieved by most countries with the advent in renewable technologies [2] and the evolution of micro grids [3–5], which has helped in meeting the growing energy demand. The population is predicted to increase around 36% by 2036 and it is expected that the energy demand will grow twice as fast [1]. Coal is a stable source of fossil fuel, globally distributed and can be a reliable source for the next 150 years or so [6, 7]. The consumption of energy from coal has played a vital role in the global energy mix, and will continue to play a critical role in meeting the increasing energy demand, despite the increase in renewable energy sources [8]. There has been a steady increase in the consumption of coal overall, primarily due to industrial and economic growth in India and China [9]. This is evident from the increase in use of coal in the power generation sector as shown in Figure 1.1. Asian countries consumed around 60% of coal produced globally in 2015 [1]. The primary benefits of using coal as a source of fuel for power generation are cost, ease of storage and availability which has seen a rapid increase in coal consumption.

The disadvantages are the toxic and harmful pollutants produced from coal, which are hazardous for human health and the environment such as nitrogen oxides NOx and sulphur oxides SOx as well as carbon dioxide (CO_2) which contributes towards global warming. A number of technologies have been implemented on power plants when it comes to curbing harmful pollutants such as SO_x and NO_x [10–14]. CO_2 is one of the main products from coal combustion which is one of the greenhouse gases (GHG) which contributes towards the global warming [15].

There is a decline in electricity produced from coal fired powerplants in Europe and United States [16]. This is attributed to decarbonistion of the grid, increase in the development and commercialisation of renewables followed by a significant drop in oil prices due to fracking and availability of shale gas [17]. Zamani et al. highlight that the fossil fuel dependency for energy production still remains high and the drop in coal consumption is impacted with the oil and gas prices [17]. Zamani et al highlighted the impact of the Fukushima nuclear disaster in Japan (2011) on the behaviour of Europe's coal consumption. The closure of nuclear power plants in Japan increased the consumption of liquefied natural gas (LNG) in Japan, which increased the prices of LNG. The European power utilities responded by using more coal and less gas for two years until the gas prices came down [16, 17]. Regardless, the use of coal in the power generation is going to be high which will be the driving

force in increasing the CO_2 emissions unless there are cleaner energy sources and global adaptation of climate change policies [9, 18].

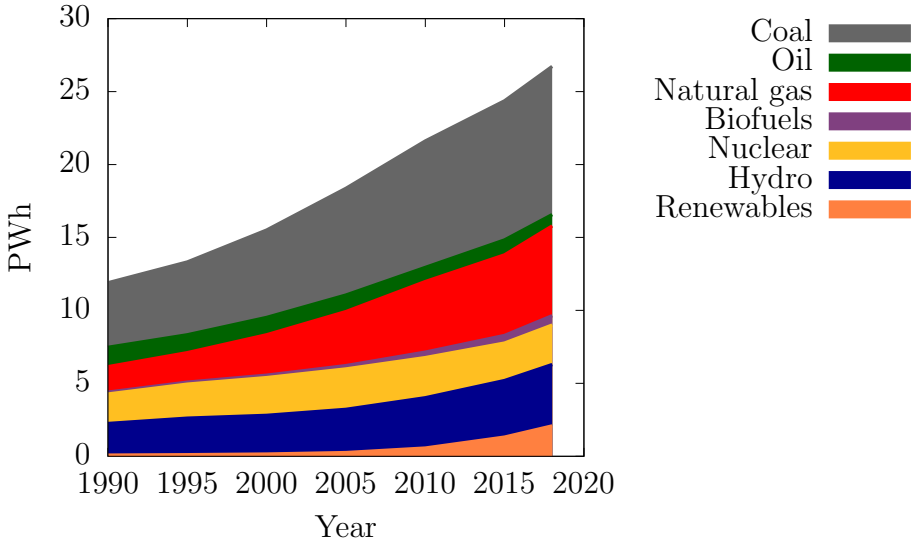

Figure 1.1: Fuel sources for power generation world wide between 1990-2018 [16].

The aim of thesis is to contribute towards a technology which has the potential to reduce the CO_2 emissions from the power plants. Oxyfuel technology is a demonstrated technology where N_2 is replaced with CO_2 and H_2O in the combustion environment for ease of CO_2 capture at the downstream of the power plant [19]. The changes in the combustion environment can introduce changes in the flame structure, efficiency of the fuel and emission from the overall power plants. The aim is to look at develop a mathematical model which focuses on ignition characteristics of a fuel which can help in accurate predictions of the flame parameters.

This chapter discusses the motivation for this thesis. Section 1.1 discuss the need of a carbon capture and storage and the different capture technologies available for capture. Section 1.3 discusses the motivation to investigate ignition characteristics for different fuels and its significance in oxyfuel conditions.

1.1 Carbon capture and storage (CCS)

A GHG is defined by either the temporary or permanent dipole propetry which traps the electromagnetic heat radiaton from earth and absorbs the outgoing heat [15]. This acts as a blanket on the earth's surface and results in increasing the average temperatures [20]. There are many GHG responsible for global warming apart from CO_2 such as CH_4, N_2O and fluorinated gases. In 2016 CO_2 accounted for 74.4% of the total GHG emissions (calculated based on CO_{2e}) which indicate that CO_2 is primarily responsible for global warming [21] and it is the biggest concern for forced climate change. Figure 1.2 shows a direct impact of increase in CO_2 on

global temperatures (pre-industrial). Currently the rise of ≈ 1.23 K is calculated due to use of fossil fuels and it is recognised that any increase beyond 2 K will be too drastic for the planet [22]. The energy demand and the trends suggest an increase the CO_2 emissions and the overall global temperatures unless there are cleaner sources of energy and changes in the government policies.

There has been a global effort in reducing CO_2 emissions which first came in the form Kyoto protocols where countries part of United Nations framework of climate change commitmented to reduce GHG emissions. Most recently the Paris agreement in 2016 brought together many countries to commit to a reduction in GHG the emissions and limiting the global wamrning temperatures well below 2 ^{o}C. Different countries submitted their Intended Nationality Determined Contributions outlining their post 2020 climate action [23]. The UK has already taken several steps towards reducing CO_2 emissions by passing the 'Climate Change Act' in 2008 [24, 25]. The Act has generated public awareness and produced few institutions, such as UKCCSRC (United Kingdom Carbon Capture & Storage Research Centre) which provides cleaner energy innovation.

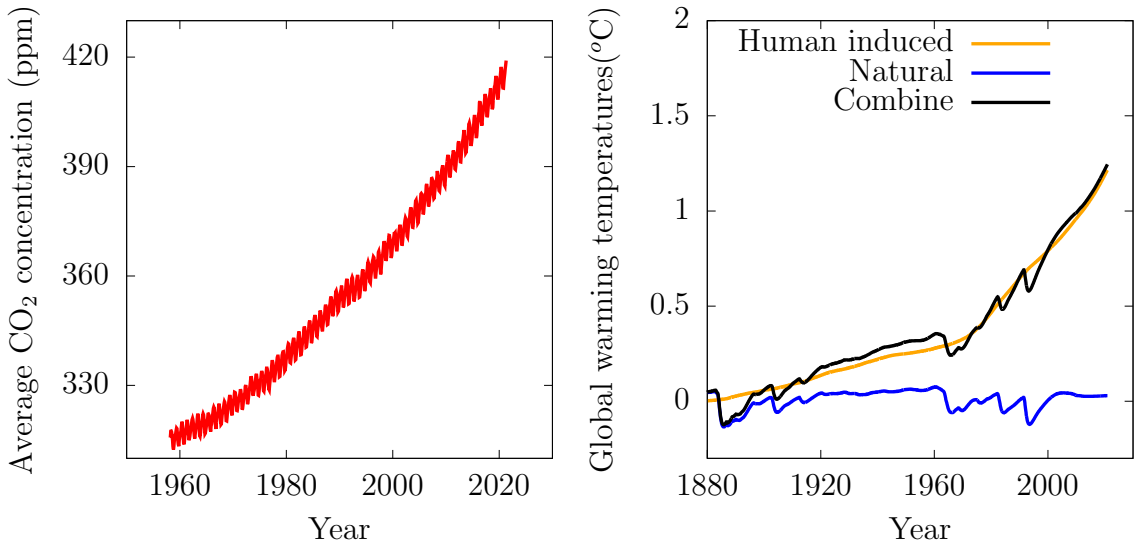

Figure 1.2: The rise in global temperatures relative to 1850-1900 due to increase in CO_2 concentration [26, 27].

As a result of GHG emissions there is a drive towards renewables, but in certain situations they fail to meet the energy demand [1]. Apart from the increase in the population and energy demand there are mainly two reasons for this:

i Renewable energy sources such as wind and solar are highly dependent on the weather conditions, which can be unpredictable and intermittent [28]. There are many research departments in the world looking at efficiently storing the excess power produced by renewables, but there are many limitations

in scaling up the power storage facility [29]. This makes supply of power unreliable and cannot be used to control the power grid [30].

ii The other obstacle with renewables is the amount of land (offshore for wind turbines) required to set the infrastructure compared to fossil fuel power plants. There are many socio-technical challenges involved which are still not understood [31–34] which stagnates the application of renewables on a large scale.

Biomass energy is agreed to be carbon neutral because the biomass consumes the CO_2 produced during its combustion which can help in reducing the overall emissions of CO_2 [35]. However, the challenge lies in the sustainability of the technology, where biomass production can be limited by the growing location, high usage of land and water for production [36–40]. Nuclear, on the other hand, has not proven to be safe [41] and cheap [42, 43]. Abbot has explained the limiting factors on scaling up nuclear power supply to meet the energy demand which highlights the debate about the nuclear waste disposal, the price volatility of the fuel and its implications on the overall cost of energy [44, 45]. It is the energy produced from fossil fuels which will allow the flexibility to meet the demand. This indicates that the fossil fuels will continue to play a significant role in future energy supply. Therefore it is essential to maintain an electricity grid system that can provide a reliable and cheap supply of energy for sustainable growth in economy but also reduce or nullify the carbon footprint at the same time. The following are some options that can reduce CO_2 :

i Increasing the overall efficiency of the coal/natural gas fired plants [46].

ii Switching/transitioning from high carbon intensity fuel, such as switching from coal to natural gas [47].

iii Installing a carbon capture facility to directly capture the CO_2 released from the power plant [47].

Increasing the efficiency of the existing coal power plants will require retro fitting or building new power plants with higher efficiency (apart for the investment point of view). In both the scenarios there will be a requirement of CO_2 clean up to meet the current emissions target. The volatility in natural gas prices makes it difficult for a smooth transitioning and reduction in dependency on coal [16]. The Carbon Capture, storage and utilisation (CCSU) is one such technology which can allow the use of fossil fuels and CO_2 can be prevented from being released into the atmosphere. The technology is to isolate CO_2 before, during or after the main fuel is combusted in a power plant and either store it or utilise it in multiple applications. The CO_2 captured is transported and stored in depleted oil & gas reservoirs/saline aquifiers or can be used for utilisation e.g. enhanced oil recovery [48]. The energy penalty associated with operaing a CCS facility is very expensive [49] and hence, it has not been commercially deployed at a significant scale. The returns from the investment in the CCS technology in the industry is debatable unless the government increases the carbon emission prices and thus there is no drive from the industry to

integrate CCS into their power station. In the UK, currently there are no commercial retrofitting power plants that accommodates CCS technology. This is because most of the UK coal power plants in operation today were built in the 1980's. Therefore the retrofitting of them with CCS facility will be not only expensive but there are also other factors, such as restrictions caused by the existing plant layout, capture bypass provisions and proximity of the facility to a sequestration site that affects the integration of CCS [50]. The Boundary dam integrated CCS project in Canada, the world's first commercial-scale CCS project at a coal-fired power plant is able to capture upto 1 Mt per year of CO_2 but the capital cost was about $C 1.5 billion where federal government funded $C 240 million which illustrates that CCS is an expensive but a useful and effective technology [51]. An in-depth analysis of technological developments and barriers are discussed in [47] which highlights why CO_2 capture is very expensive and a barrier to entry.

1.2 Capture technologies

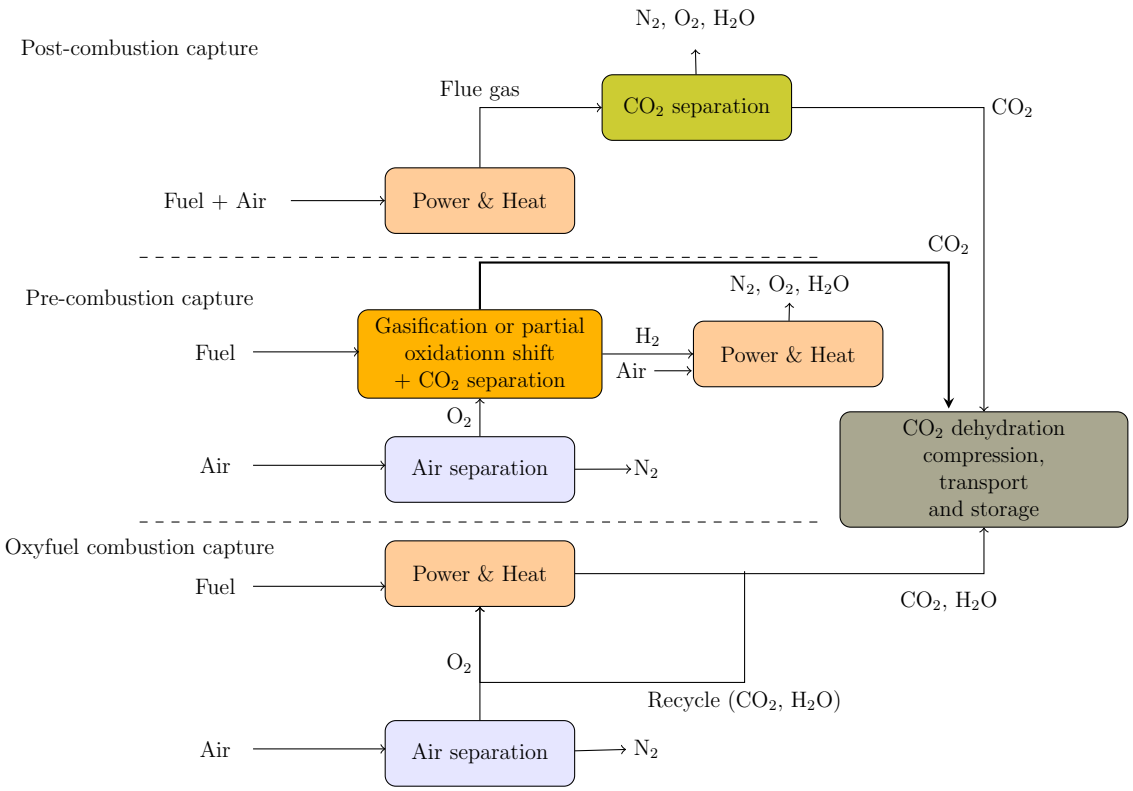

Figure 1.3: Schematic of the three main CO_2 capture technologies [52].

There is a decrease in coal power plants in the UK and this is due to more stringent Industrial Emissions Directive from 2015. This has resulted in premature closure or decommissioning of unabated coal power plants. If UK want to reduce the premature closure of the asset(coal power plants) it holds it needs to invest in CCS technology, which can negate the impact of CO_2 due to the use of coal. As the

technology is expensive government needs to incentivize the CCS or CCSU. There are three aspects to CCS i.e. CO_2 capture, transport and storage or utilisation. This section briefly discusses all the three elements of CCS. There are many technologies, which can be used to capture CO_2. The three primary technologies are pre-combustion, oxy-fuel combustion and post combustion. Figure 1.3 gives an overview and path to these technologies.

1.2.1 Pre-combustion

A pre-combustion process consists of removing CO_2 at source by converting solid, liquid or gaseous fuel into a mixture of synthesis gas, i.e. hydrogen (H_2) and carbon monoxide (CO) via *gasification* or *reforming*. The synthesis gas is then processed via a shift-conversion reaction to produce CO_2 and more H_2. The CO_2 can be separated by the absorption process. The H_2 obtained can be used as fuel to heat our homes, produce electricity or power vehicles [53, 54]. Integrated gasification combined cycle (IGCC) with CCS would be an ideal process to extract synthesis gas from coal combustion. The main drawback of this technology is the cost of building a new power plant since retrofitting an existing coal fired power plant is not a viable option.

1.2.2 Post-combustion

The post-combustion process involves separation of CO_2 from the flue gas at the exhaust of a combustion processas shown in Figure 1.3. The CO_2 is separated by a suitable solvent scrubing and later liberated for compression, transport and storage. For coal/biomass combustion, the flue gas goes though NOx and SOx (flue gas desulphurisation unit) clean up process. This is done to avoid rapid degradation of the CO_2 capture solvents and SO_2 adversely affects the capture process [55]. After getting filtered is usually passed through amine solvents such as monoethanolamine (MEA). The MEA absorbs the CO_2 and releases the CO_2 upon heating the mixture and the solvent is regenerated, which is recyled for capture process. A major challenge with the application of this technology is the low concentration of CO_2 in the flue gas which results in significant energy required for separation of CO_2 which is used from the power plant cycle. This results in a power plant efficiency penalty of approximately 10% [56]. There are other methods for separating CO_2 at the exhaust, such as cryogenic separation and high pressure membrane filtration [57].

1.2.3 Oxy-fuel combustion

Oxy-fuel combustion process involves burning fuel in oxygen diluted with the recycled flue gas (RFG) which is mainly composed of CO_2 and H_2O. Pure oxygen (O_2) is produced by an air separation unit (ASU), which separates the (O_2) and nitrogen (N_2) prior to the combustion process. The O_2 is then mixed with the RFG and the pulversied fuel is entrained into the mixture shortly before entering the burner. The O_2 rich and N_2 free environment mainly produces CO_2 and H_2O which results

in producing more concentrated CO_2 which is easier for purification of CO_2 and eliminating incondensable gases [54, 58]. It also helps in reducing NOx produced during combustion as there is a reduction in N_2. To obtain similar temperatures and heat characteristics as air-fired combustion the ratio of O_2/RFG has been reported to be about 30%/70% by volume on a dry basis [59, 60].

At the exhaust of the boiler, the flue gas goes through four steps before the CO_2 and H_2O is recycled from the flue gas. The small ash particles are removed using electrostatic precipitators which has the potential to block the recycling line and damage the burner. After that a significant fraction of moisture is removed to account for any corrosion in the pipework. In some cases the flue gases can either be recycled without drying or dried with a drying unit before re-entering the burner. As per the regulations the SOx and NOx requires a clean up which is done with desulphurisation unit and selective catalytic reduction (or non selective catalytic reduction) respectively. This is done to reduce SOx in order to avoid any corrosion in the recycle pipeline due to formation of sulphuric acid and curb the NOx emissions. For the combustion in power plant, a large volume and high purity of O_2 is required and instead of ASU, cryogenic distillation units are used. These cryogenic units generate an efficiency penalty of approximately 10% points [56]. However, emerging techologies, such as membrane separation technology can potentially use less energy than cryogenic distillation and could reduce efficiency penalty [56].

1.2.4 Transport and storage of CO_2

		SO_2	**NO**	**H_2S**	**H_2**	**CO**	**CH_4**	**N_2/Ar/O_2**	**Total**
Coal Fired Plants	*Post- combustion capture*	<0.01	<0.01	0	0	0	0	0.01	0.01
	Pre-combustion capture (IGCC)	0	0	0.01-0.6	0.8 -2.0	0.03-0.4	0.01	0.03-0.6	2.1-2.7
	Oxy-fuel	0.5	0.01	0	0	0	0	3.7	4.2
Gas Fired Plants	*Post- combustion Capture*	<0.01	<0.01	0	0	0	0	0.01	0.01
	Pre-combustion capture	0	0	<0.01	1.0	0.04	2.0	1.3	4.4
	Oxy-fuel	<0.01	<0.01	0	0	0	0	4.1	4.1

Table 1.1: Concentrations of impurities in dried CO_2 % by volume [50, 61]

Trasportation of CO_2 is fairly common in the USA for the shale gas industry and Table 1.1 shows the CO_2 purity requirement that may need to be met in order to transport CO_2 from coal or gas fired plants. Impurities can create a phase change in CO_2 which can cause pipe ruptures and release a high quantity of CO_2 into the atmosphere [62, 63]. In order to tackle the high impurities, the number of stages require to compress the gas can be increased, this results in increasing the overall cost of transport [63]. In order to reduce the probability of phase changes in the CO_2 during transport, the future pipelines would require CO_2 to be compressed above 7.38 MPa, i.e. its critical pressure [64]. Thus appropriate compression improves the transport efficiency and reduces structural damage losses.

The CO_2 currently is considered to be stored at geological formations, oceans, saline aquifers, gas or oil reservoirs. The CO_2 injected in the underground rock formation for storage posses a natural impermeable cap-rock to prevent the CO_2 to escape. In the North sea, the Utsira formation off Norway has been used for CO_2 storage since 1966 [65]. The other option is to inject the CO_2 into depleting oil reservoirs to displace the oil and increase the oil production which has proven to be a more economically viable option [51, 66].

1.3 Importance of ignition

With regards to CCS, oxy-fuel combustion is the technology where the combustion process can be changed by changing the flame environment. By changing the combustion environment, the ignition and flame characteristics change. In order to successfully apply oxy-fuel technology, ignition and flame stability should be foreseen for safe and efficient operation of power plants. The combustion process also determines the amount of CO_2 produced. In order to predict the CO_2, and other harmful emissions downstream, it is important to understand the phenomena upstream purely because it is the source at which these harmful emissions are generated. If the ignition and flame propagation phenomena is understood well then it becomes easier to control the combustion process and propose emissions control technologies.

Generally, coal fired power plants are designed and tested to meet specifications of a coal. The power plant works most effectively firing its design coal at design conditions but it is difficult to keep using the same coal due to its variability in cost and availability. Thus, the boilers have an allowable limit of coal properties which enable them to operate different coals with reduced efficiencies [67]. However, substantial deviation from design coal properties may lead to flame instability and can result in deterimental combustion performance and potentially causing serious damage to the boiler [68]. The operational issues that can affect the boiler are the pulveriser capability, incomplete combustion of fuel [69], production of pollutants beyond the regulated limits or operation of the power plant [70], flame stability [71] and also slagging [72].

Incomplete combustion of coal is characterised by measuring carbon in ash and acts as an indicator whether the fuel is releasing its potential heat. Operating with higher levels of unburned carbon leads to increasing the fuel consumption to ensure enough heat is released in the furnace and incurs additional operational losses [73]. Cloke et al. [69] tested around 16 world coals on a 1 MW pulverised fuel combustion rig and concluded that the very early stages of combustion has a dominant effect on carbon burnout. Thus, the study of ignition becomes a very important aspect when considering the application of cheaper coals. Another consequence of switching could be operating the power plant at a lower load. This situation would result in a decrease in the overall output from the power plant and this indicates a careful evaluation of true savings/cost due to fuel switching [72, 74]. Improving the

fundamental understanding of the ignition can also lead to better plant performance and flexibility by expanding the turn-down ratio of the burners. The optimum use of low value coal would be to co-fire it with the design coal or bituminous coal [75]. The effect of blending is a difficult process to predict but there has been work done in the past to predict the ignition behaviour [75–77]. Carpenter has shown that the behaviour of coal blends from bench and pilot scale tests differ from the actual performance in a utility boiler [78].

Flame stability depends highly on the successful ignition of the incoming fuel and rate of burning. A stable flame will not be generated based only on successful ignition because the exothermic reaction heat produced during ignition can be lost due to dissipation in the furnace environment before neighbouring molecules/particles can reach the activation energy (high temperature). Ignition and flame stability is a function of mixing. It is necessary for a flame to heat up to the point where the heat generation is balanced by the loss of heat during ignition. If the ignition point for a non design coal is offset with the burner design and aerodynamics, the flame formed can be unstable and violent in nature [78]. It is important to note that coals with the same proximate analysis may not ignite in a similar manner as the ignition is depended on the early heat release rather than the volatile release [76]. This provides another reason for ignition being a crucial topic on which to focus.

Fuel switching is generally based on experience and is heavily reliant on experimental tests [79]. According to authors knowledge, at the current stage, there is no ignition model in literature which could reduce the lead time in trouble-shooting and improve the development of new burners. This EngD was focused on developing an ignition model using Computational fluid dynamics (CFD), which can assist in accurate predictions of the ignition location in pulverised fuel flames.

1.4 Ignition modelling

Mathematical modelling can provide an insight into the combustion process. It allows low-cost exploration of parameters that may affect the ignition process in a burner. Experimental testing can be expensive and time consuming because of the overall set-up and operational cost. With the help of mathematical modelling it is possible to investigate the influence of various parameters on the system. Oxyfuel combustion or switching to low rank pulverised fuels (Carbon lean fuels) has been proposed as a potentially viable technology to help reduce CO_2 emissions from a power station and mitigate global warming. Changing the combustion environment from air to oxy-coal or switching to different fuels will change the ignition and flame behaviour. In other words, to achieve flexibility to operate under different conditions proposed above, the burner design should demonstrate wide range of operability, which relies on the ignition and flame characteristics.

Mathematical modelling can help predicting the changes in the ignition and the overall combustion process. Over the years CFD has been identified as an im-

portant engineering tool to evaluate ignition and flame characteristics of various combustion process. The principle fluid is modelled in a continuum medium and the macroscopic properties of the fluid are solved across a discretised space, which are represented as the transport equations for mass, momentum, energy and species. Many sub-models can be included into CFD solutions which make it a robust tool and can be applied in various engineering problems. The results obtained from CFD can be used to improve product design. Modelling coal/biomass combustion process is complex as it needs to account for interaction of turbulence, chemical kinetics, heat transfer and two-phased fluid dynamics. Each phenomena would require an accurate sub-model which can result in a reliable CFD simulation. However, in order to gain confidence in a CFD simulation, the results should be validated against experiments which can justify any modelling assumption considered.

1.5 Thesis outline

This thesis outlines the development and validation of an ignition model for simulating flames for pulverised fuel burners. This chapter highlights the background and motivation for the thesis. A review of the experimental and CFD techniques for air and oxyfuel combustion is presented in Chapter 2. Experimental and CFD modelling studies are evaluated in Chapter 2 focusing on ignition, ranging from single particle to pilot scale facilities. Chapter 3 investigates capability of three different devolatilisation network models where the results from the model are compared against the experimental data from hight temperature wire mesh experiments.

In Chapter 4, a single particle model for ignition is developed and validated against experimental data for a drop tube furnace analysing two different rank of coals. A correlation is developed between particle size and ambient O_2 concentration differentiating ignition mechanism. A number of sensitivity study are conducted to propose suitable sub-models for predicting ignition of a single particle.

In Chapters 5 and 6, CFD simulations are conducted on IFRF and Utah furnace which tested bituminous coal in coaxial burners. The facility at IFRF and Utah tested pulverised fuel flames in air and oxyfuel conditions respectively. The methodology developed to obtain the correlation differentiating ignition mechanism is used for the fuels under investigation. The benchmark CFD simulations are performed, replicating the models used in the literature for simulating the coaxial burners. The correlation developed is integrated in the benchmark model and the results from both the cases are compared with the experimental data for validation. Furthermore, sensitivity analysis is conducted on radiation models and gas phase turbulence-chemistry models for Utah furnace(oxyfuel combustion).

In Chapter 7, the ignition model developed in Chapter 5 is tested for a 250 kW pilot scale combustion facility, which had a pulverised fuel swirled burner. The model is implemented in CFD simulations with two-dimensional axis-symmetric and

three dimensional geometries. The study compares the predicted CFD simulation results with the experimental data. The final chapter, summarises the conclusions of this thesis and makes suggestions for improvements and potential future work.

2 Literature review

This Chapter focuses on investigating the work referred in the past and the current techniques to predict ignition, ranging from single particle to full scale furnace conditions. In the first half of the Chapter, a review of literature surrounding ignition of a single particle, multi particles and pilot scale burner is presented in Section 2.2. The other half of the chapter reviews the literature regarding CFD modelling where governing equations required for modelling are presented. The mathematical sub-models required for modelling coal combustion using CFD, are discussed in Sections 2.6–2.9

2.1 Single particle combustion

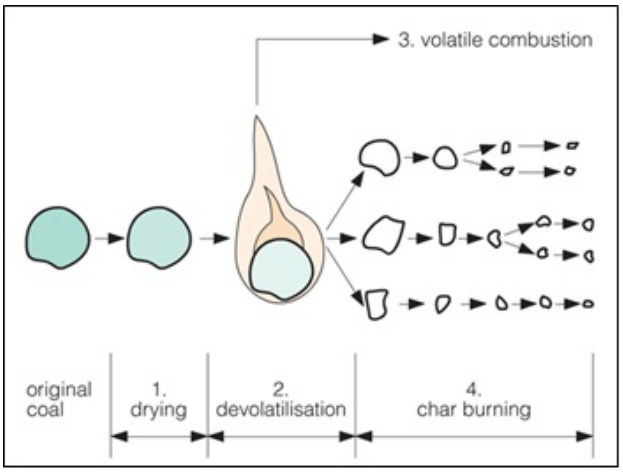

(a) Single particle combustion process[80].

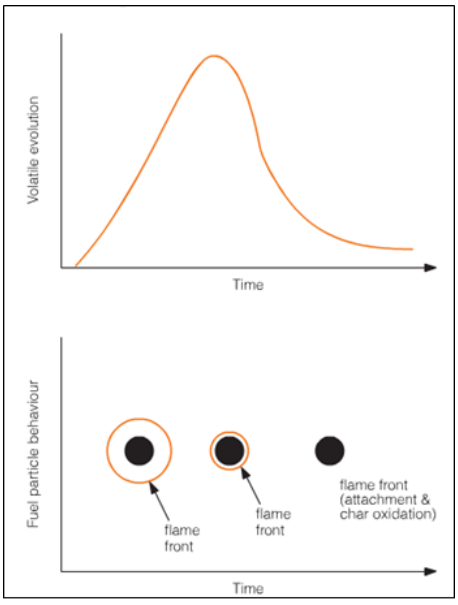

(b) Volatile Evolution and gas phase flame behaviour [81].

Figure 2.1: Single particle combustion process and volatiles evolution.

A coal particle is heated by convection and radiation as it enters the furnace. A coal particle goes through a series of stages during combustion, as illustrated in Figure 2.1a. Coal upon heating releases the moisture but complete dehydration of the coal does not occur below 350 °C [82]. As the particle approaches 400 °C, the

devolatilisation process begins and volatiles (gaseous products and vapours) from the coal particles are released. The amount of volatiles released depends on the type of coal, size and its thermal history.

The chemical process involved during devolatilisation is very complex. This complexity exists beacuse coal is a mixture of various minerals and compounds [83, 84], even if there are two coals with the same rank, the geological and elemental composition varies the way coal will devolatilises [85]. It is dependent on the type of the bonds packing within the coal [81]. The evolution of the species are subject to disintegration of the chemical bonds and the kinetics are thus highly non-linear. The result of this complexity makes it difficult to predict the devolatilisation, and minor differences in the coal, which are not necessarily prevalent from simple analysis, can have a significant impact on the behaviour. Work done by Strezov et al. [86] concluded that weaker carboxyl, hyrdroxyl and aliphatic bonds break up at lower temperatures, whereas the stronger heterocyclic components decompose at higher temperatures. The physical change during devolatilisation is primarily the swelling of the coal [87, 88]. It is during this stage, bubbles are formed inside the particle and the volatiles are released. These bubbles move to the surface and rupture releasing gases. The bubble grouping, movement and size is a function of the vapour pressure inside the bubble and the ambient pressure [88]. The volatiles are released faster through the core of the particle, and not from the surface/pores, and thus results in a build-up of internal pressure and in an initial swelling and then shrinking as the bubbles burst. This is followed by rapid contraction and this occurs until the particle re-solidifies [89].

After the volatiles are released, they react with the available oxygen. A film of gas is formed around the particle which consumes any oxygen transported towards the surface [90]. This prevents the heterogeneous oxidation of char [81]. The flame formed by the gas film and oxygen is away from the particle but comes closer and eventually adjacent as time elapses [91]. This is illustrated in figure 2.1b, as the volatile release is slowed down, there is no volatile film available to combust with the incoming oxygen. After the volatiles evolved are combusted, the remaining substance, char, burns heterogeneously and this is relatively a slow process $\approx$1000(milli seconds) slower than the volatile reaction [92]. This process dominates the total time a coal particle would take to burn. Thus, the ignition of coal mainly relies on the devolatilisation process in the furnace conditions as it is the volatiles that react faster and are responsible for initiating the increase in temperature [93]. Char combustion mainly involves oxidation of carbon to CO or CO_2 at the surface [94]. CO_2 oxidation is dominated at low temperatures and CO at high temperatures [95]. This process is controlled mainly by the rate of oxygen diffused into the particle.

2.2 Basics of ignition and flame propagation

Ignition can be defined as the non-stationary process which can be divided into three stages:

i The fuel initially absorbs the heat (endothermic process), initiating formation of free atoms/radicals (reactants).

ii The free atoms diffuse with the available O_2 forming a reactant mixture.

iii The mixture starts reacting, releasing products and resulting in a rapid increase in the temperature. This occurs due to the exothermic nature of the reactions. *Ignition* is the point when the release of heat by the mixture is greater than or equal to that absorbed by the reactants.

The basic principle of continuous combustion is a self-sustaining exothermic reaction of the fuel and oxygen [96]. The phenomena is goverened by both chemical and physical processes. The process can be defined as the heat released from the chemical reactions and transported through the fluid in motion [96]. In terms of coal combustion, a stable and rooted flame is an indication of successful combustion of the incoming fuel. Successful ignition does not imply flame stability, as ignition will determine the point of heat release, whereas for a flame propagation, ignition should be accompained by a matched burning velocity [76].

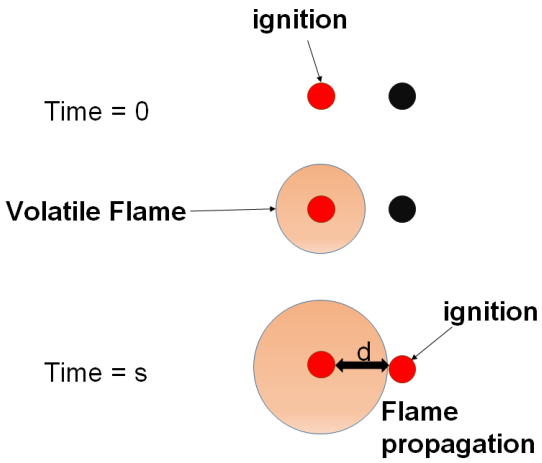

(a) Ignition of intermediate coal particle.

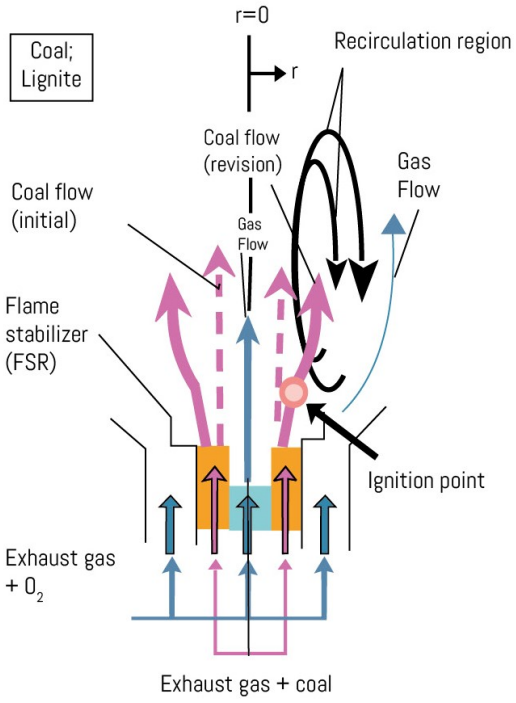

(b) Aerodynamics of a burner.

Figure 2.2: Ignition of the multiple particle combustion process [97].

The aerodynamics of a burner plays a critical role in determining the position of ignition. A typical wall fired burner is shown in Figure 2.2b. The coal particles are carried by the transport of air in the primary air register. The secondary air producing swirling air, which generates a recirculation zone of hot gas towards

the burner inlet, thus allowing the rapid heating of the incoming fuel. After the particles are introduced in to the boiler, they get caught in the recirculation region. The volatiles are released in the early stages due to the heat transfer from the recirculating hot gases and the flame. The volatiles mix with the ambient oxygen and ignite in the continuous phase 2.3.

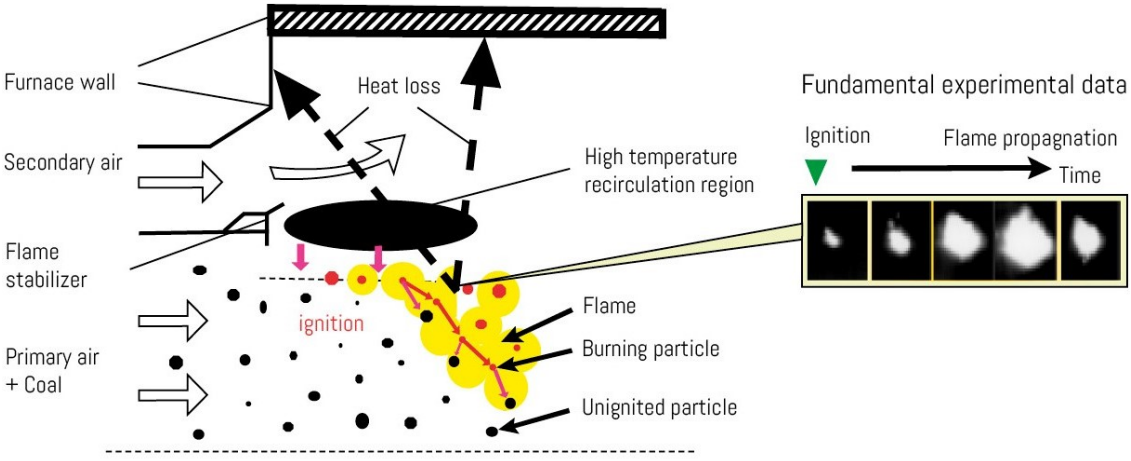

Figure 2.3: Schematic of the flame propagation in a furnace [97].

After the initial ignition, if the concentration of the particles/volatiles is high enough the heated coal particle's flame also ignite the nearby particles (Figure 2.3 & 2.2a). The clusters of ignited coal particles combine together and form a flame and ignite the other coal particles which have not been ignited and this is how the flame propagates,see Figure 2.3. The secondary air mixes with the recirculation zone and assists in completing the combustion of the coal particles (basically supplying sufficient oxygen). Generally, in a rooted flame, the particles ignite very close to the burner. This is one type of sequence for flame propagation, the particles may also get trapped in the shear layer of the flame and ignite in the layer itself which is made up of the swirling secondary air, primary air and recirculating gas forming the outer boundary of the flame. This also creates an extra layer of complexity in terms of locating ignition point. In either situation it is important to note that flame propagation is a fluctuating phenomena because of the very fast chemistry (non-linear consumption of oxygen) and mixing. Thus the ignition point is not always stable at one location but keeps shifting in a certain range. It should be realised that the mechanism of ignition in a furnace is difficult to detect because of the complex interactions between the aerodynamics, chemistry and heat transfer. Any major deviation in these interactions can change the ignition point and as a result change the shape of the overall flame.

2.2.1 Single particle ignition mechanism and modelling

The ignition mechanisms can be categorized into three regimes: *homogeneous* (HO), *heterogeneous* (HI) and *hetero-homo* (HI-HO) ignition as shown in Figure 2.4 [98]. The HO is where the ignition of the volatiles preceeds the ignition of the char,

whereas in the case of HI, the coal particle is combusted due to the direct attack of the oxygen on the surface of the particle and HI-HO is a region where ignition is due to both volatiles and direct coal combustion. These phenomena highly depend on the following properties [98]:

i Size of the coal particle,

ii Heating rate,

iii Temperature,

iv Oxygen concentration around the particle, and

v Reactivity of the coal.

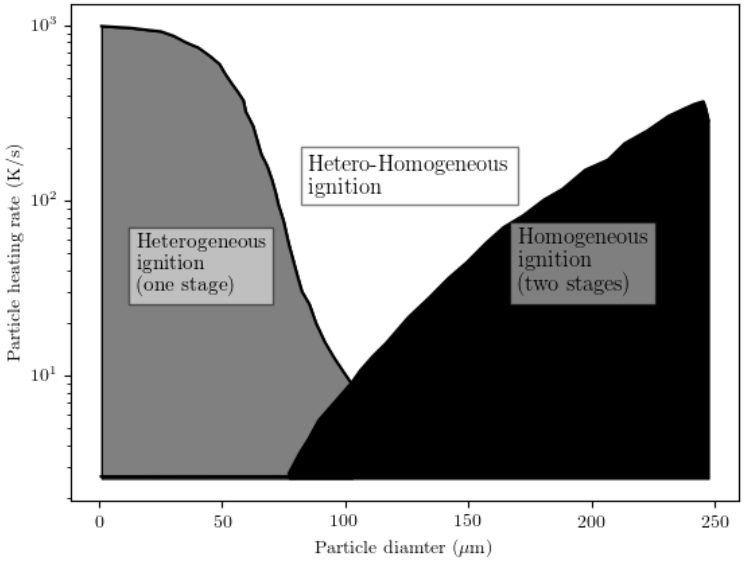

Figure 2.4: Ignition mechanism as a function of particle heating rate and particle diameter [99].

Jüntgen et al. [99] experimentally observed three ignition regimes i.e. HO, HI and HI-HO for different coals at lower heating rates ($<10^3$ °C/s). At lower heating rates, smaller particles (<100 μm) undergo HI and bigger particles (>100 μm) undergo HO as shown in Figure 2.4. The HI-HO can occur for a wide range of coals and the ignition behaviour is very difficult to predict [98]. The heating process is a significant factor as the heating rate of coal particles can affect the chemical and physical nature of its product, which is char [100]. In a furnace, typical heating rates are in the order of 10^4 – 10^5 K/s [101]. Every particle heats up independently and this depends on local factors such as particle diameter, shape, composition, etc. as well as global factors such as particle residence time, aerodynamics, surrounding combustion environment, etc. There are many other factors inside a furnace which has a secondary influence on ignition e.g. ambient conditions for the incoming

fuel. This makes the prediction of the ignition point in the furnace very difficult. Many studies have qualitatively predicted ignition behaviour but they have failed to provide a quantitative model.

Single particle modelling

In practical coal power plants, turbulence and non linear aero dynamics are present which make the study of coal ignition difficult. Examining the combustion of a single particle allows for these complexities to be neglected and provides an insight into fundamentals of coal ignition.

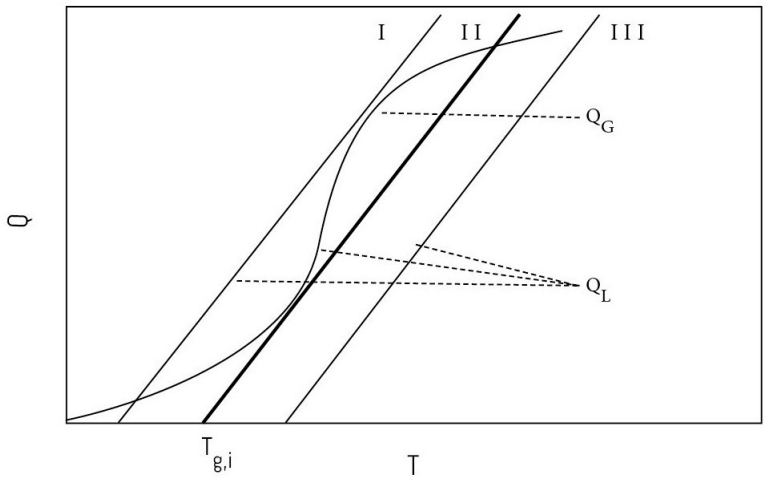

Figure 2.5: Variation of heat generation (Q_G) and heat loss (Q_L) with temperature: criterion for ignition [98].

Semenov [102] was the first person who developed an elementary model for thermal explosions which acts as the basics for simple ignition theory. He stated that the requirement for steady state ignition is that the heat absorbed by the particle is equal to the heat produced by the particle. Essenhigh and co workers were the first to investigate single particle combustion [103–105]. Single particle ignition theory was mathematically developed by Taffanel & le Floch (tangency requirement) and Van't Hoff (equivalence requirement) [98]. The theory had two criteria, the first being the heat loss Q_L is equal to the heat gain Q_G and the other being the Q_G and Q_L curves are tangent to each other. The heat rate at which the particle having mass m_o and specific heat c_p is governed by

$$m_o c_p \left(\frac{dT}{dt}\right) = Q_{\mathrm{G}} - Q_{\mathrm{L}} = Q \tag{2.1a}$$

$$m_o c_p \left(\frac{d^2T}{dt^2}\right) = \left(\frac{dQ_G}{dT} - \frac{dQ_L}{dT}\right)\frac{Q}{m_o c_p} = \left(\frac{dQ}{dT}\right)\frac{Q}{m_o c_p} \tag{2.1b}$$

where Q is the net heat supply rate to the particle. The ignition theory is satisfied

when

$$Q = 0(\text{Van't Hoff equivalence requirement}) \tag{2.2}$$

$$\frac{dQ}{dT} = 0(\text{Tangency requirement}) \tag{2.3}$$

Chen et al. [106] and later Smooth et al. [107] identified a limitation to the ignition theory and Equations (2.2) & (2.3) where the ignition can also occur if the heat produced is greater than the heat loss and suggested that $Q \geq 0$. As the temperature plays an important role in the ignition conditions, many ignition studies have focused on measuring or predicting the ignition temperature [106, 108, 109].

It is difficult to quantify the ignition mechanism i.e. HO, HI or HI-HO. A few studies have been conducted in the past which have attempted to quantify the ignition mechanism. Annamalai and Du [110] presented a mathematical model for HO or HI ignition using the Semenov and Chen criteria for the ignition, see Equations (2.2) & (2.3). It suggested that the transition to HO does not take place until the diameter of the particle is about 400 µm. The investigation considered gas at 1500 K and 23% oxygen concentration. The particle temperature was time dependant but there were clear limitations in the model, where the particle temperature being spatial uniform. In reality the particle has thermal gradients across the coal particle which changes the way that the particle behaves in the initial stages. Thermal gradients have been shown to play an important role in larger particles [111, 112]. Many hydocarbons are released during devolatilisation but the kinetics of volatiles were limited to methane. These modelling limitations were removed by Rocha and Veras who considered thermal gradients within the particle and more species were considered for the gas phase combustion using an advance devolatilisation model, i.e. chemical percolation devolatilisation-nitrogen and light gases (CPDNLG) [113]. The advantage with this model was that it can predict the amount of nitrogen and different gases released during devolatilisation. The ignition conditions were kept similar and it was found that the transition from HI to HO for different ranks of coal was very small and thus they displayed HI-HO ignition.

Improvements to a model similar to that of Annamalai was made by Zhu et al. [114] by considering intra-particle conduction but kept the volatiles reaction limited to CH_4. They found that the thermal gradients had very little effect on the transition of HI to HO. They concluded that small particles generally ignited heterogeneously (which also is dependent on the ambient conditions). Again, the simplification of assuming volatiles as CH_4 can tend to over predict the ignition phenomena. The assumption of CH_4 being released as all the volatiles was overcome by Liu et al. [115] by integrating H_2 and CO along with CH_4. They compared their modelling results with the micro gravity experiment conducted in the drop tower at the National Microgravity Laboratory. The results obtained agree well with the experiments but the conditions in a furnace are quite different. The particle size analysed here are around 2 mm at a heating rate of 150-200 K/s, which is fairly low when compared to furnace conditions. The model is not validated for particles undergoing high heating rates and thus this model did not provide high confidence

in using only a few equations for the reaction mechanism.

A similar study on single particles was conducted by Glushkov et al. [116] for low temperature (600 K) ignition by considering the interconnected process of heat and mass transfer between intermediate particles, where it is discovered that the particle undergoes HO for particles ranging from 100-1000 µm. The heat from HO is not enough for intermediate HI but multiple particles in close proximity allows surface ignition.

Wendt et al. [117] created a model assuming an axisymmetric coal particle of three different shapes by modifying the model for a single particle ignition by Annamalai and Du [110], where ignition is identified by an increase in the gas phase temperature. It considered the temperature gradient across the particle with intra-particle heat & mass transfer, external radiation and surface oxidation. The model agrees with the ignition prediction for small particles in [110] but for particles above 300 µm deviates from the results primary due to the uniform temperature assumption considered Annamalai and Du [110].

Goshayeshi et al. [118] compared the particle size, devolatilisation and chemistry models to investigate the effect on ignition delay of a single coal particle. It highlights how the current state of CFD models are not able to predict ignition. They defined the ignition delay between the particle inflection point and the peaking of CO mass fraction during devolatilisation and char combustion. Also it took into account, the simultaneous behaviour of vaporisation, devolatilisation and char oxidation, where the sequencing of the processes do not impose any restriction on the disintegration of the particle. Also they compared the detail chemistry mechanism (GRI 3.0) and flame sheet model(infinitely fast reactions) in their model. Goshayeshi concluded that to successfully predict ignition the detailed devolatilisation and gas phased chemistry models are required.

Similar work done by Veras et al. [119] to simulate char combustion and devolatilisation process simultaneously. This work was done in order to see the interaction of the char combustion rate on volatiles evolution rate during HI. It shows the effects of particle size, ambient temperature and oxygen temperature affecting the ignition process in a furnace. This work is of much significance as it gives an indication to as what occurs to the volatiles in the particle during HI.

Vascellari et al. [120] developed an ignition model for a single particle during devolatilisation, where a detailed flow is resolved near the coal particle transiently which assists in obtaining a predicting HO. This work was the next leap in ignition modelling as it considered semi detail chemical reactions of a few species rather than a few simplified equations for CH_4. The ignition model used CPD to predict the volatiles evolution where the composition was assumed to be CO, CH_4, N_2 and C_2H_2. They used the DRM mechanism [121], a reduced version of GRI mechanism, which solved about 103 reactions for 22 chemical species to maintain a trade-off between accuracy and computational cost. The GRI 3.0 mechanism is considered

to be more accurate as it includes more species and reactions but results in being computationally expensive. The integration of GRI 3.0 was done using flamelet model proposed by Pierce et al. [122] where lookup tables are generated to provide the chemistry variables. This approach was applied by Watanabe et al [123], which also includes the char gasification and oxidation reactions. It compares this approach with the detailed chemistry model (GRI mechanism) for a very small domain with scaled down parameters (coal particles being less than 5 µm in diameter) to save computational cost. The results obtained show that the flamelet modelling approach is able to predict the peak temperature of the flame with an accuracy of 4% but an error of 35% is observed when predicting the ignition position. Modifying the choice of the progress variable for the formation of the lookup table can improve the ignition phenomena but currently the detailed chemistry model provides an appropriate solution for the ignition prediction.

The model developed by Jimenez and Gonzalo-Tirado [124] analysed the volatile flame of an isolated particle. They used a single rate Arrhenius expression to simulate devolatilisation and used the kinetics from the experiments conducted previously. The composition of the volatiles was obtained from the CPD model and the composition considered was H_2O, CO_2, CH_4, CO and C_2H_2. The reactions in the gas phase are accounted for by using GRI 3.0 mechanism which considers 53 species and 325 reactions. The model focused on predicting the flame peak temperatures and voaltile flame location but did not capture the heternogenous ignition behaviour. The model also ignored the investigation of the peak temperatures produced in the flame due to the char oxidation. The results agreed with the trends but were dispersed when compared to different experiments, the errors were attributed to the assumption of no soot formation in the model. Tufano et al. [125] investigated the coupling of devolatilisation and homogeneous ignition for a single particle where they had a similar approach to model the devolatilisation using CPD. In this case, the chemical reactions were accounted by the POLIMI_TOT_1407 which included 52 species and 452 reactions. Also they compared the results for air and oxy-fuel environment where they observed that the ignition delay is reduced with a increase in O_2. The oxyfuel environment has longer delays compared to air. Tufano and co workers more recently further developed this model into an advance single particle ignition model [126], where each sub-model was developed and validated with experimental data in isolation [127],[128]. The sub-models developed are their in-house model which accounts for the detail gas phase chemistry, advance char kinetics [129], and a porous media transport model [130]. The ignition model accounted for the shortcomings discussed above e.g accounting for various species evolution in the volatiles composition based on particle properties instead of purely assuming CH_4, considering intra-particle heating etc. The overall model is computationally expensive, which a major limitation and can not be a viable option as a pre-cursor tool in industrial application. On the other hand, the methodology can be useful approach if the sub-models are simplified and the computational expense can be reduced.

Maryam et al. [131] developed a 1D ignition model to analyse large biomass

particles. The model was able to consider thermal gradients which allowed the simulation of suddenly heated particle surfaces and keeping the inner region relatively cold. The intra particle process is important for biomass as they are not easy to pulverise and they are generally fired larger in size. The results from the model show that, in general biomass ignites heterogeneously but at temperature above 523 K a significant decomposition of hemicellulose and cellulose starts and this results in the releasing of large amounts volatilies which quenches the primary HI and forms a flammable gas mixture around the particle which starts a secondary HO.

2.2.2 Experimental work on single particles

Experiments have characterised ignition by the visual detection of light omitted from the coal particles upon heating [132–134]. Similarly, some researchers have defined ignition semi-quantitatively by measuring the intensity of the light throughout a coal particle's combustion phase [135, 136]. Most of the experimental work on ignition have been conducted on either a drop tube furnace (DTF), entrained flow reactor or by TGA [137]. TGA gives experimental data that is important for the ignition modelling, such as the volatiles released but at a low heating rate below 100 ^{o}C/min which is not representative of furnace conditions [138]. These limitations are overcome by the DTF and entrained flow reactors where the heating rate of 10^4 - 10^5 K/s can be achieved with maximum temperatures about 2000 ^{o}C and more realistic conditions make it more suitable for predicting the igntion behaviour [78, 139, 140]. However, the limitations of these tests are that they may not replicate the furnace conditions due to the lack of intense turbulent conditions. The aerodynamics is very complicated and varied for different burners due to the introduction and mixing of the air at various stages to meet the combustion requirements. Thus, pilot scale testing is highly desired in order to obtain a representative performance of the combustion process. These small scale laboratory studies can be very useful to validate numerically developed sub-models of combustion. The sub-models developed can be applied in the CFD code to simulate the furnace conditions with higher confidence.

The ambient gas temperature effect the overall ignition mechanism as well as the ignition time delays. Duarte et al [140] studied four Turkish fuels, i.e. two biomass (almond shells and olive residual) and two lignite coals (Tunçbilek lignite and soma lignite) in a Mckenna flat flame burner with a varying temperatures between 1460 K - 1660 K and in TGA at 20 K/min. They found that the ignition times delay decreased with an increase in the ambient gas temperature. Another significant conclusion of the study was that both the biomass ignited homogeneously for both low and high heating rates and this was mainly due to its high volatile content. Simoes et al. [141] analysed five different biomass fuels (wheat straw, kiwi branches, vine branches, sycamore branches and pine bark) and a bituminous coal in an optical flat flame Mckenna burner. The operating temperatures were varied between 1500 - 1800 K and the results show that the biomass generally ignited homogeneously and all the fuels showed a consistent trend of decreasing ignition delay time with increasing ambient gas temperature. When the ignition time delay is compared for

the bituminous coal and the biomass fuels, biomass always took longer because of the moisture content release during the drying stage which tends to cool the gas temperature around the fuel during the ignition process.

It is experimentally shown by Fan and co-workers [142, 143], using the drop tube furnace (DTF), that an increase in O_2 concentration does not have an effect on the mechanism of the ignition but the ignition temperature reduces with an increase in the O_2 concentration. This is mainly due to the higher reactivity of the fuel-oxidiser mixture. Also it shows that bituminous coal is affected most by the O_2 concentration and temperature compared to lignite and anthracite. The rate at which the ignition temperatures decrease was much higher with between 21-30% O_2 compared to the decreased rate between 40-60% O_2.

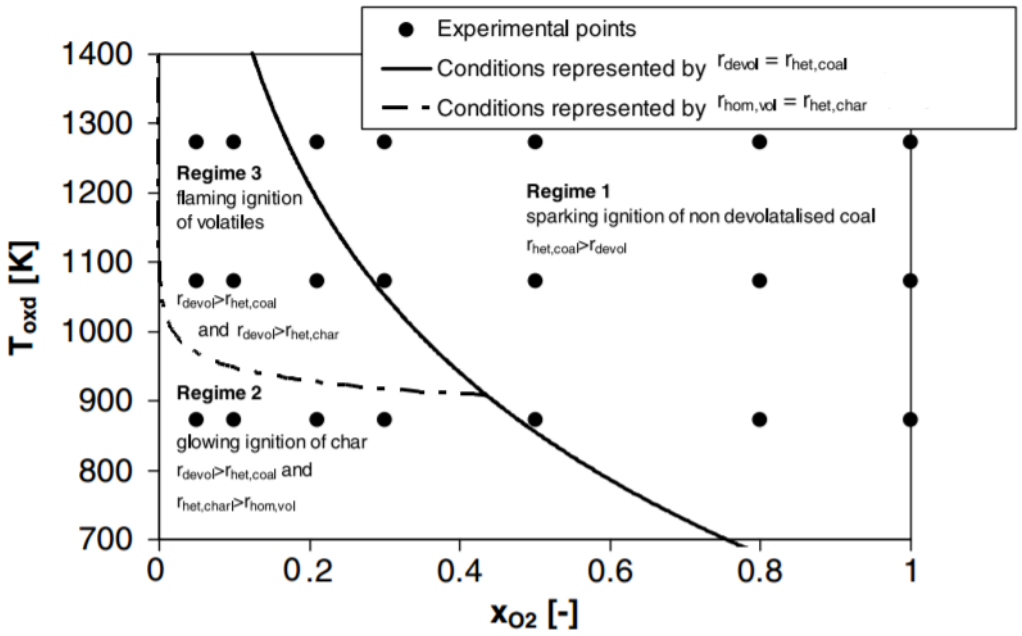

Figure 2.6: Ignition regimes for the different experimental conditions tested [144].

Ponzio et al. [144] conducted a study of single particle ignition in a batch type reactor where the O_2 influence on the ignition mechanism was monitored. After performing an experimental analysis, it was discovered that the ignition mechanism was divided into three regimes as shown in Figure 2.6. Regime 1 was the direct ignition of coal (HI), regime 2 is the direct ignition of the char mainly at low temperature and low O_2 concentration (HI), and regime 3 was the ignition of the volatiles at high temperatures and low O_2 concentrations (HO). Ponzio et al. [144] proposed a mathematical model based on the experiments where the three regime are quantified by the following conditions:

i Regime 1: The rate of coal surface oxidation is greater than the rate of devolatiliation $r_{hot,coal} > r_{devol}$.

ii Regime 2: The rate of devolatilisation exceeds the rate of oxidization of non-devolatilised coal ($r_{devol} > r_{het,coal}$ and that the rate of oxidation of the char surface is higher than the rate of volatile combustion ($r_{het,char} >$rhom,vol).

iii Regime 3: The rate of devolatilisation exceeds the rate of oxidization of non-devolatilised coal ($r_{devol} > r_{het,coal}$) and that the rate of volatile combustion is higher than the rate of oxidation of char surface ($r_{hom,vol} > r_{het,char}$).

Jovanovic et al. [145] implemented this theory in a commercial CFD software, where he considered the simultaneous evaporation, devolatilisation and char combustion rather than a sequential process in the combustion model and they were unable to predict the ignition position in an entrained flow reactor for oxyfuel conditions. The ignition position was identified based on the temperature change of the particle and the regimes suggested by Ponzio above [144]. They also conducted experiments for a high volatile Russian coal of 85 µm diameter in a vertical reactor at the ignition test facility in Warsaw, Poland. The facility is able to handle high temperatures that are similar to the DTF which makes the results comparable to the furnace conditions (excluding the aerodynamic behaviour). They tested the coal in air and oxyfuel conditions. Also, the experimental ignition points for varying conditions are determined based on the observation of the first visual flame in the reactor. The ignition results compare well with the numerical model predictions but the reaction mechanism was limited to one equation which is not sufficient to capture a detail homogeneous ignition and the ignition criteria are taken from an experiment which uses relatively larger coal pellets for analysis [144]. Another limitation of the study, is that the species evolving was kept as a single hypothetical component $C_xH_yO_z$ which is converted into CO_2 and H_2O. This over simplifies the species evolving and the final products they are converted to. Further, this approach increases the error in predicting HO. Later this work was extended to study different devolatilisation models to predict the ignition [93]. They kept the reaction mechanism limited to two equations for CPD and single rate models but increased the reactions for a FG (functional group) model which showed improvements in the ignition mechanism and prove to be a better devolatilisation model. The improvements can be attributed to the behaviour of the overall model and the increase in the reaction equations integrated. This work was replicated by Zou and Zheng [146] to study the ignition mechanism but had similar limitations.

Conflicting experimental data is given in the literature for definitions of the ignition regimes. For example, the effect of a change in the oxygen concentration was studied by Annamalai and Du [110], where at lower O_2 concentration HO was the outcome but the transition point varied with particle diameter. The transition from HO to HI was at 15% O_2 concentration for 100 µm diameter, at 23% O_2 for a 300 µm and at 30% O_2 for a 600 µm diameter. This phenomena is contradicted by the experimental analysis in [147] where at 10% O_2 concentration the particles with 600, 800 and 1000 microns ignites at the surface (HI). The contradictions not only arise due to limitations in the visualisation technique and modelling assumptions but also the differences in the bituminous coal used for validating the model and the experimental analysis. Another study by Howard and Essenhigh [148] stated that

HI occurs for particles of 0-15 µm diameter, 15-65 microns is HI-HO and beyond that is HO but this was experimentally validated only for one coal. Another study by Sun et al. [149] in TGA concluded that, the ignition of small size particles occurs heterogeneously.

The influence of the coal rank and particle size is well documented in the work performed by Chen et al. [150] where they suggested that the ignition mechanisms, for small to large (37 to 4000 μm) particles goes from HI-HO to HO. In addition, varying the coal rank from lignite-bituminous-anthracite displays HO,HI-HO and HI using differential thermal analysis (DTA) and thermogravemetric analysis (TGA). The influence of the coal rank on the ignition was analysed by Faundez et al. [139] experimentally in a laminar entrained flow reactor where subbituminous, low volatile bituminous and semianthracite coals undergo HI and high volatile bituminous coals undergo HO. A similar work by Conti et al. [151] suggests a similar finding where carbon rich coal, such as anthracites, ignite at higher temperatures with more activation energy being required.

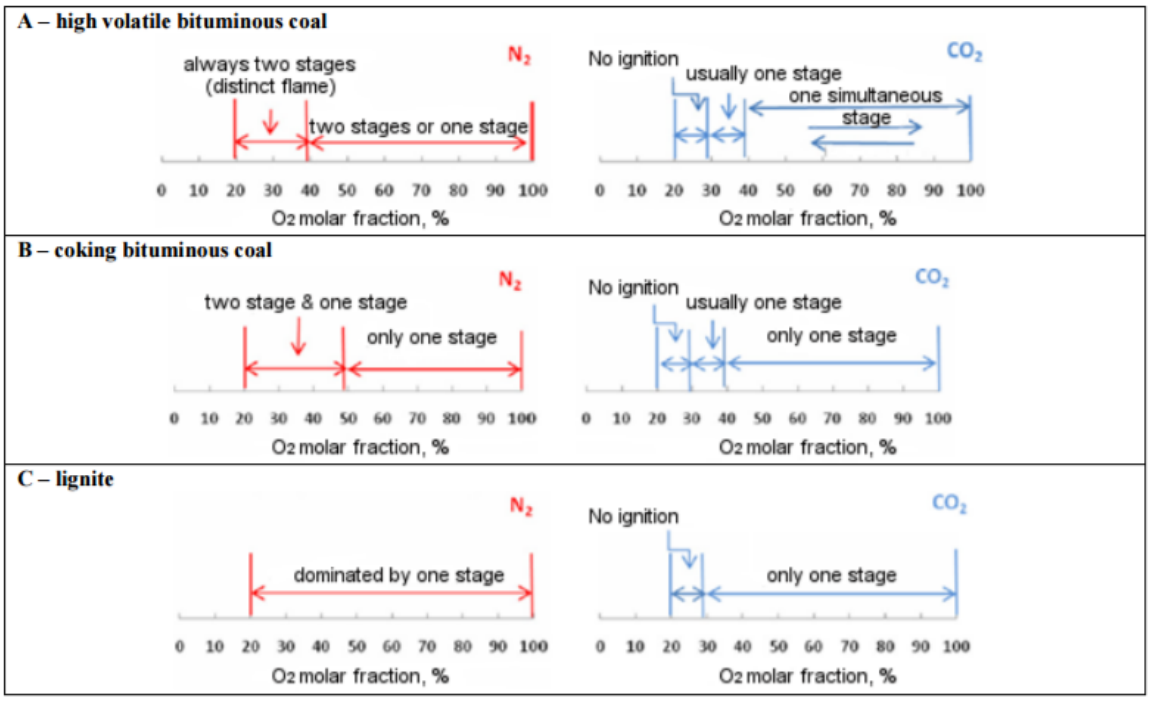

Figure 2.7: Comparison of results from coal particles combustion in different gaseous atmospheres (two-stage combustion: homo- and heterogeneous, one-stage combustion: heterogeneous or no ignition) [152].

The poor ignition behaviour of coal in oxy-fuel conditions was first answered by Kiga et al. [153] where they described the ratio of c_p/R of CO_2 is an important property which delays the combustion process. Many researchers have looked into the ignition behaviour of coal and biomass in oxy-fuel conditions [142, 154**?** –156] and the experimental studies by Shaddix and co-workers have shown that in order to

obtain the ignition characteristics similar to that of air, the O_2 concentration should be about 30% (depending on the coal rank), the devolatilisation and ignition delay reduces with higher O_2 concentrations. The rate of devolatilisation is decreased due to the higher mass diffusivity of the volatiles in CO_2, whereas an increase in O_2 increases the mass flux of oxygen to the volatiles flame, which thereby increases the rate of devolatilisation. Khatami et al. [152] also studied three different coal ranks under O_2/N_2 and O_2/CO_2 (oxy-fuel) environments by varying the O_2 concentration in a DTF. The results are shown in Figure 2.7 and these show the influence of the O_2 concentration on the ignition mechanism. It was observed that in oxy-fuel conditions that the volatile flames are suppressed and the fuel undergoes HI. In air the bituminous coals combusted in two stages but at high O_2 concentration it combusted heterogeneously without producing a volatile flame. In the operating conditions in the DTF, the furnace wall temperature for the experiment was set to 1400 K and the effect of the particle size variation was not taken into account and this was kept in a range between 75-90 µm while O_2 was varied from 20 -100%.

A similar study was performed by Riaza et al. [157] on the same facility by extending the study to different ranks of coal (anthraccite, semi-anthracite, medium-volatile bituminous and high-volatile bituminous) which ranged for particle sized between 75-150 µm. The ignition behaviour was anaylsed based on the observations performed in high speed high resolution cinematography and three colour pyrometery. The results show that the higher rank coal (anthracite and semi-anthracite) ignites HI and bituminous coals ignite HO. The ignition temperature increased with increasing the coal rank. The increase in the O_2 concentration reduces the time and temperature required for the ignition, which was previously observed in the experiments conducted in DTF [152]. When the N_2 is replaced by CO_2, with the same oxygen levels, the intensity of the combustion process is impaired. The combustion temperature is reduced and the burnout times of the particles are increased. Further, on increasing the O_2 concentration restores the intensity of the combustion process. Riaza et al. [158] used the same facilities to evaluate four different biomass particles (sugarcane bagasse, pine sawdust, torrefied pine sawdust and olive residue) at the same conditions used in [157]. It was discovered that the all biomass ignited homogeneously and it had very little difference on the way they combusted. The oxy-fuel conditions again impared the intensity of the combustion process and was restored when the O_2 concentration was between 28-35%.

There has been conflicting studies in the literature when comparing the pyrolysis in air and oxy-fuel conditions. Rathnam et al. [159] and Al-Makhadmeh et al. [160, 161] reported that the pyrolysis rate is higher in oxy-fuel conditions at temperatures above 1000 K in DTF whereas below 1000 K it is the same as air. On the other hand, Brix et al. [162] found no differences in the pyrolysis rate for the bituminous coal in DTF. Borrego and Alvarez [163] analysed high and low bituminous coals in DTF and found that the oxyfuel conditions reduced the pyrolysis rate. Wall et al [164] obtained higher volatiles in the oxy-fuel environment for the experiments conducted in DTF at 1673 K. They attributed the increase in volatiles to the Boudouard reaction and concluded that the phenomena is rank dependent

and may require further investigation.

Flammability limits of the gas determine where HO begins. The flammability limit is defined as the limit within which a gaseous mixture in air can ignite. The volatiles ejected from the coal particles need to ignite or propagate gaseous combustion and determining the flammability limits can assist to detemine the onset of HO. The upper and lower flammability limits are governed by the mixture of the fuel and oxidant. The mixture is quantified as fuel rich region if the fuel to air ratio is greater than one, the mixture is fuel lean region where the fuel to air ratio is less than one. The degree of mixing, oxygen concentration and temperature are important variables for determining the flammability limit at which the fuel-air mixture is present [165, 166]. In gaseous combustion systems, many reduced chemical mechanisms have been used to simulate a detail flame [167–170]. In order to quantify HO, having a reduced chemical mechanism in a single particle model becomes important.

Table 2.1: The main parameters influencing the ignition delay times

		Ignition time delay	**References**
Ambient gas temperature	Increase	Decreases	[140, 141, 152, 171]
O_2 concentration	Increase	Decreases	[142, 143, 152, 154]
CO_2 concentration	Increase	Increases	[152, 154]
Coal	Increase in coal rank	Decreases	[139, 150, 152]
Biomass	-	Reduced influence	[140, 158]

To summerise, single particle ignition experiments have focused on the following parameters:

i Coal particle ignition temperature.

ii Change in coal surface temperatures during ignition.

iii Determining the combustion mechanism HI, HO or HO-HI.

iv Monitoring the particle burnout time as a function of the particle size and changing temperature.

v Determining the ignition delay (the period between when the coal ignites and a visible flame can be observed).

vi Quantifying the mass loss with varying the heating rate (devolatilisation process).

vii Obtain the kinetic constants for the reactions at given measurement conditions [137].

As described in this chapter, the literature can be contrary in quantifying the ignition and flame propagation mechanism. This mainly arises due to the experimental set-up, measurement methodology, using different coals/biomass for analysis

and different operating conditions. It is because of variations in these factors that the ignition phenomena is very complicated. In order to quantify the ignition mechanisms, a single particle ignition model would be desirable and the model should be flexible enough to simulate various single particle experiments to include different heating rates. The model should account for variation in coal rank, particle diameter, ambient gas composition. Also, the model should be capable of being able to simulate the simultaneous vaporisation, devolatilisation and char combustion. The advantage of such a model will be that it will provide an understanding of the main governing phenomena of particle ignition.

2.2.3 Multiple particle ignition

There have been only a few studies that bridges the gap between single particle combustion and pilot scale studies. Similar to single particle combustion, a few modelling and experimental analysis have been conducted on a stream of coal particles. Cassels and Libemann [172] first studied coal clouds experimentally and since many researchers have focused on investigating the specifics of combustion. Xiangyang et al. [173] developed a model for predicting the transient ignition of HO or HI. The model considered a cylindrical cloud of pulverised coal particles where HO occurs for a dense cloud while HI for a diluted cloud. The HI occurs at lower temperatures and transits to HO at a higher temperature. The HO time reduces as the temperature increases for denser clouds since more volatiles are available. The results suggested that the ignition is highly dependent on particle number density, particle size, coal volatile matter, cloud radius, and ambient conditions.

The modelling approach by Xiangyang [173] was taken further by Wang et al. [174] who maintained the same ignition criteria but in a stationary phase. Wang et al. [174] discovered that the ignition time delay in a stream of particles reduces with an increase in ambient temperature and oxygen concentration. The shortcomings of the model are that it fails to simulate any convective heat transfer as the particle is simulated at stationary conditions. Experimentally, the cloud of coal particles burn in a turbulent jet flow and the quantification of the ignition in such conditions is difficult. This is mainly due to the velocity with which the coal disintegrates and it is difficult to track a particle in the early stages of combustion, which can describe the onset of the ignition. There have been many imaging technologies where higher frames per second can ease the quantification but these are relatively expensive. Therefore, generally the global behaviour of the flame is monitored and the ignition is quantified based on the intensity of the flame [175–178].

There is a significant impact of the ambient temperature on the ignition behaviour of the coal and this was highlighted by Ye et al. [136]. They studied the ignition behaviour of dispersed coal and analysed three different types of coal (lignite, high ash bituminous and low ash bituminous) in a Hencken burner, by varying the ambient temperature between 1200 - 1800 K and the oxygen mole fraction in the range 10-30%. The ignition delay times are indicated by 10% of the maximum intensity of the flame and the ignition delay time is reduced with an increase in the

temperature and this is mainly because of early release of volatiles as a consequence of higher heating rate. This is because of this early volatiles release, the HO and formation of the volatile flame is dominant at higher temperatures otherwise the ignition phenomena is simultaneous (HO-HI) at temperatures below 1500 K. Also the ignition delay decreases with an increase in the O_2 concentration. Coal rank also plays an important role in the ignition time, the differences are mainly attributed to the volatiles content in the coal. The bituminous coals exhibited a lower ignition time when compared to lignite.

Another important factor, which contributes towards ignition is the fuel to air ratio and the activation energy. It has been highlighted in the Section 2.2.2 the importance of the O_2 concentration and the heat that the reactants recieve but the concentration of the fuel is also important [179]. Man and Gibbins [180] analysed 13 coals of different rank in a 20 l explosion chamber in order to investigate the effect of coal concentration in a O_2/CO_2 atmosphere. The ignition was measured when the pressure ratio of the vessel exceeded 2. They varied the energy released by the igniter and found that the higher rank coals required more energy to ignite, whereas lower rank coals can be ignited at lower energy levels. This is mainly due to the amount of volatiles released by low rank coals, which means that the volatiles in a gaseous state could combust more easily undergoing HO. Higher rank coals mainly contain carbon, which takes relatively more time for cobustion as the ignition would be due to the surface oxidation. The fuel concentration required also decreased with an increase in O_2. The importance of the particle concentration is described by Taniguchi et al. [181], where they distinguished the ignition and flame propagation phenomena. They improved the flammability limit by adjusting the burner design to increase/shift the coal concentration in the region where the oxygen concentration is higher.

Taniguchi et al. [97] qualitatively analysed the ignition process by dividing the combustion regime into three separate regions, i.e preheating region, ignition region and continuous flame region. The ignition region in this work was defined as the region where the flame visually initiates and clouds of burning particles were formed due to the ignition particles. CFD analyses have been performed by Yamamamoto et al. [182, 183] in an attempt to qualitatively define the region where ignition occurs and this is defined as the region where particles individually ignite and produce bright spots just after the lift-off region and the flame propagation is defined at the initial stages of the flame. They simulated the experimental conditions using LES and RANS and compared the results obtained by quantitatively using the gas temperature and the lift height. They discovered that the $k - \epsilon$ turbulence model is unable to accurately simulate the flow, whereas, the LES results agree well with the experimental data.

An attempt was made by Muto et al. [184] to simulate the dispersed coal particles ignition conditions by using detailed chemical reaction mechanism. They analysed the region where two stream of fluid are mixed and the primary stream transports the coal particles and the secondary stream mixes with the primary in the mixing

plane. CPD-NLG was used as model devolatilisation and the composition of the volatiles species was $H_2, H_2O, CO, CO_2, CH_4, C_2H_2, C_2H_6, C_3H_6, C_3H_8, C_6H_6$. A detail chemical reaction mechanism was considered where about 158 species and 1804 reactions were applied to simulate the flame combustion. This model provides an insight into multi particle detailed interactions and gives detail combustion characteristics. A major limitation of the model was that the coal particles were pre heated upto 2000 K in the mixing plane in order to simulate the radiative heating. This would result in releasing high volatiles in the mixing plane and a forced ignition would be observed rather than radiative heating between the particles. This work was improved by Rieth et al. [185], where they extended the work to three-dimensional turbulence modelling where they considered particle heating. The model provides an insight into the mechanism of solid particle ignition and burning, stabilised by hot combustion products as well as the flame structure and combustion mode. It was observed that ignition initially occurs at very lean conditions when particles are entrained in to the hot gases. Subsequently volatile combustion proceeds in non-premixed as well as premixed combustion modes, characterized by means of the flame index, with an overall higher heat release in non-premixed zones. At later times, two flames can be clearly distinguished, an upper flame burning into the air carrying the particles and a lower flame burning into the lean products. In all the small scale experimental rigs, it is difficult to get inflame measurements to validate the CFD model. The experiments where the impact of recirculation is minimal, is suitable for model validation. The investigation on coaxial burners [85, 186–189] can prove to be ideal for modelling and validating multi particle ignition as the flame lift-off are sensitive to ignition phenomena. The testing conducted by Mitchel et al. [186] in IFRF furnace has tested a number of flames on co-axial burners and has reported inflame measurements for combustion parameters. Many numerical modelling studies have been conducted on that furnace but not with a particular focus on ignition.

2.2.4 Ignition in furnace/pilot scale studies

As mentioned above, ignition is a very fast phenomena. There have been plenty of experimental studies in litertaure examining pulverised fuel flames [190–194]. It is diificult to quantify ignition source and mechanism due to non linear complex turbulence and chemistry interactions. The inflame measurements of the combustion properties close to the burner can provide an insight to the ignition and flame characteristics. Such pilot scale facilities are few due to the operational and equipment costs. CFD simulations can play a critical role in visualising such a fast phenomena [195, 196], as it can capture the region where the ignition is initiated. With the advent in comuptational resources, there has been a rapid development in numerical studies in the literature developing sub-models for pulverised fuel flames but there is lack of dedicated study on ignition. Asotani et al. [197] predicted the ignition behaviour in a tangentially fired boiler by comparing the CFD and experimental results qualitatively. The CFD simulation is performed focusing on the radiation properties of the particles as the heat transfer prior to ignition is mainly due to radiative heat transfer [198]. The CFD model is verified by qualitatively comparing

the results obtained with the experimental captured images.

Al-abbas et al. [199] analysed the behaviour of lignite in a 100kW furnace at different oxyfuel ratios and air-fired conditions, both experimentally and using CFD. The model was validated by comparing the temperature distribution profiles and species concentration (O_2, CO_2 and H_2O) profiles at the most intense combustion location of the furnace. Another study on the ignition was conducted by Khare et al. [200] which monitored flame temperatures experimentally using pyrometry and was compared to CFD model. It was concluded that the ignition delay occurs at partial loads and in results obtained by the oxy-fuel cases. The ignition is defined as the point where the temperature of the flame starts increasing. The temperature profiles do not compare well with the CFD results due to the lack of boundary conditions and limitations in the sub-models.

As mentioned about the work performed by Taniguchi et al. [181] in predicting flame stability, they proposed a model for predicting the lean flammability limit based on the flame propagation velocity, flammability limits and fuel concentration. The model first defined a basic flame propagation phenomena based on two particles, where the distance between the particles, capability of the ignited particle to ignite the adjacent particle and the speed at which they ignite was analysed. This was verified for both fundamental and pilot scale experiments for a wide range of coals. The model was replicated using CFD where the flammability limit is predicted based on the flame propagation velocity which are dependent on the fuel concentration and flame propagation. The flammability limits was judged based on the minimum flame propagation velocity for a certain amount of fuel and oxidizer, which was calculated using the experiments previously. This flammability analysis defines the overall flame stability. A RANS case when compared to experiments does not provide a clear indication of flame stability whereas the LES case was able to replicate the experimental flame characteristics. RANS is generally used to capture a steady state behaviour whereas flame stability is an unsteady phenomena which makes it difficult to analyse flame stability using RANS. The flammability analysis in this work was conducted using RANS case near the recirculating region and the results for the flame stability correlated well with the experimental data. The assumption used in their CFD model was that the coal particles ignite homogeneously. In summary, the model proposed was able to define the parameters, which indicates flame stability using a RANS model in CFD and this was verified with the experimental pilot scale studies.

2.3 Governing equations

The CFD models are developed based on Finite control volume (FCV) method. Consider Figure 2.8a, where the closed volume defines the control volume CV and CVS is a closed control volume surface which is sufficiently large. The equations obtained by applying the fundamental physical principles to FCV are in integral form and these equations can be manipulated into partial differential equations. These

method can be classified into two forms, the first being an Eulerian approach where the CV is fixed and the equations obtained after manipulation are called the conservation form of the governing equations. The other approach is shown on the right of Figure 2.8a is known as as the Lagrangian approach which are a non-conservation form of the governing equations where the control volume is moving and changing in shape with the fluid and the behaviour of the same fluid is analysed. Certain flow analyses require the combination of both the Eulerian and Lagrangian approach. Pulverised fuel flames are generally modelled using combination of the two approaches where the gas phase is modelled as continuous phase and the particles are modelled using the Lagrangian method. Recently, there has been attempts in the literature where both the phases are modelled using Euler-Euler approach [201]. The approach generates few numerical instabilities and hence not widely adopted. The governing equations in this chapter are determined in Cartesian co-ordinates which are used to describe transport equations.

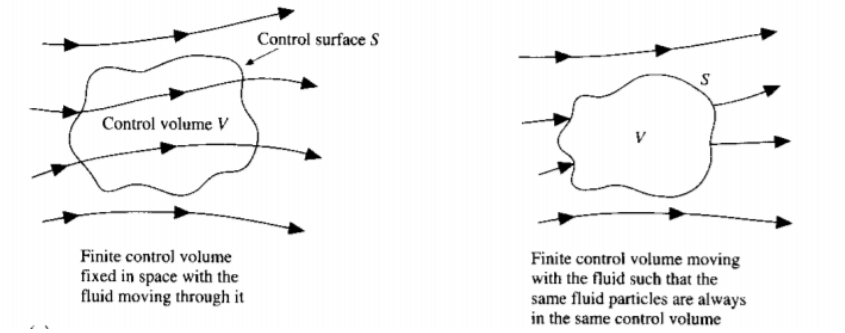

(a) Finite volume approach.

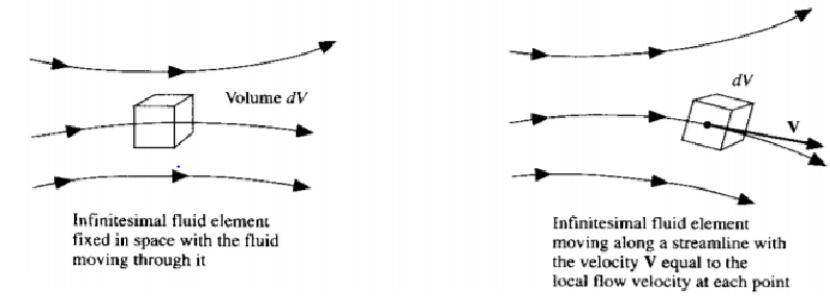

(b) Infinitesimal fluid element approach.

Figure 2.8: Schematic models of the flows [202].

The fluid is modelled in a continuum medium, where the macroscopic properties determine the continuous fluid flow. The macroscopic property Φ includes the velocity, pressure, density, temperature and species concentration. The fluctuations in the fluid flow in a control volume is described by the partial differential equation, which includes any source or sink of Φ into account:

$$\underbrace{\frac{\partial \Phi}{\partial t}}_{\text{time derivative}} + \underbrace{\frac{\partial \Phi u_j}{\partial x_j}}_{\text{convective term}} = \underbrace{\frac{\partial}{\partial x_j}\left(D\frac{\partial \Phi}{\partial x_j}\right)}_{\text{diffusion term}} + \underbrace{S_\Phi}_{\text{source term}}, \tag{2.4}$$

where t, D, x_j and u_j represents time, diffusion constant, spatial vector component and velocity vector component, respectively.

2.3.1 Conservation of mass

$$\frac{\partial \rho}{\partial t} + \frac{\partial}{\partial x_j}(\rho u_j) = S_m \tag{2.5}$$

In equation (2.5), ρ stands for the density and is valid for reactive and non reactive flows where the first law of thermodynamics is taken into consideration. S_m is the mass added to the continuous phase from the dispersed phased (e.g., due to vaporization of liquid droplets) and any user-defined sources.

2.3.2 Conservation of momentum

By using Newtons's second law, F=ma or $F_i = \partial_t(\rho u_i)$ using equation (2.4) the conservation of momentum is given by

$$\frac{\partial}{\partial t}(\rho u_i) + \frac{\partial}{\rho u_i u_j} = \frac{\partial}{\partial x_j}\tau_{ij} - \frac{\partial p}{\partial x_i} + \rho g_i, \tag{2.6}$$

where the ρ, u_i, p and g_i represents density, velocity, pressure and gravitational forces, respectively. The stress tensor τ_{ij} is given by:

$$\tau_{ij} = \mu\Big(\frac{\partial u_i}{\partial x_j} + \frac{\partial u_j}{\partial x_i}\Big) - \frac{2}{3}\mu\frac{\partial u_k}{\partial x_k}\delta_{ij}, \tag{2.7}$$

where μ denotes the dynamic viscosity and δ_{ij} is the Kronecker delta ($\delta_{ij} = 1 if i = j and \delta_{ij} = 0 if i \neq j$).

2.3.3 Species transport equation

The mass fraction Y_k for species k is the ratio of mass of species k in the mixture m_k, with respect to the total mass of the mixture m_{total}:

$$Y_k = \frac{m_k}{m_{total}} \tag{2.8}$$

The species transport equation becomes

$$\frac{\partial}{\partial t}(\rho Y_k) + \frac{\partial}{\partial x_j}(\rho Y_k u_j) = \frac{\partial}{\partial x_j}\Big(\rho D_k \frac{\partial Y_k}{\partial x_j}\Big) + S_{Y_k}, \tag{2.9}$$

where S_{Y_k} is the source term which determines the production and destruction of chemical species. The term D_k represents the diffusion coefficient assuming Fick's first law [96].

2.3.4 Energy equations

Energy is neither created nor destroyed and it can only be converted into other forms of energy and thus it is always conserved. The energy in combustion simulations takes the form of chemical and thermal energy. The specific energy equation can be used to define the energy equation, i.e. $E = H - \frac{p}{\rho} + (u_1^2 + u_2^2 + u_3^3)/2$, as follows:

$$\frac{\partial}{\partial t}(\rho E) + \frac{\partial}{\partial x_j}(u_j(\rho E + p)) = \frac{\partial}{\partial x_j}\Big[\frac{\mu}{\sigma_h}\frac{\partial H}{\partial x_j} - \sum_j^k H\rho D_k \frac{\partial Y_k}{\partial x_j} + (\tau u)\Big] + S_{rad} + S_{rxn}, \tag{2.10}$$

where S_{rad} is the source terms for the radiation, S_{rxn} is the source term for any change in enthalpy due to chemical reaction, the dynamic viscosity and Prandtl number are given by μ and σ_h, respectively and the Prandtl number is given by:

$$\sigma_h = \frac{c_p \mu}{K_{th}}, \tag{2.11}$$

Prandtl number represents the rate of thermal to viscous forces where c_p and K_{th} represents specific heat and thermal conductivity.

$$Le = \frac{K_{th}}{\rho c_p D_m} \tag{2.12}$$

2.4 Particle description

Coal combustion is a multiphase flow, as the density of the particles are high relative to the continuous phase, it is necessary to model both the phases separately. In this section the coupling between coal particles and the continuous phase is briefly discussed The particles in the continuous phase occupy a small mass fraction and thus they are tracked using Lagrangian frame of reference. The particles are coupled with continuous phase using source terms described in Equations above. The particles in this research has been assumed to be spherical and have uniform heating (thermal gradient absent) for model simplicity. In the Lagrangian tracking, the particle position, trajectories and the velocity are mainly described by the drag forces and the gravitational forces acting on the particle. For a spherical particle, the forces are calculated using Equations (2.13) and (2.14).

$$\frac{dx_p}{dt} = u_p \tag{2.13}$$

$$\frac{du_p}{dt} = F_D(u_g - u_p) + \frac{g(\rho_p - \rho_g)}{\rho_p} \tag{2.14}$$

where x_p is the position of the particle, u_p is the velocity f the particle, F_D is the drag force and ρ_g is the density of the continuous fluid. The drag force on the particle in turbulent flows is calculated using Equation (2.15).

$$F_D = \frac{3}{4}\frac{\mu C_D Re}{\rho_p d_p^2} \tag{2.15}$$

$$Re = \frac{\rho_g d_p |u_p - u_g|}{\mu} \tag{2.16}$$

where C_D is the drag coefficient and Re is the Reynolds number. The value of C_D is calculated by assuming the particle shape i.e spherical. Apart from the drag forces, there are other forces such as thermophoretic (caused due to thermal gradients) and Brownian forces (interaction of the two phases at a molecular level) which can be added into Equation (2.14) but calculating these forces for each particle is expensive. As the density of the particles are high, these forces are often ignored and the more dominant forces described above are taken into consideration.

The heat transfer between the particle and the surrounding is calculated by accounting the mass loss, chemical reactions, convective and radiative heat transfer. The underling assumption being the particle is uniformly heated.

$$m_p c_p \frac{dT_p}{dt} = \dot{Q}_{devol} + \dot{Q}_{char} + \dot{Q}_{con} + \dot{Q}_{rad}$$

As the particle heats up and experiences devolatilisation, there is heat and mass transfer with the continuous domain. There is a small reduction in the particle temperature as the volatiles are released in the gas phase. The heat loss from the particle is proportional to the mass loss and the latent heat of evaporation of the volatiles. Mathematically it is represented in Equation (2.17)

$$\dot{Q}_{devol} = -\dot{m}_{p_{vol}} \Delta H_{vol} \tag{2.17}$$

$\dot{m}_{p_{vol}}$ is the mass loss due to devolatilisation and ΔH_{vol} is the latent heat of evaporation of the volatiles. Similarly, the heat released during char combustion is represented by Equation (2.18) where $\dot{m}_{p_{char}}$ is the mass loss due to char combustion and ΔH_c is the heat heat released from char combustion, which is absorbed by the particle.

$$\dot{Q}_{char} = \dot{m}_{p_{char}} \Delta H_c \tag{2.18}$$

The convective heat exchange between the particle and the ambient gas is expressed using Equation (2.19) where Nu is the Nusselt number, which describes the ratio of convective to conductive heat transfer across a boundary.

$$\begin{aligned} \dot{Q}_{con} &= \frac{A_p K_{th} Nu (T_g - T_p)}{d_p} \\ Nu &= 2 + 0.552 Re_p^{1/2} Pr^{1/3} \end{aligned} \tag{2.19}$$

$$\dot{Q}_{rad} = \epsilon \sigma A_p (T_{rad}^4 - T_p^4) \tag{2.20}$$

The most dominant heat transfer to the particle is the radiative heat transfer, which is represented by Equation (2.20) where σ is the Stefan-Boltzmann constant. The

different models used to produce the value of radiation temperature T_{rad} is discussed in Section 2.5.

$$m_p c_p \frac{dT_p}{dt} = -\dot{m}_{p_{vol}} \Delta H_{vol} + \dot{m}_{p_{char}} \Delta H_c + \frac{A_p K_{th} Nu (T_g - T_p)}{d_p} + A_p \epsilon \sigma (T_{rad}^4 - T_p^4) \tag{2.21}$$

The final form of the heat transfer equation to the particle is shown in Equation (2.21). The value of Nusselt number can be simplified for spheres in accordance with correlation provided by Rans-Marshall in Equation (2.19) [203].

2.5 Radiation modelling

In furnace conditions, thermal radiation is the dominant heat transfer process when the particles enter the furnace as it is dependent on the fourth power of the temperature [198]. The radiation heat transfer equation (RTE) is described as follows:

$$\underbrace{\frac{I_\lambda(r,s)}{dt}}_{\text{Rate of change}} = \underbrace{k_\lambda I_{\lambda,b}(r,s)}_{\text{Emissions}} - \underbrace{(k_\lambda + \sigma_{s,\lambda}) I_\lambda(r,s)}_{\text{Absorption}} + \underbrace{\frac{\sigma_{s,\lambda}}{4\pi} \int_{4\pi} I_\lambda^{'}(s_i) \Phi(s_i, s) d\omega_i}_{\text{Scattering}} \tag{2.22}$$

λ represents an arbitrary wavelength, r and s describes the position and direction and $I_\lambda(r,s)$ describes radiation intensity for a specific λ with respect to its position and direction. The radiation becomes attenuated as it travels through the participative media. The attenuation is mainly due to scattering and absorption of the gases and particles present in the combustion environment. k_λ and $\sigma_{s,\lambda}$ represents the absorption and scattering coefficients which describes the amount of attenuation. A scattering phase function $I_\lambda^{'}$ also contributes to the scattering of radiation which is dependent on the direction and wavelength.

$$\begin{aligned} \nabla . q_\lambda(r) &= k_\lambda (4\pi I_{\lambda,b} - G_\lambda) \\ G_\lambda &= \int_{4\pi} I_\lambda(r,s) d\omega \end{aligned} \tag{2.23}$$

In Equation (2.10) the S_{rad} term is described by the radiative flux $q_\lambda(r)$ represented in Equation (2.23). The radiation heat transfer is called gray if it is assumed that the radiation is independent of λ which implies that integration over the spectrum is not required in Equation (2.22). There are many methods to solve the RTE, Monte Carlo is one such method based on the statistical methods to track the radiation intensity. The method tracks a certain amount of rays until the intensity of the ray are terminated by absorption by the wall or the gas. The accuracy of the method is improved as the number of rays tracked are increased which is also directly proportional to the computational time required. Discrete transfer method (DTM) [204] is another ray tracing method where the rays are tracked between two surfaces and the directions are predefined. Similar to Monte Carlo method the

accuracy can be improved by increasing the number of rays tracked.

Discrete ordinates [205] is the most popular method applied in combustion problems [206]. Instead of ray tracing the RTE is solved by discrete solid angles which are based on the Cartesian grid. The RTE is converted into coupled differential equations which solves for each direction over the solid angle 4π, the number of directions discretised is user dependant. The scattering term becomes a weighted summation of the directions chosen as input.

The radiative heat transfer at the molecular level is generally quantified by the change in the energy level of the interacting molecule. Tri-atomic molecules such as CO_2 and H_2O show a strong emission/absorption properties in the infrared spectrum [207]. On the other hand, in the combustion environment N_2 and O_2 do not absorb or emit radiation [208]. Hence CO_2 and H_2O plays a more significant role in radiative heat transfer but the mass fractions are relatively low for combustion in air and thus the combustion gases are generally treated as gray. Considering the same modelling assumptions may induce errors, when simulating oxyfuel combustion cases as it has higher mass fraction of CO_2 and H_2O. Calculating radiative heat transfer for each spectral is computationally expensive and difficult due to large variation in the spectral absorption coefficient as solving each RTE will scale up linearly. There has been developments in spectral models which reduces the computational time effort for predicting radiative heat transfer. The modelling approaches are categorised in three groups i.e. line-by-line models, band models and global models. In this section only global models are discussed which are extensively applied in solving combustion problems as it is computationally cheap and have provided reasonable results [209–211].

Global models provide mean values of absorption and emissivity based on the temperature , pressure and gas mixture. Tables or polynomial correlations are created from experiments or the narrow band models [208]. The Weighted Sum of gray gas model (WSGG) is one such model that is developed on the basis of polynomials dependent on temperature, partial pressure of species and the path length. The model uses a number of gray gases and one transparent gas to represent the entire spectrum. The modelling constants developed by Smith et al. for air conditions are extensively used in the literature where the polynomials are available for partial pressure ratios of H_2O/CO_2 of 1 and 2. These polynomials are not applicable in the oxyfuel conditions as the partial pressure ratios are very different. Many models have been developed in the literature adapted for oxyfuel conditions based on narrow band models [212] and modification of WSSG constants based on the partial pressure ratio[209, 212]. The full spectrum k-distribution method (FSCK) is another global modelling technique to represent the entire spectrum. This model has gained popularity as it has proven to improve the overall results [213]. The investigation by Yang et al. [195] has shown that the impact of radiation model is minimal for pilot scale studies whereas it has a greater impact(more sensitive) for combustion simulations of a complete furnace as the beams are tracked for longer distance.

2.6 Turbulence Models

Turbulence is a state of the fluid, which can be characterised by random and chaotic 3-D vorticity. Turbulence dominates the flow phenomena which increases properties such as the drag, heat transfer, mixing and energy dissipation. In the coal combustion process, the mixing rate of species is influenced by the turbulent flow. The flow can be quantified by the Reynolds number [214] which is the ratio of inertial to viscous forces acting upon fluid,

$$Re = \frac{uL}{\upsilon} \tag{2.24}$$

where u, L and υ are the velocity, characteristic length and kinematic viscosity, respectively. High Reynolds numbers indicate turbulent flow whereas small Reynolds numbers indicate laminar flow. The other major properties of turbulence is the chaotic nature of the flow and higher diffusivity of the flow. Diffusivity enhances mixing and heat transfer, which is mainly due to the eddying motion observed in a wide spectrum of sizes of length. The numerical approach to simulate turbulent flow completely would be to solve the Navier-Stokes and continuity equations, this is known as the Direct Numerical Simulation (DNS). Computationally this method is not viable to solve these equations for combustion problems and therefore other methods should be used to describe turbulent flow:

i Direct numerical simulation: This methodology resolves all the scales of eddies and it does not require any additional turbulence model. The unsteady Navier-Stokes equations are solved for a very fine grids which is able to resolve the Kolmogorov length scales. At high Reynolds numbers, Kolmogorov theorised that the small-scale eddies lose their directional orientation and become isotropic and the smallest scales of turbulence are known as Kolmogorov scales η_L [215]. The energy dissipation takes place in a very small time step, to resolve the fast fluctuations. This is very expensive technique to resolve the fluid flow.

ii Large Eddy Simulation (LES): This particular method resolves the unsteady Navier-Stokes equations by tracking only the large eddies and models the small eddies. A fine mesh is desired in to apply this method, and a good mesh will be very close to a DNS mesh. This makes this method computationally expensive relative to RANS.

iii Reynolds-averaged Navier-Stokes (RANS) equation: This method focuses on the statistical mean flow and simulates the mean flow properties interacting with turbulence. The turbulence flow is computed using different eddy viscosity models It is the cheapest and the fastest method to simulate turbulence but a grid independence study is highly recommended.

The selection of the turbulence model for RANS or LES application depends on the complexity of the flow physics, practice established for a specific problem, level of accuracy required, computational resources available and the amount of time

available per simulation. As coal combustion is a very complex and non-linear phenomena, the overall computational cost increases with the use of other sub models and thus the RANS method may be more suitable for industrial application. There will be compromise in terms of accuracy but in-order to maintain a balance between accuracy and computation cost, RANS is a viable option.

Reynolds averaging
The flow simulated with the RANS method then consists of statistical mean values. The instantaneous values are decomposed into time averaged and fluctuating components:

$$u = \bar{u} + u^{'} \tag{2.25a}$$
$$\Phi = \bar{\Phi} + \Phi^{'} \tag{2.25b}$$
$$\tag{2.25c}$$

where Φ denotes a scalar quantity, such as the pressure, energy or species concentration and $\bar{\Phi}$ and $\Phi^{'}$ are the statistical mean and fluctuating components respectively. The statistical mean is averaged between the initial time and a large time (theoretically infinity) for a steady flow. The density- weighted averaged equations for combustible flow can be represented by

$$\frac{\partial \rho}{\partial t} + \frac{\partial [\rho \bar{u_j}]}{\partial x_j} = 0, \text{(Reynolds Continuity equation)} \tag{2.26}$$

$$\frac{\partial [\rho \bar{u_i}]}{\partial t} + \frac{\partial [\rho \bar{u_i} \bar{u_j}]}{\partial x_j} = -\frac{\partial [\rho \overline{u_i^{"} u_j^{"}}]}{\partial x_j} + \frac{\partial \tau_{ij}}{\partial x_j} - \frac{\partial p}{\partial x_i} + \rho g_i, \text{(Reynolds Momentum equation)} \tag{2.27}$$

$$\frac{\partial \rho \bar{Y_k}}{\partial t} + \frac{\partial [\rho \bar{Y_k} \bar{u_j}]}{\partial x_j} = -\frac{\partial [\rho \overline{u_i^{"} Y_k^{"}}]}{\partial x_j} + \frac{\partial}{\partial x_j}\Big(\rho D_k \frac{\partial \bar{Y_k}}{\partial x_j}\Big) + S_{Y_k}, \text{(Reynolds Species transport equation)} \tag{2.28}$$

$$\frac{\partial \rho \bar{h}}{\partial t} + \frac{\partial [\rho \bar{h} \bar{u_j}]}{\partial x_j} = -\frac{\partial [\rho \overline{u_j^{"} h^{"}}]}{\partial x_j} + \frac{\partial}{\partial x_j}\Big(\frac{\mu}{\sigma_h} \frac{\partial h}{\partial x_j}\Big) + \frac{\partial \rho}{\partial t} + S_{rad} \text{(Reynolds Energy equation)} \tag{2.29}$$

In the Reynolds momentum equation, a non-linear term $\overline{u_i^{"} u_j^{"}}$ is the Reynolds stress term which is unresolved and is caused by the variations in the turbulent fluctuations which can be closed by eddy viscosity models or Reynolds stress models. Prandtl introduced the concept of the mixing length with a boundary layer where for the wall bounded turbulent flows, the eddy viscosity factor varies with the distance from the wall.

There are a range of models in literature that are used to simulate turbulence, the most popular being k-ε and k-ω models [216–221] which provides a solution to the closure problem by introducing a further two transport equations. On of the main drawbacks to these eddy viscosity methods is that all turbulence is treated as isotropic, which can be inaccurate assumption in cases with dominant anisotropic turbulence. In case of high swirling flows in burners these models can provide inaccurate solutions and therefore an alternative model is required. Reynolds stress model (RSM)[222–224] have been developed which have additional transport equations to account for the Reynolds stress terms, however the additional equations require further constants to close specific terms. It is clear that it is important to have an accurate turbulence model if the swirling behaviour during combustion is to be captured. Studies done in [225–229] has shown the advantage of RSM model over other eddy viscosity models especially around the near burner region where ignition is really important.

2.7 Devolatilisation Models

The decomposition of a single particle is often modelled sequentially in four stages:

i Evaporation/drying: The particle is heated and the moisture is evaporated.

ii Devolatilisation: The volatile matter is released.

iii Volatile Combustion: The volatile matter released in the continuous phase reacts with the oxygen present around it.

iv Char combustion: The remaining material is char and ash, where char combusts slowly with the oxygen and

v Ash loading: The mineral matter in the coal is heated and this is followed by the inert heating law after the char combustion.

.

Each stage for the particle is governed based on mass loss from the particle and heat transferred to the particle. The drying process of the coal particle begins as soon as the particle temperature reaches its evaporation temperature when it loses all its moisture. The devolatilisation process begins after the particle temperature exceeds the evaporation and boiling temperature between 600-700 K. The remaining char particle is combusted with oxygen after all the volatile matter has been released.

Coal pyrolysis and coal devolatilisation are the two terms used to describe the process of coal conversion. The thermo-chemical decomposition of the organic matter at high temperatures in the absence of oxygen is known as pyrolysis, whereas devolatilisation occurs in the presence of oxygen [230]. The physical changes during this process is the softening of the coal and undergoing plastic deformation. The bonds inside the coal start disrupting and breaking and volatiles are released but they are still contained in the particle. Bubbles are formed inside the particle which

leads to the internal swelling of the particle, and finally the bubbles burst and the volatiles are released [231]. This process is followed by the particle shrinking and rapidly contracting, this occurs until the particle re-solidifies [83, 231]. The volatiles are released when the particle temperature is between 600-700 K [83, 232, 233] and they are transported via the pores in the coal structure. During this process, the volatile matter that is release is made up of tar or heavy hydrocarbons ($C_aH_bO_c$), light hydrocarbons (C_aH_b) and light gases such as CO, CO_2, H_2 and H_2O. The emitted gaseous species mix homogeneously in the gas phase. The solid residue that remains is known as char, and it mainly consists of carbon and ash. It is generally difficult to predict the species evolving from the coal particle and hence they are modelled as empirically defined species which are predicted from proximate and ultimate analysis.

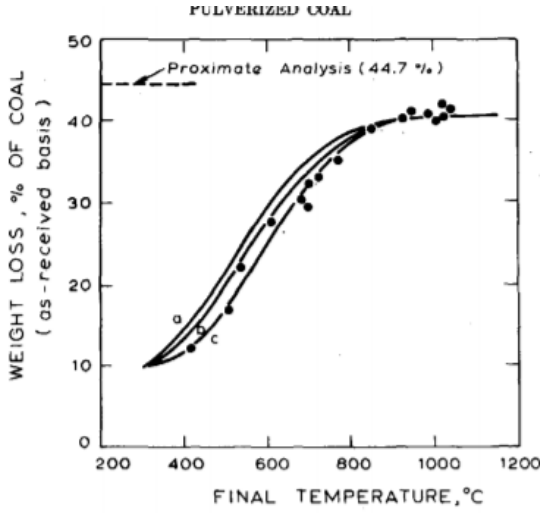

(a) Effect of final temperature on devolatilization weight loss from Montana lignite [points data (experimental time = 5 to 20 sec, mean particle diameter=70 μm, atmosphere=helium)] [234].

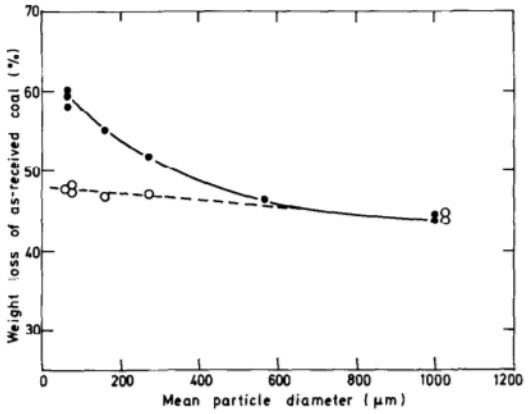

(b) Effect of particle-size on weight loss from coal heated in helium and hydrogen atmospheres. (Final temperature = 1000^{o}C; residence time = 5-20 s; nominal heating rate = 650-75O^oC/s; • hydrogen = 7 MPa; ∘ helium = 1 atm) [235]

Figure 2.9: Effect of the particle size and temperature on the volatiles release.

The devolatilisation process is generally represented in the form of a single rate Arrhenius expression as shown in Equation (2.30).

$$\frac{dm_p}{dt} = -m_{vol}A_{vol}exp(\frac{-E_{vol}}{RT_p}) \tag{2.30}$$

where m_{vol} is the mass of the volatiles and A_{vol} and E_{vol} are empirical parameters fitted to experimental data. At higher temperatures, the amount of volatile matter that evolves can be larger than that measured in the proximate analysis. This is also referred to as the high temperature volatile yield [236]. In furnace conditions, the volatile matter released is generally higher then that measured during the proximate analysis. The ratio between high temperature volatiles yield over volatiles measured by the proximate analysis is known as the Q factor. Experiments conducted by Kimber et al. [237] and Badzioch et al. [238] demonstrated that at higher

temperatures the volatile yield increases and the Q factor increases in the range 1.3 to 1.8. Anthony et al. [234] experimentally studied the rapid devolatilisation of bituminous and lignite coal, where parameters such as temperature, residence time, heating rate, particle size and pressure were varied. The effect of the particle final temperature showed a clear variation of the volatile release as shown in Figure 2.9a. Another experimental study, by the same authors [235], showed that if the final temperature of the coal is kept constant and the size of the particle is varied, the amount of the volatiles released decreases with an increase in the particle size, Figure 2.9b, which shows the amount of volatiles released is dependent on the heating rate and the final temperature of the coal.

Generally for CFD modelling the percentage of volatiles released from each coal particle, the volatiles measured during the proximate analysis is multiplied by a constant called Q_{vol} factor which gives the high temperature volatile yield. Once the ratio is set, it does not vary in accordance to the final temperature of the particle. The model will release the same amount of volatiles set at high temperatures even if the coal particles are heated at lower temperatures. This limitation in the combustion modelling sometimes over predicts the volatile release for the particles at lower temperatures and under predict the volatiles release if the particle is heated higher than the temperature used to measure the Q_{vol} factor.

In CFD modelling, the particle heating is generally calculated using the Equation (2.21) where it assumes that the temperature is uniform throughout the particle, and neglects any internal resistance to heat transfer. In reality there is a temperature gradient across the diameter of the particle which may affect the release of moisture, volatiles and char oxidation [111, 112]. Even if the temperature is considered to be uniform, it is a common CFD modelling assumption that char oxidation occurs after the particle has been fully devolatilised [239, 240] but it can occur simultaneously without following the sequencing processes or even before the volatiles are released (HI). This limits the detection of HI not possible.

The rate at which the volatiles are released from the particles can be modelled using a single rate Arrhenius equation which is empirically fitted to experimental data or results from other models, which was first proposed by Badzioch and Hawksley [238]. A single rate can be inadequate to determine the volatile release [241] because the volatile evolution is sensitive to heating rate and the single rate is not capable of adjusting to the higher heating rate [242]. Thus, there are many devolatilisation models used to predict the the volatile release. The method proposed by Kobayashi et al. [236] and Ubhayakar et al. [243] is to use the two competing rate model. The milestone report by Fletcher et al. [244] for the Sandia National Laboratories conducted experiments and compared the results produced after using the unknown constants proposed by both the competing rate models and found that the Ubhayakar et al. [243] model provides a better agreement with the experimental data. There are mainly three network models, namely, Chemical Percolation Devolatilisation (CPD), Flashchain and Functional group-depolymeroisation vaporisation cross linking (FG-DVC). These network models have been developed in the

past which requires the detail composition of the coal and chemical structures to predict accurate volatile release and a semi composition of the species evolved which are discussed.

2.7.1 Chemical Percolation Devolatilisation (CPD)

The network models were proposed because it is not practical to describe the complete devolatilisation process in the simulation. The CPD model uses the elemental composition to describe the coal structure and percolation statistics to describe the generation of tar precursors based on the number of cleaved liable bridges in an infinite coal lattice. It was first proposed by Grant et al. [245], and later developed by many researchers, for predicting some specifics during devolatilisation, e.g.nitrogen released during the volatile evolution [246]. Many researches have used the model to simulate the coal devolatilisation process in their combustion models [113, 120, 247–249]. Yan et al [250] produced a paper of significant interest where they modified the CPD code to include the thermal gradient across the particle and this enhances the kinetic rates of the volatiles evolved during the devolatilisation process. Fletcher and co-workers optimised this model for various applications and this has made it a very reliable model for many coal combustion problems over the years [251–255].

CPD assumes that the coal has a molecular network of aromatic ring clusters of many types, sizes and a variety of chemical bridges of different bond strengths. Only two types of bridges are considered, i.e. liable and stable/char bridges. These bridges and bonds breaks are based on the activation energy. The bridges are modelled based on the chemical structure determined from ^{13}C NMR (solid state nuclear magnetic resonance) spectroscopy. Generally, the solid-state spectroscopy data is generally unavailable as it is expensive experimentaly and thus a non-linear correlation was developed by Genetti et al. [246, 256] that predicts the chemical structure parameters of the coal based on proximate and ultimate analyses of the coal. The parameters include:

i the average molecular weight per side chain (M_δ),

ii the average molecular weight per aromatic cluster (M_{cl}) ,

iii the ratio of bridges to total attachments and (p_o),

iv the total attachments per cluster (σ +1).

The correlation by Genetti [246] was based on 30 different coals from different research centres in the USA. This enabled data for different ranks of coal to be included in the correlation. The complete data of these coals is provided in [246] and the four variables of the correlation are calculated using a quadratic fitted curve:

$$\begin{aligned}\text{Variable for CPD model} \;=\; & c_1 + c_2X_2 + c_3X_C^2 + c_4X_H + c_5X_H^2 + c_6X_O \\ & + c_7X_O^2 + c_8X_{\mathrm{VM}} + c_9X^2{}_{\mathrm{VM}}\end{aligned}$$

The correlation only describes the average variance of the ^{13}CNMR parameters as a function of the elemental composition and ASTM volatile matter. The accuracy of the structural properties is reduced when the correlation is used in the model. This becomes a limitation for unusual coals and the correlation exhibits limits on the structural properties to be used in the model. The solution obtained outside the limits are extrapolated and the results cannot be trusted [246]. The coal structural properties is mainly based on the coal rank but it is shown in [246, 257] that the maceral/lithotype content of the coal plays a vital role in defining the coal properties.

Rezaei et al. [85] studied two coals with similar proximate and ultimate analyses which suggests that subtle differences in the coal structural properties plays a key role in the stability of complicated turbulent flames which may have implications on the coal ignition mechanism in furnace conditions. Work done in [118] concludes that CPD is a better model than the Kobayashi model and it is able to predict ignition delay in a much more comprehensive way when coupled with the detailed gas-phase chemistry. Also Andrew et al. [258] has shown the limitations of six different single and competing rate models even after modifying them to match the CPD model results. After modification, they fail to predict the devolatilisation process over an entire range of heating rate and thus it is was concluded that CPD is a more reliable devolatilisation model. A sensitivity analysis on the ignition conducted for a Russian coal (high volatile bituminous) by Rastko et al. [93] suggests that the CPD and FG-DVC (Functional Group Deployment Vaporisation Cross Linking) agrees well with the ignition behaviour in an entrained flow reactor compared to the single rate and competing rate models. It is concluded that the FG (Functional group) model compares better than the other models.

2.7.2 Functional group-depolymerization vaporisation cross linking (FG-DVC)

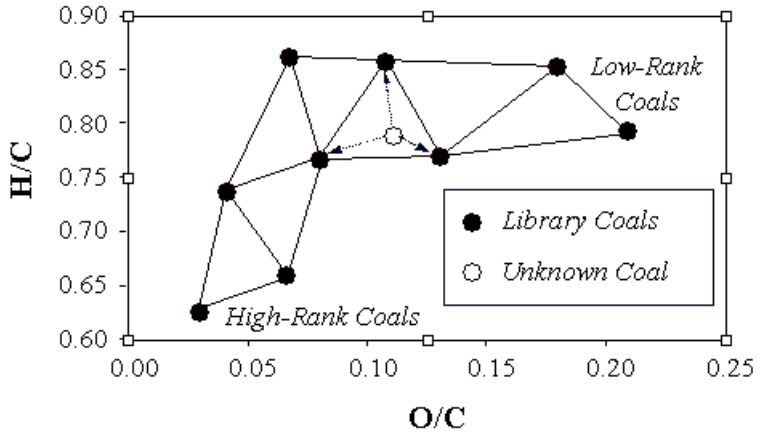

Figure 2.10: Illustration of an interpolation scheme used to create FG-DVC input files for a coal with an unknown pyrolysis behaviour [259].

The FG-DVC model relies on elemental composition to predict devolatilisation behaviour in the absence of experimental data. The FG model considers the specific functional group to decompose and predict the light gases evolved and the DVC model describes the de-polymerisation of the macromolecular network (bridge breaking, cross-linking and tar formation) [260]. The model relies on the TG-FTIR (thermogravimetry—Fourier transform infrared) spectroscopy data which assists in the prediction of the kinetic rate for species evolution [261]. In the absence of TG-FTIR data of coal, the model creates a TG-FTIR file based on the elemental composition (coal rank). The model has experimental data of nine coals which forms a two-dimensional triangular mesh (each coal acts as a node and three nodes together make a triangular grid) on a H/C vs O/C coalification diagram or the Van Kervelen diagram as shown in figure 2.10. For an unknown coal, the elemental composition determines the appropriate triangular grid boundary it falls under and the structural parameters were interpolated from the parameters corresponding to the three coals as shown in figure 2.10. If the coal is outside the mesh, the model extrapolates the structural parameters [262]. These can induce errors as it is assumed in the model that the coal with the same rank classification behaves in a similar manner. The model requires an accurate elemental composition which positions the coal in the Van Kervelen diagram. Coals with high sulphur content can cause difficulties in obtaining the calculated oxygen content by difference and the calculation of the hydrogen can be obscured by the moisture present during the analysis [261]. Again, this model is targeted towards simulating the mean pyrolysis behaviour of the coal which can result in producing discrepancies. FG-DVC has an advantage of predicting the species evolved as well as the amount of NH_3 and HCN that is released for a given coal (Helpful for NO_x modelling) but for better accuracy, the TG-FTIR file is highly desired. The species evolved can be useful in predicting the reactant involved during the ignition process.

2.7.3 Flashchain

Details of this particular network model is well documented in [263–270]. The model could also predict the kinetics of the volatiles released based on an ultimate analysis [271]. It is the building block of the PC Coal lab developed by Niksa and co workers. The code is not bounded by any experimental data requirement, other than the ultimate and proximate analysis. Particle size is taken into consideration and the resistance to volatiles escape increases with an increase in size, which sometimes over predicts the total yield for larger particles. Many other researchers have predicted devolatilisation kinetics using a modified single kinetic rate equation and they have achieve satisfactory results [250, 272–274].,

2.8 Volatile combustion

In order to capture a detailed chemistry in the flow accurately, it is favourable to predict the species evolved during devolatilisation and use detailed chemical reactions. Detailed chemical reactions requires accounting for intermediate species.

Calculating each intermediate species involved in the reaction requires an impractical amount of computational power. This is due to the increased number of transport equations and the solution becomes numerically stiff when coupled with the reactions. It is because of this reason that the unneccesary chemical reactions in the specific combustion problems are discarded. Mechanism such as GRI. 3.0 mechanism [275], FFCM [276], Aramco [277] etc have been used in the past to calculate detailed chemical reactions for various hydrocarbons fuels. GRI 3.0 considers methane combustion which considers 325 reactions for 53 species. The combustion process in diffusion flames is limited by mixing [96] but there are regions in the flame, which are controlled by the kinetics. The reaction rate of the volatiles can be dominated by either mixing, kinetics or the combination of both in diffusion flames [278]. Based on these phenomena three hypothesis can be discussed where it is assumed that $t_{turb} > t_{react}$, $t_{turb} < t_{react}$ and $t_{turb} \cong t_{react}$. The term t_{turb} implies to the time taken by large eddies to break up and reduce to small eddies where molecular interactions can occur and t_{react} represents the time required for the species to react completely to equilibrium. These hypothesis are explained in detail in [278, 279].

2.8.1 Turbulence-chemistry interactions

There are many turbulence chemistry models used in combustion CFD. The most commercially used for RANS simulation are described in this section. The reaction rate for turbulent flows are calculated using the following approach:

i Finite rate chemistry model: Turbulence chemistry interactions are ignored, the reaction rates are determined by the finite rate chemistry by only computing the chemical source terms using general reaction rate expressions. In other words, it is assumed that the time scale for the chemical reactions are greater than the mixing ($t_{turb} < t_{react}$). This model is more applicable in laminar flow where the flame is controlled by the reaction rate at which a fuel is burnt.

ii Eddy dissipation model (EDM): This model assumes that the reaction rate is very fast compared to the turbulent mixing rate and mixing is the rate limiting factor ($t_{turb} > t_{react}$). The chemical reactions are assumed to achieve instantaneous equilibrium as soon as the reactants are mixed. This model was developed by Magnussen and Hjertager [280] which was on the basis of the Eddy Break-Up model(EBU) proposed by Spalding [281]. The EBU determines the local reaction rate by the rate of break-up of the eddies. In EDM, the reaction rate was determined by the mean concentration of the reactants, rate of dissipation of the turbulent eddies and the turbulent kinetic energy. The overall reaction rate would be calculated based on the presence of a minimum number of reactants and products. The model neglects the kinetically controlled regime, which is important to ignition. However in high temperature regions, where kinetics are much faster than mixing, the model works reasonably well. This model is generally preferred in the industrial applications where as it provides a good compromise between accuracy and computational expense. The mathematical representation of the reaction rate

in this model is given by the two following equations:

$$R_{k,r} = \nu^{'}_{react,k} MW_k A\rho \frac{\varepsilon}{k} min_{\Re}\left(\frac{Y_{k_{\Re}}}{\nu^{'}_{\Re,r} MW_{\Re}}\right) \tag{2.31}$$

$$R_{k,r} = \nu^{'}_{react,k} MW_k AB\rho \frac{\varepsilon}{k} \frac{\sum\limits_{P} Y_{k_P}}{\sum\limits_{j}^{N} \nu^{"}_{j,r} MW_j} \tag{2.32}$$

where,

k	=	species
r	=	reaction
$R_{k,r}$	=	the net reaction rate to produce k
Y_{k_p}	=	the mass fraction of any product species,P
$Y_{k_{\Re}}$	=	the mass fraction of a particular reactant,$\Re$
A	=	an empirical constant equal to 4.0
B	=	an empirical constant equal to 0.5
$\frac{k}{\varepsilon}$	=	large eddy mixing time scale

Combustion proceeds when k/ε>0 is accompanied with reactants and products. In this model, every reaction has the same turbulent rate, and this is due to the intermediate species reactions not being considered in this model and global reactions are generally applied. Detailed reactions (intermediate reactions) are based on the Arrehenius rate and this is different for each reaction. Therefore this model fails to look into the ignition mechanism where the intermediate reactions play a vital role.

iii Finite rate-eddy dissipation model(FRED): To overcome the limitations of the EDM, Eaton et al. [278] proposed a model where the reaction rate is calculated based on the minimum rate of dissipation of the eddies for reactants and products and the chemical reaction rate (Arrhenius rate). The reaction rate for this model is calculated as follows:

$$\bar{R}_{k,r} = min\Bigg(\underbrace{\hat{R}_{k,r}}_{\text{Arrhenius term}}, \bar{R}_{k,r}{}^{(\text{react})}, \bar{R}_{k,r}{}^{(\text{prod})}\Bigg) \tag{2.33}$$

The Arrhenius reaction rate is calculate based on the equation:

$$\hat{R}_{k,r} = (\nu^{'}_{prod,k} - \nu^{'}_{react,k}) MW_k \Bigg(g_{forward} \Pi_{k,react} CT^{\alpha_{react,k}}_{react,k} - g_{backward} \Pi_{k,prod} CT^{\alpha_{prod,k}}_{prod,k}\Bigg)$$

where ν_{prod} and ν_{react} are the stoichiometric coefficient for product species and reactant species, respectively, CT_r and CT_p are the volumetric concentration

of the reactants and products, and there are related to their concentration exponents, $\alpha_{react,k}$ and $\alpha_{prod,k}$. The backward constant $g_{backward}$ is defined by the equilibrium hypothesis where,

$$g_{backward} = \frac{g_{forward}}{G_k} \tag{2.34}$$

$$g_{forward} = A_k \bar{T}^{\beta_k} exp\left(\frac{-E_k}{R\bar{T}}\right) \tag{2.35}$$

iv Eddy dissipation concept model(EDC): This model [282] is an extension of the EDM that allows inclusion of detail chemical mechanism in turbulent flows, the flow domain (finite volume) is subdivided into the reaction space, known as fine structures, and non-reaction zone. Inside the fine structures, reaction takes place at the molecular scale where the energy has been dissipated. The model was derived by describing the dissipative process in detail and this allows simulation of the detailed chemical kinetics of the combustion process. The model is based on three key factors:mass fraction in the fine structures, mass transfer rate between the fine structures, and the surrounding fluid, reacting fraction of the fine structures. This model becomes computationally expensive as it simulates detailed kinetics and also the mechanisms are invariably stiff (convergence issues).

2.8.2 Simplification of the species evolved and the reaction mechanisms

In terms of a RANS simulation, using detail chemistry model for volatiles combustion will be computationally expensive. Hence using global reactions mechanism for modelling such a comptational expensive flow is practical. It is also depended on the choice of turbulence-chemistry model. The use of global mechanism has been demonstarted in the past, Westbrook and Dryer [283] developed a set of global reaction mechanisms and validated the reactions with experiments using different hydrocarbon fuels, where they assumed that the hydrocarbons oxidises into CO_2 and H_2O. They observed that the 1-step mechanism was over predicting the flame temperature. Therefore it was concluded that the formation of CO and H_2 is significant and thus Dryer and Glassman [284] introduced a global 2-step mechanism for methane oxidation. The global 2-step mechanism used by Peters et al. [285] in simulating a 2.4 MWth swirling burner flame assumed that the volatile matter from the coal oxidises to CO, CO_2, H_2O and N_2. The amount of the CO_2 was predicted based on the assumption that the carbon in the volatiles completely burn to form CO. The 3-step reaction mechanism developed by Hauntman [286], which introduced the oxidation of hydrocarbon to CO & H_2 which are further oxidised to CO_2 & H_2O. Ruckert [287] presented a comparison of different global mechanism for coal fired boilers and used a different reaction rate for the irreversible CO and H_2 oxidation. A four step mechanism was presented by Jones and Linstedt [288] because the other mechanisms were incapable of accurately predicting H_2 & CO in flames. A reversible H_2 reaction and one water shift reaction was taken into

consideration.

The volatiles released are generally composed of hydrocarbons ($C_aH_bO_c$), light hydrocarbons (C_aH_b) and light gases (CO, CO_2, H_2, H_2O). The hydrocarbons react with the available oxygen to form carbon dioxide and water whereas nitrogen and sulphur react to form NO_x and SO_x. It is difficult to quantify the evolved species as it is highly dependant on the heating rate and fuel chemical structure. In order to model species evolved, a simplification is required based on the fuel ultimate and proximate analysis. In coal combustion, volatiles can be computed as a single species $C_xH_yO_z$ giving the reaction:

$$C_xH_yO_z + \alpha O_2 \rightarrow xCO + \frac{y}{2}H_2O$$

$$\alpha = \frac{x-z}{2} + \frac{y}{4}$$

$$CO + \frac{1}{2}O_2 \rightarrow CO_2 \tag{R2.1}$$

(R2.2)

Coal also comprised of other elementary substances such as Nitrogen and Sulphur and therefore volatiles are modelled to contain nitrogen and sulphur species ($C_aH_bO_cN_dS_e$). These simple reactions can be enhanced by the addition of nitrogen and sulphur.

$$C_xH_yO_zN_dS_e + (\frac{x}{2} + e - \frac{c}{2})O_2 \rightarrow (1-f_{vc})xCO + f_{vc}xCO_2 + (\frac{y}{2})H_2 + (\frac{d}{2})N_2 + eSO_2 \tag{R2.3}$$

Equation (Equation (R2.3)) represents a simple two step global mechanism where the conversion of CO to CO_2 is considered. Hauntman in his model assumes that the carbon in the volatiles first burn to CO and then CO is converted to CO_2 where H_2 is converted to water:

$$C_xH_yO_zN_dS_e + (\frac{x}{2} + e - \frac{c}{2})O_2 \rightarrow xCO + (\frac{y}{2})H_2 + (\frac{d}{2})N_2 + eSO_2$$

$$CO + \frac{1}{2}O_2 \rightarrow CO_2$$

$$H_2 + \frac{1}{2}O_2 \rightarrow H_2O \tag{R2.4}$$

These reactions in EDM are limited and beyond 3-step is not useful because the reactants burn whenever there is turbulent mixing and thus incorporating multiple intermediate reactions does not substantially increase the accuracy. Whereas in other models the chemical reactions can be increased in order to improve the accuracy but this is very expensive in 3-D simulations of coal combustion. Application of fewer equations using EDC has been demonstrated for a very simple case as it is able to track the rate at a molecular level but very impractical for industrial applications.

2.9 Char combustion

After the volatiles are released then the remaining substance is known as *char*. Char is a porous hollow sphere and it disintegrates as it reacts with oxygen. In reality the char reaction rate is complex and is controlled by porosity, pore size, surface area, O_2 available and the reactivity of the particle itself. Also the coal rank has an effect on the rate at which char is burned.

2.9.1 Char reaction and combustion regime

Char burns heterogeneously and mainly reacts with O_2, CO_2, H_2 and H_2O [107]. The reaction between H_2 and char is smaller than the other species, approximately three orders of magnitude [91, 107, 289]. According to single film theory [290], the char particle is assumed to be surrounded by a boundary layer of the gas CO. The CO for small particles ($<100\mu$m) oxidises to CO_2 outside the boundary layer, whereas CO_2 and CO may oxidise inside the boundary layer for larger particles (>1mm) [291]. The char reactions are given by

$$\mathrm{C(s)} + \frac{1}{2}\mathrm{O_2} \rightarrow \mathrm{CO_2} \tag{R2.5}$$

$$\mathrm{C(s)} + \mathrm{H_2O} \rightarrow \mathrm{CO} + \mathrm{H_2} \tag{R2.6}$$

$$\mathrm{C(s)} + \mathrm{CO_2} \rightarrow 2\mathrm{CO} \tag{R2.7}$$

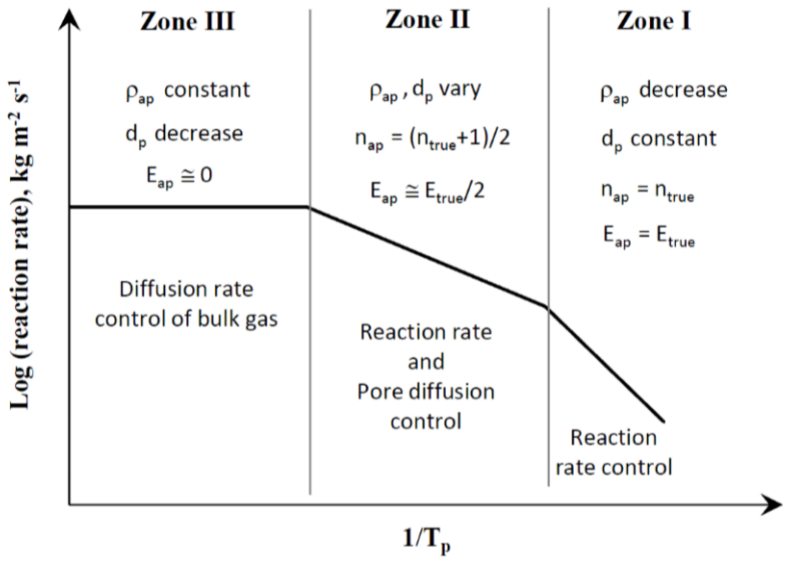

Figure 2.11: Combustion regimes of coal combustion [107].

A general regime of coal combustion is shown in Figure 2.11. At low temperatures, the combustion chemical reaction is rate limited (Zone I). For higher temperatures, the combustion process is controlled by the chemical reaction rate and diffusion through pores (Zone II). On increasing the temperature further, the combustion

process is limited by only the diffusion rate (Zone III). The apparent density, ρ_{ap} in zone I decreases while the particle diameter d_p remains constant. This is due to the diffusion gas reacting from the surface towards the centre of the particle through the pores and cracks. It is the opposite in zone III, where the density remains constant and the diameter decreases [292].

2.9.2 Global reaction rate

Levenspie provided a way to calculate the global reaction rate of coal and the char particle [293]. The chemical kinetics is assumed to control the entire combustion of char in zone I and thus the burning rate per external surface area $R_{s,c}$ is equal to the chemical reaction rate.

$$R_{s,c} = R_{ch,c} = R_{Kin,c}(P_{O_2})^{n_{ap}} \tag{2.36}$$

where, $R_{ch,c}$ is the chemical reaction rate, $R_{Kin,c}$ is the kinetic rate, P_{O_2} is the partial pressure of O_2 at the surface of the particle and the n_{ap} is the apparent order of the reaction.

2.9.3 Intrinsic model

In order to simulate the zone III combustion, Baum and Street [233] considered the overall reaction rate to be limited by the diffusion of oxygen neglecting the chemical kinetics. To simulate zone II, Field [294] proposed a kinetic/diffusion model where the kinetic rate is included and it is assumed that the diffusion is either by diffusion or the kinetic reaction of char. The diffusion rate coefficient is given by:

$$D_o = C_{diff}\frac{[(T_p + T_\infty)/2]^{0.75}}{d_p} \tag{2.37}$$

and the kinetic rate, similar to the Arrhenius equation, is given by

$$R_{s,c} = A_{k,char}e^{-(Ea_{k,char}/RT_p)} \tag{2.38}$$

which gives the char combustion rate assuming a spherical shape of the particle with an external surface area of A_p ($=\pi\ d_p^2$):

$$\frac{dm_{p,char}}{dt} = -A_p P_{O_2}^{n_{ap}}\frac{D_o R_{s,c}}{D_o + R_{s,c}} \tag{2.39}$$

This model fails to account for char swelling, internal diffusion of the reactant gas in the porous char and the intrinsic rate of chemical reaction of the reactant with the internal surface of the char particle. The model proposed by Smith [295] is a correlation between an overall burning rate of char per external surface area and the intrinsic chemical reactivity and this is simplified as:

$$R_{s,c} = \eta\frac{d_p}{6}\rho_p A_g R_{k,c} \tag{2.40}$$

where η is the effectiveness factor and it is introduced because of the decrease in the oxygen concentration from the surface to the centre of the particle. It describes the ratio of the actual combustion rate to the rate attainable if no pore diffusion resistance existed (particle oxygen constant) and is given by:

$$\eta = \frac{3}{\phi^2}\Big(\phi coth\phi - 1\Big) \tag{2.41}$$

where, ϕ denotes the Thiele modulus [296]

$$\phi = \frac{d_p}{2}\Big[\frac{\Omega\rho_p A_g R_{i,c} P_{O_2}}{D_e \rho_{ox}}\Big]^{0.5} \tag{2.42}$$

where ρ_{ox} is the density of the oxidant in the bulk gas and D_e is the effective diffusion coefficient in the particle pores. When the pores are very small ≈ 0.001 μm the oxygen molecules collide more frequently with the walls of the particle than the other molecules, and such diffusion is known as Knudsen diffusion which takes into account in the effective diffusion.

$$D_e = \frac{\varepsilon}{\tau^2}\Big[\frac{1}{D_{Kn}} + \frac{1}{D_o}\Big]^{-1} \tag{2.43}$$

where D_{Kn} and D_o are the Knudsen and bulk molecular diffusion coefficients, and ε is the porosity of the char particle given by $\varepsilon = 1 - \rho_p/\rho_t$. The Knudsen diffusion coefficient is given by:

$$D_{Kn} = 97.0\bar{r}_p\sqrt{\frac{T_p}{MW_{ox}}} \tag{2.44}$$

2.10 Summary

2.10.1 Experiment and modelling

The single particle studies in the literature provide an insight into many different phenomena, which are generally neglected in many numerical models. There are many studies dedicated on quantifying HO, HI or HO-HI. The other studies have focused on the effect of the devolatilisation process coupled with the ignition phenomena. The effect of coal rank, particle size, oxidizer concentration and ambient gas temperature on the ignition phenomena have been studied experimentally and numerically. A few studies have been performed the effect of the particle temperature during ignition. There are contradicting predictions sometimes because of differences in experimental set up, operating conditions and fuel analysed. The most significant studies are highlighted as follows:

i Work done by Du and Annamalai [110] on the prediction of transient ignition of single particle of coal has become the corner stone of all the new single particle model developed in the past few years.

ii The study by Veras et al. [113] in implementing the particle gradient and using the CPDNLG devolatilisation model in developing a single particle model

is a massive step towards simulating single particle ignition. The contribution from Goshayeshi et al. [118] shows that in order to obtain an accurate ignition delay model then the integration of the detail gas phase chemistry is important.

iii The modelling study on volatile flame by Jimenez et al. [124] has the potential to be further developed in ignition studies and it can also be extended to HI.

iv The experimental contribution from Ponzio et al. [144] for a single particle study on defining the affect of the oxygen concentration and temperature has been very significant but has its own experimental limitations. The ignition criteria used by Jovanovic et al. [145] in CFD simulations of a particle is good contribution in mathematically defining ignition mechanism.

v The model developed by Tufano and co-workers [126] is probably the most advance single particle combustion model but is computationally very expensive. However, a simplified version of the model will be suited for quantifying ignition mechanism for a particle.

vi Khatami et al. [134] studied the variation of the oxygen concentration for three different ranks of coal in DTF which provides a good understanding of the basic phenomena of HO, HI or multi stage HO-HI.

There are a few experimental studies that have focused on the ignition of the stream of coal particles and tried to bridge the gap between single particle phenomena and multi particle ignition. Many experiemntal investigations focused on the intensity of the flame and quantified ignition based on the percentage of flame intensity detected. Taniguchi et al. [97] qualitatively predicted the ignition in experiments by dividing the combustion regime into three regions. The ignition region was defined based on the visual detection of the particle clouds burning. Yamamamoto et al. [183] defined the ignition in a similar way for CFD simulations of a pilot scale combustion process in RANS and LES. They highlight that the RANS is not suitable for quantifying the proposed ignition model, even in the absence of swirl and recirculation. The experimental work done by Shaddix and co workers [154, 155, 297–299] in the laminar flow reactor on multi-particle combustion has been useful in understanding some of the coal ignition characteristics. The experiments conducted on co-axial burner [85, 186–189] can be useful literature for modelling multi particle ignition, as the inner recirculation region of the flame is absent (less sensitive to turbulence model) and the flame lift-off is generally sensitive to ignition phenomena.

There are plenty of studies in the literature where a pilot/full scale test facility are studied experimentally or numerically [300–304]. They generally focus on the overall behaviour of the flame as the numerical models used were developed to focus on the global combustion process rather than the ignition process itself. Asotani et al. [197] qualitatively compared experimental images with post processed CFD contours in order to indicate ignition, assuming that the primary source of heat transfer is radiation. The study by Taniguchi et al. [181] on flame stability is very important as it simulates a RANS model and highlights the limitation of the method. They

created a model based on the flame propagation velocity and fuel concentration for a few particles and validated the predictions against the experimental data. The useful parameters from the pilot scale RANS simulation are extracted, analysed and validated for flame stability. The experimental studies which provide in flame data close to the burner can be useful for model validation as it is sensitive to the ignition phenomena.

2.10.2 CFD modelling

There are many limitations in the use of commercial CFD sub-models. The following are a few identified during the literature search which affects the simulation of ignition.

i The devolatilisation models require experimental data which in general is difficult to obtain for unknown coals and thus it requires the integration of a suitable network model.

ii The coal combustion process is restricted by the sequencing of vaporisation, devolatilisation and char combustion.

iii The particle heating is calculated using a lumped equation where thermal the gradient across the particle is neglected. The intra particle heat and mass transfer should be taken into account especially when modelling ignition of a particle.

iv The CFD code is unable to permit HI or simultaneous HO-HI.

v The restrictions of the turbulence chemistry model, in terms of integrating the detailed chemistry with the turbulence mixing. The EDC and FRED models are able to integrate detailed chemistry but is computationally expensive and the equations are very stiff for practical applications.

vi The current models used in the literature fail to predict the source of ignition in pulverised fuel flames or predict the combustion behaviour close to the burner. Despite this, previous studies have managed to demonstrate that accurate coupling of various sub-models have come close to predicting inflame parameters.

3 Investigation of different devolatilisation network models

Coal combustion modelling using CFD requires a variety of inputs that act as precursors to the overall combustion model. The experimental data of the coal under investigation would be ideal, however, this is generally unknown and expensive to generate. This chapter focuses on investigating devolatilisation network models, the output from the models are used in the CFD calculations of coal combustion. In this chapter, three widely used devolatilisation models are validated against the High Temperature Wire Mesh (HTWM) experimental values for 36 coals. These 36 coals are from different geographical regions of the world and varies in coal ranks. This study will validate and provide confidence in the devolatilisation model to be used for investigating novel fuels for future CFD simulations. The novelty of this study is investigating three different network models, testing 36 different coals and concluding the optimum devolatilisation to be used for investigating virgin coal.

3.1 Devolatilisation models

Three devolatilisation models are tested in this section, namely, CPD, FG-DVC and Flashchain, which is a building block of the PC-Coal Lab software package. The basic concept of all the three models is to form the type of bonds in the coal, based on the elemental composition, and decomposes, based on the boundary conditions. The decomposition occurs based on the kind of bonds and structural property of coal which varies for different coal. These models are able to predict the major species and the high temperature volatile release during devolatilisation. Measurements by Gibbins et al. [305] during HTWM experiments provide the values of high temperature volatile and the nitrogen partitioning. The aim of this investigation is to compare predictions from all three devolatilisation models with the experimental data which can provide confidence in using this model as a precursor for future CFD calculations.

The experiments used a very fine mesh made up of molybdenum, which can operate at high heating rates. This type of mesh assists in the investigation of the coal pyrolysis and char gasification reactions at high pressure and heating rate. The coal samples were placed between the two layers of wire mesh, which were weighed before and after the pyrolysis in order to determine the HTVY. The coal sample were heated up to 1873.15 K with a heating rate of 10000 K/s which is similar

to that experienced in a furnace. The operating conditions of the experiments are summarised in Table 3.1. In the experiments, 36 different coals were analysed, and the coal properties and its origin are highlighted in Table 3.2.

Table 3.1: HTWM devolatilisation experimental conditions for the 36 coals [305]

Experiment type	High temperature Wire Mesh(HTWM)
Heating rate	10000 K/s
Final temperature	1873.15 K
Hold time	2 s
Amount of coal	10-12 mg
Size of the coal	125 - 150 µm

Table 3.2: Coal origins, properties and high temperature wire mesh test results [305]

Coal	Country of origin	TGA micro-proximate analysis Ash(wt% db)	VM (wt % daf)	Elemental analysis(%daf) C	H	N	HTWm volatile yield (% daf)	Volatile N (% coal N)
1	VEN	4.3	38.3	83.0	5.5	1.8	54.3	58.2
2	COL	9.4	38.6	82.8	5.6	1.8	59.1	62.2
3	COL	3.0	38.5	77.4	5.2	1.6	60.7	74.2
4	BLN	8.9	32.4	80.8	4.8	1.9	50.9	68.4
5	BLN	9.8	32.0	81.1	4.7	2.0	50.7	65.4
6	COL	3.5	38.7	78.1	5.2	1.8	60.4	72.0
7	SA	13.1	28.5	82.0	4.4	2.2	43.7	64.5
8	BLN	11.8	35.3	80.1	5.0	1.9	54.5	68.1
9	SA	17.3	30.2	82.0	4.6	2.0	47.8	63.4
10	BLN	11.8	36.7	81.7	5.4	2.1	52.0	67.9
11	IND	4.5	40.9	79.7	5.5	1.8	58.2	68.4
12	NSW	11.6	38.2	83.9	5.4	1.9	56.4	68.7
13	RUS	9.6	37.4	81.7	5.3	2.6	55.2	72.1
14	VEN	6.1	40.3	81.6	5.4	1.7	59.0	68.6
15		10.3	46.0	76.8	6.0	1.5	63.8	77.8
16	RUS	6.8	32.2	80.2	4.9	2.4	44.3	66.8
17	CHI	9.4	33.0	83.8	4.9	1.2	46.6	55.8
18	POL	16.2	35.1	88.0	5.6	1.7	50.1	66.7
19	SA	22.5	30.2	84.6	4.6	2.2	49.2	64.8
20	IND	0.3	47.8	71.1	5.2	0.9	61.2	74.7
21		21.6	37.2	83.3	5.5	1.6	49.7	65.3
22		5.4	39.7	81.2	5.6	1.7	53.0	58.1
23	RUS	10.4	36.7	84.5	5.6	2.8	49.6	66.1
24	IND	12.8	48.1	81.2	6.6	1.5	63.3	71.8
25	SA	10.6	36.2	78.9	5.1	2.2	50.6	69.8
26	IND	4.2	41.3	77.4	5.6	1.8	60.5	71.6
27	SA	18.8	29.5	79.7	4.4	2.0	45.1	63.7
28	COL	5.4	39.0	82.3	5.7	1.7	52.5	57.5
29	BLN	9.7	38.3	81.9	5.7	1.7	55.7	65.2
30	BLN	8.4	37.9	80.2	5.5	1.7	52.3	60.3
31	BLN	10.1	36.5	81.6	5.5	1.6	50.7	60.5
32	US	17.4	33.7	87.4	5.5	1.8	49.5	59.2
33	COL	5.3	37.6	79.9	5.4	1.8	54.1	61.3
34	COL	6.1	38.8	79.1	5.4	1.6	53.0	61.4
35	BLN	13.2	34.2	82.8	5.1	1.8	54.1	64.0
36	BLN	17.0	31.3	82.3	5.0	1.8	49.6	54.0

On analysing the coals under investigation based on the ASTM coal classification [306], it was observed that the coal rank varies from Semi-anthracite to Sub-bituminous coal B which covered a wide range of coal ranks. The coal rank classification showed that none of the coals have extreme properties, including such

as anthracites and peat.

CPD is an open source code developed by the Sandia National Laboratory and the University of Utah [246]. The fundamentals of the model are described in Section 2.7.1 but the solid state spectroscopy data was not available for the 36 coals under investigation and thus the ^{13}C NMR calculator developed by Genetti et al. [246] was used to predict the average chemical structure parameters in the form M_δ, M_{cl}, p_o and $\sigma + 1$. These output parameters, together with the ultimate analysis of the coal, are used as the input to the CPD model. Out of the 36 coals, 4 coals were out of the range of the interpolation data set of the ^{13}C NMR calculator, i.e. coal no. 15,18,24 and 32. The calculations suggest that the results for the four coals are not reliable but are included in the analysis to check the relative error in the final predictions. The Van Kervelen diagram of the coals under investigation and the library coals used by the ^{13}C NMR calculator for correlations are shown in Figure 3.1. It can be observed that the model uses a wide range of coals for generating the correlations and thus, is able to predict the devolatilisation kinetics and mass loss during devolatilisation process for a majority of the coals under investigation.

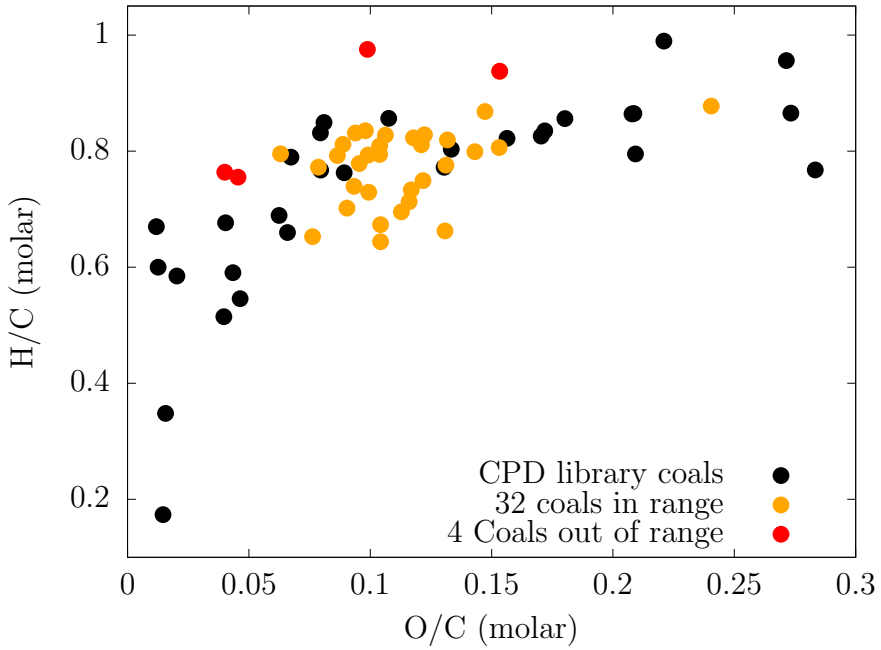

Figure 3.1: Coalification chart of the 30 coals used for the CPD model and the coals under investigation [246, 305].

FG-DVC is semi commercial and is developed by Solomon and workers [260, 261]. The code for the FG-DVC model was available at the University of Sheffield and the methodology to use the model is described in Section 2.7.2. Similar to CPD, in the absence of detail experimental data then the FG-DVC generates the input parameters for the model based on the elemental composition of the coal. The elemental composition defines the position of the coal in the triangular mesh of nine

library coals on the Van Kervelen diagram. The coals fitting inside the mesh produce reliable interpolated input files for the model whereas the input files generated for the coals outside the mesh are extrapolated and cannot be relied on. It can be observed from Figure 3.2 that 20 coals are inside the two dimensional mesh and 16 coals are outside the mesh which implies that the prediction cannot be relied on and may have relatively high error. The CPD model has a better spread in comparison with FG-DVC and its library coal includes a few anthracites, bituminous, sub-bituminous and lignites. This spread in the CPD model in comparison with the FG-DVC model, has an advantage when it comes to predicting the devolatilisation behaviour.

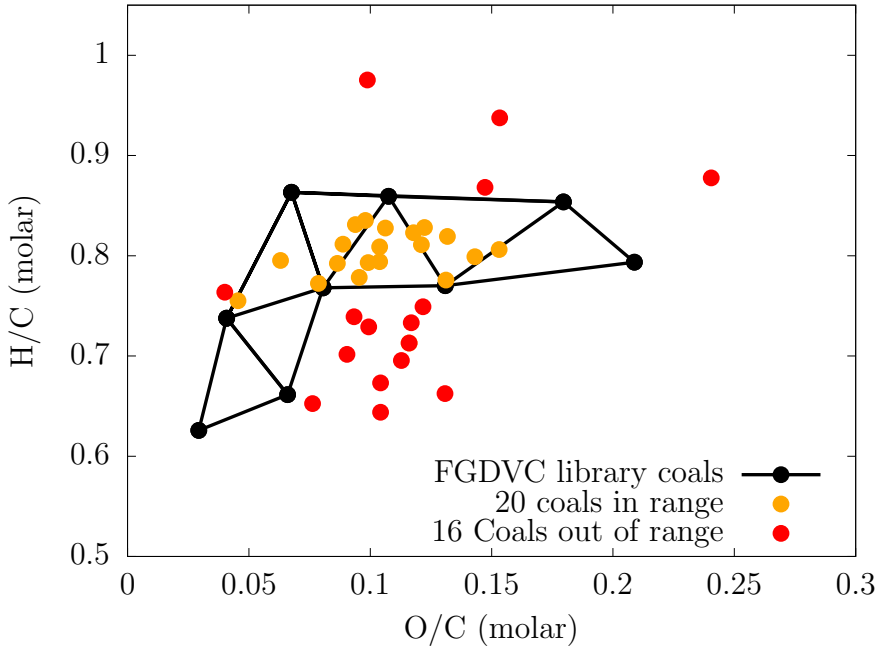

Figure 3.2: Position of the 36 coals on the triangular mesh of the FG-DVC model. [262, 305].

The PC Coal Lab software was developed by Niksa and his group which requires licensing. The industrial partner, Doosan Babcock Ltd uses the PC Coal Lab to predict many pre-cursors for the CFD calculations of coal. The primary input for the model was also elemental and proximate analysis similar to CPD and FG-DVC. The devolatilisation results for the 36 coals investigated in this work were provided by Doosan Babcock Ltd. The coals under investigation are in the interpolation range of the PC-Coal Lab library coal.

There were few limitations when using the coal elemental analysis for the devolatilisation predictions. The elemental data required were that of carbon, hydrogen, nitrogen, oxygen and sulphur. However, the elemental data available is only for C, H and N and the value for sulphur was kept at zero (as the sulphur content is relatively negligible in most coals) and oxygen was calculated by difference (100 -

C% - H% - N%). This allowed the user to keep the structure of the coal the same for the CPD,FG-DVC and the PC-Coal Lab. It is highly debatable as to whether the real structure of the 36 coals are not analysed and totally different coals are used for comparison of the experimental results. (A parametric study was conducted by varying oxygen and sulphur content for the FG-DVC model but the results on comparing with the experimental results kept getting worse and therefore it was decided to keep sulphur at zero). Finally, the codes are independent of the particle size and therefore it will be difficult to comment on the accuracy of the results. Since different coals under investigation may have a size effect on the overall devolatilisation behaviour.

All three models provide the particle mass loss with time which enables the user to obtain the kinetics of the devolatilisation. The final value of the mass loss is used for comparison with the measured values provided by the experimental data. The results for the mass loss and nitrogen evolved during devolatilisation are presented in Figure 3.3. The PC Coal Lab provides an excellent agreement with the measured data while the CPD, apart from the four coals that are outside the of range provides a reasonable agreement with the experimental results. It is evident from Figure 3.3 that this FG-DVC model is not capable of analysing a wide variety of coals and FG-DVC is the least reliable for the devolatilisation behaviour. The coals in this range exhibit a wide range of error for FG-DVC, whereas few coals that are out of the range of the interpolating mesh are able to predict well the final mass loss during devolatilisation. However, it would be a heuristic approach to rely on the results as a few out of the range coals exhibit a large error in the mass loss. It is important to highlight that the missing TG-FTIR files for the coals under investigation could have improved the prediction of the behaviour for the FG-DVC model. This investigation shows that the FG-DVC model is more dependent on the accurate experimental data while the CPD and PC Coal Lab interpolation scheme are more reliable in predicting the mass loss during volatile release. The nitrogen partitioning in CPD is dependent on the following correlation:

$$f_{st} = max(0.5, 0.0182 * (C_{daf}\%) - 1.062) \tag{3.1}$$

where the value of f_{st} determines the amount of nitrogen inside the char particle which probably had a significant impact on the overall predictions. According to Genetti et al. [246] the value of f_{st}, the fraction of nitrogen in the char is higher for high rank coals, only the coals 18 and 32 had a value higher than 0.5 which are out of the range of the interpolating library coals. As a result of the correlation The rest were capped at a value of 0.5. The impact of this value is evident in the prediction of the nitrogen evolved where the prediction is clustered around 60% nitrogen evolution. The results suggest that the assumptions in the CPD model provides reasonable predictions and can be used for future calculations. The volatiles evolution stops after reaching a particle temperature of 1400 K for all three models and no volatiles are released after. The CPD and PC Coal Lab models release nitrogen even after the volatiles are released but the FG-DVC code stops as soon as the volatile release is stopped which results in an under prediction of the

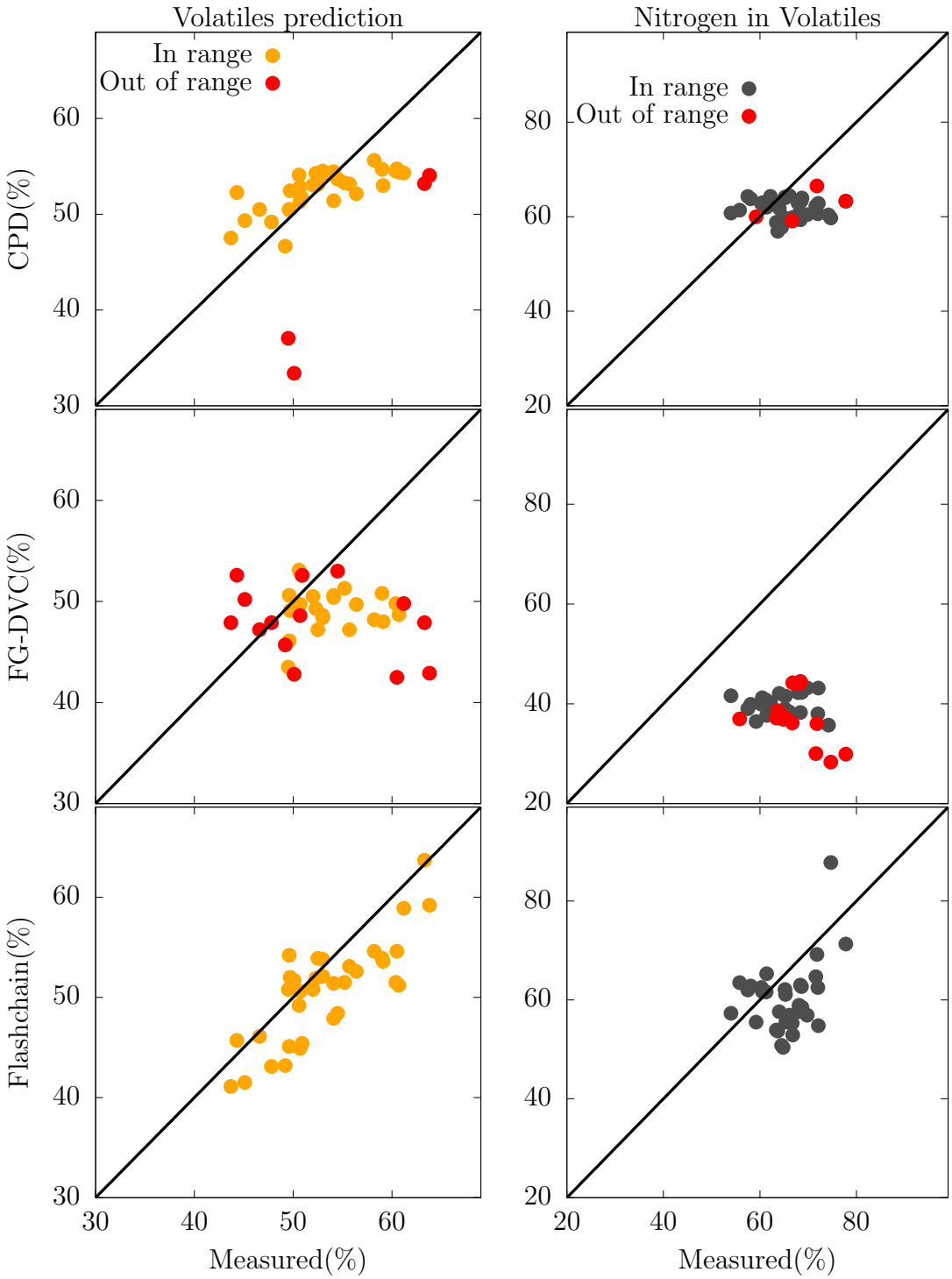

Figure 3.3: Comparison of the predicted Volatiles(left) and Nitrogen in volatiles(right) vs experimental for the 36 coals by CPD, FG-DVC and Flashchain.

nitrogen evolved. This may depict a greater error in the results when comparing the predicted and measured values for the FG-DVC model which is shown in Figure 3.3. A comparisons of the three models displays the accuracy of the models prediction. It was concluded that the PC Coal Lab is able to predict the Devolatilisation behaviour better than the other two models for the 36 coals investigated. However, at the same time the CPD is a good alternative option as it is an open source model and can be integrated in any future combustion model without any licensing requirement unlike the PC Coal Lab.

3.1.1 Summary

i Three network models for predicting the devolatilisation behaviour of the coals have been evaluated and compared against the experimental data of 36 different coals.

ii The PC-Coal Lab covers a wider range of coals for the correlation compared to the other two models whereas the FG-DVC accommodates very few coals, thus making it the least effective model for investigating the devolatilisation behaviour of coals.

iii Both the PC-Coal Lab and the CPD model have a reasonable agreement with the experimental data set, however some limitations were identified in this work for the FG-DVC model. As the PC-Coal Lab entails a license cost, the CPD proves to be a better and less demanding model of the three models investigated.

4 Mathematical model for ignition of a single particle

It is well established from the conclusions of previous investigation that visualising a single particle combustion process in absence of turbulence will enable quantifying the ignition mechanism. This chapter develops a model to simulate the ignition process of a single particle and validate the model against experimental results for air and oxy-fuel cases. A sensitivity analysis is conducted on the different reaction mechanisms for better accuracy. The validated model is then used to generate a correlation between particle diameter and oxygen concentration, which describes the ignition mechanism of the particle.

The CFD simulation for combustion of a single particle can suggest the shortcomings of standard modelling approaches used in simulating pulverised fuel flames, e.g. a common modelling assumption that char combustion occurs after complete devolatilisation. Treating all the particle sizes with this assumption can induce errors. CFD simulations for ignition of a single particle will allows the process of devolatilisation and char combustion to coincide and can indicate the impact of those assumptions. Quantifying the ignition mechanism is of industrial relevance as it can qualitatively indicate the flame stability, flame size and improve the existing burners fuel flexibility. Hence, the model will not only suggest improvements for the CFD modelling of pulverised fuel flames but will also provide economic benefit to the industry in modification and operation of the power plant.

The different modelling approaches for simulating single particle ignition are discussed in Section 2.2. The ignition of a coal particle are generally modelled using a lumped mass assumption, which ignores any thermal gradients inside the particles. The significance of thermal gradients for modelling a particle's ignition is discussed in Chapter 2. There are char combustion model, which accounts for the changes inside the particle but does not model the flow variations outside the particle [307–310]. The models developed by Yang et al. [311] and Tufano et al. [126] resolved the flow the inside as well as outside the particle. The approach provided an insight into the conversion process inside the particle during the combustion of a particle. This study focuses on adopting a similar methodology to quantify ignition mechanism.

The novelty of this investigation is to obtain a correlation for critical particle diameter which can quantify the ignition mechanism with respect to the ambient

O_2 concentration. According to the author, the quantification methodology has not been implemented in the literature to differentiate the ignition mechanism for varying O_2 concentration and particle size. The precursors and sub-models used to predict the thermo-conversion are open source and derived from coal proximate and ultimate analysis, which are validated in the past for different applications but have not been implemented together in the past to predict the ignition mechanism.

This Chapter is divided into three sections, Section 4.1 describes the experiment chosen for modelling, the model structure, case set up and the mathematical equations used in the model are described in Section 4.3 and the results of the model are discussed in Section 4.4.

4.1 Reference experiment

There have been a number of experimental investigations to quantify the ignition mechanism and combustion characteristics of a single particle, which are summarised in Section 2.2.2. Experiments conducted in DTF, entrained flow reactor and most recently in Hencken burner's are able to replicate the heating rate experienced in a furnace by the particles. The experimental work described in Section 2.2.2 concluded that ignition mechanism of a single particle is dependent on the ambient gas composition, particle size, heating rate and fuel rank. Work done by Khatami et al.[134, 152, 157, 312–314] varies all the above parameters in a DTF and primarily focuses on the ignition delay of the particles at different conditions. The authors observed HO, HI and HO-HI ignition mechanisms for extensive conditions which make it a suitable study to validate this particular model.

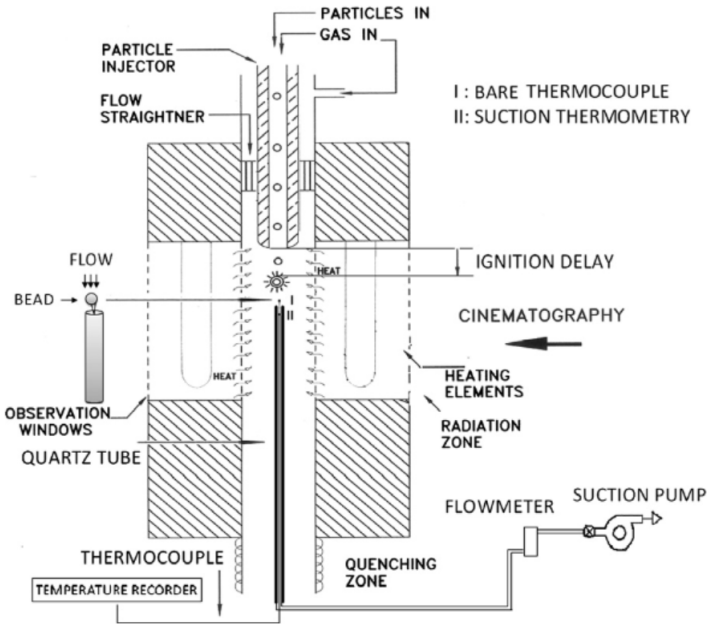

Figure 4.1: Schematic of the drop-tube furnace and the gas temperature measurement setup inside the furnace [134].

The schematic of the laminar flow DTF is shown in Figure 4.1 where the temperature of the wall is kept constant at 1400 K. The cavity in which the particle heats up is 25 cm long providing enough residence time for particles to ignite. A sealed transparent quartz tube was fitted around the furnace. The ignition videos were obtained using a high speed cinematographic camera, through the observation ports available at the sides of the furnace. Three colour pyrometry is used to calculate the temperatures in the domain. The pyrometric observations were conducted from the top which followed the path of the particle. The gas temperature inside the DTF was measured from the tip of the injector at the centreline using a thermocouple.

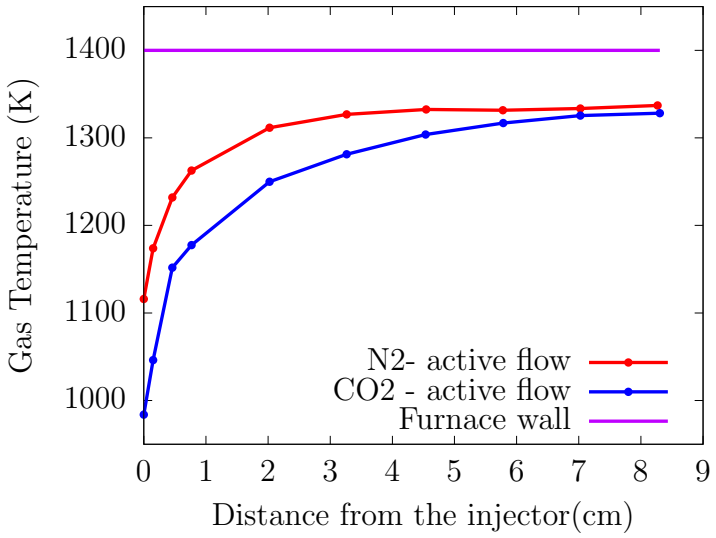

Figure 4.2: Centreline gas temperatures in different ambient conditions (corrected for radiation) [134].

The heating rate experienced by the particles ranged from 5000 -10000 K/s. The measured values of the ambient gas temperatures are shown in Figure 4.2, the values shown are corrected for radiation on the thermocouple. There is a visible difference in the gas temperatures for O_2/N_2 and O_2/CO_2 condition. It can be seen that in the early stages of the furnace that the heating rate experienced by the particle is not constant. This change in the heating rate is important to account for when considering particle temperature and species evolution from the particle which will have an overall impact on the ignition model.

Four different coals varied across three ranks, varying under O_2/N_2 and O_2/CO_2 conditions were tested in the DTF and their respective ignition delay were measured i.e. one bituminous coal, one sub-bituminous coal and two lignites. The two lignites undergo similar ignition mechanism and thus only one lignite is discussed in the study. Their fuel properties and ignition mechanism is described in Tables 4.1 and 4.2 respectively. The moisture content of sub-bituminous coal and lignites were tested prior to experiment which was different to the one provided from Penn state coal sample bank. The change in moisture content, changes the proximate analysis

of the coal tested in the DTF and thus this study uses those values for consistency.

Table 4.1: Proximate and Ultimate analysis of the coals used in this study

	PSOC -1451	DECS-26	DECS-11
Rank and fuel source	Bituminous High Volatile A Pittsburgh #8, Pennsylvania	Sub-bituminous B River basin, Wyodak, Wyoming	Lignite A Beulah, North Dakota
Proximate analysis as received and(upon re-evaluating moisture)			
Moisture (%)	2.5	26.3 (13.1)	33.4 (13.2)
Volatile matter (%)	33.6	33.1 (39.0)	37.4 (48.6)
Fixed carbon (%)	50.6	35.1 (41.4)	22.9 (29.8)
Ash (%)	13.3	5.6 (6.5)	6.4 (8.4)
Ultimate analysis (on a dry basis)			
Carbon (%)	71.9	69.8	66.2
Hydrogen (%)	4.7	5.7	4.0
Oxygen (%) (by diff.)	6.9	15.6	18.6
Nitrogen (%)	1.4	0.9	0.9
Sulfur (%)	1.4	0.4	0.7
Sodium (%)	0.06	0.09	0.66
Ash (%)	13.7	7.6	9.6
Heating value dry fuel (MJ/kg)	31.5	28.2	25.7

Table 4.2: Ignition mechanism observed by Khatami et al. [134, 152] in DTF.

O_2 (mole fraction)	Bituminous coal	Sub-bituminous coal	Lignite A
N_2 background			(All fragmented)
21%	HO	HO	HO
30%	HO	HO	HI(HO-HI)
40%	HO	HO	HI(HO-HI)
50%	HO or HI (HO-HI)	HI(Fragmentation)	HI(HO-HI)
60%	HO or HI(HO-HI)	HI(Fragmentation)	HI(HO-HI)
70%	HI(HO-HI)	HI(Fragmentation)	HI(HO-HI)
80%	HI(HO-HI)	HI(Fragmentation)	HI(HO-HI)
CO_2 background			(All fragmented)
30%	HI	HI	HI
40%	HI	HI	HI
50%	HI	HI(Fragmentation)	HI
60%	HI	HI(Fragmentation)	HI
70%	HO-HI	HI(Fragmentation)	HI
80%	HO-HI	HI(Fragmentation)	HI

HO:Homogeneous ignition HI:Heterogeneous ignition HO-HI:Simultaneous ignition

Only two ranks of coals are simulated in this study (Bituminous and and Lignite A). These two coals are tested for a range of conditions and exhibit different types of ignition mechanism in the DTF. These conditions will suffice enough to validate the ignition model for different fuels and across conditions. Experimentally, the HO mechanism for Bituminous coal is described by the combustion of volatiles in the gas phase outside the particle, the HI on the other hand is described by simultaneous combustion of volatiles i.e. very close to the particle surface or by oxidation of the char. In case of Lignite, the volatiles burn before or after the fragmentation of the particle. The experimental observation for bituminous coal show both the ignition mechanism over 50% O_2 content due to the difference in the chemical and physical structure of the coal [152, 314]. Another contributing factor for such a behaviour is that the particles at those conditions are in transition phase and hence it exhibited dual ignition mechanism. The transition of ignition mechanism was also observed by Molina and Shaddix for bituminous coal [155].

4.2 Computational domain for case set up

It will be favourable to simulate a particle moving through an entrained flow reactor or a DTF but it will require modelling of the complete domain and the movement of the particle itself (dynamic meshing). In addition to the governing equations in gas phase, the thermo chemistry conversion of particle happening inside the porous particle increases the computational time required. Hence, to reduce the computational time, a leaf was taken from wind tunnel testing where the body under investigation is static and the fluid flows over the body. In this CFD model the particle is static and the ambient gas flows over it at low velocity. This particular approach has been implemented in the past [126, 311, 315] to validate various single particle combustion models. It is important to model the particle as a porous shell to simulate the thermal conversion inside the particle. This will enable the thermal resistance as well as the resistance to the transport of species via particle pores.

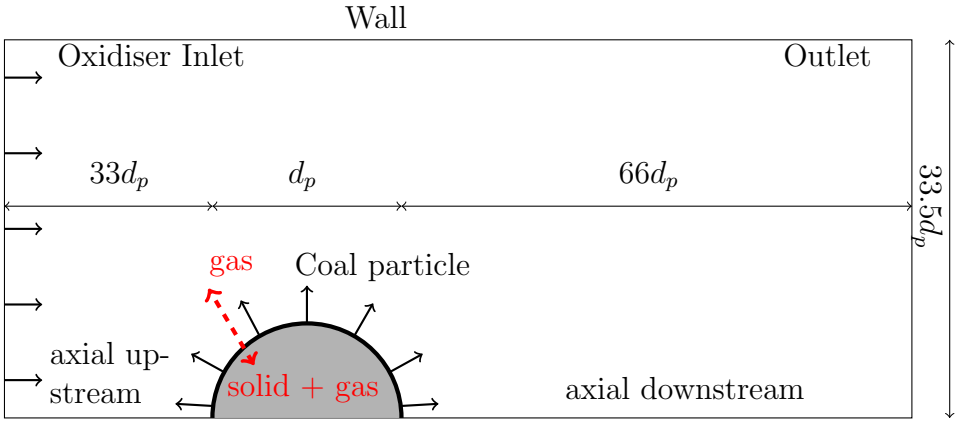

Figure 4.3: Computational Domain(not to scale)

The model configuration is shown in Figure 4.3, which can replicate a DTF or an entrained flow reactor. In order to reduce the computational time a 2D-

axisymmetric flow is considered where the particle is assumed to be a sphere. The geometry is modelled in a way that the particle diameter d_p will determine the height and width of the domain. The length of the domain in the direction of the flow is $100d_p$ and $33.5d_p$ wide in radial direction. The geometry scales with the change in size of the particle, it is done because the far field flow do not affect the particle as the flow is laminar in the DTF. A similar geometry is used by Tufano et al [126] to simulate combustion of single particle combustion in the Hencken burner used by Molina and Shaddix [298].

The flow in the case set-up is separated in two zones, i.e. the flow inside the particle and the ambient gas flowing over the particle. At t = 0 s, the particle is modelled as a porous medium with uniform porosity across the particle which consists of both solid and gas phase(pores inside the particle). In the model the particle is static, the gas flows over the particle and thus to replicate experimental heating rate the incoming gas temperature needs to be adjusted according to the temperature experienced in the DTF.

The velocity of the particle was not measured experimentally but rather it was calculated [134]. In the model in order to replicate similar time temperature profiles experienced by the particle, it is assumed that the gas that flows over the particle is equal to the experimental particle velocity. The overall particle velocity is calculated by calculating the particle terminal velocity in the experiment, which is around 0.02 m/s. The particle terminal velocity is calculated using Equation 4.1 [134].

$$V_t = (\rho_p d_p^2 g)/(18\mu) \tag{4.1}$$

where, μ is the dynamic viscosity, V_t is the particle terminal. The particle terminal velocity changes due to particle mass loss and the buoyancy effect due to volatile gases and flame around the particle are neglected. This may reduce the overall particle velocity experienced in the experiments. The model assumes that the terminal velocity is achieved instantly by the particle as it enters the furnace. These assumptions may overpredict the velocity of the particle inducing a small error which over predicts the heating rate of the particle. In reality, the particle will never achieve terminal velocity due to continuous thermo-conversion processes but this assumption will suffice for further investigation.

The particle terminal velocity increases with increase in particle size and thus the heating rate for each particle size will be different. There are four particle size investigated in this Chapter i.e. 50 μm, 90 μm, 150 μm and 200 μm. The temperature experienced by different particle sizes with respect to time in different conditions are shown in Figures 4.4 and 4.5. The temperature profiles during the experiments did not change with increase in O_2 concentration and hence the same temperature profiles can be used for various concentration of O_2. Many researchers have ignored the cooler temperature around the injectors and used a constant temperature profile in the domain phase for model simplification [110, 131, 316, 317]. The model in this work accounts for this variation by setting up a temperature gradient between particle-inlet and transiently changing the inlet temperature (see more details in

Section 4.3.4).

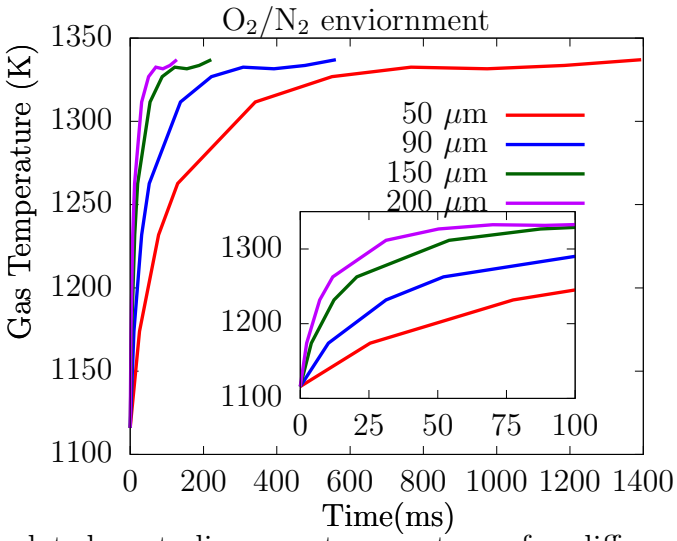

Figure 4.4: Calculated centreline gas temperatures for different particle size in O_2/N_2 conditions.

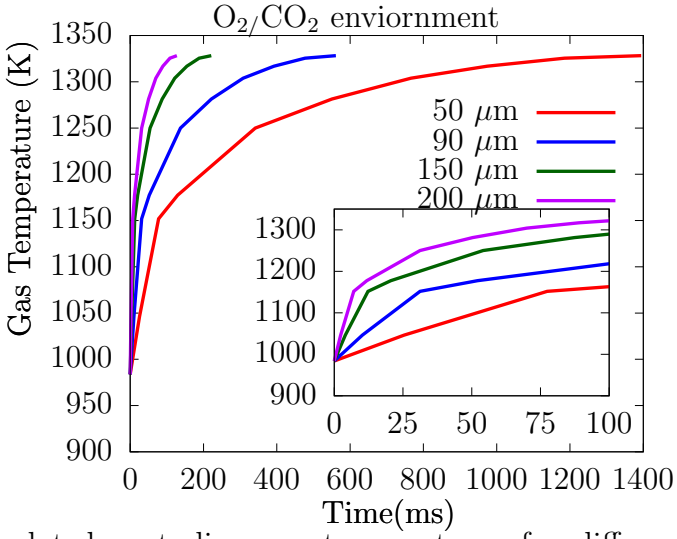

Figure 4.5: Calculated centreline gas temperatures for different particle size in O_2/CO_2 conditions.

The velocity of the ambient gas which flows around the particle at t = 0 s in the model is the experimental velocity of the particle + the ambient gas velocity (0.02 m/s) measured experimentally. The inlet conditions are initialised in accordance with the velocity and temperature of the ambient gas, for e.g. when t = 0 s a particle with diameter of 90 μm will experience a gas velocity of 0.27 m/s and there will be a temperature gradient across the domain from inlet (1255 K) upto particle (1115 K) whereas there will be a constant temperature of 300 K from particle upto the outlet. The temperature of the inlet will increase with increase in time upto 1330 K. This

initialisation simulates the particle entering the furnace and replicate accurate heat transfer to the particle. The calculations of time and temperature profiles discussed earlier in this section will govern the temperature field at t=0 s. Radiation in the domain is neglected apart from the heat transfer at the particle surface as it is one of the main mode of heat transfer into the particle in the initial stages of particle heating. This approach has been implemented in the past by various authors to simulate the contribution of radiation [126, 307, 309, 310, 317]. Particle upon heating decomposes with the process of devolatilisation and char conversion which leads to chemical reactions, heat and mass transfer between the porous particle and the gas phase. Ignition is detected by the increase in temperature relative to the ambient gas and concentration of species like OH within the particle or gas phase. The model can be easily extended to three dimension and different shapes of the particle for biomass ignition. The following assumptions are made in the model :

i The main ambient gas passing over the particle is laminar as the flow inside the drop tube furnace is laminar.

ii The radiation heat exchange exists only at the particle exterior surface and is neglected everywhere else in the geometry.

iii At t=0 s, particle is assumed to have uniform porosity which increases locally with mass loss from the particle.

iv The mass loss during thermo chemical conversion do not change the particle volume.

v The gas and solid components inside the particle are in thermal equilibrium i.e. the temperature of the gas inside the porous particle is same as the particle on evolution from the particle.

vi The transport of species from the particle to the gas phase is governed by Darcy's law.

4.3 Mathematical model

The transient simulations were performed using ANSYS Fluent v19.0. The gas phase is governed by the conservation equations described in the Section 2.3. The governing equations for the gas phase inside the porous particle are in a similar form of equation 2.4 which are modified to account for the variation in the porosity. The governing equations are coupled with the governing equations of gas phase using source terms with the help of User Defined Function (UDF's) and User Defined Scalars (UDS's) in Fluent. The details of the operation and applicability of UDF's and UDS is described in Fluent UDF manual [318]. This section describes the governing equations used to model the flow inside the particle. The general form of UDS in Fluent is same as Equation (2.4) which is solved as an additional transport equation. Four UDS's are used in the model to pre-define the volumetric mass source of four components of the particle, i.e. moisture, volatiles, char and ash. The ash in the particle is assumed to be inert and hence the density is constant. The particle

in the model is stagnant, the diffusive and convective terms are hence neglected and the changing variable in the UDS's is the unsteady term which described the change in the values of overall density with time (which is made up of the four scalars). The mass loss of the particle or the rate of change of the scalar values is described below.

$$\frac{\partial \rho_p}{\partial t} = \frac{\partial \rho_m}{\partial t} + \frac{\partial \rho_v}{\partial t} + \frac{\partial \rho_c}{\partial t} + \frac{\partial \rho_a}{\partial t} \tag{4.2}$$

The mass balance in solid phase is given by Equation (4.2), where ρ_m for water, ρ_v for volatiles, ρ_c for char and ρ_a for ash are the density of the solid phase which are defined by the UDS ($kg/m^3 - s$). The procedure to calculate the value of the UDS is described in section Section 4.3.1. As the particle heats up transiently, the thermochemical conversion takes place and the change in the particle density is described by:

$$\frac{\partial \rho_p}{\partial t} = S_m = -\dot{r}_M - \dot{r}_V - \dot{r}_C \tag{4.3}$$

where S_p is the the net mass loss rate due to the particle drying ($\dot{r}_M$), volatile release ($\dot{r}_V$) and char combustion ($\dot{r}_C$). Coal upon heating releases the moisture but complete dehydration of the coal does not occur below 350 °C [82]. The mass of the particle moisture per unit volume is given by ρ_m and the rate of moisture loss is given by Equation (4.4) [311]

$$\frac{\partial \rho_m}{\partial t} = -\dot{r}_M = -\frac{(T_p - T_{boil})\rho_m c_{pm}}{\Delta H_{latent} \partial t} \tag{4.4}$$

where, T_p represents the temperature of the particle, T_{boil} represents the boiling temperature of water and ΔH_{latent} is the latent heat of evaporation (2.260 x 10^3 kJ/kg). The devolatilisation rate for different species is derived represented by a single rate Arrhenius equation, namely

$$\frac{\partial \rho_v}{\partial t} = -\dot{r}_V = -\rho_v A_v exp^{\frac{E_v}{RT_p}} \tag{4.5}$$

The kinetics for the devolatilisation are obtained from the CPD. Then they are fitted into single rate parameters giving the pre-exponential factor (A_v) and the activation energy (E_v). The kinetics for each species evolved during devolatilisation are split by multiplying Equation 4.5 by the mass fraction of the species evolved. The species evolution and the mass fraction of each species is discussed in Section 4.3.1. The reactions in the gas phase are calculated using FFCM or Westbrook-Dryer reduced mechanism. The char mass loss in the particle is determined as follows:

$$\frac{\partial \rho_c}{\partial t} = -\dot{r}_C = -\dot{r}_{C_{\mathrm{O_2}}} \frac{MW_{\mathrm{C}}}{\Omega_{\mathrm{O_2}} MW_{\mathrm{O_2}}} - \dot{r}_{C_{\mathrm{O_2}}} \frac{MW_{\mathrm{C}}}{\Omega_{\mathrm{O_2}} MW_{\mathrm{O_2}}} - \dot{r}_{C_{\mathrm{CO_2}}} \frac{MW_{\mathrm{C}}}{\Omega_{\mathrm{CO_2}} MW_{\mathrm{CO_2}}} - \dot{r}_{C_{\mathrm{H_2O}}} \frac{MW_{\mathrm{C}}}{\Omega_{\mathrm{H_2O}} MW_{\mathrm{H_2O}}} \tag{4.6}$$

The char reaction rates are represented in the following form for coal [129],

$$\dot{r}_{Ci} = A_{ci} exp^{(\frac{-E_{ci}}{RT_p})} [CT_{Char}][CT_{react,k}]^{\alpha_{react,k}} \tag{4.7}$$

for biomass[308, 319] ,

$$\dot{r}_{Ci} = T_p S_{char} A_{ci} exp^{(\frac{-E_{ci}}{RT_p})} \varepsilon [CT_{char}][CT_{react,k}] \frac{\rho_c}{\rho_p} \tag{4.8}$$

The biomass char kinetics have an extra term to account for the reaction order $\alpha_{react,k}$ which is assumed by Bryden et. al. [308] to be a unity. Thermal annealing is ignored as it will not have a major impact in the overall ignition phase. The reaction involved in the coal char consumption and biomass char consumption due to the oxidation and gasification are presented in Tables 4.4 and 4.5 respectively. Here i represents the reaction number, k represents the reacting species, $[CT]$ represents the volumetric concentration of the reacting species, Ω is the stoichiometric coefficient, S_{char} is the specific internal surface area ($\frac{m^2}{m^3}$)of the char porous structure and MW is the molecular weight of the species involved in the reaction.

Table 4.3: Species added as source terms S_{Y_k} in the particle gas phase due to moisture loss and devolatilisation

Species	Source term (S_{Y_k})
H_2O	$S_{H_2O} = \dot{r}_M$
N_2	$S_{N_2} = Y_{N_2} * \dot{r}_V$
CO	$S_{CO} = Y_{CO} * \dot{r}_V$
CO_2	$S_{CO_2} = Y_{CO_2} * \dot{r}_V$
CH_4	$S_{CH_4} = Y_{CH_4} * \dot{r}_V$
H_2	$S_{H_2} = Y_{H_2} * \dot{r}_V$
C_2H_4	$S_{C_2H_4} = Y_{C_2H_4} * \dot{r}_V$

Table 4.4: Char reactions, kinetic constants and heat of reactions for coal

Reaction	A_{ci} (m/s)	E_{ci} (kJ/kmol)	Reaction order	ΔH_c (kJ/kg)	Ref.
$C + \frac{1}{2} O_2 \longrightarrow CO$	$1.5e^9$	$1.6e^5$	$[C][O_2]^{0.78}$	9208.33	[129]
$C + O_2 \longrightarrow CO_2$	$7.3e^7$	$1.35e^5$	$[C][O_2]$	32808.33	[129]
$C + CO_2 \longrightarrow 2\,CO$	$8.1e^7$	$2.07e^5$	$[C][CO_2]$	14416.6667	[129]
$C + H_2O \longrightarrow CO + H_2$	$2.6e^8$	$2.03e^5$	$[C][H_2O]$	10941.66	[129]

Table 4.5: Char reactions, kinetic constants and heat of reactions for biomass

Reaction	A_{ci} (m/s·K)	E_{ci} (kJ/mol)	ΔH_c (kJ/kg)	Ref.
$C + \frac{1}{2} O_2 \longrightarrow CO$	0.658	74.8	9212	[308]
$C + CO_2 \longrightarrow 2\,CO$	3.42	130	14370	[319]
$C + H_2O \longrightarrow CO + H_2$	3.42	130	10940	[319]

The governing equation for gas species transport inside the particle is given by

$$\frac{\partial}{\partial t}(\varepsilon\rho_g Y_k)+\frac{\partial}{\partial x}(\varepsilon\rho_g Y_k u_x)+\frac{\partial}{\partial y}(\varepsilon\rho Y_k u_y) = \frac{\partial}{\partial x}\Big(D_{k_{eff}}\frac{\varepsilon\rho_g\partial Y_k}{\partial x}\Big)+\frac{\partial}{\partial y}\Big(D_{k_{eff}}\frac{\varepsilon\rho_g\partial Y_k}{\partial y}\Big)+S_{Y_k} \tag{4.9}$$

where ε is the porosity of the particle and the diffusivity of each specie is calculated using kinetic theory in the domain and in the particle it is a function of porosity and Knudsen diffusion. Fluent does not allow separating the diffusivity of porous and non porous phase. Hence the transport property was calculated using a UDF. The equations used for calculating diffusivity in the particle are as follows:

$$D_{k_{eff}} = \big[\frac{1}{D_{k_m}} + \frac{1}{D_{k_{Kn}}}\big]^{-1}\cdot\frac{\varepsilon}{\tau} \tag{4.10}$$

$$D_{k_{Kn}} = \frac{d_{pore}}{3}\cdot\sqrt{\frac{8RT_p}{MW_k\pi}} \tag{4.11}$$

$$D_{k_m} = \frac{1-X_k}{\sum_{l,l=k}\frac{X_l}{D_{k_l}}} \tag{4.12}$$

$$D_{k_l} = 0.0188\frac{\Big[T_p^3\cdot\big(\frac{1}{MW_k}+\frac{1}{MW_l}\big)\Big]^{0.5}}{P_{abs}\cdot\varsigma_{k_l}^2\Omega_D} \tag{4.13}$$

$$\varsigma_{k_l}^2 = 0.5(\varsigma_k+\varsigma_l) \tag{4.14}$$

$$\Omega_D = f(T^*) \tag{4.15}$$

$$T^* = \frac{T}{(\frac{\varpi}{\sigma})_{k,l}} \tag{4.16}$$

$$(\frac{\varpi}{\sigma})_{k,l} = \sqrt{(\frac{\varpi}{\sigma})_k(\frac{\varpi}{\sigma})_l} \tag{4.17}$$

D_{k_m} is the diffusion coefficient of species k in mixture m, $D_{k_{Kn}}$ is the Knudsen diffusion coefficient obtained from [320], τ is the tortuosity of the particle, X is the mole fraction of species, D_{k_l} is the diffusion in binary mixture, ς_{k_l} and the ϖ_{k_l} are the Leonard-Jones parameter which are also known as the characteristic length and the energy parameter. The kinetic theory used is based on Chapman-Enskog formulation to obtain the binary diffusion coefficients [321, 322]. The diffusion in the domain is calculated using D_{k_m} and inside the particle it is calculated using $D_{k_{eff}}$.

In order to maintain conservation of species, the species evolved in the pores of the particle (gas phase) due to the decomposition of the solid structure of the particle are hooked in the term S_{Y_k} of equation 4.9 for each specie. The values of mass fraction of each specie are given in Tables 4.3 and 4.6. The methodology to calculate the values of mass fraction of species presented in Table 4.3 are discussed in Section 4.3.1.

Table 4.6: Species added as source terms (S_{Y_k}) in the particle gas phase due to char combustion

Species	Source term (S_{Y_k})
O_2	S_{O_2}= - $\left(\dot{r}_{C_{O_2}}\right)_{CO} - \left(\dot{r}_{C_{O_2}}\right)_{CO_2}$
CO_2	S_{CO_2}= - $\dot{r}_{C_{CO_2}} + \dot{r}_{C_{O_2}} \frac{MW_{CO_2}}{\Omega_{O_2} MW_{O_2}}$
H_2O	S_{H_2O}= - $\dot{r}_{C_{H_2O}}$
CO	S_{CO}=$\dot{r}_{C_{O_2}} \frac{MW_{CO}}{\Omega_{O_2} MW_{O_2}} + \dot{r}_{C_{CO_2}} \frac{MW_{CO}}{\Omega_{CO_2} MW_{CO_2}} + \dot{r}_{C_{H_2O}} \frac{MW_{CO}}{\Omega_{H_2O} MW_{H_2O}}$
H_2	S_{H_2}=$\dot{r}_{C_{H_2O}} \frac{MW_{H_2}}{\Omega_{H_2O} MW_{H_2O}}$

The changes in the mass fraction of the species due to gas phase reaction are not described in Table 4.3. There are no additional source terms required to hook into the model, as Ansys Fluent Finite rate model is able to account for the variation of the species because of the gas phase reactions in the species transport equation.

$$\frac{\partial(\varepsilon\rho_g)}{\partial t} + \frac{\partial}{\partial x}(\varepsilon\rho_g u_x) + \frac{\partial}{\partial y}(\varepsilon\rho_g u_y) = S_{m_{char}} + S_{m_{vol}} \tag{4.18}$$

The gas phase density (varying with ideal gas law) is calculated Equation (4.18). The S_m is the mass source terms added in order to conserve the mass of the particle in the gas phase. The source terms required conserving the species continuity/density due to devolatilisation and moisture release is given by:

$$S_{m_{vol}} = S_{H_2O} + S_{N_2} + S_{CO} + S_{CO_2} + S_{CH_4} + S_{H_2} + S_{C_2H_4} \tag{4.19}$$

The source term $S_{m_{vol}}$ added to conserve the mass inside the particle in gas phase is the summation of all the species released during moisture and devolatilisation phase. Similarly, the source terms for each specie to maintain overall gas density/continuity conservation due to char reaction are given as follows:

$$S_{m_{char}} = -(-\dot{r}_C) = \dot{r}_{C_{O_2}} \frac{MW_C}{\Omega MW_{O_2}} + \dot{r}_{C_{O_2}} \frac{MW_C}{\Omega MW_{O_2}} + \dot{r}_{C_{CO_2}} \frac{MW_C}{\Omega MW_{CO_2}} + \dot{r}_{C_{H_2O}} \frac{MW_C}{\Omega MW_{H_2O}} \tag{4.20}$$

The energy conservation equation for the gas phase is governed by Equation (4.21).

$$\varepsilon\rho_g\frac{\partial H_g}{\partial t}+\frac{\partial(\rho_g u_x H_g)}{\partial x}+\frac{\partial(\rho_g u_y H_g)}{\partial y}=\frac{\partial}{\partial x}\Big(\rho_g c_{pg} k_{eff_g}\frac{\partial T_g}{\partial x}\Big)+\frac{\partial}{\partial y}\Big(\rho_g c_{pg} k_{eff_g}\frac{\partial T_g}{\partial y}\Big)+S_{rxn} \tag{4.21}$$

where enthalpy in an individual cell is calculated using $H_g = \sum_{k=1}^{k=n} Y_k c_{p_k} T_k$. Similarly the thermal conductivity, k_{eff_g} is calculated using $k_{eff_g} = \sum_{k=1}^{k=n} Y_k k_{eff_k}$. The value of thermal conductivity for individual specie is calculated using kinetic theory and the specific heat capacity c_{p_g} is calculated using the piecewise polynomial function which varies with change in temperature(in built in Fluent). The energy transferred from reaction is added as a source term S_{rxn} in the cell. Similarly, the conservation equation for the solid phase is given by equation 4.22

$$\rho_p\frac{\partial H_p}{\partial t}=\frac{\partial}{\partial x}\Big(k_{eff_p}\frac{\partial T_p}{\partial x}\Big)+\frac{\partial}{\partial y}\Big(k_{eff_p}\frac{\partial T_p}{\partial y}\Big)+S_{rxn}+S_{rad} \tag{4.22}$$

The value of source term due to reaction is integration of all the heat release from the combustion for e.g. the heat release from char reaction is defined by $S_{rxn_{char}} = \sum \frac{\partial \rho_c}{\partial t}\Delta H_c$. The value of k_{eff_p} and c_{p_p} is calculated using the correlation in Equations (4.23) and (4.24) provided in [323] and [324] respectively.

$$k_{eff_p}=\Big[\frac{Y_c}{1.47}+\frac{Y_H}{0.0118}\Big(\sqrt{\frac{273.15}{T_p}}\Big)\Big]^{-1} \tag{4.23}$$

$$c_{p_p}=\begin{cases}1.15(kJ/kg)\text{if } T_p \leqslant 573.15K\\ 1.15+2.03e^{-3}(T_p-573.15)-1.55e^{-6}(T_p-573.15)^2 1.15(kJ/kg)\\ \text{if} T_p \geqslant 573.15\end{cases} \tag{4.24}$$

As thermal equilibrium is assumed between the gas and solid phase the energy equation for the particle, which includes both gas and solid phase is governed by combination of Equations (4.21) and (4.22) which is represented in Equation (4.25). Thermal equilibrium assumption defines the temperature field of the particle where the gases inside the pores reaches the temperature of the solid instantaneously. In this approach the temperature increase due to reaction inside the particle is going to be for both the phases (i.e. the energy released is added to a cell containing both solid and gas phase of the particle).

$$\varepsilon\rho_g\frac{\partial H_g}{\partial t}+\rho_p\frac{\partial H_p}{\partial t}+\frac{\partial(\rho_g u_x H_g)}{\partial x}+\frac{\partial(\rho_g u_y H_g)}{\partial y}=\frac{\partial}{\partial x}\Big(k_{eff}\frac{\partial T}{\partial x}\Big)+\frac{\partial}{\partial y}\Big(k_{eff}\frac{\partial T}{\partial y}\Big)+S_{rxn}+S_{rad} \tag{4.25}$$

The value for effective thermal conductivity of the particle is given by Equation (4.26).

$$k_{eff} = \varepsilon k_{eff_g} + (1-\varepsilon) k_{eff_p} \tag{4.26}$$

$$S_{rad} = \frac{A_{p_{surface}}}{V_{p_{surface}}} \epsilon\sigma(T_{wall}^4 - T_p^4) \tag{4.27}$$

Radiation is ignored everywhere in the domain apart from the surface of the particle. The source term S_{rad} is only added to the surface cells of the particle and is ignored everywhere else. This approach has been validated in multiple studies to account for the radiation contribution [126, 131, 307–310, 316, 317]. The value of S_{rad} is given by Equation (4.27) where σ is the Stefan-Boltzmann constant and ϵ is the emissivity of the particle. The porosity of the particle increases as the particle loses mass upon heating. The porosity of the particle varies according to equation 4.28.

$$\frac{\partial \varepsilon}{\partial t} = \frac{\rho_{true} - \rho_p}{\rho_{true}} \tag{4.28}$$

where,

$$\rho_{true} = \frac{\rho_{p0}}{1-\varepsilon_0} \tag{4.29}$$

ρ_{p0} and ε_0 are the initial particle density and porosity. The momentum of the species in x-direction in the porous media is governed by the following equation:

$$\begin{aligned} \frac{\partial(\varepsilon\rho_g u_x)}{\partial t} + \frac{\partial(\varepsilon\rho_g u_x u_x)}{\partial x} + \frac{\partial(\varepsilon\rho_g u_y u_x)}{\partial y} &= -\frac{\partial \varepsilon p_g}{\partial x} + \frac{\partial}{\partial x}\Big(\mu \frac{\partial u_x}{\partial x}\Big) \\ &+ \frac{\partial}{\partial y}\Big(\mu\Big(\frac{\partial u_x}{\partial y} + \frac{\partial u_y}{\partial x}\Big)\Big) - \frac{\mu}{K} u_x - \frac{C_2}{2}\rho_g u_x u_x \end{aligned} \tag{4.30}$$

The last two terms on the right side includes two parts a viscous loss (Darcy) and an inertial loss term where K is the permeability and C_2 is the inertial resistance factor.

$$K = \frac{d_{pore}^2 \varepsilon^3}{150(1-\varepsilon)^2} \tag{4.31}$$

$$C_2 = \frac{3.5(1-\varepsilon)}{d_{pore}\varepsilon^3} \tag{4.32}$$

The value of permeability and the inertial resistance factor is obtained from the correlation proposed by Yang et al. [311] described Equations (4.31) and (4.32) where, d_{pore} is the local pore diameter inside the particle.

$$u_x = -\frac{K}{\mu}\frac{\partial p}{\partial x} \tag{4.33}$$

The local superficial velocity of the gases are calculated based on the permeability and the pressure gradient in the particle. The equations presented above are for conservation of momentum in x direction the governing equations are similar for y direction.

4.3.1 Model Precursors

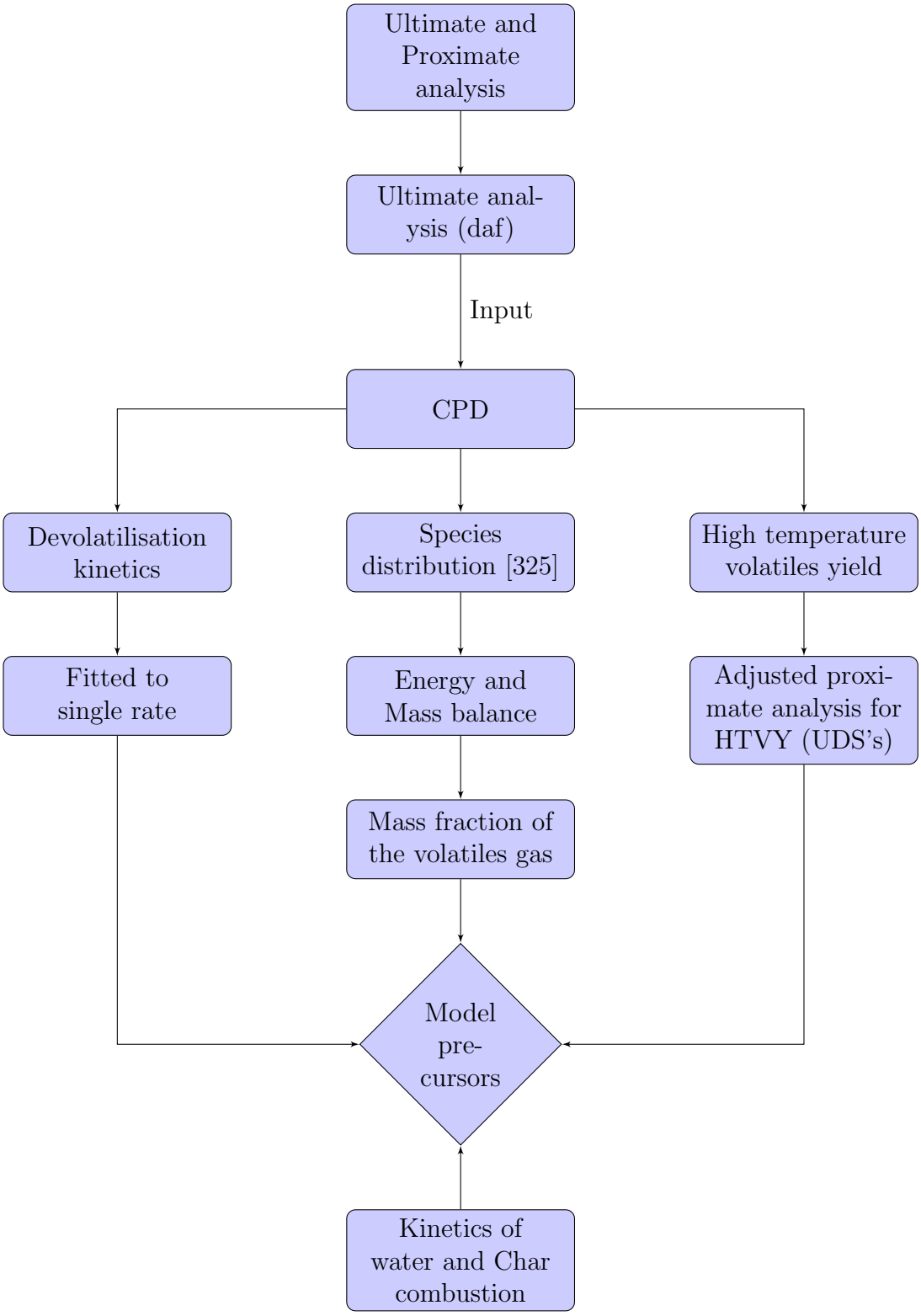

Figure 4.6: Methodology for the model precursor

There are three important precursors required for this model, kinetics of the fuel, mass fraction of the devolatilising species and the split of particle solid components (the value of four UDS's). These parameters are not available because of the experimentation cost. The only parameters generally available for a virgin fuel are the proximate & ultimate analysis and the heating value of the fuel. A methodology shown in Figure 4.6 is used to obtain all those parameters. The kinetics of water and char mass loss are discussed in Section 4.3 and it has already been concluded in Section 3.1 that the CPD provides an accurate predictions for volatiles evolution kinetics. The total volatiles released is determined using CPD.

Methodology for using the CPD model devolatilisation

Table 4.7: Chemical structure parameters of the coal

	Basis	Bituminous	Lignite A
Carbon (%)	daf	83.31	73.23
Hydrogen(%)	daf	5.45	4.43
Nitrogen(%)	daf	1.62	0.996
Oxygen(%)	daf	7.99	20.58
ASTM Volatile(%)	daf	39.91	62.023
M_δ		30.7	37.9
MW_{cl}		351	284.9
P_o		0.501	0.631
σ +1		4.97	5.16
C_0		0	0.113

M_δ: the average side-chain molecular weight, MW_{cl}: the average molecular weight of an aromatic cluster, P_o: the fraction of intact bridges of total attachments, σ +1: the average number of attachments per cluster and C_0: the population of char bridges.

The CPD requires coal's ultimate and proximate analysis, the heating rate of the coal particle and the final temperature. The work done in Section 3.1 used the CPD model, which used constant heating rate as input. It was important to account for the variation in the heating rate of the particle. There is another version of CPD, which allows particle time-temperature profiles as input. A series of sensitivity analysis was conducted on the CPD model to use the correct methodology to obtain accurate devolatilisation kinetics. The coal used for investigation was the bituminous coal described in Table 4.1. The other input values for the CPD model are calculated from the proximate and ultimate analysis of the coal according to Genetti et al. [246]. The input values for the CPD model for the coals under investigation are described in Table 4.7. The first sensitivity focused on the impact of final temperature with constant heating rate where the heating rate was set at 5 x 10^3 K/s and final temperature of the particle varied from 1200-2500 K. The results in Figure 4.7 (top right) suggest that final temperature had negligible impact as input

on the volatile release profiles. The other sensitivity was conducted on the impact of heating rate with constant temperature where the heating rate varied from 5 x 10^1 - 5 x 10^5 K/s and temperature was kept constant at 1300 K. An addition case was investigated in the same analysis where the input parameters were set at 5 x 10^5 K/s and 2500 K as final temperature in order to see the combined effect on the CPD model predictions. The results in Figure 4.7 (top left) show that there is a small and subtle impact on the devolatilisation behaviour where the volatile release rate profiles changes and there is an increase in HTVY with increase in heating rate. The increase in final temperature from 1300 K to 2500 K at 5 x 10^5 K/s had negligible impact on the overall profiles. Thus showing that the heating rate is an important factor and should be accounted for by calculating the devolatilisation kinetics.

The heating rate of the coal under analysis is not constant as it is moving through a temperature profile in the DTF and hence time temperature profiles are used as input to provide accurate heating rate of the coal particle. The time temperature profile for a single particle was obtained by setting up a a simple case in Fluent to simulate inert heating of the particle. The case consisted of a simple rectangular box initialised with the temperature profile described in Figure 4.4. The initial particle temperature is 300 K and wall temperature was set at 1400 K. A time temperature profile is obtained for a desired particle size, from the particle tracks. This was done to account for the variation of ambient temperature experienced by the particle in the drop tube. There will also be an impact of combustion of char and volatiles on the overall heating rate and hence it was decided to investigate the devolatilisation behaviour for temperature profiles of two cases which includes combustion of volatiles (i.e. the cases with ambient O_2 concentration of 21% and 80%), they are discussed later in detail in Section 4.4 . The results are shown in Figure 4.7 (bottom left), it also compares the results from the case where heating rate is set at 5 x 10^3 K/s and final temperature is set at 1300 K. This was chosen for comparison as experiments suggests that the particle experiences average heating rate of 5 x 10^3 K/s in the drop tube reactor. The profile with constant heating rate shows that there is significant impact of variable heating rate and it is not recommended for further investigation. The results show that the volatile release profiles with inert heating are very close for the profiles with the two cases where combustion of the volatiles is included. They start to deviate at particle temperature of $\approx$ 950 K when particle for the combustion cases ignites and there is sudden spike in heating rate. The deviation is not significant for the inert heating cases and the profiles are very close to each other. A comparison of the HTVY is shown for the four cases in Figure 4.7 (bottom right). There is difference of 1.5% in the final predictions of HTVY between inert and the two cases with combustion. This shows that higher heating rate after combustion did not change the final volatile release significantly. Using detail kinetics to predict the combustion behaviour of a particle is computationally expensive. The investigation, which includes the combustion does not change the volatile release profiles significantly and recalculating the temperature profiles iteratively for each condition will be computationally expensive and not impact the solution significantly as the three profiles are very similar to each other. Hence, it

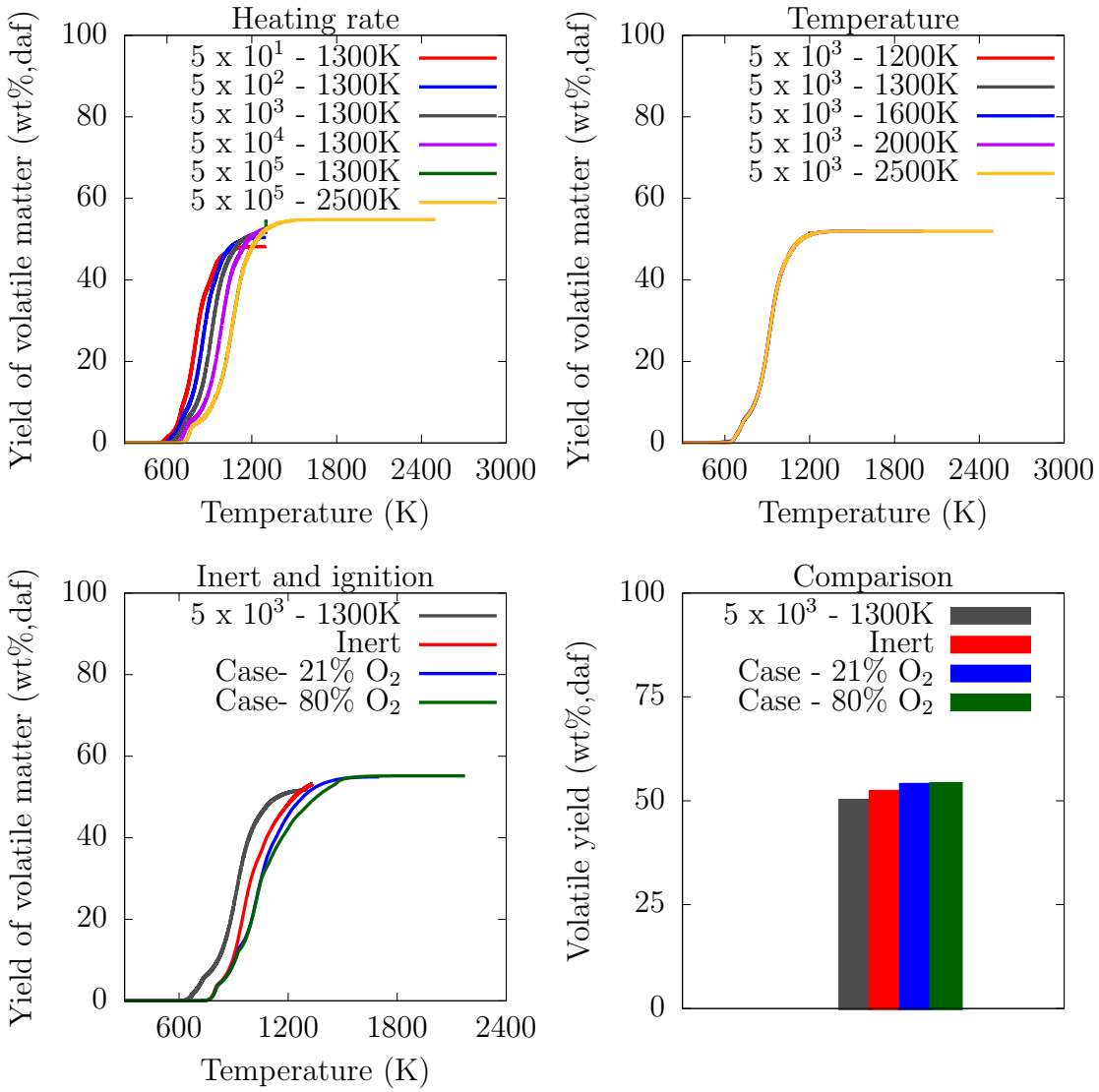

Figure 4.7: Sensitivity analysis on the heating rate and the final temperature to be used as an input for the CPD model.

was decided to use the particle temperature profiles from the inert heating of the particle which will provide a good agreement with the experimental conditions.

The CPD model provides results, which are used in predicting the devolatilisation kinetics, high temperature volatile yield and species distribution. The kinetic rate for devolatilisation are fitted into single rate Arrhenius expression and its E_v and A_v are obtain. The HTVY is also obtained from the CPD, which provides the q_{ratio}. The model does not take into consider the change in the molecular structure during the decomposition phase and hence it is important to account for the HTVY while calculating the UDS's. The proximate analysis of the fuel provides the mass fraction of moisture, volatiles, char and ash. In order to account for the HTVY the volatiles mass fraction is multiplied by the q_{ratio}. It is assumed that the increase in

the final volatiles is from the reduction in overall char content. The final values of the UDS's are calculated based on Equation (4.34).

$$UDS's = \begin{cases} \rho_m = & \rho_p Moisture_{ar} \\ \rho_a = & \rho_p Ash_{ar} \\ \rho_v = & \rho_p q_{ratio} Volatiles_{ar} \\ \rho_c = & \rho_p - \rho_m - \rho_a - \rho_v \end{cases} \tag{4.34}$$

The species evolved during the devolatilisation of coal is a very complex process to predict as it consists of heavy tar, light hydrocarbons, water, CO_2 and many other species. It hence requires a simplification, which are good representative of the volatiles evolved. The volatiles released can be assumed to decompose according to the Reaction **??** which is stoichiometrically consistent [325]. It uses the ultimate analysis of the fuel in dry ash free basis and uses splitting factors to decompose volatiles into H_2s, N_2, CO, CO_2, CH_4, H_2, C_2H_4 and C_6H_6. In Reaction R4.1 a, b, c, d and e are the mole fraction of component C, H, O, S, N. ζ_{CO}, $\zeta_{C_2H_4}$ and $\zeta_{C_6H_6}$ are the splitting factors for dividing the amount of carbon and oxygen to different species.

$$\begin{aligned} \mathrm{C_aH_bO_cS_dN_e} \longrightarrow\ & \mathrm{dH_2S} + (0.5\,\mathrm{e})\mathrm{N_2} + (\zeta_{\mathrm{CO}}\mathrm{c})\mathrm{CO} + 0.5\,\mathrm{c}(1-\zeta_{\mathrm{CO}})\mathrm{CO_2} + \\ & [(1-2\,\zeta_{\mathrm{C2H4}} - 6\,\zeta_{\mathrm{C6H6}})\mathrm{a} + 0.5\,(\zeta_{\mathrm{CO}}+1)\,\mathrm{c}]\mathrm{CH_4} + \\ & [0.5\,\mathrm{e} - 2\,(1-\zeta_{\mathrm{C2H4}} - 4.5\,\zeta_{\mathrm{C6H6}})\mathrm{a} + (\zeta_{\mathrm{CO}}+1)\,\mathrm{c} - \mathrm{d}]\mathrm{H_2} + \\ & a\,\zeta_{\mathrm{C2H4}}\mathrm{C_2H_4} + \mathrm{a}\zeta_{\mathrm{C6H6}}\mathrm{C_6H_6} \end{aligned} \tag{R4.1}$$

The assumptions presented by Petersen and Werther [325] are applied here as well with the addition of $\zeta_{C_6H_6}$ is kept to zero for modelling simplicity and reduction in computation time of the reactions from C_6H_6. It is a good assumption that heavy hydrocarbons are reduced to methane of other light gases and just from the perspective of ignition detection it can be neglected. Similarly, soot modelling is also ignored for reducing the computational time. The procedure for mass and energy balance is as follows:

i The ultimate analysis and proximate analysis provided are converted to dry ash free basis (daf). The calorific value of the fuel is converted to daf basis by using the correlation provided by Given et.al [326]. This provides the heat energy contribution from the volatiles.

ii The HTVY predicted from the CPD are used to generate the ultimate analysis of the volatiles in daf basis.

$$Moles_{volatiles} = \begin{cases} C_{vol} = & (C_{daf} - FC_{daf_{CPD}})/Vol_{daf_{CPD}})/MW_C \\ H_{vol} = & (H_{daf}/Vol_{daf_{CPD}})/MW_H \\ O_{vol} = & (O_{daf}/Vol_{daf_{CPD}})/MW_O \\ S_{vol} = & (S_{daf}/Vol_{daf_{CPD}})/MW_S \\ N_{vol} = & (N_{daf}/Vol_{daf_{CPD}})/MW_N \end{cases} \tag{4.35}$$

The ultimate analysis of the volatiles(daf) lead to the mole fraction of each component using Equations (4.35) and (4.36). This mole fraction is nothing but a, b, c, d and e in Reaction R4.1.

$$\begin{cases} a = & C_{vol}/\sum Moles_{volatiles} \\ b = & H_{vol}/\sum Moles_{volatiles} \\ c = & O_{vol}/\sum Moles_{volatiles} \\ d = & S_{vol}/\sum Moles_{volatiles} \\ e = & N_{vol}/\sum Moles_{volatiles} \end{cases} \tag{4.36}$$

iii The total energy of the volatile species should match with the overall energy contributed by the volatiles. The splitting factors in the Reaction **??** are calculated using iterative guessing where each species is ≥ 0. The split factors are adjusted until the summation of the calorific value of all the volatiles species matches the above calculated calorific values of volatiles.

4.3.2 Ignition criteria for the model

The criteria for homogeneous ignition is evident by the increase in domain temperature accompanied with increase in volatiles combustion products such as OH [120, 135, 327, 328] or CO [329, 330] Mathematically it can be detected when $\left(\frac{dT_g}{dt}\right)_{max}$ condition is achieved after the heat up stage, caveat being that the rise in domain temperature is not because of heterogeneous ignition. The ignition of volatiles can happen inside the particle, on the surface of the particle or in the domain but only the latter is quantified as homogeneous ignition. In this study the homogeneus ignition is quantified by the increase in the domain temperature and the increase in the OH mass fraction in the domain.

The heterogeneous ignition can be quantified using the inflection condition proposed by Du and Annamalai [110] which was based on the theory of thermal explosion postulated by Semenov [102]. This criterion has been applied in many single particle studies for detecting heterogeneous ignition [117, 131, 316, 330–332]. The inflection condition can be mathematically represented by $\frac{d^2T_p}{dt^2} = 0$ and $\frac{dT_p}{dt} \geqslant 0$. As the particle heats up due to the heat transfer from the ambient conditions the heat transfer rate reduces. The inflection condition is described as the point (time) when the heating rate of the particle starts increasing due to energy released from

the reactions inside or at the surface of the particle. The increase in the heating rate could also be due to the development of the volatile flame (heat transfer during homogeneous ignition). Thus, the reactions on the surface and inside the particle are monitored to quantify heterogeneous ignition.

Mathematically only one of the ignition mechanism will initiate first. According to the experimental definition of the heterogeneous ignition, the ignition can be due to simultaneous burning of char and volatiles close to the surface. The basic understanding of the simultaneous combustion of volatiles and char imply that the ambient O_2 has managed to diffuse through the outer flame or the volatiles concentrated region up to the surface or inside the pores of the particles.

Many research groups simulating a single particle model who ignored the flow inside the particle observed that the overlapping of volatiles burning on the surface of the particle during heterogenous ignition but did not quantify the simultaneous ignition mechansim [110, 117, 119]. There are no accurate methods in the literature to quantify such a mechanism, which has made it difficult in the past to quantify such a phenomena [333]. Most recently, Lili et al. [316] defined that in order to detect simultaneous ignition, the ignition delay time for both the mechanisms should happen close to each other. It also described that after the simultaneous ignition is established, most of the volatiles burn inside the particle heterogeneously or in other words inside the solid boundary of the particle. The research did not obtain a correlation or provide any mathematical quantification for detecting simultaneous ignition. In order to mathematically quantify the criteria to detect such a condition, the difference between the ignition delay time for both the mechanism should be very small. The parameters influencing such a scenario (mechanism) will be the fluctuations in reaction rate (indicated by the combustion products) and the increase in heating rate in both the phases which should happen one after the other in short space of time. The difference in the ignition time delay are very small for the particles under investigation and thus the time difference for the overlapping of both the mechanism will be a fraction of the time of which ever ignition happens first. As the ignition mechanism are fast and small in time scale, to quantify the overlapping mechanism a reasonable assumption of addition of 10% to the which ever ignition happens first will prove to be sufficient barrier for the second ignition to initiate. Any additional time taken for the second ignition mechanism to initiate will imply that the first ignition process has a pronounced relevance and the overall ignition process for the particle is dominated by the first mechanism. For e.g. if volatiles ignite first in the domain and then heterogeneous ignite inside the particle after that, the mathematical criteria for simultaneous ignition will be as represented in equation 4.37.

$$\frac{t_{HI}}{t_{vol}} - 1 \leqslant 0.1 \tag{4.37}$$

To summarise the following criteria are used to quantify ignition mechanism in this model:

i HO will be described by significant increase in the temperature gradient of the

gas phase outside the particle accompanied with increase in mass fraction of OH[120, 135, 327, 328]. The criteria is similar for reduced mechanism, instead of monitoring OH, the reaction rate of methane is monitored.

ii HI can be quantified in three ways

a) When the volatiles released in the domain fail to reach flammability limits and the ambient oxygen diffuses inside the particle which leads to particle undergoing char mass loss with increase in the overall particle temperature due to char reaction [152], i.e. the inflection condition.

b) The increase in particle temperature (inflection condition) due to combustion of volatiles inside the particles [316] with increase in OH in the particle accompanied with rise in particle temperature (surpassing the ambient temperature). Similar to HO, methane reaction rate is monitored instead of OH for global reaction mechanism [98].

c) HI due to simultaneous combustion of volatiles and/or char inside the particle boundary and in domain phase which are quantified by the time it takes for OH to increase inside the particle. The time is calculated based on formulation described in equation 4.37.

4.3.3 Validation of the particle heat up and devolatilisation

It was important to obtain confidence in the methodology of the model for the particle heat up and mass loss during thermochemical conversion. Hence, the results are compared with Fluent's default model for particle heat up and devolatilisation. The model in Fluent does not account for any thermal gradient across the particle and assumes uniform heating. The particle heat up equation also known as lumped model equation is described in Equation (2.21).

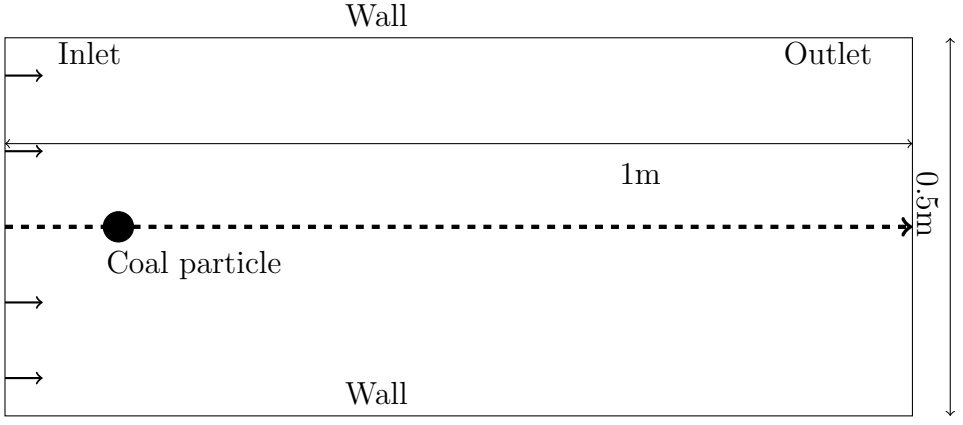

Figure 4.8: Computational Domain(not to scale).

In order to calculate the inert particle heating of the Fluent lumped model equation a case set up is required. The configuration is shown in Figure 4.8. The geometry is a rectangular box (similar to drop tube furnace) with a particle injected in a hot domain which is carried by pure N_2. The different particle sizes

simulated are 50, 90, 200 and 1000 μm. The geometry inlet temperature was set at 1300 K, the wall temperatures at 1400 K, the initial particle temperature at 300 K with zero slip velocity, gas inlet velocity of 1e-3 m/s and the domain is initialised at 1300 K. The density of the particle is 1180 kg/m^3. The particle c_p and k_{eff_p} is calculated using Equations (4.23) and (4.24). The time temperature profiles are calculated for a purely N_2 environment. The particle is assumed to be inert and does not undergo any mass transfer.

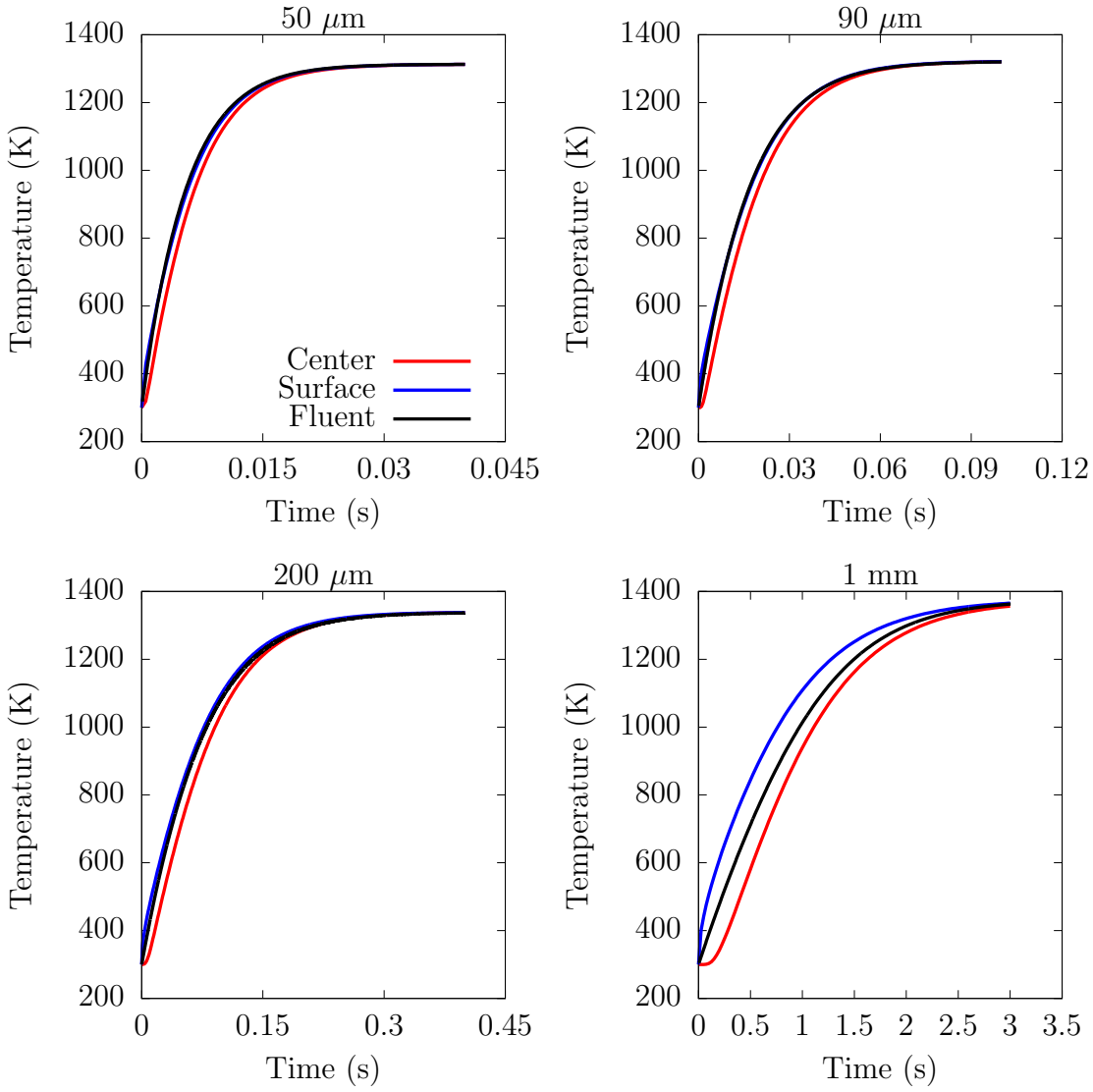

Figure 4.9: Comparison of the particle heat up between the model and the Fluent lumped model for different particle sizes.

In the porous coal particle model the same conditions are considered with the exception of particle being stationery and the ambient N_2 flows over it at the same velocity. The comparison results for the time temperature profiles of different particle sizes are shown in Figure 4.9. There is a decrease in heating rate with an increase

in particle size due to increase in thermal resistance. The impact of thermal gradient is pronounced with increase in the particle size, which is evident by the lag in the increase in heating rate at the center of the particle. The assumption of lumped model generates error for particle size ≥ 250 μm, which was also observed by Lu et al. [310]. The predictions of the time temperature profile between the model and Fluent lumped model is fairly good and hence the modelling methodology can be used for further investigation.

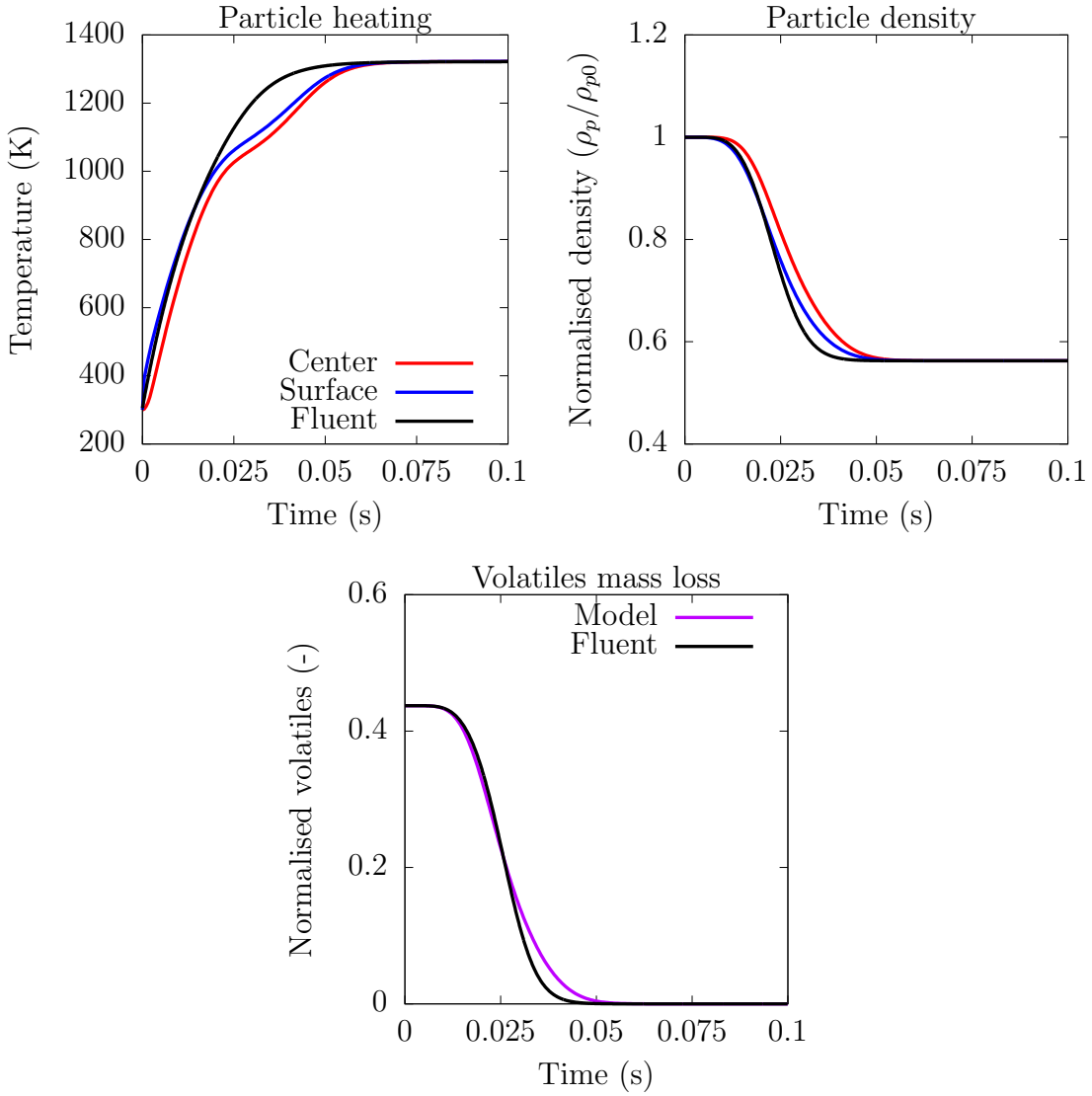

Figure 4.10: Comparison of the particle volatiles mass loss between the model and the Fluent default model.

A similar strategy is used to validate the devolatilisation model where the particle in the fluent default model is assumed to lose mass uniformly throughout the particle. The same boundary conditions as mentioned above is used with the addition of particle having an initial porosity of 17% for a particle diameter of 90

μm. The coal used for validation is the bituminous coal described in Table 4.1. The mass transfer from particle to gas phase, change in particle porosity and the transport of volatile species inside the pores is governed by the equations described in the Section 4.3. The particle devolatilisation kinetic rate is calculated using the methodology described in Section 4.3.1 using the CPD model. In this part of the validation, reactions are ignored, the char mass loss is ignored and the particle is simulated on dry basis i.e. the validation is purely focused on devoltilisation. The devolatilisation kinetics obtained after fitting the CPD results in a single rate expression are E_v = 5.61 x 10^4 kJ/kmol and A_v = 5.6 x 10^4 s^{-1} . The same kinetics are used in Fluent to predict mass loss due to devolatilisation. The input parameter are kept the same wherever possible to obtain consistency.

The default Fluent model does not account for the porosity change in the particle during devolatilisation as it assumes uniform mass loss. The impact of change in porosity and transport of volatiles species through the pores is evident in the heating rate of the particle in the model. As the devolatilisation starts the particle strts displacing the N_2 in the pores with the release of volatiles in the pores. As the devolatilisation rate increases the early released volatiles are displaced. The thermal equilibrium assumes that the volatiles released in the pores are at the same temperature as particle. The volatiles when transported through the pores into the domain reduces the heating rate as it briefly convective cools the solid surface of the particle accompanied with a generation of a cool film surrounding the particle relative to the domain. These two phenomena when compared to the Fluent's default model reduces the devolatilisation of the particle. In the model, once the volatiles are released through the pores and are diffused away, the heating rate is increased and the temperature reaches the domain temperature achieving equilibrium state. In the Fluent default model the heating of the particle is not interrupted due to the evolution of the volatiles. The difference in the volatiles loss is shown in Figure 4.10 where there is decrease in the mass loss rate in the model and is evident by the lag in the model when compared to the Fluent's default model. The two model shows similar mass loss rate and the trends are in good agreement with each other, hence the methodology used in the work can be used to simulate devolatilisation.

4.3.4 Boundary conditions for the O_2/N_2 cases

The numerical set up used a 2-D axisymmetric flow, which is meshed in ICEM with 35326 cells. The simulations are performed in Ansys Fluent v19.0. The viscous model was set to Laminar and the finite rate chemistry was used to ignore the turbulent chemistry interaction. The coupled scheme was used for pressure velocity coupling, all the discretisation are set to second order and the transient formulation was calculated using bounded second order implicit. In terms of the materials properties of the species, the viscosity and thermal conductivity of each were calculated using kinetic theory and the C_p was calculated using a polynomial function which is inbuilt in Fluent.

At t=0, T_p = 300 K, T_{wall} = 1400 K, T_g and u_g varies with particle size and are initialised in accordance with Figures 4.4 and 4.5. For e.g. a 90 μm particle case the maximum domain temperature in O_2/N_2 conditions is around 1250 K(from the inlet but around 1150 K at the particle surface) which increases transiently upto 1300 K. Similarly, for oxyfuel conditions the maximum domain temperature starts from 1100 K increasing to 1300 K.

$$\left(\rho_g D_{k_{eff}} \frac{\partial Y_k}{\partial x}\right)_p = \left(\rho_g D_{k_m} \frac{\partial Y_k}{\partial x}\right)_{domain} \tag{4.38}$$

$$\left(\rho_g D_{k_{eff}} \frac{\partial Y_k}{\partial y}\right)_p = \left(\rho_g D_{k_m} \frac{\partial Y_k}{\partial y}\right)_{domain} \tag{4.39}$$

$$\left(k_{eff} \frac{\partial T}{\partial x}\right)_p = \left(k_{eff_g} \frac{\partial T}{\partial x}\right)_{domain} \tag{4.40}$$

$$\left(k_{eff} \frac{\partial T}{\partial y}\right)_p = \left(k_{eff_g} \frac{\partial T}{\partial y}\right)_{domain} \tag{4.41}$$

The diffusion and thermal conditions for the species mass fractions and the temperature fluxes for both the phases the above equations are used. The diffusion coefficeints and thermal conductivity inside the particle is account by Equations (4.11) and (4.26). The particle is initially saturated with the same gas as ambient gas which satisfies a zero gradient conditions across the particle and domain. The S_{rad} is the radiation absorption at the external surface and is neglected everywhere else [330]. Initially, the particle pores are saturated with the ambient gas and as the particle heats up, the species are evolved in the pores of the particles, after which the ambient gases in the pores (including the oxidant) are pushed outwards in the domain.

Initial porosity (ε_0) was kept at 17% and 25% for bituminous and lignite coals respectively [314, 334]. The value of d_{pore} and ρ_{p0} = 1180 kg/m^3 are obtained from the values provided in [334]. The mass loss due to devolatilisation predicted by the CPD model fitted into a single rate expression. The results for both the coal are reliable as both the coals under investigation are CPD library coals [246]. The other parameters for both the coals are described in Table 4.8.

Lastly, volatiles homogeneous gas phase kinetics are described by using two mechanism, FFCM [276] which has 38 species and 291 reactions and Westbrook-Dryer mechanism [283] which uses 6 species and 3 reactions. The FFCM includes reactions for C_{0-2} and is validated for methane combustion but also includes limited reactions for C_2H_4. A sensitivity was conducted where the predicted volatiles species was assumed to compose of H_2S, N_2, CO, CO_2 and CH_4. This approach is applied in multiple studies in literature for modelling simplification [110, 117]. The splitting factor ζ_{CO} kept as unity which predicted a higher mass fraction of CH_4. There is also an over prediction of the heat release (around 9%) from the volatiles species when checked for the heat balance of the volatiles calorific value. The sensitivity is conducted to compare the predictions with reduced mechanism and simpler

hydrocarbons. The reduced mechanism is used to test if the model can provide accurate results with Westbrook-Dryer mechanism, which could significantly reduce the computational time required by the model.

Table 4.8: Model Precursors

		Bituminous coal	Lignite
Devolatilisation Kinetics	A_v (s−1)	5.60 x 10^4	5.30 x 10^3
	E_v (kJ/kmol)	5.61 x 10^4	4.16 x 10^4
	HTVY	1.30	0.93
Modified Proximate analysis (ar)	Fixed Carbon (%)	40.48	33.04
	Volatiles (%)	43.73	45.36
	Moisture (%)	2.5	13.2
	Ash (%)	13.3	8.4
Split factors	ζ_{CO}	1.0	1.0
	$\zeta_{C_2H_4}$	0.387	0.0934

4.4 Results and discussion/validation of the ignition model

This section discusses the model behaviour in O_2/N_2 and oxyfuel conditions and the development of corelation for critical particle diameter. The first part focuses on the validation of the model, the experimental parameters used for validating the model are ignition delay time [134] and the peak flame temperature [152]. The experiments were conducted for particles in the range of 75-90 μm and the model is validated against the upper limit i.e. 90 μm. The second part extends the model for different diameters and produces a correlation differentiating the ignition mechanism for different particle sizes at varying O_2 concentrations.

4.4.1 O_2/N_2 cases

Bituminous coal

The sequence of the combustion for the Bituminous coal is illustrated in Figures 4.13–4.15, the simulation of the combustion process is upto the point where the volatiles have devolatilised completely. The overall burnout times of each particle are fairly high and thus it was decided to simulate the ignition process and the impacts it have on volatile combustion. There are two cases used as reference examples to describe the combustion behaviour at various time instance. The results of the two reference cases are for the bituminous coal simulated with FFCM mechanism under air conditions and 80% O_2 in N_2 which are showed in Figures 4.11 and 4.12. As there will be a small recirculation zone downstream of the particle the

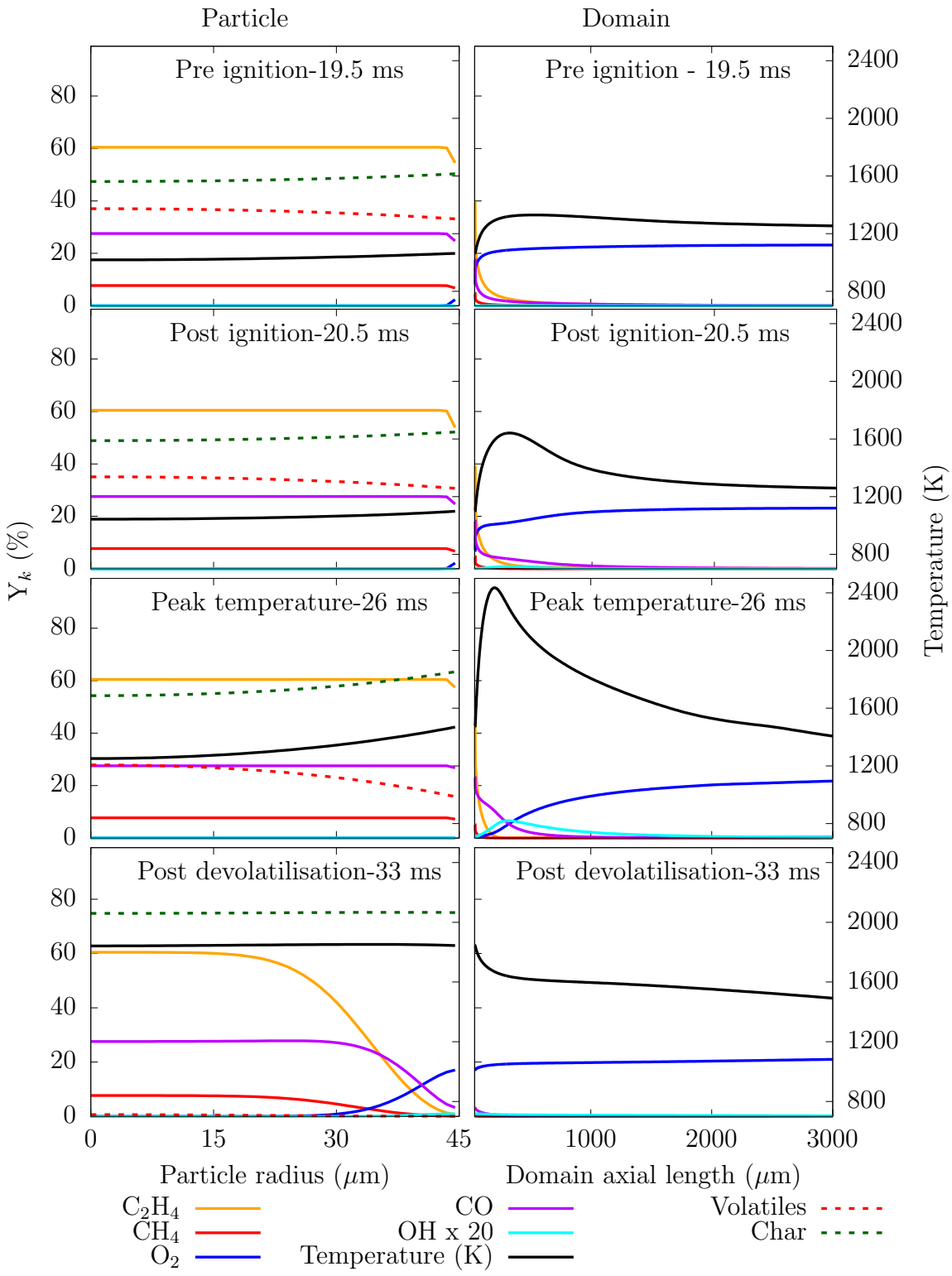

Figure 4.11: Temperature and species distribution in the particle and domain for air conditions at different time instances using FFCM. The plots are at the axial location of the geometry near the particle surface and the recirculation region (i.e. downstream of the particle).

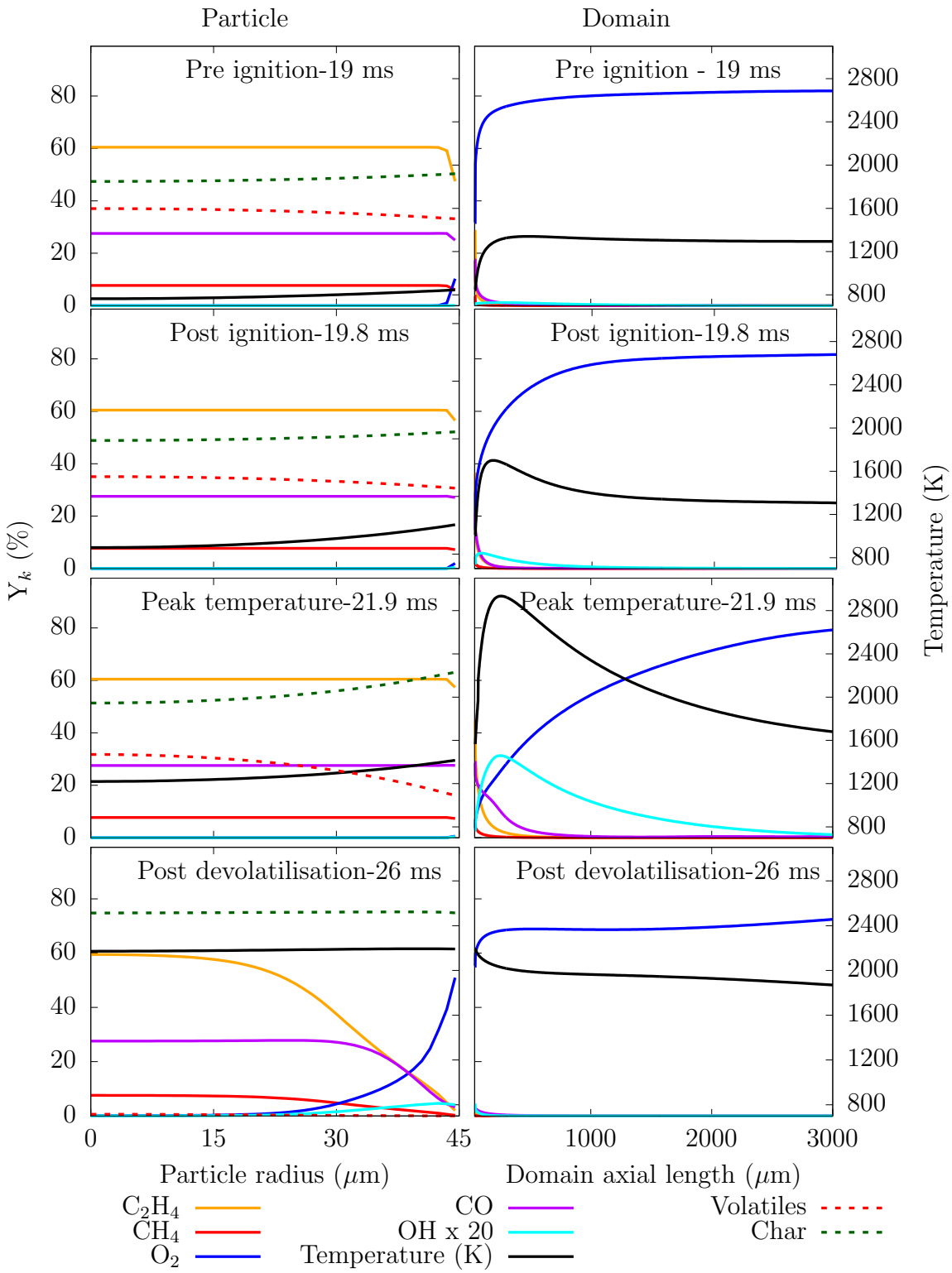

Figure 4.12: Temperature and species distribution in the particle and domain for 80% ambient O_2 conditions at different time instances using FFCM. The plots are at the axial location of the geometry near the particle surface and the recirculation region (i.e. downstream of the particle).

volatiles and the ambient O_2 mixes and ignite first in the wake formed downstream of the particle (right side of the particle). The region of interest was in the vicinity of the particle surface and around the small recirculation region down stream of the particle. Hence, it was decided to represent the profiles from the center of the particle to a small distance down stream of the particle (This was done to get a better understanding of ignition). The profiles in Figures 4.11 and 4.12 are along the axial plane of the overall geometry. (The results do not represent that the particle's thermo-conversion is symmetrical in nature. As the combustion of the volatile flame happens close to the particle, only a small region of interest is presented in Figures 4.11 and 4.12). The results in the Figure 4.13 describes the maximum temperature of particle and gas phase domain for simulations using FFCM (left) and Westbrook-Dryer mechanism(right). Figure 4.14 describes the maximum OH mass fraction produced in the particle and the domain when using FFCM and minimum reaction rate of CH_4(right) to describe the consumption rate of CH_4 while using Westbrook-Dryer mechanism. The normalised maximum volatiles and char mass loss is shown in Figure 4.15. The ignition mechanism is quantified based on the time taken for the volatiles to burn inside and outside the particle as described by Equation (4.37) in Section 4.3.2. In this section particle size of 90 μm is simulated varying from air to 80% O_2 in N_2 conditions. Each condition exhibited its unique combustion history but the general combustion behaviour stayed the same. The generic behaviour of the thermo-chemistry conversion of the bituminous coal in O_2/N_2 cases is discussed in this part of the section.

As the particle is placed in a hot environment, there is a steady increase in the particle temperature in the radial direction(from surface to the interior of the particle) due to ambient heat transfer to the particle (convective and conductive and the radiative heating at the surface). At first, the moisture evolves with respect to the temperature of the particle followed by the volatiles release, both dependent on the thermal gradient in the particle. The kinetics are such that there is very brief overlap between the moisture release and initiation of devolatilisation. The species are released in the pores of the particle, which pushes the gas inside the pores outside the particle into the domain. As the outer edge gets heated first, the early moisture and volatiles are released from the outer edge of the particle. It is observed in the simulation results that a small amount of devolatilisation from the edges of the particle is enough to saturate the particle pores with the volatiles and also create a small volatile cloud around the particle. The temperature of the evolved gas species and the particles are at lower temperature relative to the ambient gas, this forms a relatively cool envelope around the particle, which reduces the heating rate briefly. The increase in porosity and the reduction in heating rate, decreases the rate of transport of volatiles in the domain after initial devolatilisation which was also observed by Veras et al. [119]. It briefly promotes diffusion of O_2 back towards the particles and volatile cloud surrounding the particle, which was displaced initially. At this point the volatiles released are not in flammability limits because either the O_2 around the particle has not diffused significantly (decreased O_2 concentration) or the temperature of the volatiles is fairly low for ignition. As time increases, the ambient gas diffuses with the volatiles and gradually increases

the volatiles temperature and increases the O_2 concentration in and around the volatile species. Combustion is not established until the volatiles released from the particle reaches flammability limits. Once volatiles reaches flammability, there is a sudden rise in the domain temperature, which indicates ignition. The combustion of volatiles can also be signified by increase in OH mass fraction [120, 135, 327, 328]. Figure 4.14 shows the increase in OH mass fraction in the domain and particle just after the ignition. The volatile flame encircle the particle, the effect of rise in surrounding temperature results in accelerating the particle heating which in turn increases the volatile release from the particle and the inner core. This creates a feedback loop between volatile mass transfer, combustion of volatiles and particle heating which can be seen in Figure 4.15 where the devolatilisation is accelerated after the increase in temperature.

After ignition, the flame temperature in the domain reaches peak as the volatiles release in the domain peaks (Figures 4.13 and 4.16). The volatile release reduces which gradually reduces the flame temperature. Due to this phenomena flame from moves close to the surface with depleting volatiles and into the particle. Meanwhile, a certain amount of volatiles released in the core of the particle fail to reach the surface due to the resistance of the porous structure. While approaching peak temperature, a tiny amount volatiles burn inside the particle boundary, which generally happens close to the surface of the particle (primarily due to fast reaction of volatiles with the diffusing O_2). The reactions inside the particle is controlled by the O_2 diffusion and it can be said that the reaction is diffusion controlled. In case of air conditions the volatile flame is lifted in the particle wake and takes longer time to burn in the domain and it also takes longer time for flame front to reach the surface and inside the particle. This is denoted by the production of OH inside the particle which begin to increase after 6.5 ms (i.e. $\approx$ 26.5 ms) of combustion of volatiles in domain whereas in case of 80% O_2 in N_2 the OH starts appearing with a time delay of 1 ms signifying combustion of volatiles inside the particle.

The volatile flame front (reaction zone) shifts towards the particle surface from the domain with the following phenomena. It is observed in the simulation results that the peak temperatures are sustained for longer duration or the volatile flame in the domain burns for longer time with decrease in ambient O_2. As the reactivity is high for cases with higher ambient O_2 the volatiles released react faster which consumes the volatiles in the domain faster and reaches higher peak temperature but for a shorter time. The higher peak flame temperature also result in greater amount of volatiles loss (dotted red lines) from the particle when compared for the two reference cases in Figures 4.11 and 4.12 by comparing the instantaneous plots at respective peak temperatures. After reaching the peak temperature, the flame begins to cool down and reduces the heat transfer rate. As the volatile flame begins cooling down,the devolatilisation rate starts reducing, this results in decreasing the overall pressure inside the particle and the volatiles release rate in the domain starts reducing Figure 4.16. The depletion of volatiles in the domain results in further diffusion of O_2 towards and inside the particle and burn the volatiles released in the pores of the particles. This phenomena happens in both the reference cases but

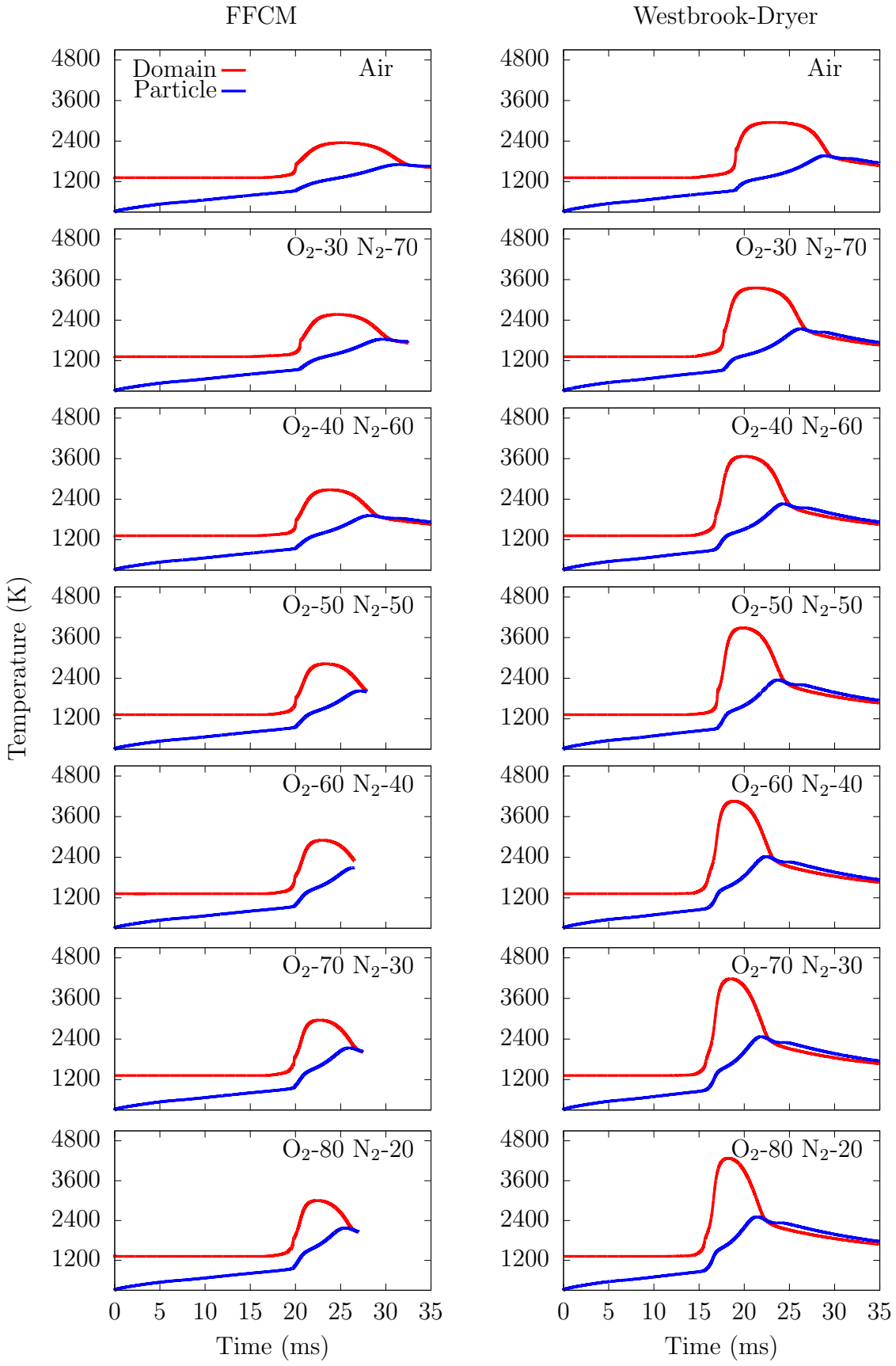

Figure 4.13: Maximum temperature of the domain and particle for Bituminous coal at different ambient conditions.

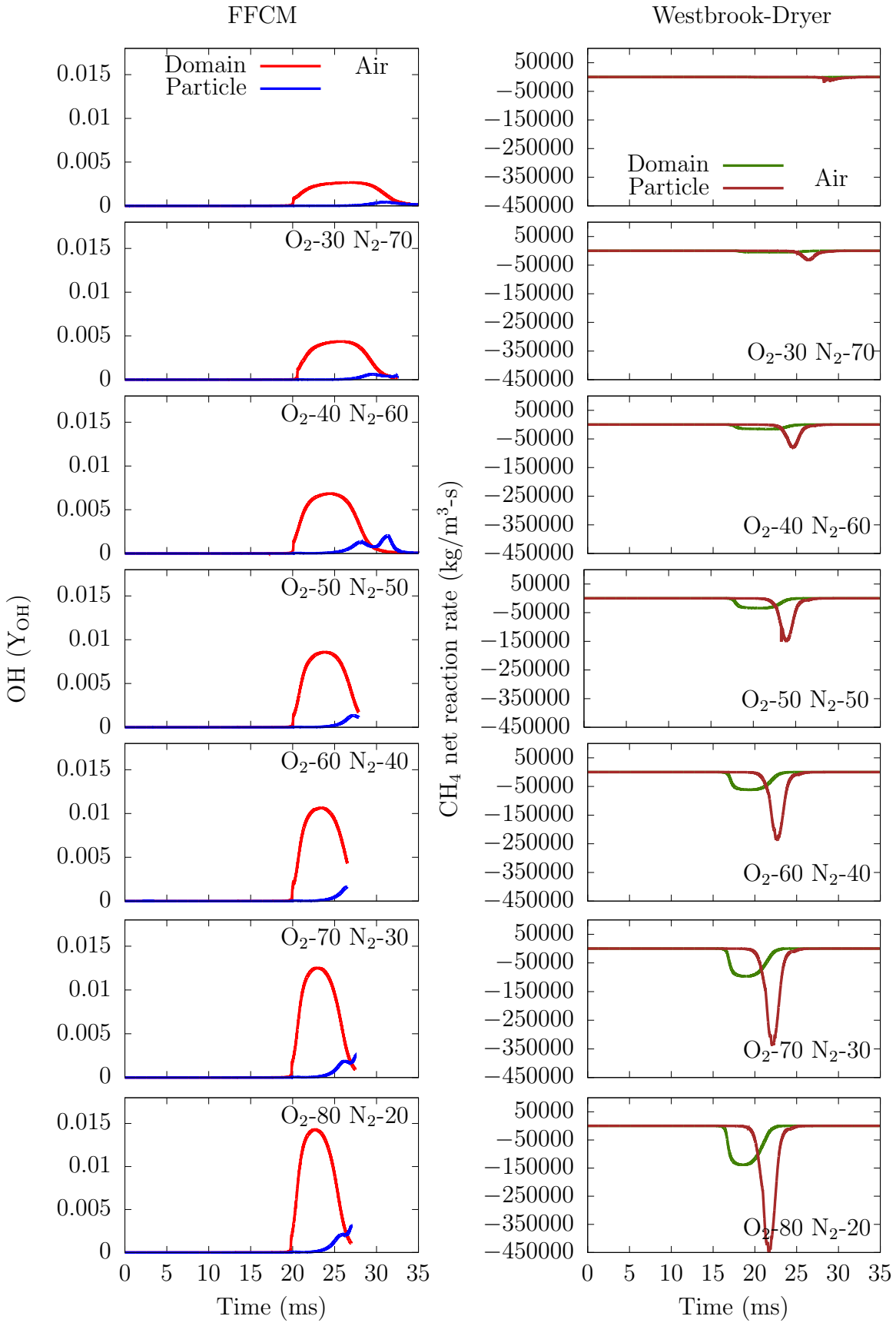

Figure 4.14: Evolution of OH (Detailed mechanism) and methane reaction rate (Westbrook-Dryer) for Bituminous coal.

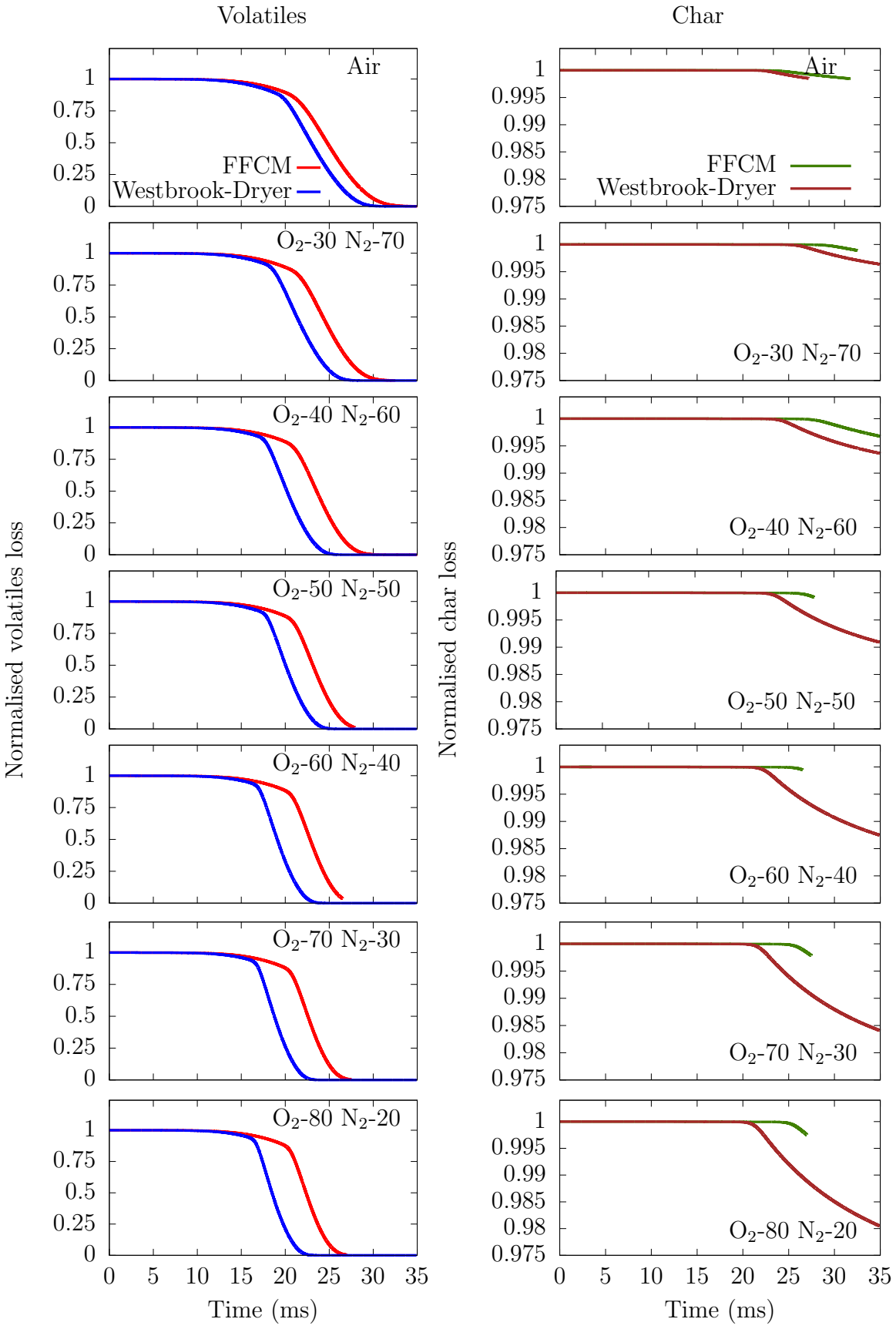

Figure 4.15: Volatiles and Char mass loss for Bituminous coal. The plots are obtained using maximum value of volatiles in the particle. This provides an insight into impact of ignition on the particle.

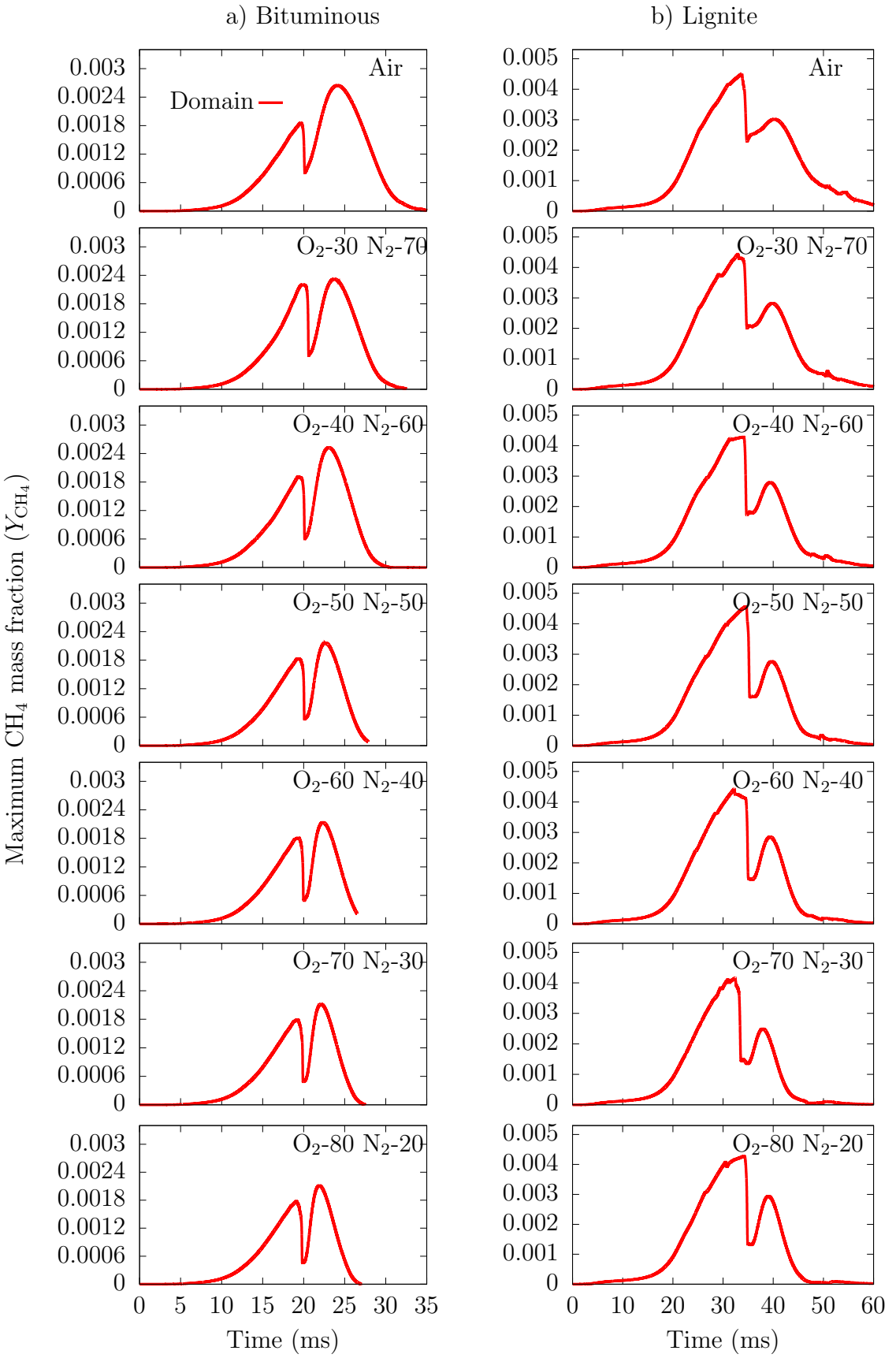

Figure 4.16: Maximum methane mass fraction in the domain for a) Bituminous and b) Lignite

as the volatile flame is sustained for longer in the domain for air conditions, the amount of volatiles burn in the particle is much lower compared to the case of 80% O_2 in N_2. This is signified by the production of OH in the particle before and after ignition. It can be observed in the instantaneous plots when the flame reaches it's peak temperature in Figures 4.11 and 4.12. A small amount of volatiles are combusted at the particle surface for ambient O_2 of 80% case (formed OH with a mass fraction of around 1 x 10^{-3}) but for air case it is negligible where OH mass fraction is $\approx$ 1 x 10^{-5}. This shows that the fundamental combustion behaviour is very similar but the combustion history is very different which allows the quantification of the ignition mechanism as homogeneous for air case and HO-HI for the latter. The increase in OH mass fraction in the particle is also shown in Figure 4.14, which confirms the combustion of volatiles inside the particle pores which combust inside the boundary of the particle surface. During the combustion of volatiles in both the phases there is feeble char mass loss at the surface (not shown in the Figures) which does not contribute significantly in the overall combustion process. As the volatiles are combusted, the products of volatiles combustion such as CO, CO_2 and H_2O diffuses in the particle pores. They react with char accelerating the char mass loss and increases the particle temperature. Figure 4.15 shows the initiation of char mass loss as the particle finishes the devolatilisation process. The contribution of char happens downstream in the furnace which increases the particle/flame temperature is not described as it does not play a vital role in the ignition stage of the particle. The ignition delay time are calculated/quantified based on the sharp increase in the domain/particle temperature and OH mass fraction.

Validation of the model

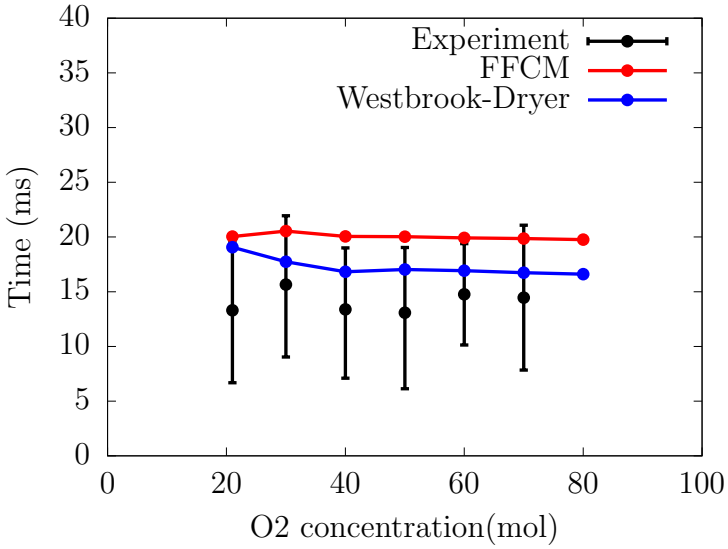

Figure 4.17: Model validation using reduced mechanism and detailed mechanism by comparing ignition delay time for Bituminous coal with particle size of 90μm(simulation) and 75-90μm(experiment).

The model is validated by comparing three parameters i.e ignition time delay, peak flame temperatures and the ignition mechanism. The results shown in the Figure 4.17 shows a comparison for the model prediction and the experimental result of ignition time delays for bituminous coal in O_2/N_2 environment. The model predictions for the ignition time delay are in good agreement with the experimental data for both the mechanism. The modelling predictions are within the error limits of the experimental results. The model predictions are in the range of upper error limits as the particle size in the experimental work ranged from 75-90 μm and the model predicts the ignition time delay for 90 μm. As stated previously the reduced mechanism predicts shorter ignition delay due to its increase in CH_4 mass fraction. The ignition time delay predicted by the FFCM reaction mechanism are approximately constant for different O_2 concentration, whereas there is a slight decrease in the ignition delay time for Westbrook-Dryer mechanism for cases with ambient O_2 between 21% to 40% and a constant time delay after that. The comparison provides confidence in the model and can be used with both the mechanism to predict the ignition delay times of individual coal particles.

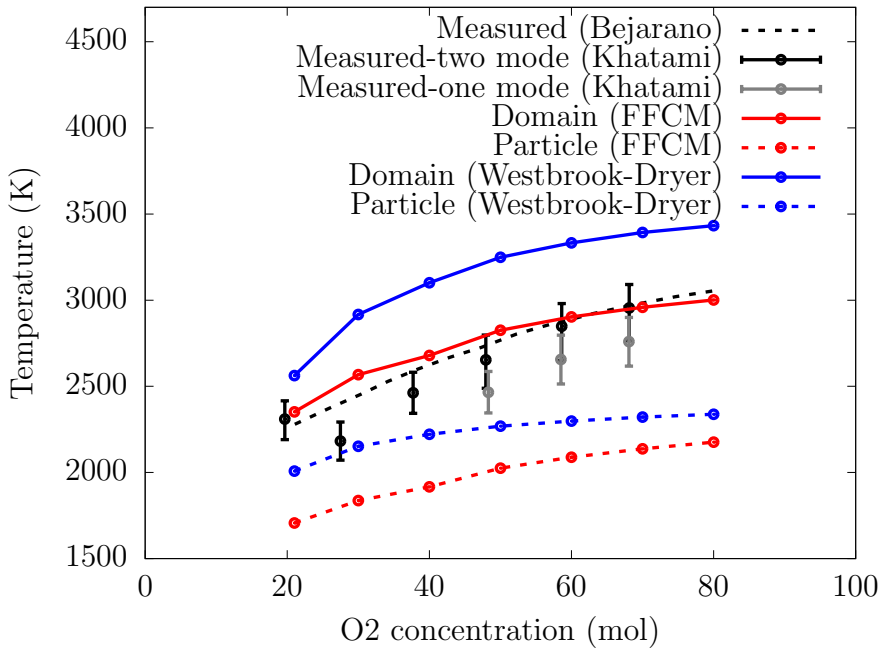

Figure 4.18: Comparison of Peak temperatures of domain and particle using FFCM and Westbrook-Dryer mechanism for Bituminous coal.

The validation of the peak temperatures predicted by the model for each condition provides confidence in methodology used in obtaining modelling pre-cursors. Levendis and co-workers presented the experimental data in multiple publications. The maximum flame temperatures were deduced using the three colour pyrometry for the bituminous coal which are presented in [152, 334]. The experimental ambient conditions used in [334] are same as the one used for model case set up except for the O_2 concentration and hence the results can be used for direct comparison.

The experimental ambient concentration of O_2/N_2 presented in [152] are not exactly the same but the trends of peak flame temperature are used for validating the methodology. The advantage of comparing the trends of the peak temperature is that Khatami et al. differentiates the peak temperatures with respect to the ignition mechanism. The comparison of the results between the experiments and the model are shown in Figure 4.18. There is an overlap in the measured values of the peak temperatures for one and two mode ignition which suggest that the two different mechanism display similar peak temperatures. The model with both the mechanism is able to predict the trend of increase in flame temperature with increase in O_2 concentration. The primary reason being increase in reactivity of the volatiles. The model predicts the peak temperatures for the particle size of 90 μm and thus the predictions are in the upper error limit of the trends. The model predictions with FFCM reaction mechanism are in excellent agreement with the measured results. The flame temperatures are over predicted when the reduced mechanism of Westbrook-Dryer is used. The main reasons for the limitations are discussed previously. A contributory factor could be the energy and mass balance for reduced mechanism had 9% error(i.e 9% increase in total calorific value) which is over predicting the flame temperatures.

According to the model definition for ignition mechanism, the coal particle ignites heterogeneously with increase in ambient O_2. The ignition is quantified primarily based on time taken for the particle heating rate (inflection condition) and the OH mass fraction or the consumption rate of methane which depends on the reaction mechanism used. The heterogeneous ignition is also quantified based on the inflection condition which is indicated by the particle heating rate. In 4.19 particle heating rate of two cases are described i.e. air conditions and 80% O_2 in N_2. In the case of air conditions the particle heating rate increases as the volatile flame in the domain encircles the particle and it drops until the domain reaches to its peak flame temperature. There is an inflection point around 25 ms, which confirms that flame front is away from the surface. It also confirms that in air conditions the particle ignites homogeneously.

In case of 80% O_2 in N_2 there are three inflection points on the heating rate curve which coincides with the formation of OH in the particle. The first one is after the volatile combustion in the domain due to brief combustion of volatiles inside the particle. This was possible as the higher O_2 concentration enables diffusion inside the particle even before the combustion of volatiles in the domain which was not in flammability limits and achieved flammability just after the initial combustion of volatiles in the domain. The first peak was brief and the heating rate dropped significantly quickly. The second inflection point signifies the flame front where the volatiles burn simultaneously in the particle and in the domain (confirmed by OH formation). The particle heating rate drops briefly as the reaction rate of the volatiles inside the particle drops (This is due to the end of devolatilisation where the pressure inside the particle drops and volatiles are not pushed towards the surface at the same rate as before) and picks up as the volatiles in the domain depletes completely. There is an increase in O_2 diffusion into the particle which

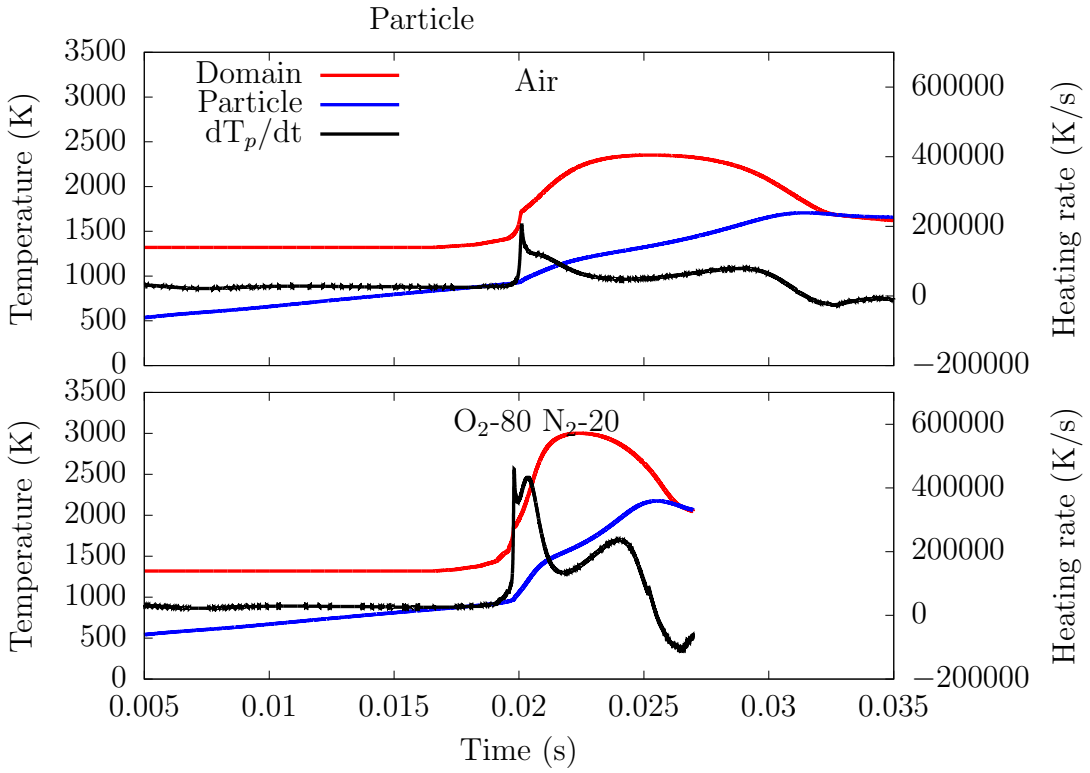

Figure 4.19: Particle heating rate used to quantify the ignition mechanism.

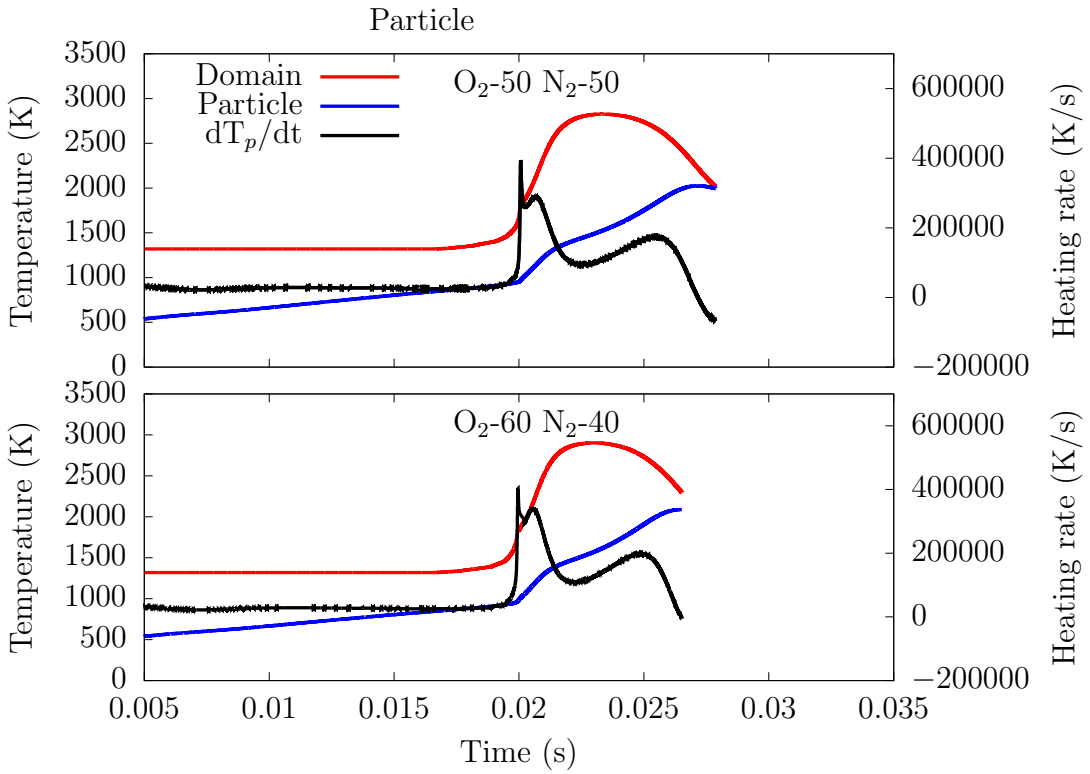

Figure 4.20: Particle heating rate to quantify the transition of the ignition mechanism.

reacts with the char and the volatiles inside the pores of the particle. The time scale for the presence of second inflection point is very small which according to the ignition criteria demonstrates that the particle experiences heterogeneous ignition. It should also be highlighted that particle experiencing HI(HO-HI) combust a much greater amount of volatiles inside the particle which can be seen by comparing the OH mass fraction produced during combustion of the particle. This is generally ignored when modelling combustion of particles in a large scale furnace.

Table 4.9: Comparison of the ignition mechanism between experiments and model

O_2 concentration	Ignition mechanism	
in N_2 background	Experiment [134, 152]	Model
21%	HO	HO
30%	HO	HO
40%	HO	HO
50%	HO or HI(HO-HI)	HO
60%	HO or HI(HO-HI)	HI(HO-HI)
70%	HI(HO-HI)	HI(HO-HI)
80%	HI(HO-HI)	HI(HO-HI)

The comparison for the ignition mechanism predictions are shown in 4.9. In ambient conditions of $\leqslant$40% O_2 concentration in N_2 background, homogeneous ignition of bituminous coal particles are predicted by the model which are in agreement with the experimental observations. The model is also able to predict the experimental observations of heterogeneous ignition of coal particle for $\geqslant$70% which is due to simultaneous combustion of volatiles and char. There is a transition of ignition mechanism between 40-70% O_2 concentration and the experimental observation suggests that coal particles displayed both the ignition characteristics due to differences in the physical and chemical properties. The model can only predict one mechanism for a certain condition and mathematically it is not possible to predict two ignition mechanism for one condition. The results in Figure 4.20 show similar heating rate curves for ambient O_2 of 50 and 60 % in N_2. The inflection points are apart by 1 ms i.e for conditions at 50 % ambient O_2 the increase in heating rate occurs at 23 ms and 22 ms for 60% ambient O_2. The model predicts the transition of the ignition mechanism for the bituminous coal happens between these two conditions i.e. 50-60% ambient O_2 which is in agreement with the observations and predictions made in [312]. Hence, the model is able to define the transition of ignition mechanism and performs well for differentiating between the ignition mechanism. The model predictions are in good agreement for the ignition behaviour of a particle and thus can be used for future investigation of ignition mechanism.

Impact of O_2 concentration

The increase in the O_2 concentration did not significantly affect the ignition delay times of the bituminous coal. The phenomena of volatiles released and a formation

of volatiles rich region around the particle is consistent because there is very little difference in the heating rate of the particle, which is attributed to the volumetric heat capacities of O_2 and N_2. The diffusion of O_2 in the volatiles and reaching flammability limits almost happens at similar times. The peak temperature of the volatile flame increases with increase in O_2 concentration making a brighter flame which matches with the experimental results [134, 142, 143, 152]. This is due to higher reactivity of volatiles with increase in O_2 concentration. The increase in reactivity of volatiles at higher O_2 decreased the overall burnout times of the volatiles or increase the consumption rate of volatiles, resulting in increasing the peak of OH mass fraction in the domain. The increase in peak temperature also results in quicker devolatilisation (post ignition) and this increased the volatiles release rate from the particle into the gas phase(which also includes the pores in the particle). The higher volatiles reactivity implied that the volatiles are consumed at a higher rate in the domain. This is evident in Figure 4.16 where the second peak of CH_4 reduces with increase in O_2. It also explains the observation made in the experiments that there is reduction in the volatile flame size as the volatiles burn very close to the particle [152]. The increase in O_2 also increases the diffusion of O_2 inside the particle, resulting in the volatiles combusting inside the particle and the initiation of char mass loss. It is evident in Figure 4.14 that the OH formation inside the particle happens early with increase in ambient O_2. The char and the volatiles inside the particle competes for the diffused O_2 inside the particle leads to a brief time of simultaneous combustion, which can be seen from Figure 4.15.

The particle size chosen experimentally exhibit a complete transition in ignition mechanism and thus there were instances when particles examined in certain conditions displayed multiple mode of ignition. This has been attributed to physical and chemical properties of the particle. At higher O_2 content($\geqslant$50%) the experimental observation states that the coal displays both ignition mechanism i.e. HO-HI or HO. It is clear from the model that there is this point where the particle burns simultaneously but it ignites first in the domain. Experimentally, it is very difficult to capture this phenomena as homogeneous flame burns very close to the particle at higher O_2 concentrations and then it switches to simultaneous combustion very quickly ($\approx\leqslant$ 3ms). In addition, the flames burns bright which makes it difficult to capture such a phenomena. The general trend from the model suggests that there is simultaneous combustion at low O_2 concentrations but the time overlap is much greater than the cases with higher O_2 due to lower reactivity and longer burnout times in the domain. This reduces the O_2 diffusion in the particle. As a result the simultaneous combustion of volatiles is feeble that it is no significant enough to be detected during visualisation but with increase in O_2 content and increase in O_2 diffusion, this phenomena amplifies and leads to quicker simultaneous combustion and reduction in the time for observation of a relatively smaller volatile flame. This particular model is able to clear the doubts presented experimentally regarding the reduction in the flame size and the simultaneous combustion behaviour of the particle at higher O_2 concentrations. According to the criteria set for defining ignition mechanism in the model, the model is able to define the transition points where the ignition mechanism changes for bituminous coal as later shown in Figure 4.23.

In summary the increase in O_2 does not impact the ignition time delay but increases the O_2 diffusion. The increase in O_2 diffusion increases the tendency of the particle to ignite heterogeneously. The other contributory factor of heterogeneous ignition is the shorter volatile burnout times due to higher reactivity which increases the O_2 diffusion in the particle.

Impact of the reaction mechanism on the model predictions

A major advantage of using the reduced mechanism is reduction in the compuatational time. It also makes this model more applicable for industrial use where time and computational power are massive constrains. In terms of volatiles evolved, there is an increase in mass fraction of methane for Westbrook-Dryer mechanism when compared to FFCM because the mechanism does not include species such as H_2 or any heavy hydrocarbons. This increases the amount of CH_4 around the particle during devolatilisation and predicts an early ignition when compared to the FFCM mechanism as heavy hydrocarbons take up more time to reduce in simpler hydrocarbons. The peak flame temperature predicted by the global mechanism are very high and not practical. Apart from higher CH_4, the contributory reason for high temperature might be neglecting reactions for H_2 in the global mechanism [335]. Higher flame temperatures leads to quicker devolatilisation and early volatiles burnout. This also results in early char mass loss as shown in Figure 4.15.

As mentioned previously the particle at higher O_2 content displays both simultaneous (one mode) ignition as well as gas phase ignition and then char loss (two mode). Figure 4.18 shows a comparison of the peak flame temperature with the model. The FFCM mechanism are in excellent agreement with the prediction with the flame temperatures, whereas Westbrook-Dryer mechanism over predicts the flame temperature. It was difficult to distinguish the ignition type at higher O_2 content because of the quicker switch to volatiles burning inside and close to the surface of the particle. The experimental results shows that the maximum difference between the upper limits for peak temperatures of the two different modes are around $\approx$ 200 K. There are also instances when the limits of experimental peak temperature overlap which shows that there was not much to distinguish between the two ignition mode experimentally. The difference in the temperature maybe due to reduction in the volatiles content for those particles exhibiting one mode which was explained by Howard and Essenhigh [148]. The particle size used in the calculation are for 90 μm and hence the results are compared with the upper limits of the error bars in Figure 4.18. The peak temperature predicted by the FFCM model are in 5-8 % error for HO-HI (one mode).

A major limitation of using global mechanism is the absence of OH radicals in the reaction which fails to signify detection of ignition mechanism. Instead the net reaction rate of CH_4 is monitored which provides an insight to burning of volatiles inside and outside the particle as shown in Figure 4.14. An increase in the reaction rate of CH_4(i.e negative) suggests the beginning of the ignition and consumption

rate of CH_4. The ignition mechanism can also be quantified based on the time history of the consumption rate of CH_4 in the domain and particle. The time gap between which volatiles ignite in the domain and the volatiles burning inside the particle reduces with increase in O_2 content (similar to OH monitoring). The results show a similar trend as FFCM in predicting the ignition mechanism. The only major limitation for using the reduced mechanism was the prediction of volatile species which over predicts the CH_4 released and that drives the flame temperature to non practical levels.

Model extension to different particle sizes

The comparison of peak flame and particle temperatures for the four particle sizes are shown in Figure 4.21. There is a steady increase in peak temperatures with increase in particle diameter and O_2 concentration. The temperature predictions with Westbrook-Dryer mechanism are unrealistic and are not reliable. The FFCM mechanism provide a more realistic peak temperatures for different particle sizes. The increase in flame temperatures are attributed to increase in volatile content with increase in size. Accompanied with the particle size distribution, the predictions of the peak temperatures provide an insight into the operating temperatures of the coal furnace. This can help in modification of burner design or changing the aerodynamics to control the emissions (e.g. NOx) of the furnace.

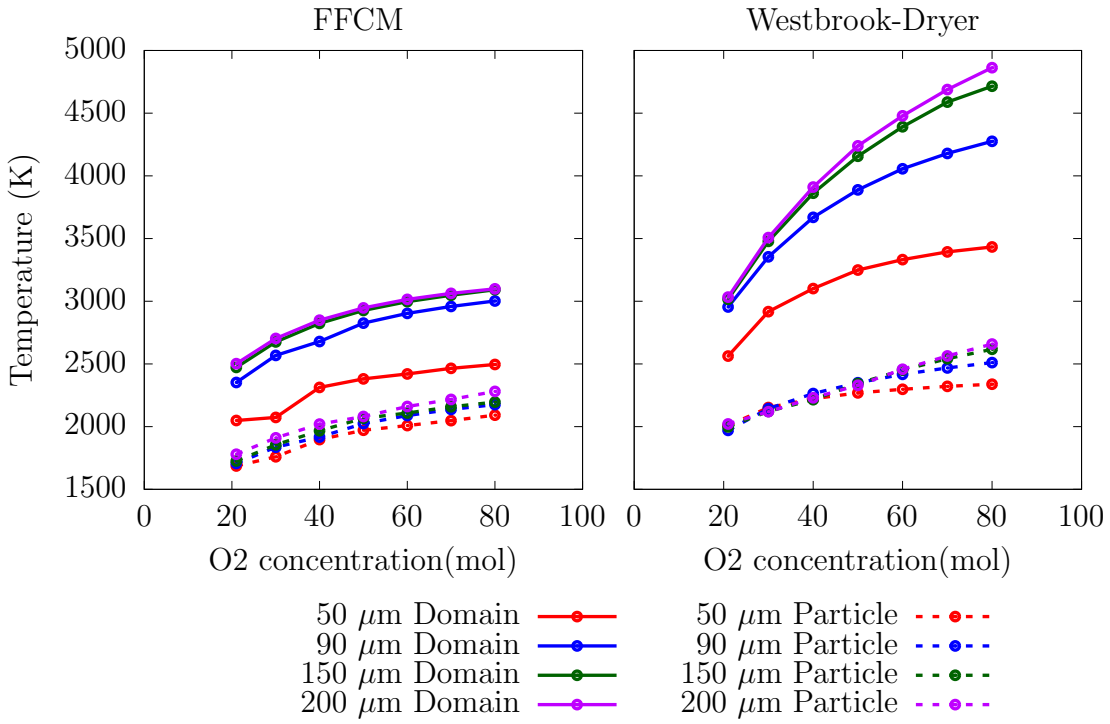

Figure 4.21: Peak temperatures for different particle size for bituminous coal using FFCM kinetics (left) and Westbrook-Dryer(right).

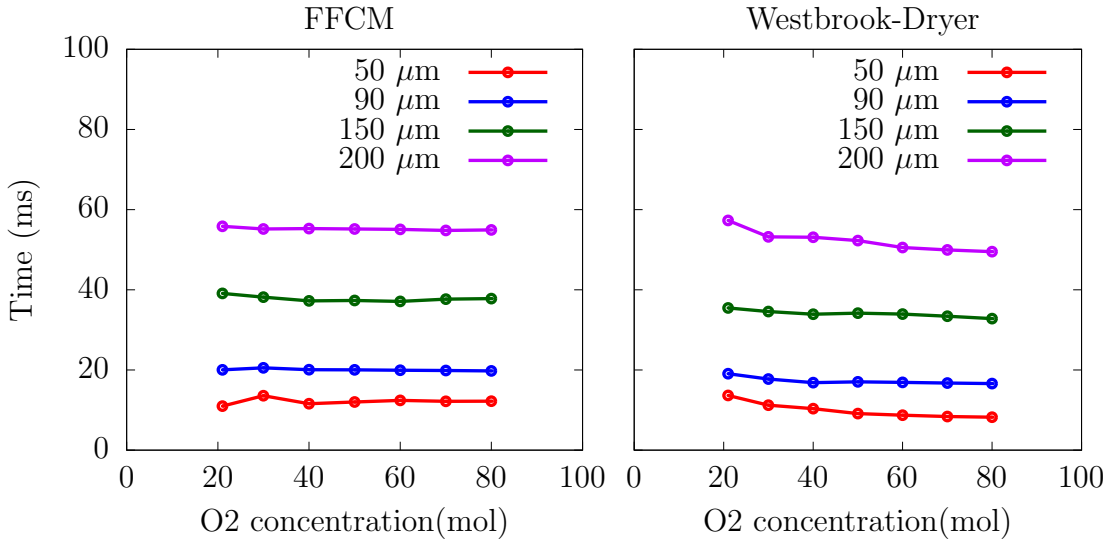

Figure 4.22: Ignition delay times for different particle size for bituminous coal using FFCM kinetics (left) and Westbrook-Dryer(right).

The variation in particle size also impacts the ignition delay time of the particle. The ignition delay time predictions for the four particle size are presented in Figure 4.22. There is a general trend of increase in ignition time delay with increase in size. The other evident trend is that the ignition time delay stays approximately constant for same particle size with increase in O_2 concentration. The parameters influencing the ignition delay times are the particle heating rate, the volatile content and the velocity of the particle (In the model, the velocity of the gas). The primary factor decreasing the heating rate is the increase in surface area of the particle (Equation (2.21)), and the factor accelerating the heating rate is the velocity of the particle as it travels faster into the furnace. It should be noted that in the model, the ambient gas which passes over the particle at higher velocity and thread through the cooling region around the injector faster. The results suggest that the impact of increase in the surface area reduces the heating rate, which results in longer ignition time delay. The reduction in heating rate reduces the volatile release rate and hence increase the time taken for the volatile concentration to reach above lower flammability limits. Hence the increase in particle size also increases the ignition temperature required as the bigger particles will require longer times and will travel further in the furnace (In the model it ignites at a higher ambient gas temperature which flows over the particle). Another contributory factor for increase in time is the transport of volatiles as it has to overcome the particle resistance and the volatile transport reduces the heating rate(as observed in Section 4.3.3 which increases with particle size. The increase in particle size (increase in volatile content) increases the volatile burnout time and there is a reduction in burnout times with increase of O_2 concentration due to increased reactivity.

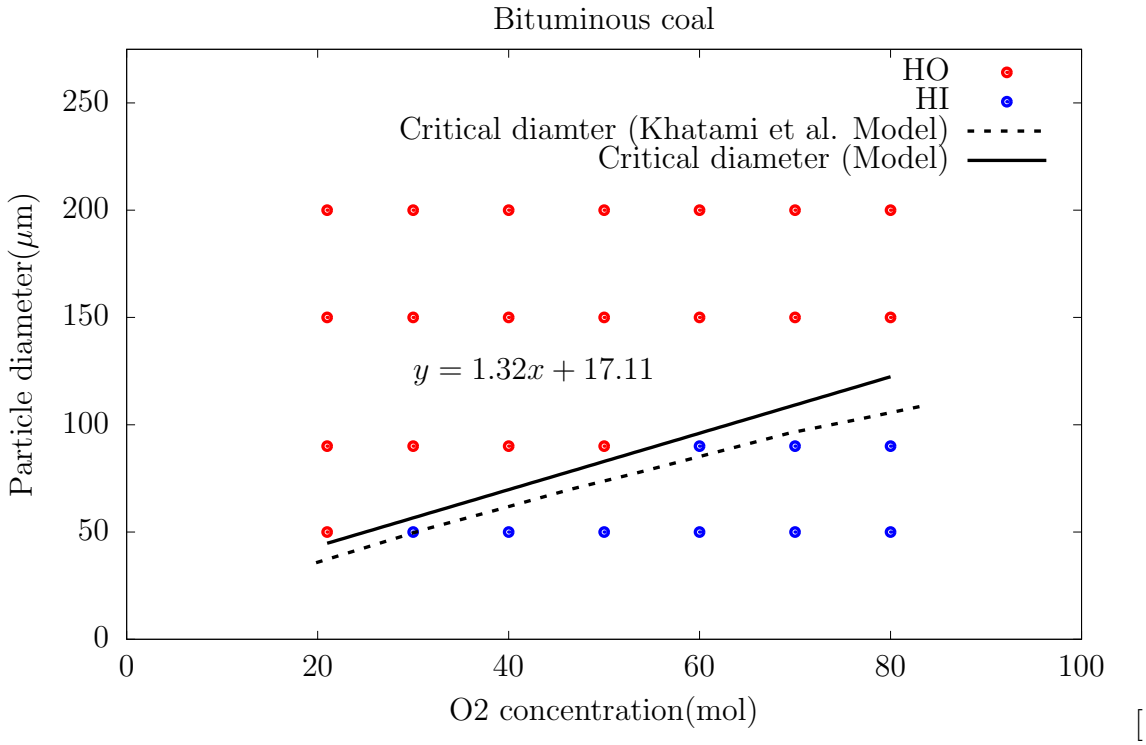

Figure 4.23: Ignition mechanism and correlation of critical particle diameter for the bituminous coal particles in O_2/N_2 conditions.

The concept of critical particle diameter was introduced by Howard and Essenhigh [148], where they reported that the ignition mechanism is a function of particle size. The particles below or equal to the value of critical particle diameter ignites heterogeneously(HO-HI) whereas above that ignites homogeneously. The concept was based on the lack of volatiles concentration enveloping the particle whose reaction zone is close to the particle surface for a given particle size, it enables diffusion of O_2 in the particle initiating simultaneous combustion of char and volatiles on or inside the particle surface. A correlation is developed between the ambient O_2 and particle size based on the assumption that the relationship between ambient O_2 and particle size is either linear or a quadratic fit. The basic methodology to produce the relationship is that the critical diameter fit should pass between the ignition transition points. In case of bituminous coal, the transition of ignition mechanism happens twice. Once for 50 μm and second for 90 μm which enables a linear correlation. The particles in a coal furnace are fired with a size distribution for a better control over the flame aerodynamics. The results highlighting the ignition mechanism and the critical particle diameter with increasing O_2 concentrations for the four particle sizes is shown in Figure 4.23. A limitation of this correlation is that the heterogeneous ignition is accounted for particle burning simultaneously and not for a particle experiencing pure char ignition/combustion due to lack of volatiles or volatiles diffusing away from the particle surface. Inaddition, Howard and Essenhigh [148] discovered that such behaviour is observed for particle sizes of $\leqslant 15\mu$m. Hence, it important to account for the this behaviour which generally

depends on grindability of the coal, burner optimisation and the particle size distribution (which determine the mass fraction contribution of small particles) when applying this correlation.

The transition of ignition mechanism for particle diameter of 90 μm has been discussed previously. The higher volatile content for particle diameter of 150 and 200 μm illustrate consistent homogeneous ignition. The particle diameter with 50 μm ignite heterogeneously except at O_2 concentration of 21% (molar) which ignites homogeneously. The tendency of smaller particles to ignite heterogeneously was also observed in [98, 119, 148, 336]. The lack of volatiles and increase in O_2 content (increase O_2 diffusivity) results in simultaneous combustion of volatiles inside and outside the particle. At 21% O_2 the diffusion is longer in the particle and results in favouring the homogeneous ignition. The model is able to quantify the ignition mechanism across different conditions as shown in Figure 4.23 for bituminous coal. It illustrates that the smaller bituminous coal particles are sensitive to ignition mechanism because of its volatile content, heating rate and O_2 concentration. The capability of model to quantify ignition mechanism produces a linear correlation for critical particle diameter. A correlation which differentiates the ignition mechanism with respect to particle size and O_2 concentration. The correlation obtained can be used in quantifying the ignition mechanism and improving the ignition/combustion modelling of pulverised fuel burners, which burns a variety of particle sizes. The critical diameter correlation was also modelled by Khatami and co-workers [312] using the equation proposed by Howard and Essenhigh [148]. That particular model requires few key experimental values such as ignition time delay, ignition temperature, O_2 around the particle surface and the amount of volatiles evolved prior to ignition. The correlation predicted by Khatami and co-workers is presented in Figure 4.23. The correlation is very close to the predictions by the single particle model in this chapter. The model used by Khatami et al. requires accurate experimental parameters, and it is tricky to investigate a novel coal. In such scenario the methodology used in this chapter can be used to predict the correlation of critical particle diameter. There is another limitation for applying this correlation in a simulation of a pilot scale facility. It is difficult to quantify for the amount of volatiles burning inside the particle. This limitation is overcome by making a few modelling assumptions and this is discussed in the next chapter.

Lignite

The tendency of particle fragmentation increases with decrease in coal rank. The particle fragmentation is attributed to the mechanical strength of the particle, the porosity, particle surface structure and the chemical composition. The Scanned Electron Microscope (SEM) results show that the lignites before combustion have rough abrasive surfaces and further analysing a partially devolatilised particle suggests that the cracks on the particle increases compared to its raw form [312]. Other studies in which lignite particles were tested experimentally after the removal of moisture demonstrated that the particles displayed fragmentation on further heating which is because of the increase in the porosity (which also increases the pres-

sure from the devolatilised volatiles on the walls of the particle) which results in increasing the cracks on the particle surface [337, 338]. This model does not take any fragmentation into consideration due to lack of modelling data (mechanical strength of the coal particles at high temperature) in the literature but it should be able to detect the ignition mechanism and the ignition delay time accurately as this phenomena will be dominated by the combustion of the volatiles.

The combustion sequence of the lignite coal is shown in Figures 4.16 and 4.24–4.26. The combustion sequence and the general trends for the combustion of lignites are similar to the one of bituminous coal. The ignition process for the particle diameter of 90 μm using FFCM mechanism is discussed in this part of the section. The moisture content and the initial porosity of the lignite particle is higher when compared to bituminous coal. This results in greater mass loss of the particle in shorter time and reduction in the heating rate of the particle. The heating rate is reduced because of the water released from the particle in the domain at lower temperature which reduces the average ambient temperature around the particle. This results in increasing the time for devolatilisation and eventually the ignition of the particle.

As the devolatilisation begins the volatiles from the particle outer edges are ejected in the domain but fail to ignite as they do not reach the lower flammability limits. A reason being the high moisture content which dilutes the O_2 diffusion in the volatiles ejected and delaying the ignition process. The longer ignition delay increases the amount of volatiles released in the domain when compared to the bituminous coal, which is evident in Figure 4.16. The higher mass loss of the particle and longer ignition delay time increases the porosity of the particle which enhances the diffusion of the O_2 into the particle. The combustible volatile and O_2 coexisted inside the particle as the particle temperature is relatively low for eith volatiles or char to react. This phenomena increases the probability of simultaneous ignition/combustion of volatiles inside and outside the particle. Once the O_2 diffuses with the volatiles inside and/or outside the particle and reaches flammability limits, ignition is achieved. This is signified by the increase in OH as shown in Figure 4.25. In air conditions the particle ignites homogeneously as small delay is evident in the combustion of volatiles inside the particle. The particle simulated in O_2 concentration of 30% is in the transient phase and is close to be quantified as igniting homogeneously but the results suggests that they ignite heterogeneously. The onset of ignition for the lignite particles $\geqslant$ 30% is due to simultaneous burning of volatiles inside and outside the particle, i.e. heterogeneously.

After ignition the overall flame temperature increases and undergoes the feedback loop of increase in devolatilisation rate similar to bituminous coal. Experimentally, the particles fragments just after the ignition and spherical flames are observed. It results in increasing the O_2 available for volatiles and fragmented char to combust. As the fragmentation is not accounted in the model, the volatiles inside the particle are not exposed to the ambient O_2 (increase in O_2 mixing). Hence, the peak flame temperatures predicted by the model will not be accurate after the ignition is achieved for lignites. The main objective of the model is to predict the ignition mechanism accurately and hence this limitation of modelling ignition of lignites are

acknowledged at early stage of the analysis. The lignite cases are simulated beyond the devolatilisation of the lignite particle to investigate the fate of volatiles which may impact the peak temperature of the flame.

Impact of the ambient O_2 concentration

The higher moisture content displaces the O_2 further away from the particle which was saturated inside the pores and concentrated around the particle. The volatiles released from the outer edge, fails to reach the flammability volumetric fraction due to the relatively cooler gas surrounding the particle and the lack of O_2 concentration. The increase in the ambient O_2 concentration enhances the diffusivity of the O_2. The ignition delay time remains approximately constant, which can be attributed to the heating rate which stays constant during the initial heat transfer phase. The constant heat transfer implies similar devolatilisation rate and hence it releases similar amount of volatiles (see Figure 4.16). The higher rate of O_2 diffusion with the volatile inside and outside the particle does not reach achieve faster flammability and hence did not impact the ignition delay times. The longer delay in ignition accompanied with increase in O_2, increases the tendency of the volatiles to combust simultaneously/heterogeneously with increase in O_2. It is evident in Figure 4.25 where the time gap for the increase in OH mass fraction inside and outside the particle during the ignition almost reduces to zero with increase in ambient O_2. The comparison between the model predictions and the measured values for the ignition delay times are shown in 4.28. It shows that the model predictions and trends using FFCM mechanism are in good agreement with the experimental values. The model can be used to predict the ignition time delays for lignites.

The increase in ambient O_2 also reduces the volatiles burnout time in the domain, which results in quicker depletion of volatiles in the domain. The shorter burnout times also increases the O_2 diffusion in the particle. This increases the rate of combustion of volatiles and the amount of volatiles combusting inside the particle which is illustrated by the OH peaks inside the particle. The combustion of volatiles inside the particle after the ignition coincides with the char consumption of the outer surface of the particle. The increase in O_2 content also increases the overall reactivity of the volatiles, which increases the peak flame temperature. Comparing the peak flame temperature with the experiment in Figure 4.28 shows that the model underpredicts the flame temperature. The difference in the peak temperature is due to the exposure of the volatiles to the ambient O_2 after the fragmentation, which increase the domain/flame temperature. The maximum particle size after fragmentation were 30 μm. In the model the particle resistance still exists (volatiles ejection in the domain and O_2 diffusion in the particle) which results in slower combustion rate of the volatiles and longer overall burning rate of the volatiles (which includes the combustion of volatiles inside the particle as well). This suggests that the model predictions of volatiles burning inside the particle after the ignition are underestimated and will require to incorporate a fragmenting model which enhances O_2 mixing with the volatiles/char.

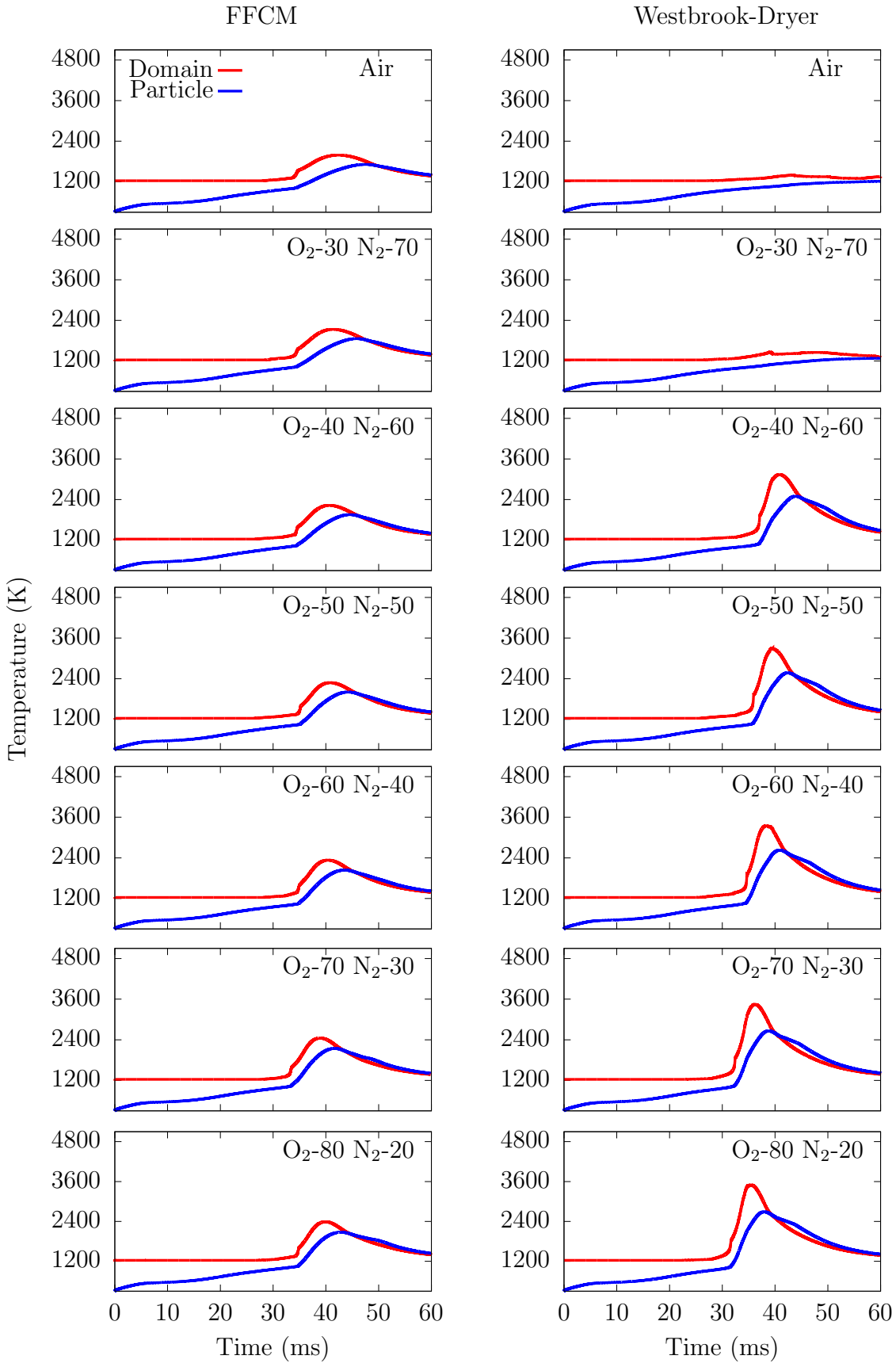

Figure 4.24: Maximum temperature of the domain and particle for Lignite at different ambient conditions.

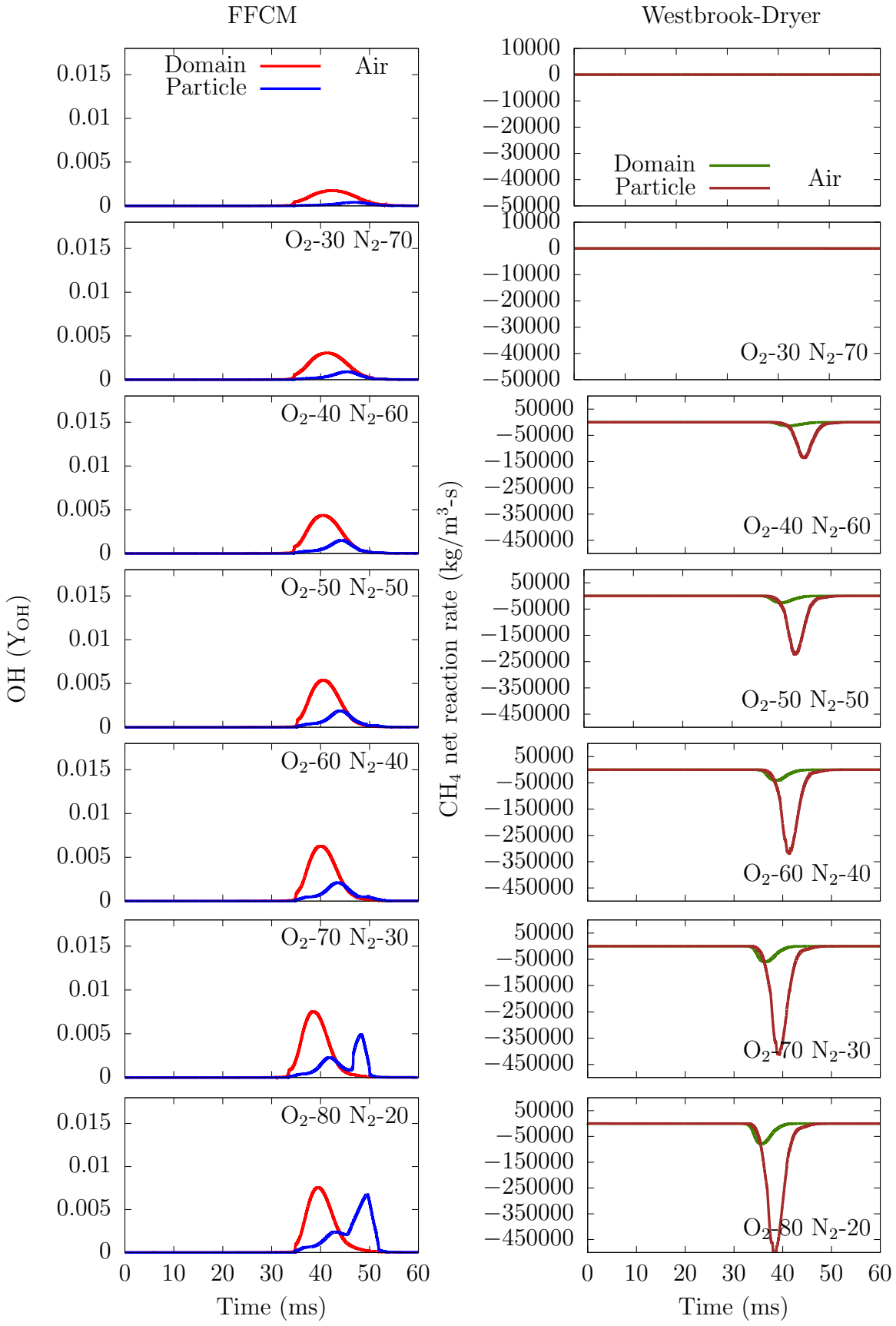

Figure 4.25: Evolution of OH (FFCM) and methane reaction rate (Westbrook-Dryer) for Lignite.

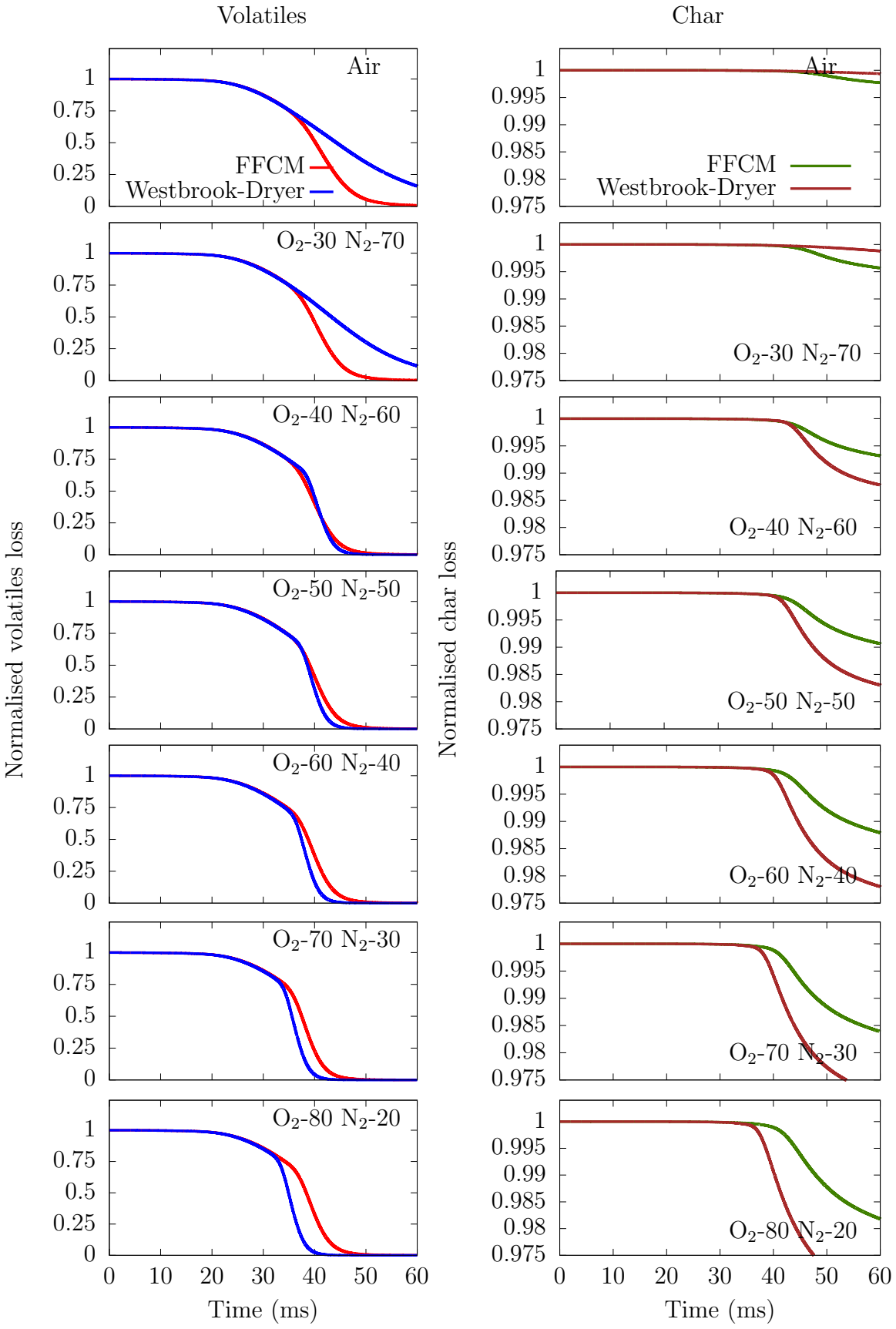

Figure 4.26: Volatiles and Char mass loss for Lignite.

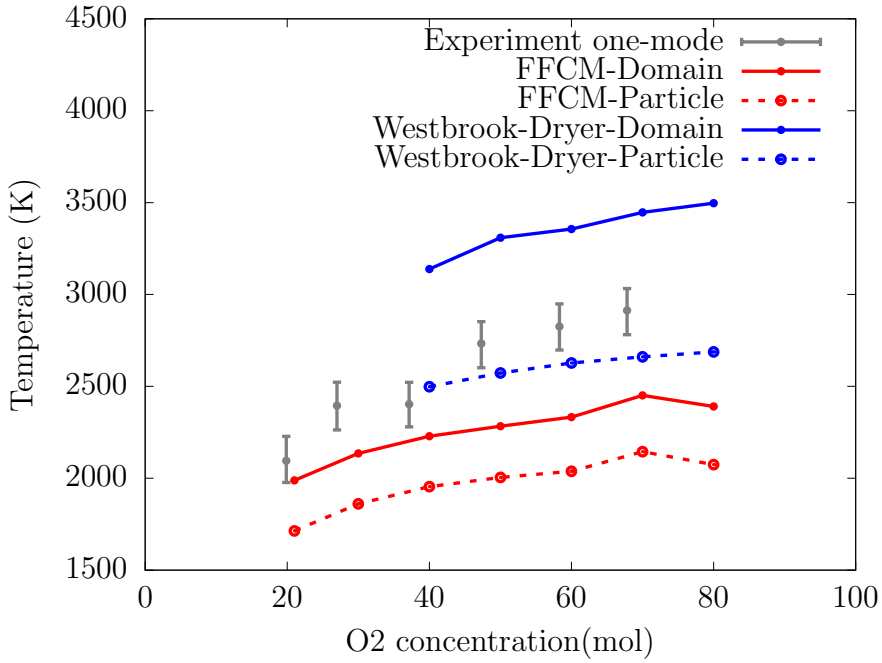

Figure 4.27: Comparison of Peak temperatures of domain and particle using FFCM and Westbrook-Dryer mechanism for Lignite.

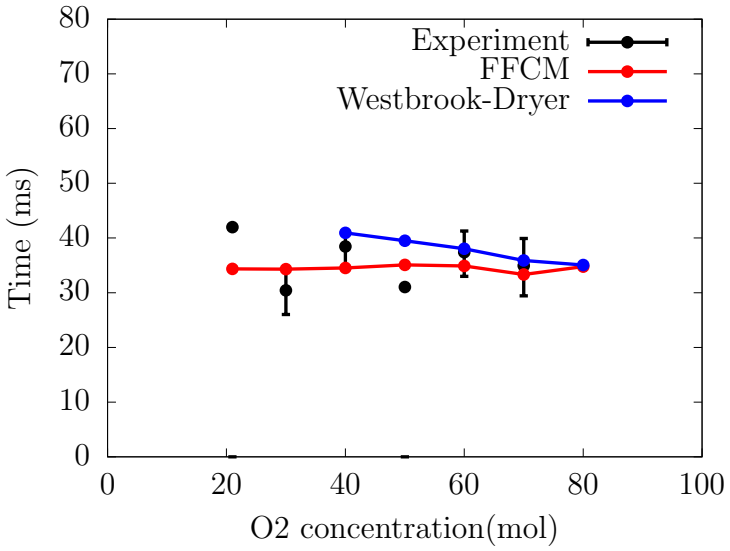

Figure 4.28: Model validation using reduced mechanism and detailed mechanism by comparing ignition delay time for Lignite with particle size of 90μm(simulation) and 75-90μm(experiment).

In summary, the increase in O_2 increases the lignite particles to ignite heterogeneously. The increase in the O_2 has no significant impact on the ignition delay times but the longer delay enhances the O_2 diffusion in the particle which promotes heterogeneous ignition. The increase in O_2 concentration increases the rate of combustion of volatiles after the ignition, which in turn increases the peak flame temperatures. The peak flame temperatures predicted by the model are under predicted because the fragmentation of the particles are neglected in the model.

Impact of the reaction mechanism on the model predictions

There are similar advantages and disadvantages for using Westbrook-Dryer mechanism as discussed in section above for bituminous coal. The model with Westbrook-Dryer mechanism is not capable of simulating the combustion of the volatiles in few conditions and fail to ignite in certain conditions. It evident from Figure 4.25 which describes the net reaction rate for CH_4 inside and outside the particle. It demonstrates that the CH_4 consumption rate increases for the particles in ambient O_2 >40%. The global mechanism fail to detect any ignition at O_2 concentrations of 21% and 30%. This is due to high moisture content around the volatiles which dilutes the O_2 diffusion. Minotti et. al [339] has shown that Westbrook-Dryer mechanism fail to ignite at lower temperatures and/or at various equivalence ratios. The higher moisture content around the particle also increases the ignition delay time prediction as seen in Figure 4.28 where the global mechanism takes longer to predict ignition delay compared to FFCM mechanism.

The dilution of O_2 results in low concentration of O_2 with the volatiles and the O_2 does not meet the temperature and the equivalence ratio criteria required for the global reaction mechanism to activate ignition. Hence, the volatiles evolved failed to meet the volumetric concentration required for the ignition and diffuse away which results in no volatiles combustion. The model suggests that the O_2 diffuses in the particle and manages to initiate char mass loss igniting the particle heterogeneously but at a much longer time dealy. This particular time delay is longer when compared to the experiments and the predictions with FFCM mechanism. Thus the predictions are not accurate at lower O_2 concentration. The ignition time delay predicted for the ambient conditions O_2 $\geq$40% are well within the error range and suggests that they are reliable. The ignition delay times for reduced mechanism are higher when compared to FFCM model because of the limitations of the conditions it can be used to simulate [339] and absence of few species. There is a small decrease in the ignition time delay for increase in O_2 ($\geq$40%) which suggests that the increase in O_2 also enhances the O_2 diffusion and the volatiles reach flammability limits quicker.

The cases with the ambient conditions O_2 $\geq$40% over predicts the peak flame temperatures for global mechanism as observed in case of bituminous coal. The reasons for the over predictions are similar to the one discussed for bituminous coal. This shows that for the O_2/N_2 cases, the Westbrook-dryer mechanism is not suitable to simulate all the conditions for the lignite coal. However, it does manages to simulate few of the scenarios and predicted the ignition delay times well for those

limited cases. The limitations of using the Westbrook-Dryer mechanism are evident and hence it is not recommended in investigating ignition for lignites. The model with FFCM mechanism are in excellent agreement with the experimental results and thus it can be used for investigating ignition for lignites.

Ignition mechanism and correlation for critical particle diameter for the lignite.

The comparison between the model predictions and the experimental observation for ignition mechanism of lignite particles with 90 μm is shown in Table 4.10. The experimentally observed heterogeneous ignition were due to simultaneous combustion of volatiles and the char particles followed by fragmentation. The experimental results for O_2 concentration between 50-80% exhibit consistent heterogeneous ignition. In case of particles igniting between 21-40% O_2 in N_2, the particles sometimes displayed a brief, non-sooty and faint volatile flame burning which indicate homogeneous ignition of the particles. The observation were not consistent for all the particles which indicates that the particle were transitioning to Heterogeneous from Homogeneous ignition. The modelling results demonstrated that the particle transits to heterogeneous(HO-HI) ignition at ambient O_2 concentration of $\approx$ 30%. The results for the lignite particles igniting at 30% O_2 in N_2 were close to be quantified as homogeneous ignition but according to the definition of inflection condition (accompanied with increase in OH mass fraction in the particle) it was quantified as heterogeneous ignition. The transition predictions by the model are in good agreement with the experimental observation. This provides a confidence in the modelling methodology and assumptions used in predicting ignition mechanism. The model can hence be used to predict ignition behaviour for other lignites in O_2/N_2 conditions.

Table 4.10: Comparison of the ignition mechanism between experiments and model

O_2 concentration	Ignition mechanism	
in N_2 background	Experiment [134, 152]	Model
21%	HO or HI(HO-HI)	HO
30%	HO or HI(HO-HI)	HI(HO-HI)
40%	HO or HI(HO-HI)	HI(HO-HI)
50%	HI(HO-HI)	HI(HO-HI)
60%	HI(HO-HI)	HI(HO-HI)
70%	HI(HO-HI)	HI(HO-HI)
80%	HI(HO-HI)	HI(HO-HI)

Experimentally the lignite particles fragments after ignition.

The model is extended to multiple particle sizes which can generate a correlation for critical particle diameter. The plot quantifying the ignition mechanism is based on particle diameter and ambient O_2 concentration is presented in Figure 4.29. The cases investigated between 21-80% O_2 in N_2 demonstrates that the particle size below 90 μm experience heterogeneous ignition except for the one condition

described previously. The particle diameter with 200 μm ignites homogeneously for the conditions investigated. The high moisture and volatile content do not allow O_2 to diffuse inside the particle but diffuses well into the volatile cloud around the particle where it sustain a volatile flame for longer period. The transition from homogeneous to heterogeneous ignition for particle diameter of 150 μm happens at 80% O_2. The high O_2 content manages to diffuse inside the particle during the devolatilisation phase and trigger heterogeneous(HO-HI) ignition. The correlation predicted by the model implemented by Khatami et al. using the experimental values is close to the model predictions except for smaller particles in air conditions. The difference between two models was because the lignite experiences transition in ignition mechanism. As mentioned before the results for 90 μm particle was so close to be quantified as homogeneous ignition for cases with 30% O_2 in N_2, the correlation could be have been close to the model prediction of Khatami et al. [134, 152]. As the other parameters are validated and the correlation is close to the one prediction by Khatami et al., this provides confidence in the correlation developed using this methodology which can be used for further application. If the correct experimental values are available the model implemented by Khatami et al. can be used to predict the correlation of critical particle diameter for lignites which will reduce the computational time. In absence of experimental values the proposed model can be used to predict the ignition time delay and the ignition mechanism for the lignite particles.

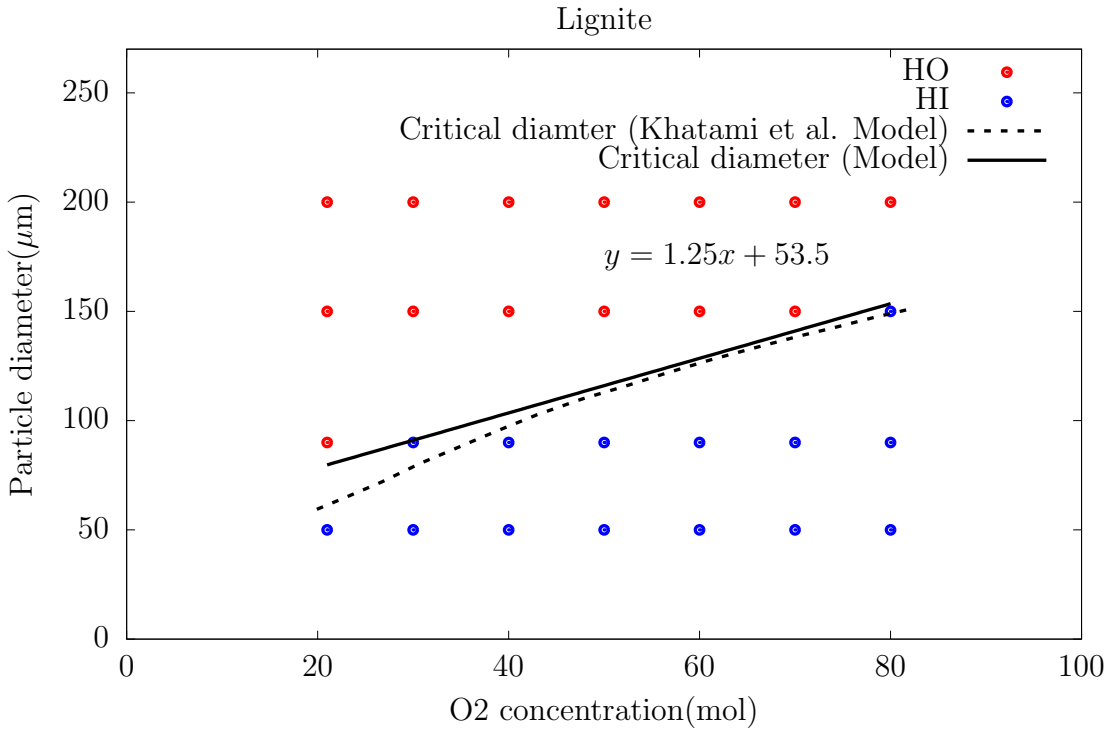

Figure 4.29: Ignition mechanism and critical particle diameter for the Lignite particles.

4.4.2 Oxy-fuel cases

This section is an extension to the modelling investigation of the bituminous coal in oxyfuel conditions tested experimentally by Khatami et al. [134, 152]. The modelling methodology is same as used in air conditions and the difference are implemented in the boundary conditions. The cases modelled for validation are of 90 μm in particle size diameter. The ambient gas concentrations varied from 30% O_2 in CO_2 up to 80% O_2 in CO_2. Similar to O_2/N_2 cases a correlation for critical diameter was obtained for oxyfuel cases using the same four particle sizes.

Boundary conditions

The ambient gas velocity for particle size of 90 μm was set to 0.127 m/s produced from Equation (4.1). The inlet temperature at t=0 is 1100 K which increases transiently and near the particle surface a temperature of 983 K. The temperature between them is a gradient described in Figure 4.5, which replicates the particle heating through a cooler region near the ejector. The temperatures are relatively lower compared to the O_2/N_2 conditions due to the heat capacity of CO_2. The wall temperature is kept at 1400 K.

The initial particle temperature is set at 300 K, the initial porosity at 0.17 and the particle density at 1180 kg/m^3. The boundary conditions for k_{eff} and D_{k_m} is set in accordance with Equations (4.26) and (4.39). The devolatilisation is calculated using the CPD where time temperature profiles are calculated from Fluent and used as input for the CPD model. As devolatilisation is a function of temperature, the results yield a similar mass loss curve and hence, the devolatilisation kinetics used are the same used in O_2/N_2 atmospheres which was also observed in [162]. The only difference observed in the volatile mass loss profile in the two atmosphere is that for oxyfuel environment the volatile loss was delayed due to lower heating of the particle. This phenomena was taken care by accounting for lower initial temperatures compared to O_2/N_2 cases. The FFCM reaction mechanism is used for simulating gas phase reactions in the oxyfuel conditions. The rest of the numerical setup is kept the same as described in Section 4.3.4.

Results and discussion

The progression of combustion for the six cases is shown in Figure 4.30. It describes the time temperature profiles and the formation of OH in the domain and inside the particle. The general combustion behaviour of the bituminous coal is similar in oxyfuel condition for ambient O_2 between 40-80%. When compared to O_2/N_2 conditions the particle heating rate was slower in oxyfuel conditions due to the lower initial ambient temperatures (close to the particle injector). In addition, CO_2 has a higher heating capacity which reduces the heating rate of the particle. The reduction in particle heating rate results in slower volatile release. The low volatile release results in longer time for the volatiles to reach lower flammability limits. The longer ignition delay also implies that the particle reach higher ignition

temperatures, which enables higher amount of volatiles to be released in the domain and it increases the porosity of the particle. The longer delay also increases the O_2 to diffusion back into the particle after the initial displacement of O_2 during moisture release and early stages of devolatilisation. The higher diffusion of O_2 in the particle before ignition enables volatiles burning simultaneously (HO-HI) in both phases just after ignition where the reaction zone of the volatiles are in both phases close to the surface.

The ignition mechanism for cases in 40% $\leqslant$ ambient O_2 ignites heterogeneously (HO-HI). This can be observed from temperature rise in the particle and the domain accompanied with the simultaneous increase in OH mass fraction in both the phases. The simulation results also revealed that the volatiles ignite after the volatile release rate peaked (not shown). This was attributed to diffusion of high concentration of CO_2 into the volatile cloud around the particle, which retards combustion. The high concentration of volatiles cloud formed around the particle fails to ignite and diffuse away from the particle, which increases the ignition delay time. Once the volatile release rate drops the diffusion of ambient O_2 increases which enabled ignition. The particle volatiles fail to ignite in ambient O_2 of 30% due to low concentration of O_2 and higher concentration of CO_2. The volatiles release fail to achieve the volumetric concentrations to achieve lower flammability, which was also observed during the experiments by Khatami et al. There were rather a small spike in temperature close to the surface, which signifies tiny small bright spots observed on the particle surface during experiments for that condition. The devolatilised char for this condition burns slowly signifying pure char combustion.

The simulation results also confirms the behaviour observed in many other high heating rate single particle combustion experiments [155, 298].The increase in ambient O_2 increases the diffusivity and reactivity in and around the particle. The increase in ambient O_2 under oxyfuel conditions has the following impact on the combustion of the particle:

i There is an increase in peak flame and particle temperature (Figure 4.31).

ii There is also an increase in peak OH mass fraction complimenting the increase in peak temperatures.

iii The particle ignition temperature decreased with increase in ambient O_2.

iv There is a steady decrease in ignition delay time with the increase in ambient O_2 (Figure 4.32).

v There is also an increase in the amount of volatiles that burn with increase in O_2 as the longer delays diffuses away the volatile cloud away from the particle. The volatiles released reaches it peak mass fraction and reduces with increase in time as it diffuses away from the particle. The ignition takes place when the mass fraction of the volatiles are on the decline. The longer ignition delay implies greater diffusion of volatiles away from the particle (Not shown in the

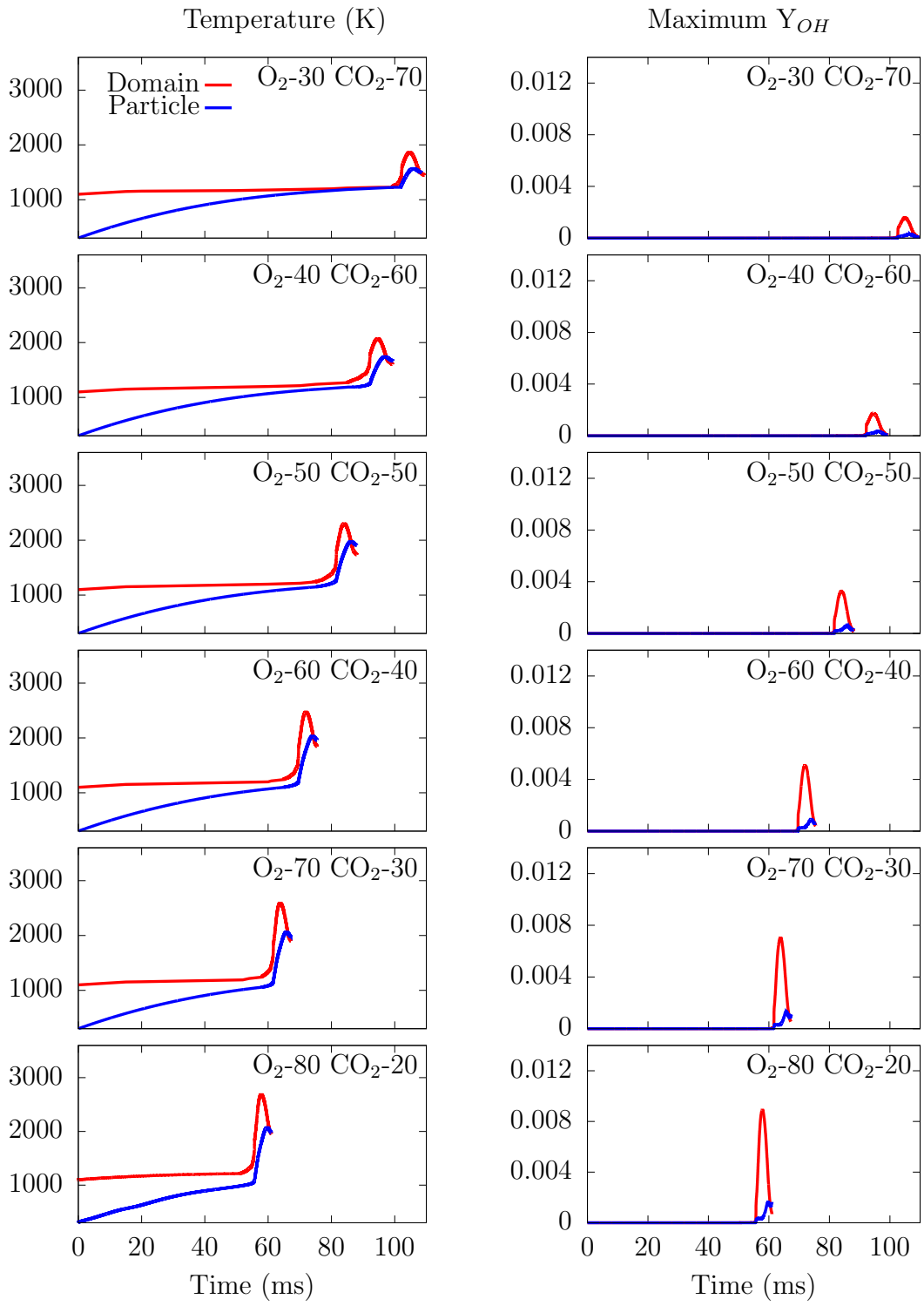

Figure 4.30: Maximum temperature of the domain and particle for Bituminous coal at different oxy conditions.

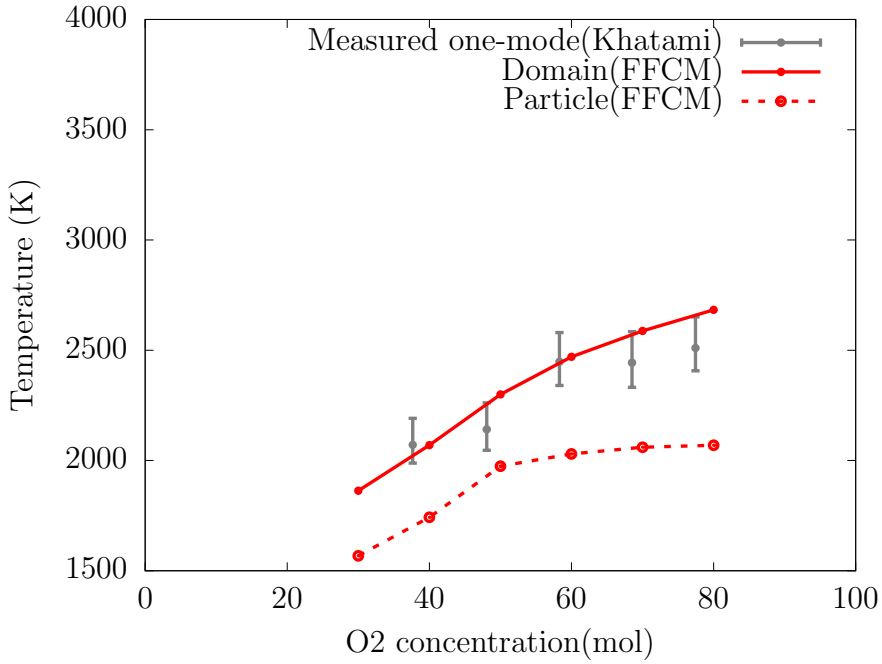

Figure 4.31: Comparison of peak temperatures of domain and particle using FFCM for Bituminous coal in oxyfuel conditions.

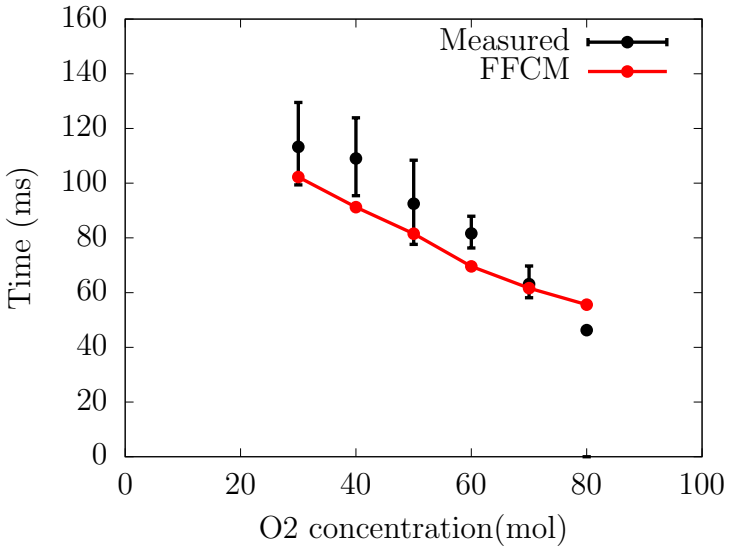

Figure 4.32: Comparison of ignition delay time for bituminous coal in oxyfuel conditions with particle size of 90μm(simulation) and 75-90μm(experiment).

plots). The reduction in volatiles content combusted is evident by the amount of OH formed during combustion of volatiles as shown in 4.30.

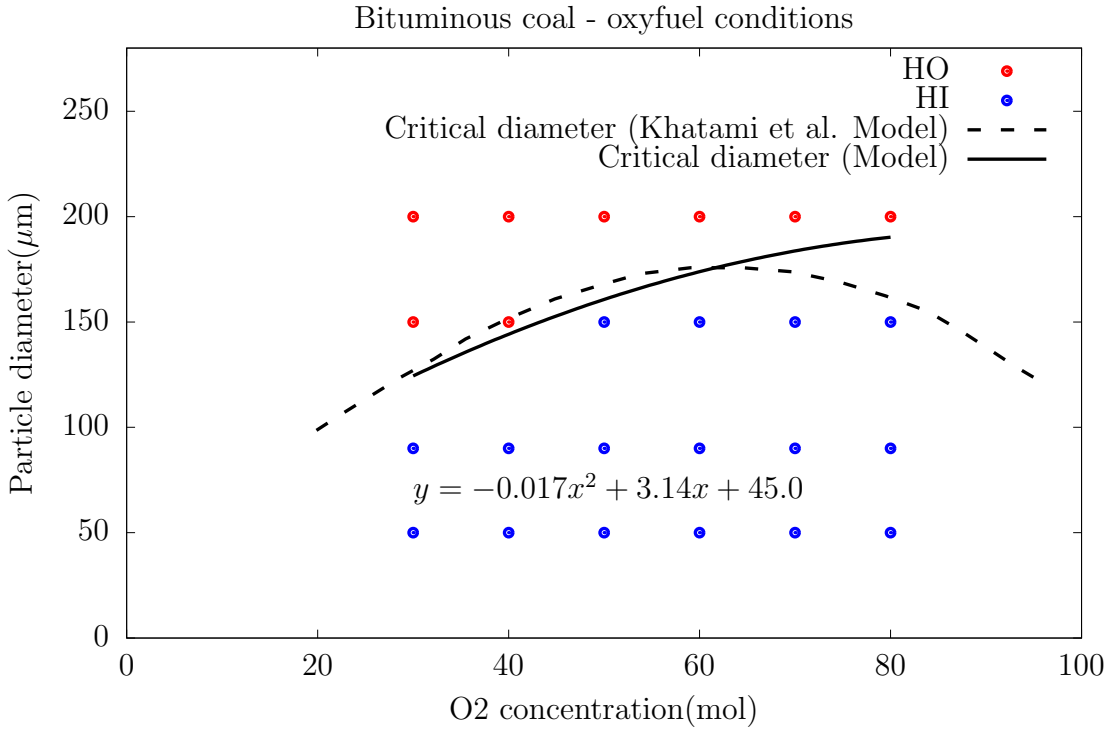

Figure 4.33: Ignition mechanism and correlation of critical particle diameter for the bituminous coal particles in O_2/CO_2 conditions.

Similar to the O_2/N_2 cases, the validation of the methodology and the overall model in oxy fuel conditions is done by comparing the experimental and simulation results. Figures 4.31 and 4.32 compares the measured results and the model predictions. The peak flame temperatures in 4.31 are in excellent agreement with the measured results. It shows that the pre-cursor calculations are accurate and the FFCM reaction mechanism is apt for predicting the flame chemistry. The peak volatile flame temperatures are calculated for cases between 30-80% ambient O_2. According to the experimental results, the case with 21% ambient O_2 the ignition was not detected hence the simulations are not conducted for below 30% ambient O_2. However, the ignition delay time is calculated for all the cases (Figure 4.32) which shows that the simulation results are under predicted for a 90 μm particle but well within the experimental error range. Hence, the model is feasible for the simulation of the ignition of single particle under oxy fuel conditions.

As the model is validated it can be extended to predict the ignition mechanism of other particle sizes which provides the correlation of critical particle diameter. The model tested three other particle sizes i.e. 50, 150 and 200 μm. the numerical set up was kept the same except for the gas velocity, transiently changing inlet temperature and the initial domain temperature. These parameters were determined

by Figure 4.5 which describes the time temperature profiles of ambient gas. The results of their ignition mechanism is shown in Figure 4.33. The ignition delay time increased with increased in size due to reduction in overall heating rate of the particle. The cases with particle size of 200 μm ignite homogeneously due higher volatiles content. The cases with particle size of 150 μm experience a transition in ignition mechanism. The transition is from homogeneous to heterogeneous(HO-HI) which happens for cases between 40-50% ambient O_2. The transition happens because of the increase in O_2 reactivity (Similar to transition observed in O_2/N_2 cases). The cases with particle size of 50 μm ignite heterogeneously(HO-HI) because smaller particle experienced a higher heating rate which enabled rapid release of volatiles. The rapid release of volatiles peaked quickly as smaller particles consist of lower quantities of volatiles. This enabled quicker diffusion of O_2 into the volatile cloud and enables ignition before the volatiles around the particle diffuse away. The peak temperatures for the 50 μm cases ranged between 1575-1750 K and was short lived compared to other particle sizes but it did burn simultaneously.

The set of results generated illustrated transition in ignition mechanism for only one particle size. This generates a limitation in obtaining correlation for critical particle diameter. In previous cases there were atleast two particle sizes where transition of ignition mechanism was observed. In order to obtain an accurate correlation, investigation of a couple more particle sizes are recommended. However, a correlation is produces which passes through the middle of the transition points for particle diameter of 150 μm were the start and end points satisfy the ignition mechanism points i.e the correlation at 80% O_2 should be below 200 μm and at 20% O_2 it should be greater than 90 μm. A quadratic correlation is obtained as shown in Figure 4.33. The correlation is in decent agreement upto 60% ambient O_2 with the model used by Khatami et al. After 60% ambient O_2 the results diverges and this is where the investigation of other particle sizes will enable a more accurate correlation. The correlation by Khatami et al. also suggests that the ignition mechanism prediction for the other particle sizes are accurate and the model suffice well across particle size and different oxy conditions. The critical particle diameter correlation generated can be used for investigating conditions under 60% ambient O_2 and investigation into few more particle size will be recommended to improve the accuracy of the overall correlation.

Sensitivity to heating rate

It is important to see the impact of heating rate on the ignition mechanism. As oxy fuel cases are most sensitive to ignition time delay, it was decided to test a couple of oxy fuel case for sensitivity analysis of heating rate. There has been extensive work in the literature highlighting the impact of heating rate. The studies generally concluded that the particle achieved early ignition i.e. decrease in the ignition delay time and decrease in particle temperature. The sensitivity was conducted on particle size of 90 μm where the ambient temperature was changed to a constant ambient temperature of 1250 K, i.e the low temperature region around the injector is ignored and a constant profile of 1250 K was set. The two oxy fuel conditions

tested were for 50% and 60% ambient O_2 concentration.

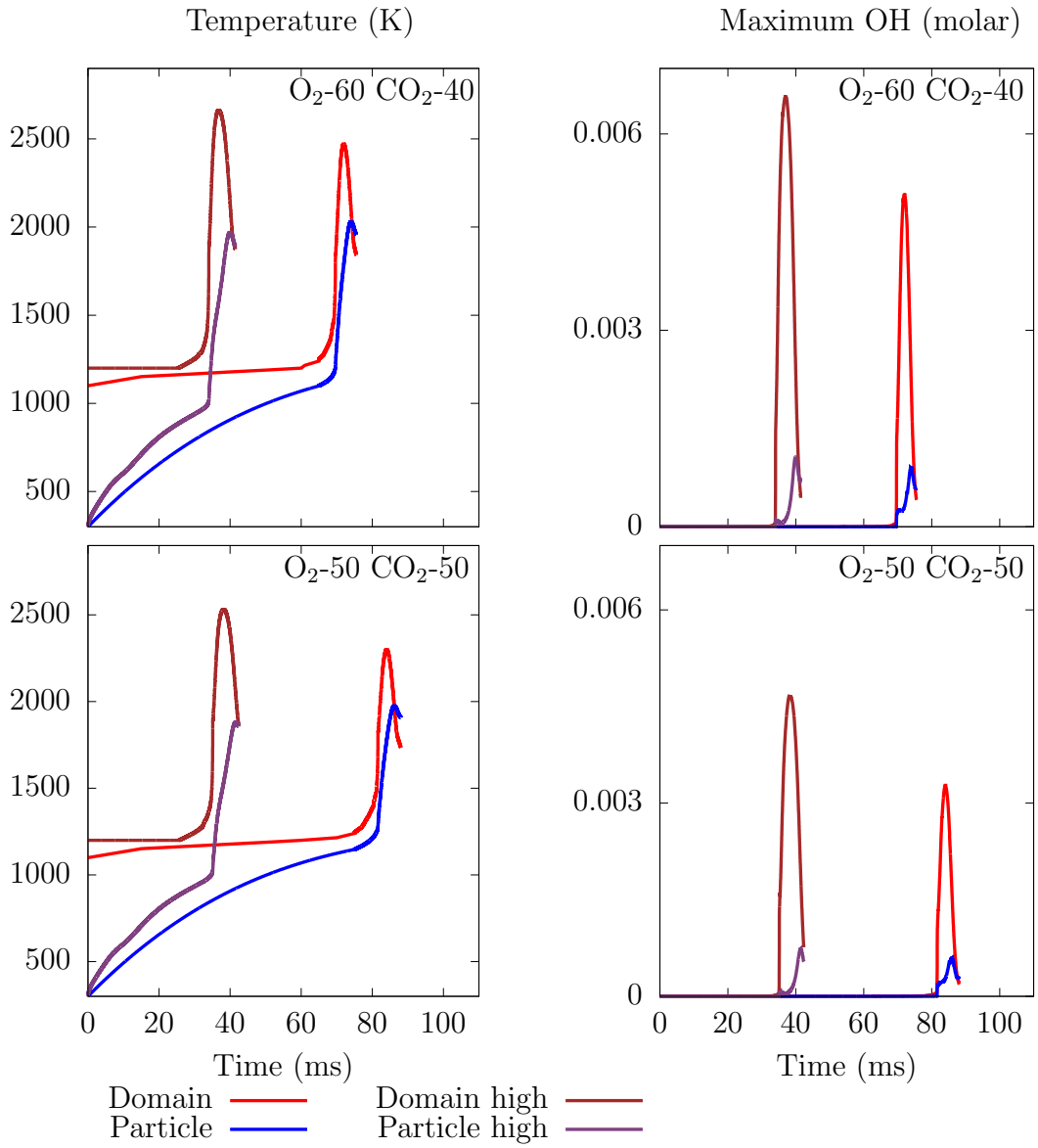

Figure 4.34: Maximum temperature of the domain and particle for Bituminous coal at different oxy conditions.

The results for the sensitivity analysis are shown in Figure 4.34. The higher heating rate resulted in higher volatile release rate, which enabled higher concentration of the volatiles around the particle. The higher release rate enabled the volatiles to reach the lower flammability limits quicker. The higher volatile concentration and the higher ambient temperature reduces the ignition delay time significantly (Table 4.11). It also shows that the particle ignition temperature also reduced $\approx$ 200 K for higher heating rate environment. The reduction in the ignition delay allowed higher amount of volatiles to be combusted around the particle, which is reflected in the peak flame temperatures and peak OH mass fraction. The reduction in the ignition delay time reduced the amount of ambient O_2 diffused back into the

Table 4.11: Impact of heating rate on flame parameters for cases with ambient O_2 concentration of 50% and 60%

Ambient O_2(%)	Ambient temperature (K)	Maximum temperature (K)	Ignition delay time (ms)	Particle ignition temperature (K)
50	Khatami et al.	2295	81.53	1201
50	1250	2522	37.5	1004
60	Khatami et al.	2467	71.2	1182
60	1250	2566	32.7	993

volatile cloud and in the particle. The volatile flame burning outside the particle at higher heating rate also reduced the diffusion of O_2 in the particle, which delayed the combustion of volatiles inside the particle. This phenomena did not change the overall ignition mechanism for the conditions tested (i.e. heterogeneous due to simultaneous burning of volatiles in both the phases) but impacted the overall ignition behaviour. On the other hand the cases replicating experimental conditions show that the combustion of volatiles are almost instantaneous in both the phases. This suggest that particle ignition mechanism will not be impacted unless there is a significant higher ambient temperatures (or greater heating rate). In pilot scale or industrial burners, particles will experience a heating rate represented in the experimental conditions by Khatami et al. where there is a gradual increase in the ambient gas (flame temperature for burners) temperature which will have a greater tendency for particles to ignite heterogeneously.

4.5 Conclusions

A mathematical model for identifying the ignition mechanism of a single particle is developed successfully. A novel approach to modelling ignition of a single particle using ultimate and proximate analysis is comprehensively presented in this study. The model was focused on replicating ignition of coal particles in drop tube furnace used by Khatami and co-worker, which experiences heating rate of 5000-10000 K/s. The model is flexible enough to replicate other high heating experiments such as entrained flow reactors. The model and the methodology developed was validated with the experimental data based on the peak flame temperature, ignition delay and ignition mechanism. The particle size validated was 90 μm in O_2/N_2 and O_2/CO_2 gas atmospheres where the O_2 concentration was varied from 20-80%. The results suggest that ignition of the coal particle is primarily due to the combustion of the volatiles. Upon validation, the model was extended to three other particle sizes, i.e. 50, 150 and 200 μm which enabled a correlation of critical particle diameter. The correlation is able to quantify the ignition mechanism of the particle based on the particle diameter and the ambient O_2 concentration. The other conclusions specific to the cases are discussed below.

4.5.1 Bituminous coal in O_2/N_2 environment

i The flame front for all the conditions transits from the domain towards the inner core of the particle after the volatiles reach the peak flame temperature.

ii The modelling predictions for the bituminous coal with 90 μm ignites homogeneously in air conditions and transits to heterogeneous ignition with increase in O_2 content which is between 50-60% ambient O_2 molar concentration. The modelling prediction for the transition are in good agreement with the experimental data.

iii The increase in O_2 had a minimal impact on the ignition delay time which are in excellent agreement with the measured data. There is an increase in the diffusion of O_2 with increase in ambient O_2 during the devolatilisation phase. This increases the tendency of particles to ignite heterogeneously as it enhances simultaneous combustion of volatiles inside and outside the particle.

iv The simulation results using the FFCM mechanism are in excellent agreement with the experimental data. The reduced mechanism proposed by Westbrook-Dryer used for the bituminous coal in O_2/N_2 atmospheres is able to detect the ignition mechanism but is not recommended for investigation as it over predicts the flame temperatures and it can lead to false overall results.

v The extended investigation to different particle sizes reveal that the the ignition time delay increases with particle size.

vi The tendency of particle to ignite heterogeneously increases with decrease in the particle size and increase in O_2 concentration.

vii Quantifying the ignition mechanism based on O_2 concentration and particle diameter provided a correlation of critical particle diameter which can be used in defining the ignition mechanism of individual particles in a pulverised fuel furnace. The correlation generate using this model is close to the correlation predicted by Khatami and co-workers using the experimental data.

4.5.2 Lignite in O_2/N_2 environment

i The increase in inherit moisture of coal increases the ignition delay time for lignites. It also increases the porosity of the coal during the devolatilisation phase. Compared to bituminous coal the longer ignition delay together with increased porosity, enhances the diffusion of O_2 inside the lignite particle and promotes heterogeneous ignition.

ii Similar to the bituminous coal, increase in the ambient O_2 increases the probability of particle igniting heterogeneously. It also increase the peak flame temperature, the devolatilisation rates and reduces the overall volatiles burnout time.

iii The FFCM model proves to be a suitable mechanism to simulate ignition for lignites in the current model. The Westbrook-Dryer mechanism failed to detect ignition for concentration of 21% and 30% O_2 in N_2. It is not recommended to be applied for investigating ignition of lignites.

iv When compared to the bituminous coal, the correlation of critical diameter suggests that the overall probability of lignite to ignite heterogeneously is higher. It also indicate that the probability of heterogeneous ignition reduces with increase in size.

v On comparing the overall modelling results for the two rank of coals, it indicates that coal properties play an important role in quantifying ignition mechanism and it is not just depended on the ambient conditions.

4.5.3 Bituminous coal in O_2/CO_2 environment

i The ignition time delay for bituminous coal is much longer in O_2/CO_2 conditions compared to O_2/N_2 ambient conditions due to lower temperatures around the injector.

ii The longer ignition delay leads to greater amount of particle volatile release and increase in porosity. This also increases the diffusion of O_2 in and around the particle, which exhibits HI due to simultaneous combustion of volatiles in both phases.

iii The modelling results for particle size of 90 μm are in good agreement with the experimental parameters. This provides confidence in the modelling assumptions and simplifications, which can be used for investigating novel fuels.

iv The correlation obtained for oxyfuel conditions are in good agreement with the one obtained by Khatami et al. but a more simulations points are desired for a better prediction of the correlation. In order to investigate furnace conditions it is recommended that the correlation is developed is based around the particle size distribution and the ambient O_2 concentration.

v There is a reduction in the overall ignition delay times of the particle at 50 and 60% ambient O_2 with increase in heating rate. There is also a reduction in the particle ignition temperature and increase in peak flame temperature but it is no impact on the ignition mechanism.

5 Modelling investigation of ignition in IFRF co-axial burner

This chapter presents the CFD simulations of an air fired coaxial burner that has been studied experimentally by Michel and Payne [186] in the International Flame Research Foundation (IFRF) industrial-scale pulverised coal furnace. This chapter investigates the impact of particle's ignition on the overall flame parameters and compares the results from the CFD simulations against the experimental measurements with a particular focus on ignition.

The single particle ignition model developed in Chapter 4 was based upon the laminar flow environment, whereas particles in industrial and pilot scale burners produce eddies due to many factors such as burner geometry, aerodynamics of the burner and turbulent mixing. Turbulent mixing is generally preferred in combustion systems to increase the residence time of the fuel and the oxidant mixture which enhances the overall combustion efficiency of a fuel [177]. In some cases the burner geometry is designed to enhance the oxidant residence time by turbulent mixing in order to reduce harmful emissions, e.g. NOx. In the process of achieving a favourable turbulent environment, the particles experience a higher velocity and heating rate [177] and this results in particles devolatilising at a high rate. In a multi-particle turbulent environment, the slip velocity between the ambient gas around the particle and the particle can easily change the gradients of the volatile concentrations and the heating rate of the particle [127, 340]. This could lead to volatiles and char burning at two separate locations in a flame. This generally poses a challenge in the quantification of the particle ignition. According to the author's knowledge there is no experimental work in the literature which has been able to quantify the ignition mechanism in a fully turbulent coal flame. This demonstrates that the visualisation of the ignition mechanism in a high speed turbulent flame is still a challenging task.

Conducting CFD simulations on pilot scale coaxial coal flames will provide an understanding of particle behaviour durning the ignition phase of the flame in the presence of turbulence. The IFRF furnace was chosen for investigation as it provides insight into the combustion process of high volatile bituminous coal under air conditions in non-swirling (type 0) burner. The impact of swirl generates internal as well as external recirculations which generally produces stable ignition close to the lip of the burner. The ignition point in type 0 burners are further away from the burner as they inherent a forward flowing low swirl flame [200]. The forward flowing

nature of the flame enables quantification of particles themochemistry behaviour. The coaxial geometry chosen, allowed efficient modelling of the coal combustion process in the absence of swirl which enabled the author to focus on the physics and the overall model which is able to predict particle's ignition in a furnace. Additionally, the uncertainty related to the accuracy of the RANS methods in simulating a swirling flow is avoided [341].

The aim of this chapter is to develop a model which focuses on ignition of particles using CFD in a turbulent environment and observe the model impact on the overall flame structure of the case under investigation. The impact of the model developed is assessed by comparing the flame parameters with the measured experimental data. The comparison of the data will provide the validation and confidence in the ignition model which is able to efficiently capture the ignition phenomena for coal particles. The validated CFD ignition model in this study can therefore be extended to perform numerical investigation on a pilot scale swirl burner. In order to determine the improvement and impact of the model, a benchmark CFD simulation was performed on the geometry chosen and tested for a grid independent study against the experimental measurements. The benchmark case sub-models are then modified by incorporating the outcomes from the previous chapter and the improvements in the overall model is validated against the provided experimental measurements. The novelty in this chapter includes the development of a combustion model for coal burners using CFD with a special focus on the ignition of coal particles in a turbulent environment.

This chapter is divided into three sections where the case descriptions, boundary conditions are described in Section 5.1. The modelling strategy for the benchmark case and the results for the benchmark case are reported in Sections 5.2 and 5.3 respectively. The application and the discussion of the results for the ignition model are described in Section 5.4. The conclusions from the study is summarised in Section 5.5

5.1 Case description

In the past, the IFRF furnace has been used to perform experimental tests on various burners [342–347]. A range of numerical studies have been conducted on this furnace [285, 348–353], however according to author's knowledge there hasn't been a model particularly focused on the ignition in the furnace. The flame chosen for the simulation is Flame B1 of the IFRF furnace No.1 documented by Michel and Payne [186]. This particular flame was chosen to simulate and validate the model because it is a lifted flame which is sensitive to the ignition mechanism. The detailed inflame measured values, such as the temperature, velocity and distribution of species are used for validation of the model. Flame B1 has been simulated in the past using the RANS methodology by Lockwood and Salooja [348], Tian et al. [353] and Stöllinger et al. [350–352]. The Stöllinger et al. methodology came closest to the measured results and therefore many of the sub-models used in this

study are common with the work done by Stöllinger et al.

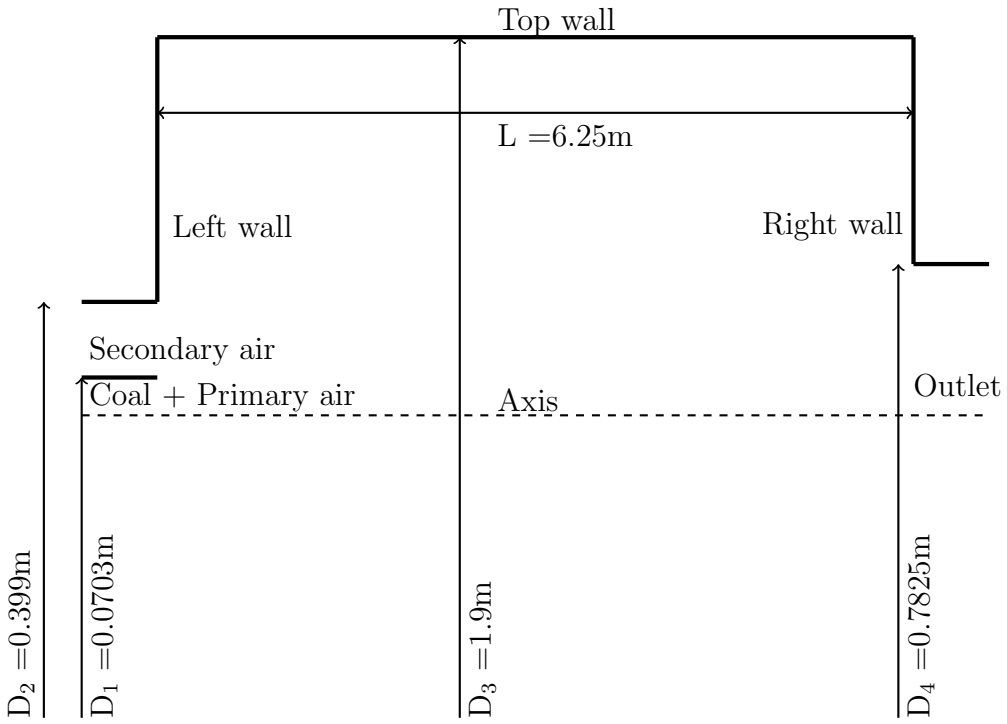

Figure 5.1: Schematic of the IFRF furnace (not to scale).

Table 5.1: Operating conditions for the IFRF furnace no.1 (Flame B1).

Primary stream		
Coal mass flow	212	kg/hr
Bulk velocity	40.7	m/s
Temperature	463.15	K
Secondary stream		
Bulk velocity	9.6	m/s
Temperature	773.15	K

A schematic of the IFRF furnace no. 1 is shown in Figure 5.1. The furnace is a rectangular cross-section (1.9 m x 1.9 m) and 6.25 m long. The primary air and coal is supplied by a central pipe with diameter of 0.0703 m and the secondary air (oxidant) for combustion is provided by an outer annulus with outer diameter of 0.399 m. Previous studies of the IFRF furnace no.1 have shown that three dimensional flow effects are weak and thus the geometry is treated as a 2-D axisymmetric where the length of the wall is adjusted according to the diameter and the value of D_3 = 2.26 m [348]. The exhaust gas and particles exit the furnace where the outer diameter is 0.7825 m. The furnace was equipped with many access ports to enable the inflame measurements such as gas velocity, temperature and

species concentration. The gas temperatures and the velocity were measured using a standard water-cooled suction pyrometer and a Prandtl-probe, respectively. All the above parameters measured are compared at various relevant locations with the simulations. The boundary conditions for the B1 flame are shown in Table 5.1.

Table 5.2: Coal properties of the high volatile bituminous coal from the Saar region.

Proximate analysis (as received)	[wt%]
Fixed carbon	59.5
Volatiles	31.0
Ash	7.5
Moisture	2.0
Ultimate analysis (dry basis)	**[%wt]**
C	74.65
H	4.7
O	11.08
N	1.12
S	0.85
Lower calorific value	31 MJ/kg

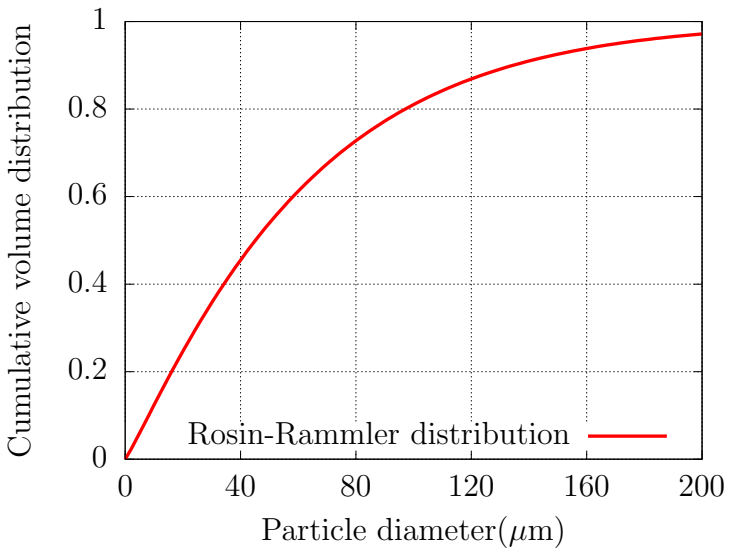

Figure 5.2: Particle size distribution using Rosin-Rammler correlation where d_e = 63 μm and n = 1.1 [352].

The coal used in this burner was a high volatile bituminous coal from the Saar region in Germany and the coal properties are shown in Table 5.2. This coal was selected as it contained very much less ash content which minimised the ash deposition on the furnace walls and this was accompanied with the high volatile content

which is more characteristic of several US coals [186]. The particle size distribution is shown in Figure 5.2 which is obtained by using the Rosin- Rammler distribution model [354]. The distribution defines the mass fraction for diameters greater than the diameter d and is governed by the equation:

$$Y_d = exp\Big[- \Big(\frac{d}{d_e}\Big)^n \Big] \tag{5.1}$$

where Y_d is the mass fraction of the particles greater than diameter d, d_e is the mean particle diameter and n is the spread parameter. The values $d_e = 63$ μm and $n = 1.1$ are obtained from the size distribution provided by Stöllinger et al. [352].

5.2 Benchmark model specifications

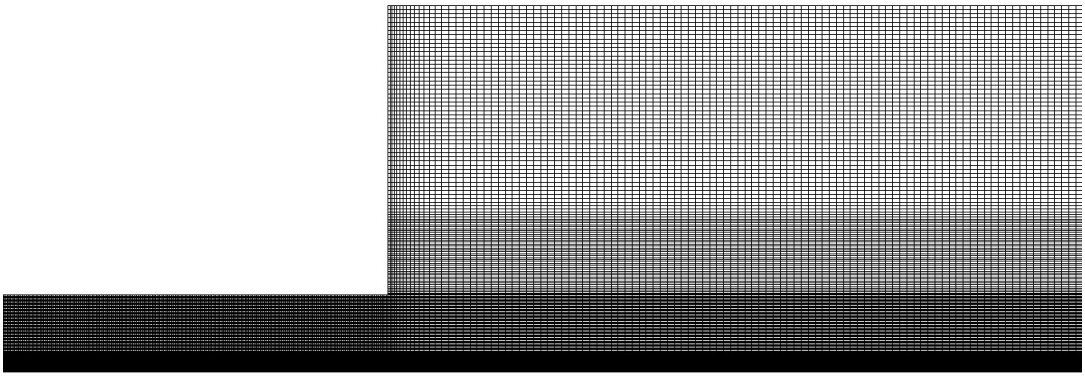

Figure 5.3: Computational mesh near the burner for IFRF furnace No. 1 used for the benchmark case.

The IFRF furnace was modelled as a two dimensional axis-symmetric cylinder. The computational mesh was generated using ICEM ANSYS which consists of 298606 structured quadrilateral cells. The cells are aligned in the direction of the flow which assists in reducing the numerical diffusion. The cells were concentrated and refined near the burner to capture the ignition phenomena. The fine mesh was generated with y+, a non dimensional wall distance greater than 12. The value of y+ was chosen to use scalable wall functions proposed by Launder and Spalding [216] for thickness prediction of laminar boundary layer and its impact on the profile of free stream flow. A near burner mesh is shown in 5.3 which is used for the benchmark simulations. A mesh refinement study was conducted in Section 5.3 in order to check the grid independence of the solution.

The CFD simulations were performed in ANSYS Fluent which consist of many advance sub models which have been used in predicting the combustion behaviour of the coal. The sub-models used are summarised in Table 7.3. The gas phase is solved with the application of the finite volume method which uses Equations (2.4)–(2.6), (2.9) and (2.10) to account for the transport properties of the continuous field as described in Section 2.3. Since, the density of the coal particles is much greater than

air and the effect of gravitation, Brownian and thermophoretic forces are negligible, the gravitational terms from the governing equations were neglected. The main force considered in the calculations are the momentum exchange between the solid and the fluid phase. The steady state turbulence is modelled using the Reynolds stress model proposed by Launder et al. [222, 223]. The constants in the model were kept the same as that used by Stöllinger et al. [352]. This model was chosen over the eddy viscosity models implemented by Tian et al. [353] because it has provided a better prediction in the near burner zone.

The dispersed phased was modelled using the unsteady Lagrangian tracking of discrete particles using the discrete random walk model to account for the impact of the turbulence on the particles motion. The particle time step size was set constant at 0.005 with 10 times steps solving. The particle distribution accounted for 15 particle diameters which resulted in 4350 particles injection solved for every 250 fluid iterations. All the particles are modelled as spheres and the particles heating was considered using Equation 2.21 where it is assumed that the particle heats up uniformly. The boundary conditions for the particles were set such that they simply reflect from the surface of the wall and escape from the outlet of the furnace. The particles are composed of moisture, volatiles, char and ash. The particles and the gas phase are non-linearly coupled by introducing source terms into the governing equations of each phase, e.g. the energy source term consists of the heat exchange between the dispersed phase, gas phase and the radiative heat transfer in the furnace. The heat exchange between the particle and gas phase leads to the change in particle mass which is dependent on the kinetics of the individual components.

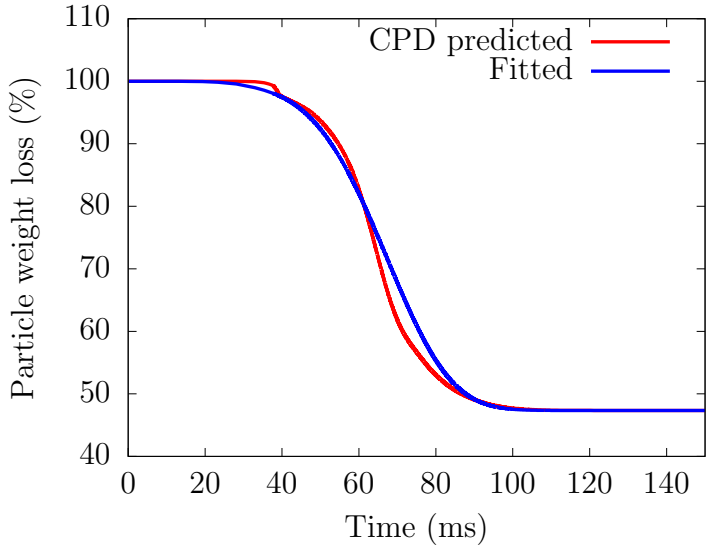

Figure 5.4: Volatiles weight loss for high volatile bituminous coal from the Saar region.

Table 5.3: Models employed for calculating the benchmark case.

Model	Model Parameters		
Turbulence	Reynolds Stress Model [352, 355]		
Gas Phase Chemistry	Eddy dissipation model [280, 355]		
	$C_{2.70}H_{4.60}O_{0.68}N_{0.0789}S_{0.0261} +$	$3.53\,O_2 \longrightarrow$	$2.7\,CO +$ $2.3\,H_2O +$ $0\,0394\,N_2 +$ $0.0261\,SO_2$
	$CO + 0.5O_2 \longrightarrow CO_2$		
Devolatisation rate	Single-step Arrhenius expression [355]		
	Pre-exponential fac. (A_i)	= 20820	
	Activation Energy (Ea_i)	= 4.696 x10^7	J/kmol
Char Combustion Model	Intrinsic model[352, 355, 356]		
	Diffusion coeff. (C_{diff})	= 5x10^{-12}	$m^3/K^{0.75}$
	Porosity (θ)	= 0.70	
	Tortuosity (τ)	= $\sqrt{2}$	
	Pore radius (r_p)	= 1 x 10^{-7}	m
	Int. Surf. A (S_a)	= 250 x 10^3	m^2/kg
	Stoichiometric coeff. (S_b)	= 1.33	
	Pre-exponential fac. (A_{ichar})	= 0.052	kg/(m^2 · s · Pa)
	Activation Energy (E_{ichar})	= 1.615 x 10^8	J/kmol
	Burning Mode (α)	= 0.25	
Radiation	Discrete Ordinates (3 x 3) [205]		
	Absorption coefficient given by WSGG constants [295, 355]		
	Particle emissivity ϵ	= 0.9	
	Particle scattering factor σ_p	= 0.9	
Particles	Eulerian-Lagrangian approach		

The mass loss due devolatilisation was modelled using the single rate Arrhenius expression as follows:

$$\frac{dm_p}{dt} = -m_v A exp\left(\frac{E_a}{RT_p}\right) \tag{5.2}$$

where m_v is the mass of volatiles. The kinetics were obtained from using CPD and fitted into a single rate expression as shown in Figure 5.4. The heating rate was set at 5 x 10^4 and the model input were obtained from the correlation by Genetti [246]. The HTVY predicted by the CPD for the bituminous coal is $\approx$ 1.58 which meant that the char mass fraction was reduced to 0.417 in the coal particles. The initial particle density was 1000 kg/m^3 and the specific heat capacity of the particle was

kept constant at 1100 J/(kg.K) [352]. A DNS investigation on coal jet flame by Muto et al. concluded that the particle swelling during devolatilisation had negligible impact on the jet flame [357] and thus the simulations were conducted without taking any swelling into considerations. The volatiles combustion was modelled by using a two-step eddy dissipation model [280]. The volatile gases were modelled as empirical species derived from proximate and ultimate analysis having a molecular weight of 50 g/mol [352].

The resulting two-step mechanism is presented in Table 7.3 and the standard mixing parameters defined by Magnussen and Hjertager [282], A and B were kept constant at 4.0 and 0.5, respectively for both the gas phase reactions. The char combustion was represented by the intrinsic model described in Section 2.9.3. The kinetics for the model were obtained from the study by Stöllinger et al. [352] and the ash in the particle is assumed to be inert [358]. The heat absorbed by the particle during char combustion is 9.6 MJ/kg. The transport properties of the species such as the diffusion coefficient, viscosity and thermal conductivity was calculated by ANSYS Fluent that are based on kinetic theory. The spatial discretisation for the transport equations was accounted by using the second order upwind scheme.

The primary and secondary inlets were set as constant velocity profiles across the surface and hence the domain was extended to obtain a fully developed velocity profile prior to the introduction of the primary and secondary flows into the furnace. The velocity and temperatures at the two inlets are summarised in the Table 5.1. The mean velocity of the particles which enter the domain from the primary inlet with the hot air has the same velocity as the carrier gas. The domain was also extended towards the outlet to avoid any recirculation at the outlet and the outlet was set as a standard pressure outlet condition. The outlet boundary condition assumed a zero diffusive flux, a constant gas temperature of 1300 K and an emissivity of 1.0. The inlets and outlets are treated as blackbody surfaces for the radiation boundary condition to neglect any reflecting radiation. There was a difference in the way the top wall temperature was set, Tian et al. [353] set a constant temperature of 1373 K which predicted early ignition. The error in the early temperature rise by Tian et al. could be explained by analysing the experimentally measured temperature which had the form of a sinusoidal wave as shown in Figure 5.5. This discrepancy impacts on the radiative heat transfer. In order to accuratelly model the heat tranasfer the experimental values were fitted in the form of equation shown in Figure 5.5. The temperature profile along the top wall was thus set equal to the experimental fitted value which was the approach of Stöllinger et al.[352] and Fabrizio [355]. The side walls are treated as adiabatic walls and assumed to have an emissivity of 0.8 [352, 355]. The discrete ordinates model was used to solve the radiative heat transfer equation with the angular discretisation of 3 x 3. The particle emissivity and scattering factor was set to 0.9 and the particle to wall radiation interaction was incorporated [355]. An extensive work was conducted by Fabrizio [355] on the sensitivity of the gas absorption coefficient and it was concluded that the WSGG model approach provided a more accurate method which predicted the incident heat flux particularly well and hence the constants from the WSGG approach were employed.

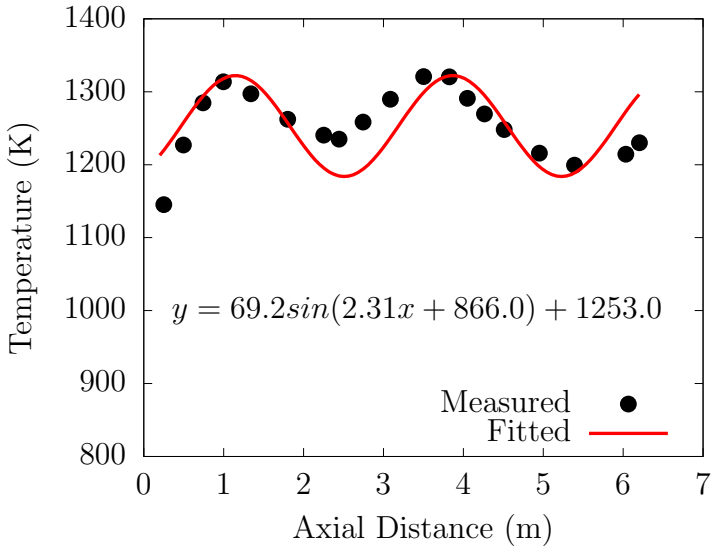

Figure 5.5: Average wall temperature along furnace top wall.

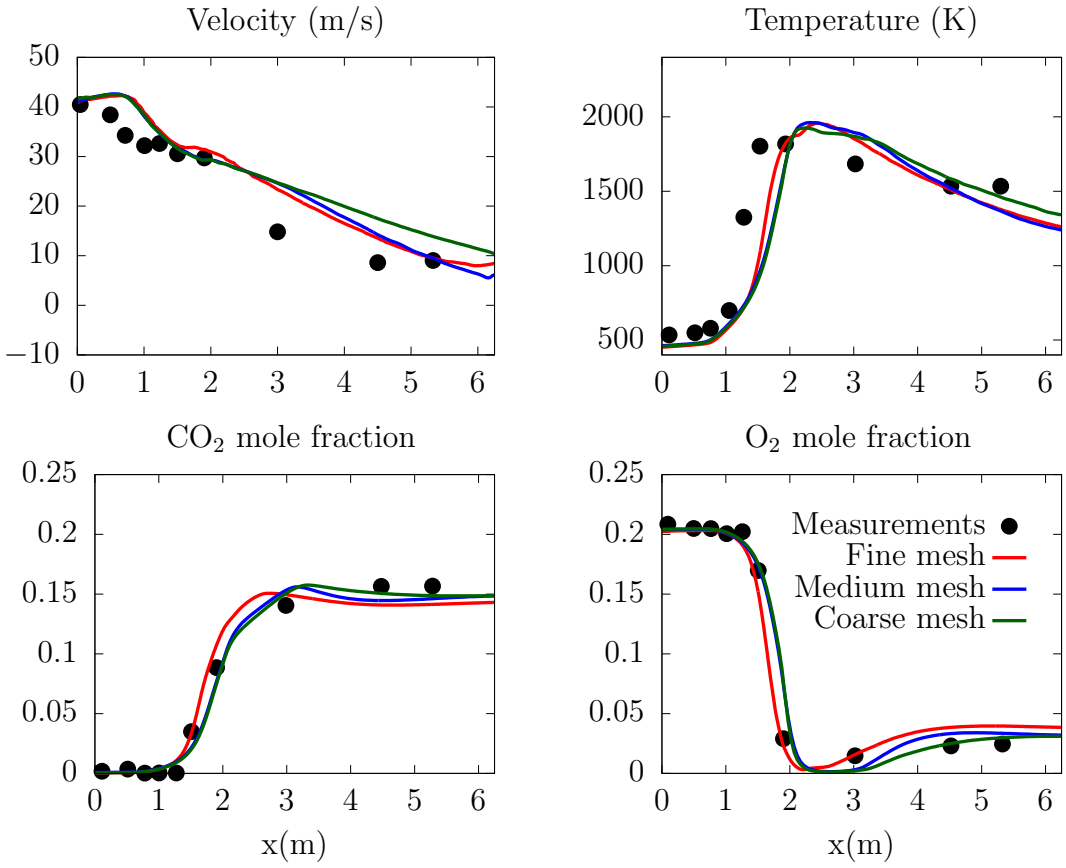

Figure 5.6: Mesh sensitivity analysis showing axial mean plots along the centreline of the furnace for gas phase: velocity, temperature, CO_2 and O_2.

The sequence of the particles combustion process is set as a consecutively occurring process, i.e. the process of water evaporation, volatile release and char combustion occurs one after the other. The thermo-chemical conversion processes were limited by the fact that each conversion was not allowed to start before the previous one finishes, i.e. the char combustion does not start until all the volatiles from the particles are released. The standard modelling approach is that the particles are treated as uniformly heating spheres which releases volatiles in the gas phase and then they combust in the gas phase and hence the benchmark model does not permit combustion of volatiles inside the particle. As the focus of this thesis is on ignition modelling, only the standard modelling approaches are considered for many phenomena. It is acknowledged that the application of the simplified models may generate a significant errors in the overall predictions.

In order to analyse the solution dependence on the grid a mesh sensitivity analysis was conducted using three meshes with 75898, 148778 and 298606 cells. The refinement was primarily done in the direction of the flame and focused close to the burner region and keeping the y+ constant. The boundary conditions and the case was set up as described above. The mesh sensitivity results shown in Figure 5.6 are with the benchmark case and the results show little improvement with refinement. The results demonstrate, as expected, that the solution is most sensitive downstream of the flow which is most prevalent in the velocity field. As the fine mesh provided the best agreement, it was decided to use this mesh for all future analyses. In order to avoid any inconsistencies, the benchmark case was also simulated using the fine mesh.

5.3 Benchmark Case results

The benchmark case was simulated using a fine mesh and the results obtained are compared with the measured data in Figures 5.7–5.10. The experimental observed ignition distance is between 0.8-1.0 m and the peak temperature of 1873 K is at around 1.75 m. As the B1 flame is a lifted flame, predicting the lift-off distance will be a key factor in determining the accuracy and reliability of the model. The flame ignition point are dependent on several particle and flame parameters, namely, particle velocity, devolatilisation rate, volatiles combustion and radiative transfer. The overall particle behaviour and its interaction with flame during the ignition phase is discussed in Section 5.4.1. This section discusses and compares the gas phase predictions of the benchmark model with measured data.

Figure 5.9 compares the measured values with the simulation results for different parameters along the centreline. The results at the centreline reveals that the flame reattachment point is predicted with a delay and the sharp increase in the temperature is lags when compared to the measured values. The flame temperature is over predicted after the reattachment and it under predicts downstream of the furnace. The velocity profiles at the inlet and outlet are well predicted, however there is an over prediction in the vicinity of half way along the centreline which could

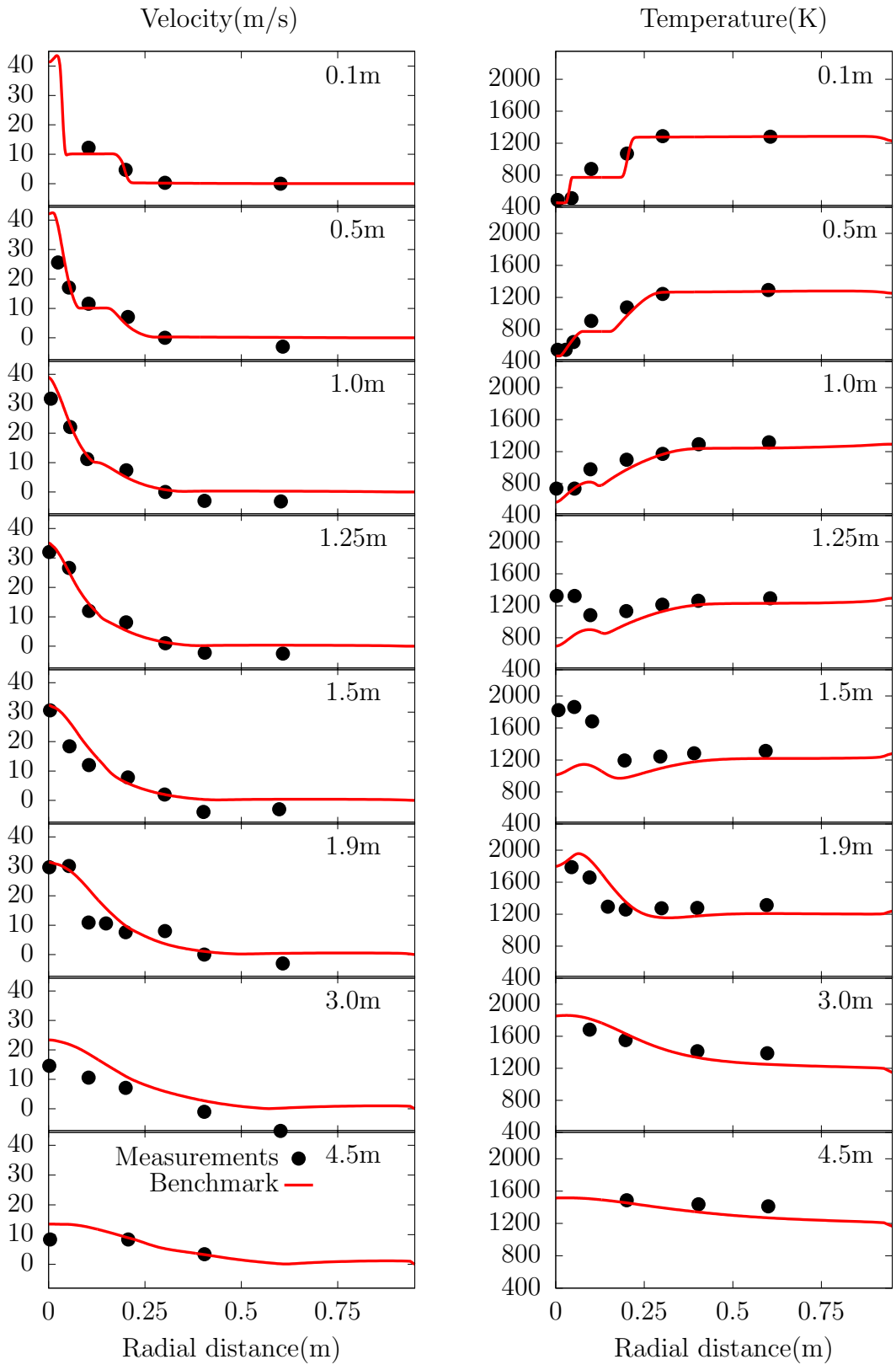

Figure 5.7: Benchmark CFD calculations against the in-flame measurements for the Velocity(left) and Temperature(right).

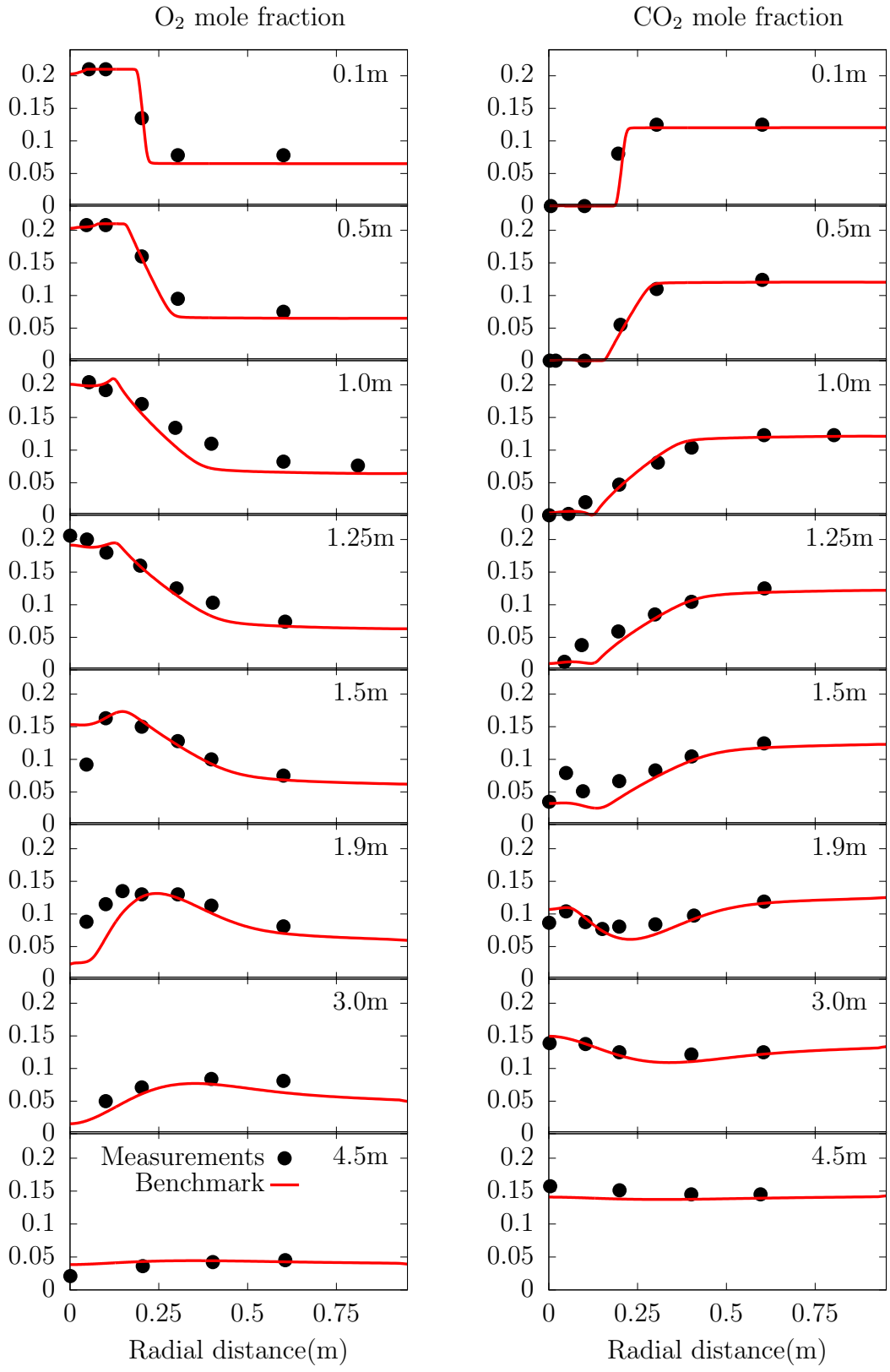

Figure 5.8: Benchmark CFD calculations against the in-flame measurements for O_2(left) and CO_2(right) mole fractions.

be due to the over prediction of the temperature field after the ignition phase. The O_2 and CO_2 concentrations are predicted well near the ignition point but as the flame temperatures are under predicted downstream, the O_2 concentration is over predicted and the CO_2 is under predicted.

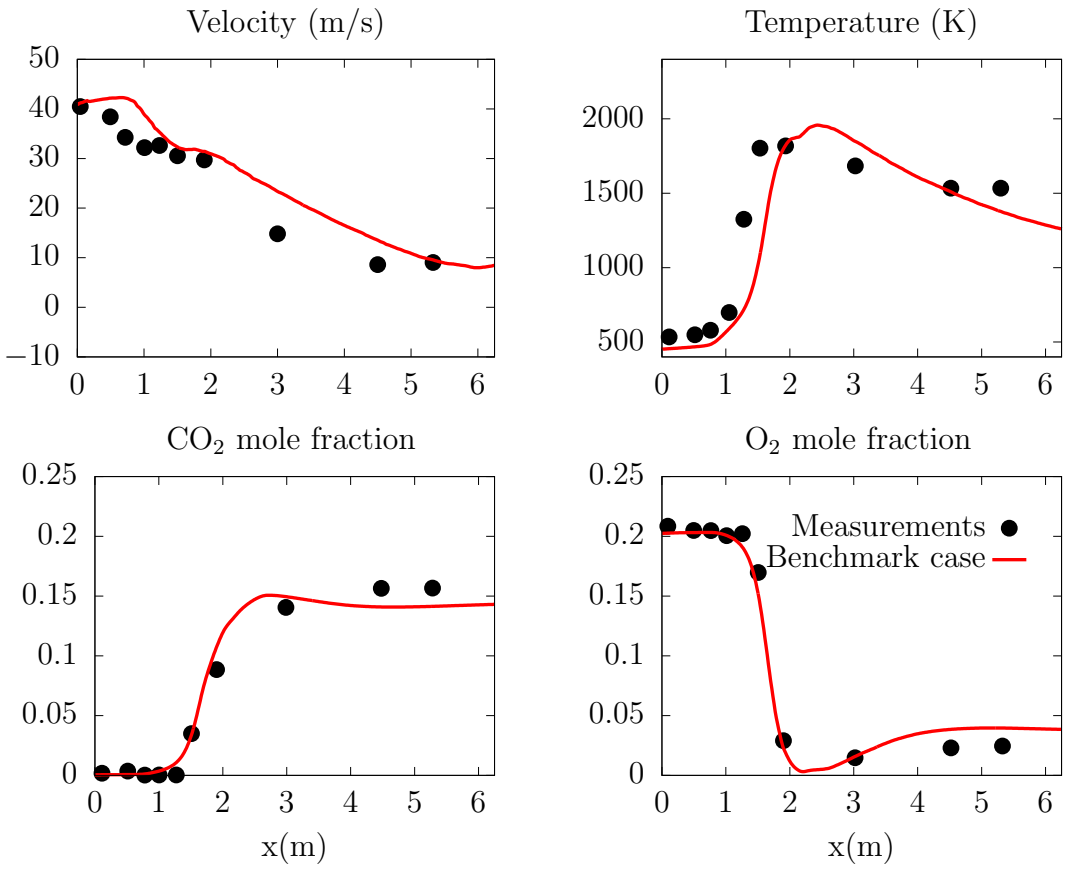

Figure 5.9: Axial mean plots for the benchmark case along the centreline of the furnace for the gas phase: velocity, Temperature, CO_2 and O_2 mole fraction.

On analysing the mean radial temperature profiles in Figure 5.7 with the region of interest between 1 - 1.9 m, it is evident from the measured values that the increase in the flame temperature starts between 1 - 1.25 m. The measured peak temperature values at 1.25 m of the radial distance away from the burner tip indicates early ignition, which occurs in the shear layer where both the streams are mixed. The turbulent mixing of high temperature air from the secondary flow provides suitable thermal conditions for the ignition of the particles. The increase in temperature is delayed in the benchmark simulation as the increase starts between 1.5 - 1.9 m. The discrepancies in the lift-off height could be due to high stain rates in the shear layer which generally produces local pockets/regions of extinction of the flame which in this case delays the ignition. Once the strain rate drops below a certain level then the region can establish or reestablish ignition [359–361]. Another factor influencing

the flame could be the short comings in the thermo-chemistry model which does not account for the variation of the ignition mechanism for different particle sizes are ignored. It could be a combination of these factors but only the latter of these is tested in this chapter to see the overall impact of accurate ignition modelling.

Lack of finite rate chemistry or an error in the devolatilisation and char combustion model could be a contributory factor for the delay in the ignition. If the kinetics delay in the volatile evolution or an under prediction in the HTVY will delay the gas phase combustion. Similarly, if the char combustion rate is under estimated then the heat contribution from the smaller particles in the ignition phase of the flame will be delayed. Importantly both the processes are interdependent and will be sensitive to each other in the overall predictions. The devolatilisation and char combustion model has already proven to provide good results in the past [352, 355] and hence the kinetics from both the models are reliable to use in this case. The ED model assumes that all the volatiles released are combusted as soon as they are mixed (infinitely fast chemistry) with the available O_2 at high temperature which generally over estimates the reaction rate. It is therefore, highly unlikely that the mixing rate from the ED model delays the rate of the initial combustion.

The mean radial velocity profiles radially are in good agreement with the measured data which demonstrates that the adopted Reynold stress model is able to accurately predict the flow field. The temperature field in the simulation after the ignition is able to predict the peak temperature but as the ignition is delayed, the changes in flame thickness downstream are delayed. This is evident from the temperature field at 1.9 m away from the burner tip which over predicts the temperature field.

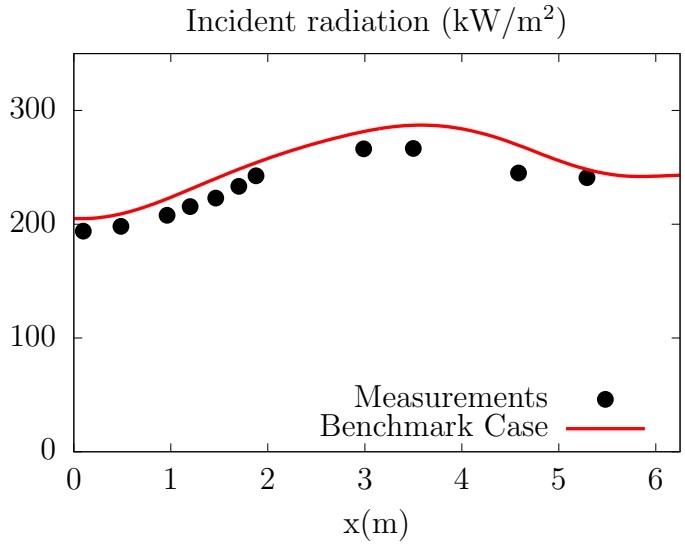

Figure 5.10: Benchmark results for the incident radiation on the top wall.

The overall simulation results of the mean mole fraction of O_2 and CO_2 are in

reasonable agreement with the measured values radially and along the centreline. On analysing the CO_2 and O_2 fields, it is found that the higher temperature field is accompanied with a higher mole fraction of CO_2 and a decrease in the mole fraction of O_2. There is a small inconsistency in the measured O_2 and CO_2 values at 1.25 m where the measured values do not follow the trend of the higher temperature and this implies lower O_2 and higher CO_2 mole fraction in and around the flame region. At the radial distance of 1.5 m, the simulation values of the O_2 mole fraction are over predicted and the value of the CO_2 mole fraction are under predicted in and near the flame region as the volatiles from the particles have not completely devolatilise and the volatiles in the continuous phase are not in flammability limits which reconfirms the delay of the ignition predicted by the benchmark model.

Finally, the furnace wall temperatures are determined by the interactive radiative,conductive and convective heat transfer between the furnace walls and the flame. The incident heat flux to the wall, presented in Figure 5.10, is over predicted throughout the length of the furnace but it has the correct shape. As it is a high volatile bituminous coal, it generally prefers two stage burning and thus the benchmark case is close to predicting the experimental values. Overall, the model predicts the flame shape and the peak temperature with a reasonable error of 10% but it fails to predict the early increase in the flame temperature between 1 - 1.25 m (suggested by the measured values) due to the delayed ignition. Thus, the results from the benchmark model are encouraging enough to investigate the influence of an ignition model which accounts for heterogeneous ignition.

5.4 Ignition model

The definition of the heterogeneous ignition of coal particles employed in this chapter is when the volatiles combust inside the particle which is indicated by the heat release and increase in the temperature. It is important to appreciate the limitation of applying the understandings from a single particle ignition model. Computationally it is not practical to solve the flow inside all the particles participating in the flame, the particles are modelled as lumped spheres exchanging heat and mass transfer uniformly via source terms. This does not allow simultaneous ignition of volatiles evolved in both phases as it was observed for certain conditions in the previous chapter. The ignition model proposed in this section enables both the modes for the ignition mechanism by allowing combustion of volatiles both inside and outside the particle separately which depends on the correlation of critical particle diameter. The correlation is based on the O_2 concentration and particle size, the particles below the critical particle diameter ignites the volatiles inside the particle(heterogeneously) and the particles above the correlation behaves the same way as the benchmark model (consecutively occurring thermo-chemical conversion). Implementing the correlation of critical diameter, bridges the gap between understanding the ignition mechanism of a single particle and identifying the ignition location for the stream of particles in a turbulent environment.

A detailed single particle study was conducted on the bituminous coal from the Saar region to obtain the correlation for the critical particle diameters with respect to O_2 concentration. The case under investigation is an air fired case and thus coal will not experience higher oxygen concentrations. The single particle model for the Saar coal was analysed using three O_2 concentration and three particle diameters. The sub models and methodology to obtain various pre-cursors for the single particle were kept the same. The boundary conditions used in the Chapter 4 for air cases were kept the same as the heating rate of 10000 K/s is high enough to simulate the furnace conditions. The simulations were conducted using a FFCM chemical kinetic package for better accuracy over the reduced mechanism. The single particle study is able to determine the ignition mechanism for different diameters based on the O_2 concentration that the particle experiences. The results are summarised by the correlation for the critical diameter as shown in Figure 5.11. The gas phase results from the benchmark case suggests that the particle do not experience an O_2 concentration higher than the inlet boundary conditions. The single particle model illustrates that only the particles under 32 μm ignite heterogeneously under pure air conditions which translates to a very small amount of mass fraction of particles igniting heterogeneously which can be seen from the Figure 5.2 describing the particle size distribution. This could be a contributing factor as to why this bituminous coal, when modelled using the two stage burning method in air conditions is able to accurately predict the trends. In addition, the benchmark case predicts the flame shape well with a maximum error of about 10%.

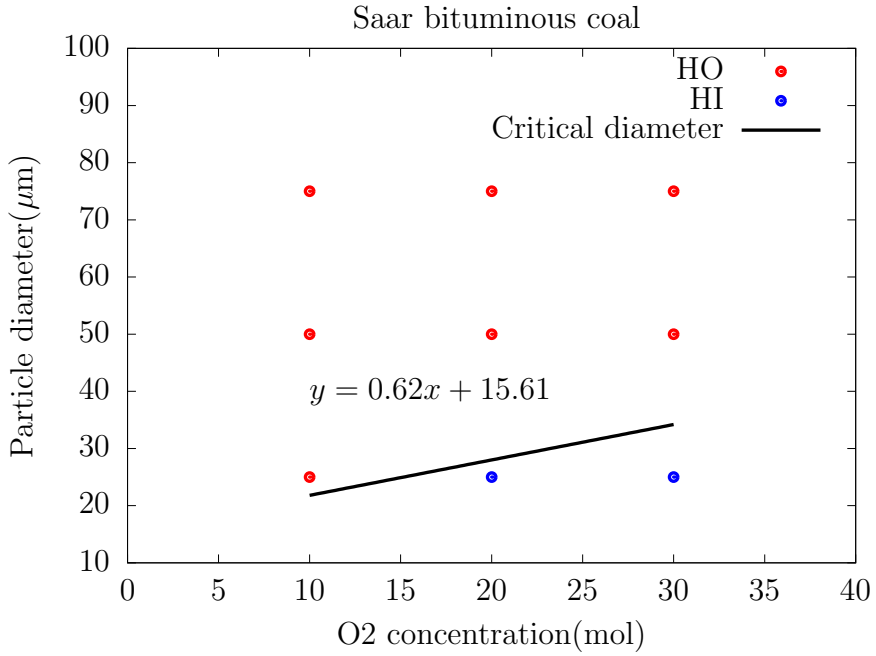

Figure 5.11: Correlation of the critical particle diameters for the Saar bituminous coal.

To analyse the sensitivity of the ignition model on the prediction of the inflame

Table 5.4: Governing laws for heat and mass transfer for a combusting particle.

Combusting particle	
Laws activated	Process
1	Inert heating
2	Water evaporation
3	Water boiling
4	Devolatilisation
5	Char Combustion

parameters, the CFD calculations of the IFRF furnace are repeated by integrating the ignition model. The ignition model was implemented by modifying the discrete phase model (DPM) which governs the particle Lagrangian trajectories and tracks the particle's thermo-chemical conversion (water evaporation, devolatilisation and char combustion). It involves the coupling of the interaction of heat, mass, species and momentum for particles and the gas phase. Each consecutively occurring thermo-chemical conversion process is defined by a law and each law was allocated an index. The law index corresponding to each heat and mass transfer phenomena which are summarised in Table 5.4. The ignition model is included in the CFD calculations by using a UDF and the UDF allows access to the source terms which couples the particle heat and mass transfer with the gas phase. The ignition model is activated when the particles are devolatilising (law 4) and for the particle sizes which are below the critical diameter values. The rest of the particles burn in a consecutively occurring process as described in the benchmark model.

As the particle initiates devolatilisation, the UDF checks the O_2 concentration of a cell along with particle size and temperature. The particle devolatilises according to Fluent's default code until the particle temperature reaches 800 K and the conditions for critical particle diameter is attained. It is a reasonable approximation that volatiles are flammable at 800 K. It will be expensive to account for the mass fraction of volatiles combusting inside each individual particle size. Thus, it was assumed that the UDF calculates the reaction of all the remaining volatiles left inside the particle as soon the particle reaches 800 K and the critical particle size conditions are achieved. This will partially devolatilse the particle depending on the devolatilisation kinetics and the vaporising temperature of the volatiles. This methodology will enable combustion of volatiles inside the particle triggering heterogeneous ignition as observed in Chapter 4. These conditions may exaggerate the combustion of volatiles inside the particle and over predict the ignition delay but will be a more accurate representation of ignition experienced by the particles and will be an improvement over the benchmark modelling methodology. The volatiles inside the particle are consumed and converted into products where there is an energy consumption from the domain for the volatiles to react and this is accompanied by the energy released in the conversion to the products which is absorbed by the particle. The net energy and products of the species evolved are added to the source

terms of the governing equations. Once the volatiles are consumed then the particles enter the char combustion phase (law 5). The increase in particle temperature accelerates char combustion. In this modelling strategy, there are no gradients for the heat and mass transfer considered within the particle, it is still considered as a lumped particle. This methodology can be applied to other CFD codes as long as it allows access to the source terms coupling the DPM and gas phase.

5.4.1 Particle ignition and its interaction in the gas phase

This section compares the particles behaviour and its impact on the continuous phase for the benchmark case and the case with ignition model. In order to quantify the ignition phenomena, Figures 5.12–5.14 are considered for analysis which describes the distribution field of the volatiles mass fraction, O_2 mass fraction, temperature field, the particle law index (thermo chemistry phase) and the heat generated due to volatiles reaction. Figure 5.12 shows that there is a very small difference in the thermo chemistry behaviour of the particles, highlighting small amount of particles initiating char combustion phase early. The small change can be attributed to the correlation of critical particle diameter which indicates that a small fraction of particles ignite heterogeneously. It is discussed below how this subtle difference impacts the gas phase and impacts the overall ignition of the flame and changes the flame predictions.

The particle distribution field presented in Figure 5.14 is superimposed on the heat of reaction field to illustrate the source of heat in the flame. The particle size shown in Figure 5.14 is capped at 50 μm in order visualise the behaviour of the smaller particles and avoid the overshadowing of the heat of the reaction field. It also reveals the position of the particles and the laws it is governed by at different locations in the furnace.

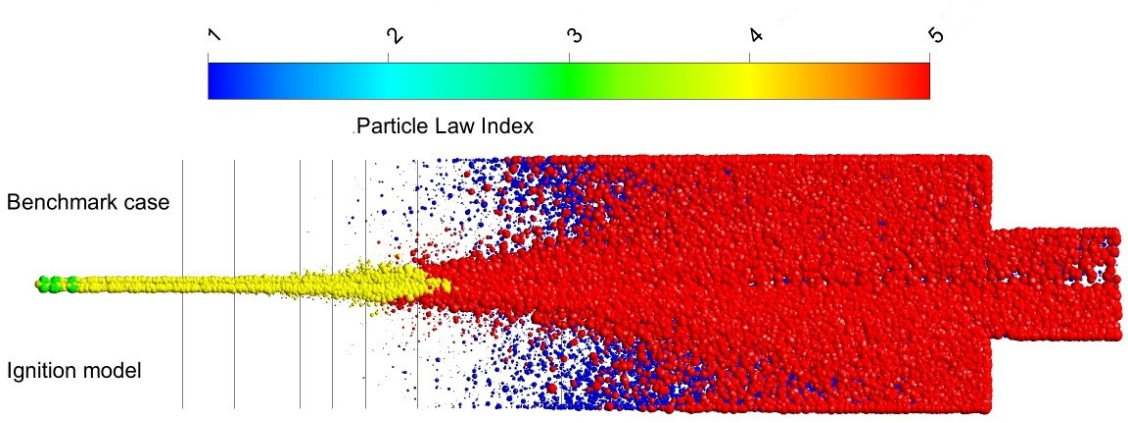

Figure 5.12: Particle distribution field defining the thermo chemistry phase of the particle (particle law). The particle sizes are not to scale but scaled relative to each other.

For both the modelling strategies, the char combustion does not start before the particle is completely devolatilised. The smaller particles devolatilise quicker com-

pared to bigger particles because of the less resistance to the heat transfer from a smaller particle surface area. Hence the smaller particles enter the char combustion phase earlier compared to bigger particles. As the bigger particles stay in the devolatilisation phase longer and their ignition mechanism are not affected, this section is significantly focused on the combustion behaviour of the smaller particles and their contribution in the ignition region.

On analysing the Figures 5.13 and 5.14 simultaneously, the benchmark case shows that the particles are already under the devolatilisation phase when it enters the furnace and this is because of the high temperature inlet boundary conditions. As the particles go through the mixing zone, the devolatilisation rate increases due to the increase in radiative heat transfer to the particles from the wall and the increase in convective-conductive heat transfer from the secondary stream. The particles release a small amount of volatiles in the early stages at around 1 m, the volatiles mix with the available O_2, reacts and releases heat in the gas phase(signifying homogeneous ignition). The heat release in the gas phase between 1 - 1.5 m, as shown in Figure 5.14b is due to combustion of volatiles which illustrates homogeneous ignition. The depletion of O_2 and the increase in the heat released are directly proportional to each other which is evident in the distribution of the O_2 field. It can be concluded that the benchmark phase ignition is primarily due to the gas phase ignition as there is no contribution from the char reaction in the early stages of the flame which is evident from the particle law indicated in Figure 5.14. The particles continue to devolatilise as they move along the furnace, and the production and combustion of the volatiles peaks between 1.25 m and 1.9 m. The small particles highlighted in Figure 5.14 show that the char combustion phase (law 5) starts at 1.7 m. The high flame temperatures around 1.8 m are a result of the simultaneous volatiles and char combustion. The high temperature flame downstream (after 1.9 m) is primarily due to the char combustion which is accompanied with a small amount of the volatile combustion (volatiles released from the bigger particles). In summary, the ignition in the benchmark models is due to the volatiles combustion because the model does not account for the particles igniting heterogeneously. Thus the overall model lacks an accurate ignition predicting capability due to this limitation.

On the other hand the ignition model modifies the way the particles behave during the devolatilisation phase. Based on the single particle correlation, the coal particles burn the volatiles and releases products in the gas phase and the enthalpy of the products increases the heat generated in the gas phase. This is evident in Figure 5.14b where there is early heat release in the gas phase due to the volatiles combustion inside the particle. The particles ignite heterogeneously in the shear layer of the mixing plane where the particles are subjected to additional heat from the secondary stream. The heat released from the heterogeneous burning in the early stages of the particles accelerates the devolatilisation phase of the particles around it as the temperature of the gas phase increases. This phenomena implies that the smaller particles enter the char combustion phase earlier compared to the benchmark case which is clearly illustrated in Figure 5.14b. This early particle

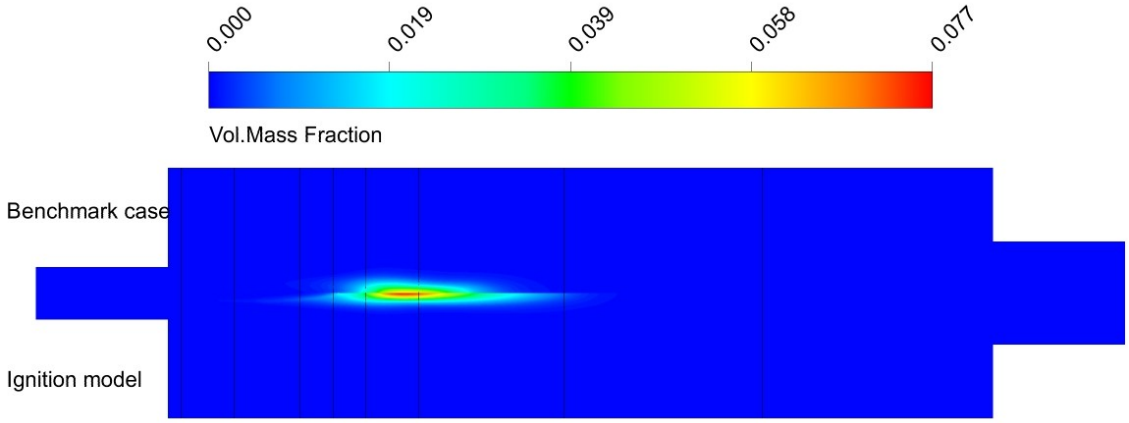

(a) Volatiles mass fraction in the gas phase.

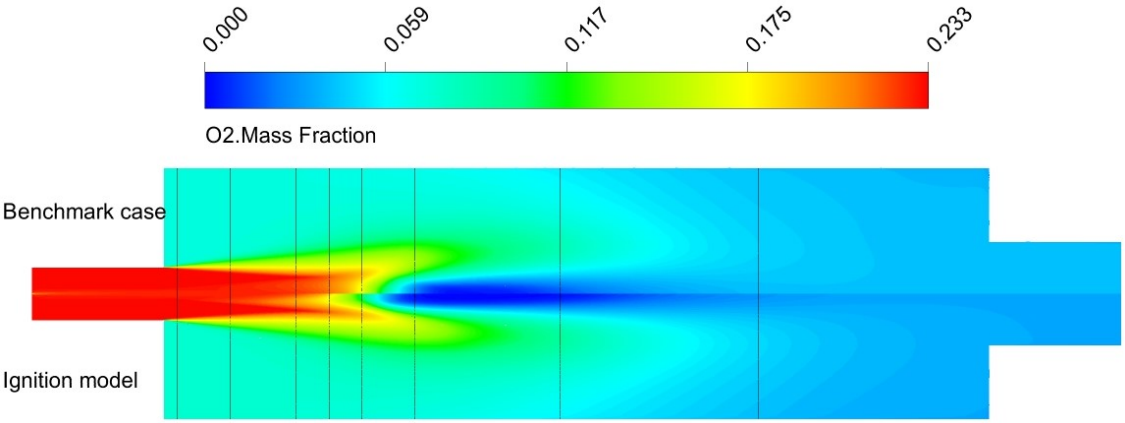

(b) CO_2 mass fraction.

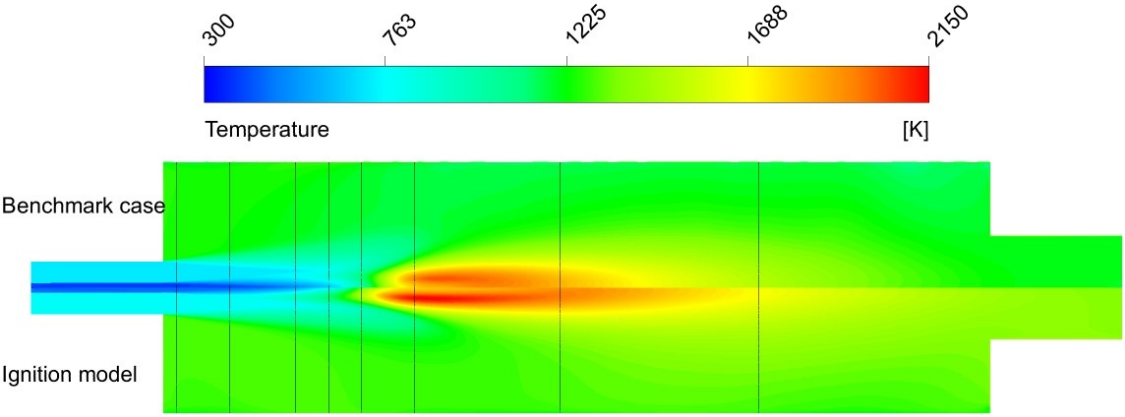

(c) Temperature field.

Figure 5.13: Comparison of the CFD simulations between the benchmark model (top) and the Ignition model(bottom) for (a)Volatiles mass fraction, (b)CO_2 mass fraction and (c)Temperature field. The lines indicate the position of the measurement ports.

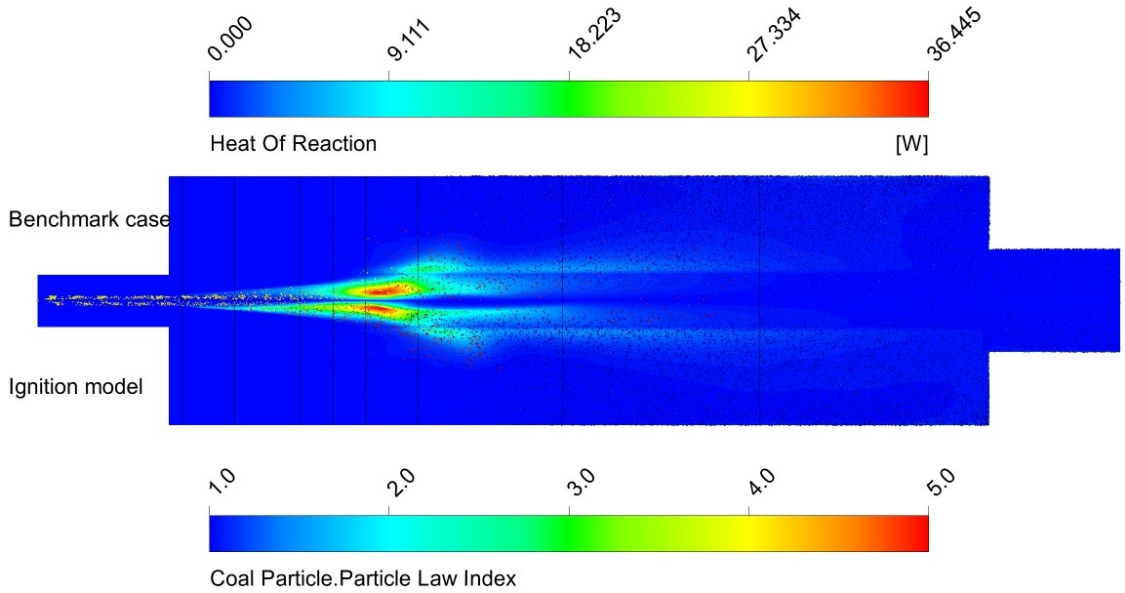

(a) Distribution field of the heat generated super imposed with the particle spread defining the thermo chemistry phase (particle law).

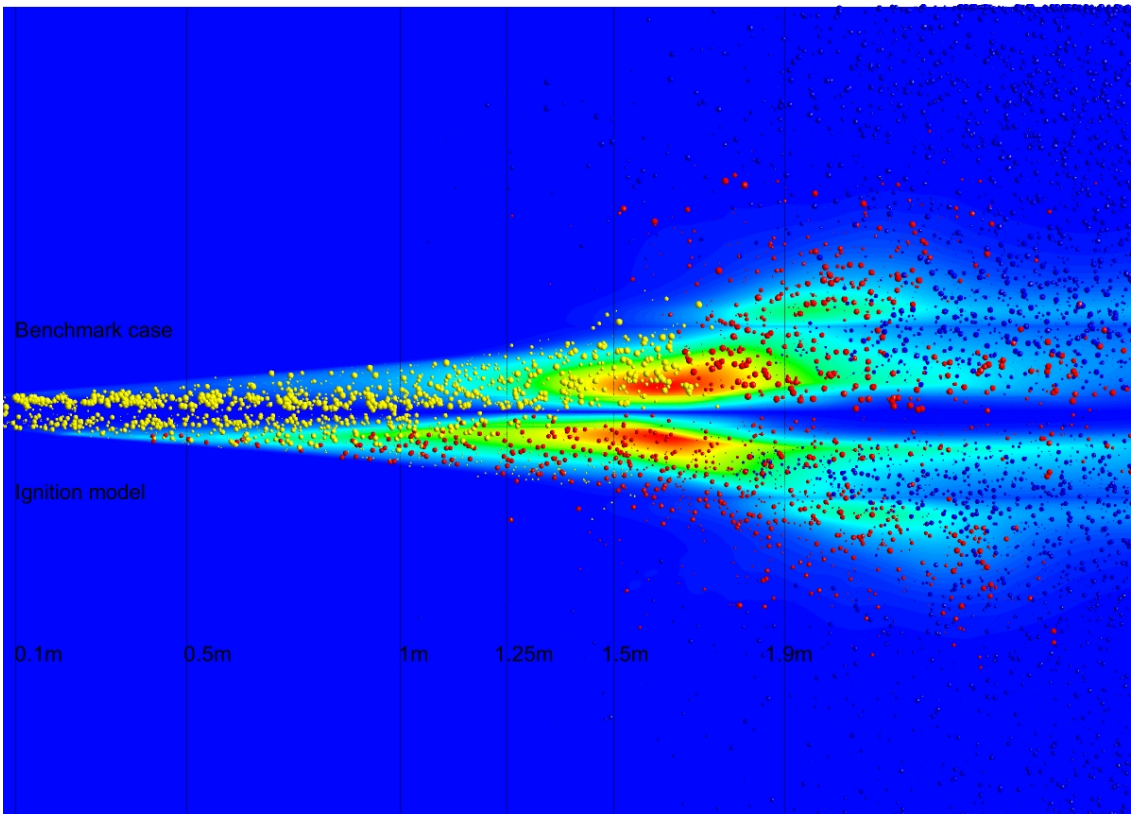

(b) A zoomed in view (close to the burner) of the distribution field for the particle visualisation.

Figure 5.14: Distribution field of the heat produced due to the chemical reactions super imposed with the particle spread defining the thermo chemistry phase (particle law). The particle sizes are capped at 55 μm for clearer visualisation of small particles.

ignition leads to increase in the gas phase temperature, early devolatilisation, early gas reactions and particles initiating the char combustion phase early compared to the benchmark case. In Figure 5.14b it is evident that the smaller particles between 1.25 m and 1.9 m are in the char combustion phase whereas Figure 5.12 shows that the bigger particles are still in the devolatilisation phase and continue to release and combust the volatiles in the gas phase. Similar to the observation in the benchmark case, the peak temperatures in the flame predictions in the ignition model is a combined result of small particles undergoing the char combustion phase and the volatiles burning in the gas phase. It may be concluded that the ignition model enables early heat release which impacts the particles around it. The ignition between 1-1.25 m can be attributed to the combination of heterogeneous combustion of the volatiles, the gas phase combustion of the volatiles and the char combustion of small particles.

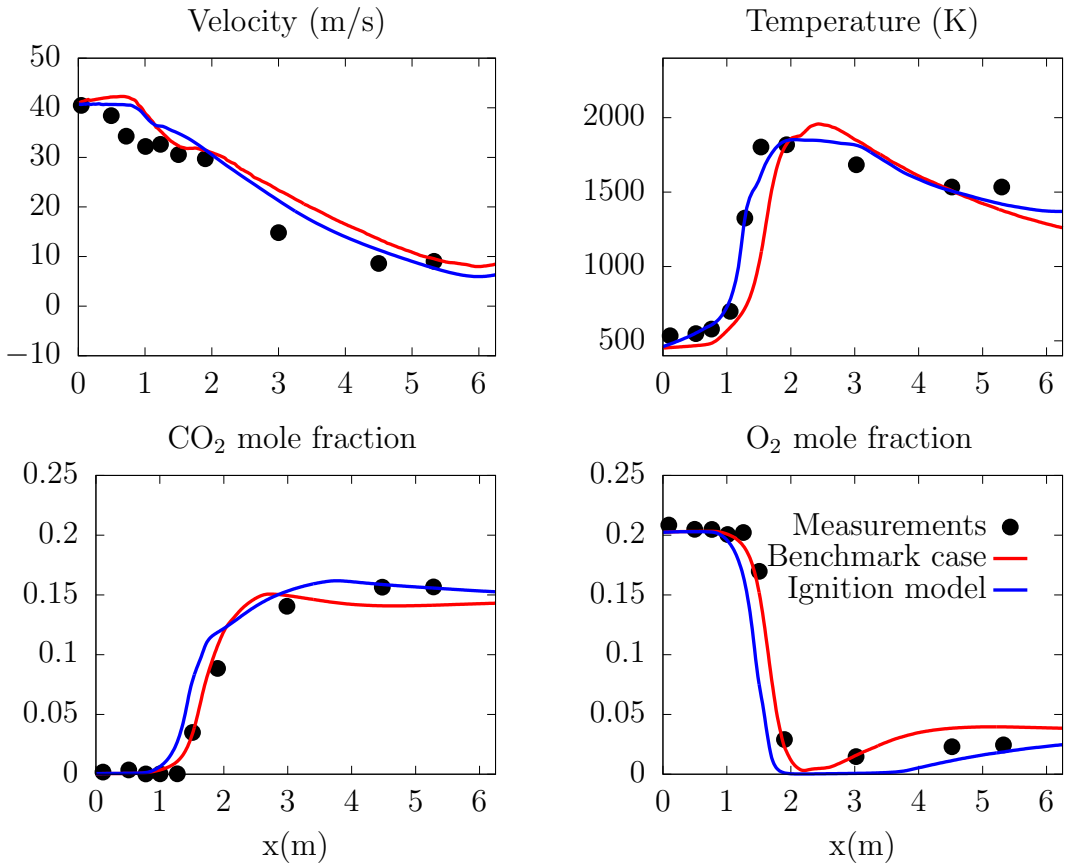

Figure 5.15: Axial mean plots for the CFD calculations with the ignition model and benchmark case along the centreline of the furnace for gas phase: velocity, temperature, CO_2 and O_2 mole fraction.

It is difficult to differentiate from Figure 5.14b the particles that ignite hetergeneously and particles that are a result of complete devolatilisation but on comparing the benchmark case and the ignition model, it is clear that there is early ignition in

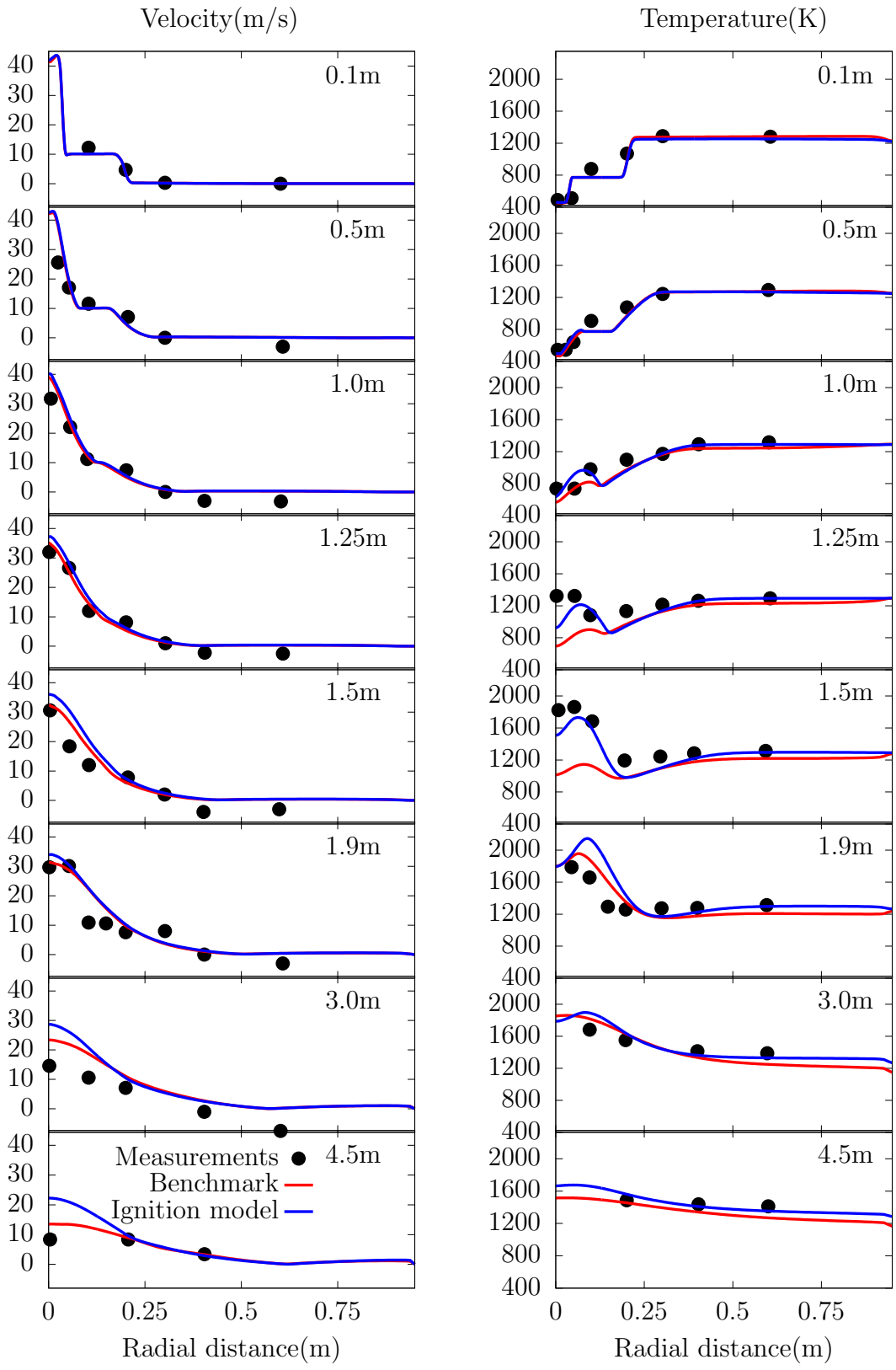

Figure 5.16: Results of the CFD calculations for the ignition model and benchmark case against the in-flame measurements for the Velocity(left) and Temperature(right).

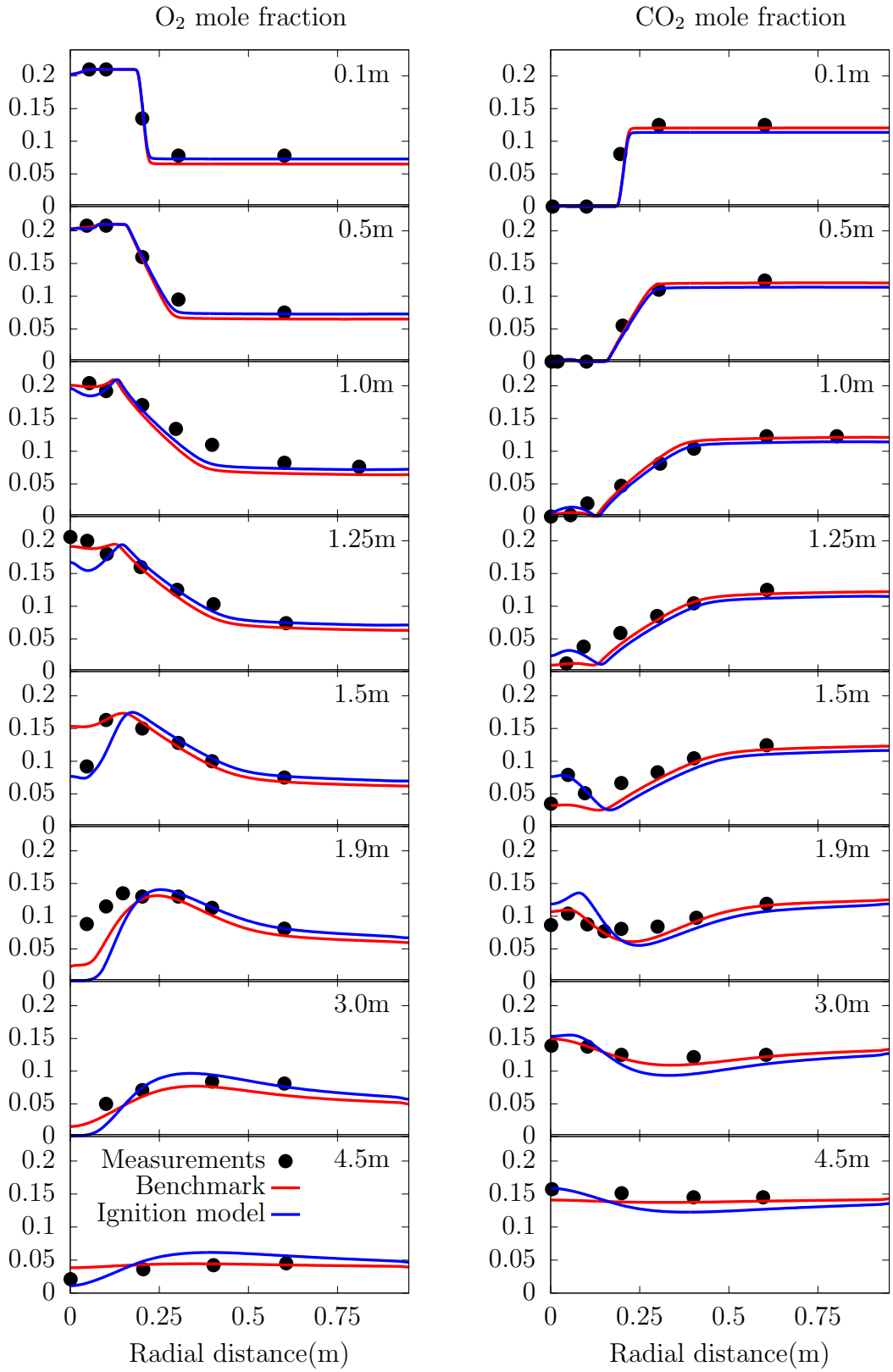

Figure 5.17: Results of the CFD calculations for the ignition model and benchmark case against the in-flame measurements for O_2(left) and CO_2(right) mole fraction.

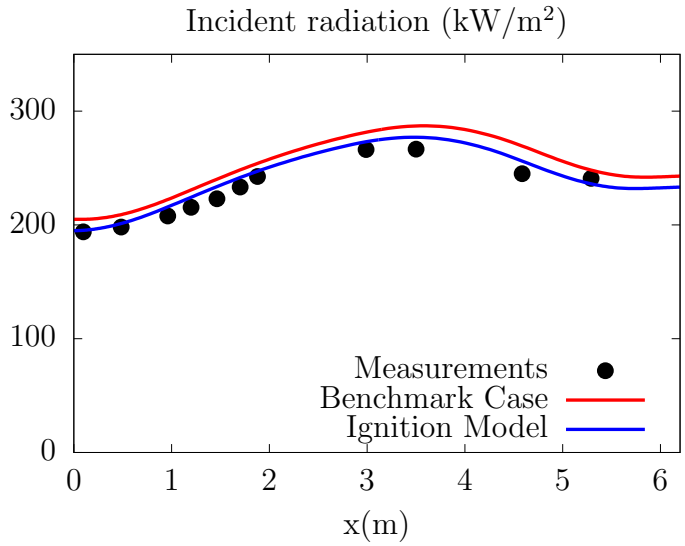

Figure 5.18: Results for the incident radiation on the top wall for the benchmark case and ignition model against the measured values.

the overall results when the ignition model is applied. Figures 5.13 and 5.14 suggest that there is ignition close to the burner and a clear reduction in the flame lift-off distance which can be attributed to the ignition model. It is practically impossible to visualise such a phenomena experimentally which propagates in small time scales and highly turbulent environments. Hence it is difficult to validate this particular phenomena of particle to particle interaction in a highly turbulent environment. The inflame measurements are used to validate the modelling impact of the particle to particle interaction on the overall flame predictions.

The comparison of the results obtained from the benchmark case and the ignition model against the inflame measured values are shown in Figures 5.15–5.18. The ignition model shows an improvement in the ignition phase, i.e. in the early stages of the flame when compared to the benchmark model. The improvement is evident in the centreline temperature profile as shown in Figure 5.15. The results demonstrate that the prediction of the lift off distance is improved by the ignition model and the gradual increase in the temperature close to the burner is predicted with an improved accuracy. Improvements in the prediction of the flame shape close to the burner is evident from Figures 5.13c and 5.16 especially at radial locations between 1 m and 1.5 m. The improvement can be attributed to the early heat release from the small particles which burn heterogeneously. The temperature field is under predicted for the radial profiles in the early part of the flame but is sensitive to the ignition and in excellent agreement with the measured values.

The velocity field is not affected as much when compared to the benchmark case. The species mole fraction of O_2 and CO_2 abide to the temperature field. The consumption of O_2 due to early ignition is highlighted in Figure 5.13b. The ignition

model compares well with the measured data close to the burner, it under predicts the O_2 concentration inside the flame at 1.9 m which could be attributed to the spike in the volatiles combustion and increase in the char reaction. This phenomena is also reflected in the temperature field where the ignition model over predicts the flame temperature. The prediction of the incident radiation along the length of the furnace improves which could be due to the changes in the flame shape. The comparison of the modelling results with the measured data suggest that the model is an improvement over the benchmark modelling strategy and the ignition modelling approach can be used with confidence for future CFD calculations.

The study in this section applied an ignition model to the CFD calculations of the IFRF furnace. The results from the ignition model show excellent agreement with the measured values which demonstrates the importance of integrating the heterogeneous ignition mechanism when simulating a coal flame. The results suggests that the methodology applied in integrating the findings from the previous chapter is accurate and is recommended to be used in CFD calculations of coal combustion.

5.5 Conclusions

A novel approach is developed to visualise ignition in a pulverised fuel turbulent flame. Since the coaxial geometry exhibits a low swirl forward flowing flame, it provided an easy insight into the history of thermo chemical conversion of coal particles. This analysis together with gas properties enabled determination of the source of ignition which has not been quantified in the literature before. The methodology highlighted the short comings in the standard CFD modelling approach of modelling pulverised fuel flame with a focus on ignition.

The investigation in this chapter applied the single particle ignition model developed and validated in the previous chapter to the CFD calculations for the IFRF co-axial burner. The IFRF facility was chosen for the CFD calculations to exhibit the impact of the ignition on the overall flame development in air conditions. The burner and furnace geometry were simplified and simulated as a 2-D axisymmetric geometry as the three dimensional flow effects are weak in these cases. The general approach to the studies were to simulate the benchmark cases first, then simulate the same cases after incorporating the ignition model and finally compare the results against the experimental results. The ignition model has been successfully integrated into the benchmark models and the main findings of the investigation are as follows:

i On analysing the benchmark case, it was difficult to determine the source of ignition and the ignition mechanism of the flame based only on the gas phase parameters. The ignition mechanism was quantified by simultaneously analysing the particle law index, gas phase parameters and the heat released in the furnace. The benchmark results suggest that the ignition is due to volatiles combustion in gas phase (homogeneous ignition) as the char combustion is

initiated downstream of the ignition zone. The peak temperatures of the flame ≈ 1.9 m is due to the combination of volatiles and char combustion.

ii The benchmark simulation was able to predict the flame parameters well and the predictions were in reasonable agreement with the experimental values and this shows that the choice of the sub-models was good. The measured values show that the flame ignites between 1.25 m and 1.5 m. The benchmark simulations could not predict the ignition location with accuracy and lagged with a 10% error which was evident when the flame parameters from the benchmark case are compared with the measured data at 1.25 m and 1.5 m.

iii The Rosin-Rammler particle distribution and the critical diameter correlation obtained from the single particle ignition study on the Saar coal suggests that very few and small particles ignite heterogeneously. This was one of the reasons why the benchmark case with the traditional thermo-chemistry model was able to predict the flame parameters with a smaller error.

iv The ignition model illustrates that the ignition is due to the combination of volatiles combustion inside the particle (heterogeneous ignition), volatiles combustion in gas phase and the char combustion of small particles. The CFD simulations results shows that the interaction between heterogeneously igniting particles and the other particles plays an important role in predicting the overall ignition and flame behaviour of coal flames.

v Inclusion of heterogeneous ignition of particles improved the prediction of the gas phase parameters in the ignition zone. The overall agreement between the measured values and the simulation are encouraging and suggest that the ignition modelling strategy used in this section can be applied with confidence in the CFD calculations of the coal combustion in air conditions.

6 Modelling investigation for a Utah coaxial oxy-fuel burner

In coal power station, oxyfuel technology has the potential to reduce the CO_2 emissions to meet the climate change targets. The technology increases the concentration of CO_2 in the flue gases. This enables high purification of CO_2 which is suitable for transport and storage. The technology requires N_2 in the oxidant supply stream's to be replaced with CO_2. As CO_2 is more effective at absorbing heat when compared to N_2, oxyfuel conditions will change the combustion environment and have implications on the overall ignition and flame parameters. This technology can be retrofitted to the existing power plants but it is important to develop an understanding of switching to this technology. The CFD modelling can provide an insight into the influence of retrofitting the existing air fired burners to oxycoal burners. The work in the chapter is an extension of the previous chapter which investigates the application of the developed ignition model in oxyfuel conditions for a Type 0 burner.

The experimental facility chosen for this modelling investigation is the oxy-fuel furnace at the University of Utah. The facility at the University of Utah is a downward firing oxy-coal combustor with 40 kW output (up to 100 kW capacity) studied by Zhang and coworkers [85, 187–189]. The Utah facility was chosen for a similar reasons as the IFRF furnace with the addition that it provided many experimental conditions which tested the ignition based on the variation of the O_2 concentration. The facility tested a number of experimental conditions which focused on the ignition and flame stability [85, 187–189, 362]. The six cases which conducted sensitivity study on the flame stand off distance due to variation of O_2 concentration in the secondary stream are used for modelling investigation. As the ignition model is sensitive to the O_2 concentration, the set of cases is able to demonstrate the significant changes in the flame stand off distance. The numerical modelling studies on this test facility range over a wide variety of modelling methodologies when quantifying the ignition of a flame [201, 329, 363–366]. The work performed by Babak et al. [329, 364] and Seidel et al. [201] used the RANS methodology whereas Julien et al. [365, 366] used a LES approach. In all three approaches, the temperature and combustion species were used to indicate the ignition point in the flame. The species chosen depended on the species included in the reaction mechanism and the turbulence chemistry model used, e.g. Babak used C_2H_2 as a pre-cursor for soot and Seidel et al. used CO as an indicator of the product species. Again they have all used different sub models and methodologies in their simulations but according to the author's knowledge there is no integration of the heterogeneous particle ignition in their modelling approach as described in the previous chapter.

The numerical modelling and the methodology in this Chapter is similar to the Chapter 5. A set of benchmark cases are simulated and compared with experimental results which are described in Section 6.2 and later the measured data is compared with the simulations of the ignition model. There are no inflame measurements available for validating the sub-models, the only available data is the computed stand-off distance based on the visual observations and it is this result that is used to validate the different models. Section 6.1 describes the oxy fuel experimental facility in Utah, Section 6.2 describes the benchmark model and its results, and a sensitivity analysis on the different modelling parameters of the benchmark case is also discussed in this section. The overall impact of the ignition model is described in Section 6.4.

6.1 Case description

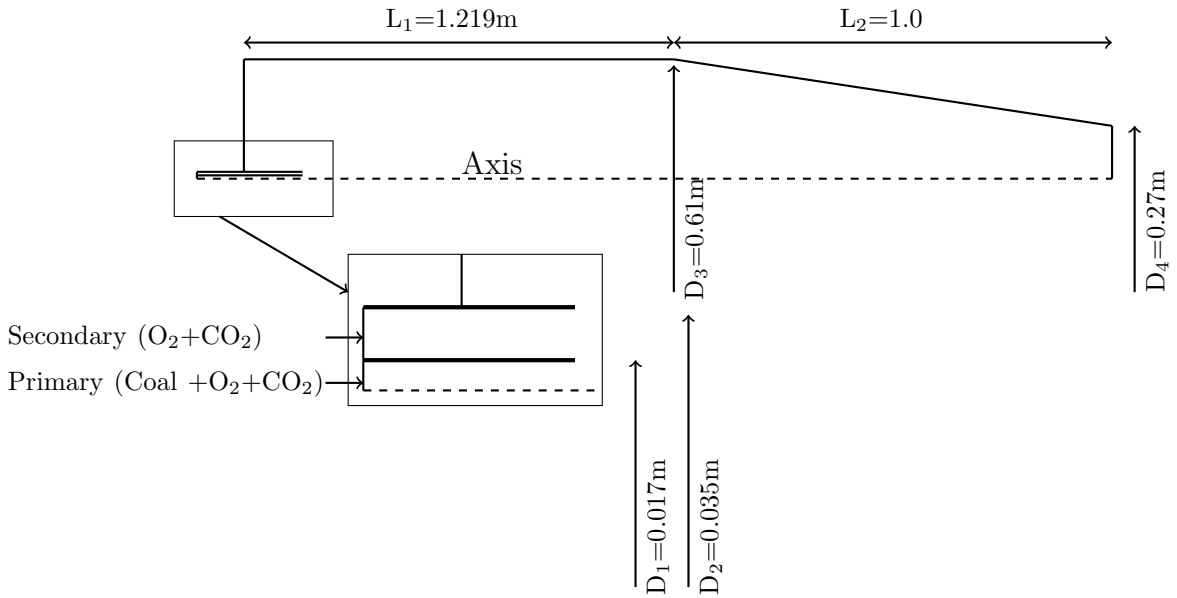

Figure 6.1: Sketch of the Utah oxy-fuel furnace (not to scale).

The experiments were conducted in a down-fired oxy-fuel furnace which is based at the University of Utah and is capable of an output up to 100 kW [187]. It is a co-axial burner with two streams where the primary stream carries the coal and the secondary stream provides sufficient oxidant for combustion. The furnace is divided into three regions i.e. the burner zone, radiant zone and the convective zone. The main region of interest is the burner zone where the flame prevails and the burner zone is 1.219 m long and the diameter width of 0.61 m. The burner has two concentric pipes for the two stream of flows which is 0.27 m long where around 0.15 m protrude into the furnace (in the burner zone) which enables the radiative heat transfer from the furnace walls to the coaxial burner. The burner zone is electrically heated by a 24 ceramic plate heater rated at 840 W each which

enables the furnace to operate upto 100 kW. In the burner zone, there are three rectangular optical windows for the flame visualisation, three circular flanges to install K-type thermocouples for the temperature measurements and three more circular flanges for flame visualisations. A schematic of the Utah oxy-fuel furnace inner dimension of the burner zone and radiant is shown in Figure 6.1. The visual observations suggest that the flame was centred and did not lean to one side and thus a 2-D axisymmetric geometry will suffice for the numerical calculations and the prediction of the flame behaviour. Zhang and co-workers tested two coals but the Utah high volatile bituminous coal was extensively tested across various conditions and hence it was used for the present modelling investigation, the properties of the coal are described in Table 6.1. The Rosin-Rammler particle size distribution was used to model the different particle sizes measured and the mean diameter chosen was 85 μm, the spread parameter of 3.5, and the fitting is shown in Figure 6.2.

Table 6.1: Coal properties of the Utah bituminous coal.

Proximate analysis (as received)	[wt%]
Fixed carbon	46.44
Volatiles	38.81
Ash	11.72
Moisture	3.03
Ultimate analysis (dry ash free)	**[%wt]**
C	77.75
H	5.03
O	15.33
N	1.44
S	0.45
Higher heating value	27.286 MJ/kg

Zhang et al. [187, 188] tested a wide range of oxy-fuel conditions in the Utah furnace. Among which, the sensitivity study conducted on the impact of O_2 from the secondary stream of the burner on the flame stand-off distance provided an important set of results. It provides data for the flame transition from a detached to an attached flame close to the burner tip. As the two key parameters in the ignition model are the particle diameter and O_2 concentration, the final results from the numerical study will be able to highlight the improvement by ignition model over the benchmark modelling strategy. The study consisted of six cases of the flame stand-off distance and the operating condition as described in Table 6.2. The coal particles are assumed to have the same velocity and temperature as the carrier gas at the inlet.

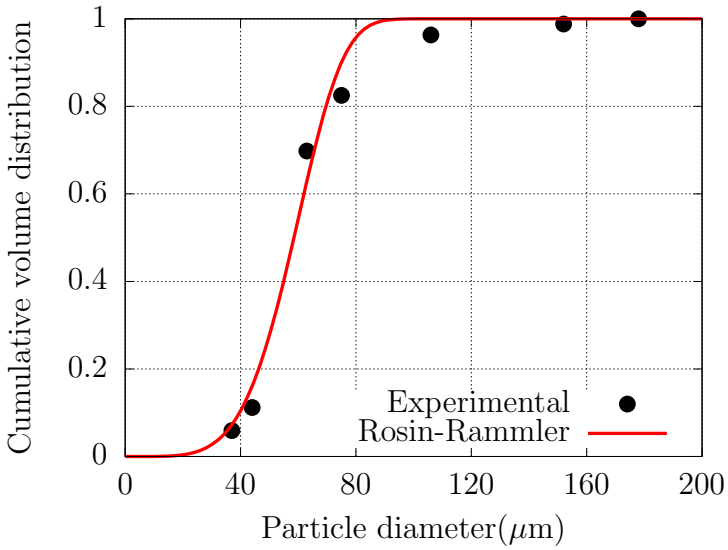

Figure 6.2: Particle size distribution using the Rosin-Rammler correlation where d_e = 63.1 μm and n = 4.845.

Table 6.2: Operating conditions for the Utah oxyfuel furnace.

	Case 1	Case 2	Case 3	Case 4	Case 5	Case 6	
Primary stream							
Coal mass flow	4.84	4.84	4.84	4.84	4.84	4.84	kg/hr
CO_2 mass flow	6.84	6..84	6.84	6.84	6.84	6.84	kg/hr
Temperature	305	305	305	305	305	305	K
Bulk Velocity	5.394	5.394	5.394	5.394	5.394	5.394	m/s
Secondary stream							
CO_2 mass flow	15.98	15.98	15.98	15.98	15.98	15.98	kg/hr
O_2 mass flow	11.052	11.52	12.024	12.528	13.032	15.336	kg/hr
Temperature	489	489	489	489	489	489	K
Bulk Velocity	14.93	15.23	15.56	15.89	16.21	17.74	m/s

Zhang et al. [187, 188] obseverd multiple steady states during the experimentation stage where the flame for certain conditions display both attached and detached ignition from the tip of the burner. Case 1 favoured a detached flame, Cases 5 and 6 displayed unimodal attached flame whereas Cases 2, 3 and 4 illustrated multimodal behaviour. This could be explained as the flame was undergoing transition from Case 1 to Case 5 and due to the complex coupling of the turbulent mixing and reaction kinetics this behaviour was observed. There could be additional factors such as change in ambient conditions, the burner operation cycle and the measurement limitations. This phenomenon was also observed by Chen and Churchill for radiantly stabalised flame [367]. This behaviour could be mathematically explained by

the Semenov theory of thermal explosions where a flame can have multiple steady state ignition points [102]. In order to overcome this behaviour and quantify the stand-off distance, 6000 images for each case were used and presented in the form of a probability density function.

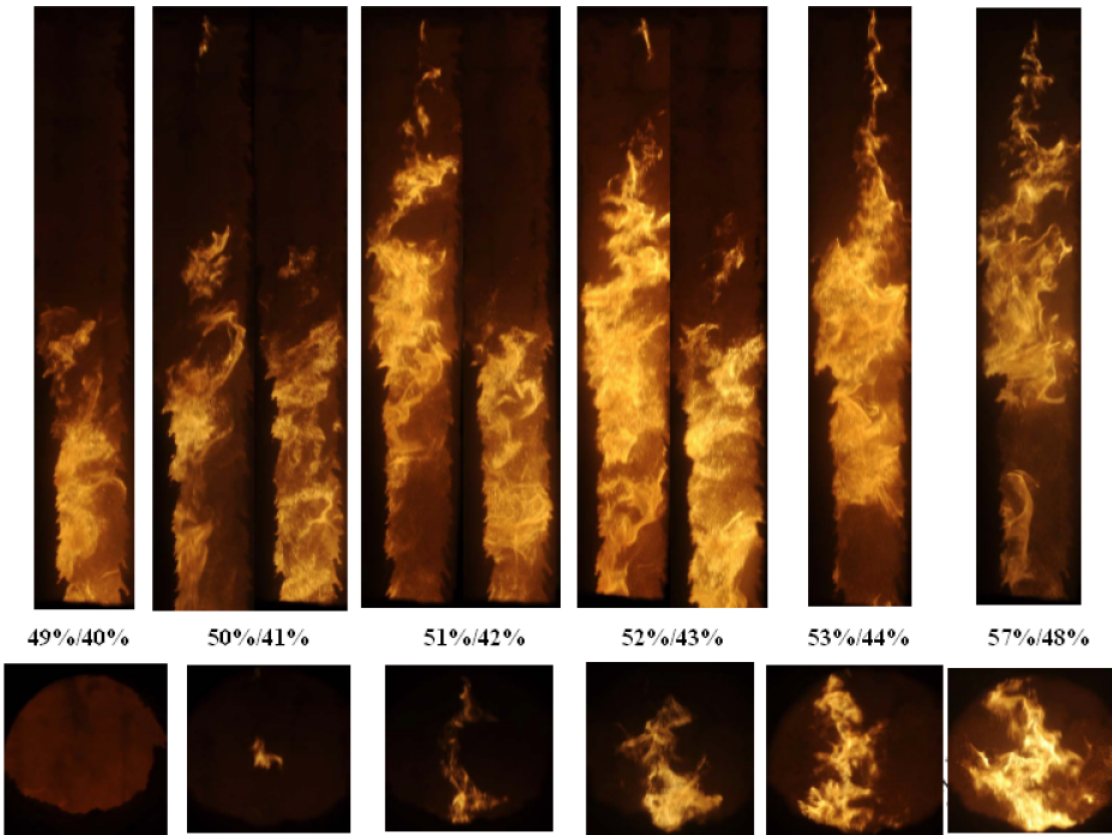

Figure 6.3: Flame images from the experiment. Circular view shows the flame behaviour close to the burner. The numbers in the image represent Secondary O_2/overall O_2 in moles.

The stand-off distance was defined as the observed distance between the burner tip and the visible ignition of the flame. The observation was done by an EPIX CMOS camera which was set up at a frame rate of 30 fps and exposure time of 8.3 ms. An image processing methodology was developed to obtain the flame stand-off distance from the images captured and the flame images from the experiments are shown in Figure 6.3. It shows the impact of increasing the O_2 concentration on the flame stand-off distance. The images from the experiments illustrates that the ignition in attached flames occurs in a thermally thin layer close to the burner and the flame cloud increases in the width downstream. The development of detached flames are very different, i.e. the ignition occurs in or around the flame cloud, away from the tip of the burner.

6.2 Benchmark case

The mesh generation and the CFD calculations were performed in ICEM and ANSYS Fluent, respectively, and a similar meshing strategy was applied as described in Section 5.2. A fine mesh generated with 112716 cells is shown in Figure 6.4 which was used for all the analysis in this part of the study. The cells are concentrated near the burner zone to accurately capture the ignition phenomena. A mesh sensitivity analysis is conducted in Section 6.3.1 in order to obtain a consistent grid independent solution.

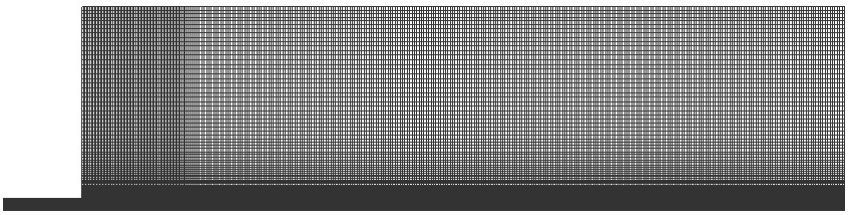

Figure 6.4: Computational grid generated for the CFD calculations of Utah furnace.

A RANS modelling approach was used to model the oxy-coal flame, the boundary condition set up and the sub-models applied were similar to the IFRF case. The gas phase is solved using Equations (2.4)–(2.6), (2.9) and (2.10) and the dispersed phase is modelled using the Lagrangian tracking of discrete particles. The continuous and the dispersed phase are non linearly coupled using source terms. Since the Reynolds stress model provided good results for modelling turbulence in Section 5.3 it was chosen to model the turbulence in this furnace. The devolatilisation is modelled using CPD [365, 366] and the predicted value of HTVY was ≈ 1.25. This reduced the total combustible char mass fraction to 0.379. The initial density of the particles was assumed to be constant at 1300 kg/m^3 [363]. The volatiles evolved were modelled as empirical species derived from fuel properties which had a molecular weight of 30 g/mol. The volatiles combustion is calculated using the two step Eddy dissipation model which has been used in the past for accounting the turbulence-chemistry interation in oxy-coal combustion [195, 302, 368, 369]. The mixing parameters A and B in Equation 2.32 for the two step reaction model was kept constant at 4 and 0.5, respectively, which was taken from Magnussen and Hjertager [282]. The char combustion is calculated using the kinetics-diffusion model proposed by Field et al. [294] and Baum and Street [233] and described in Section 2.9.3, summarised by Equation 2.39 and the kinetics were obtained from the work perfomed by Siedel [201]. Since the focus of the work is on ignition, it is acknowledge that the absence of CO_2 equilibrium dissociation reactions and gasification reactions may induce an error in the early stage predictions of the flame and hence the model is tested with the different gas phase chemistry which are coupled with different turbulence chemistry interacting model, described in Section 6.3.3. The overall transport properties of the species was calculated by using ANSYS Fluent based on the kinetic theory. The transport equations are calculated using a second order discretisation upwind scheme. The sub-models used are summarised

in Table 6.3.

Table 6.3: Sub-models employed for calculating the benchmark cases.

Model	Model Parameters		
Turbulence	Reynolds Stress Model [222]		
Gas Phase Chemistry	Eddy dissipation model [280]		
	$C_{1.52}H_{2.63}O_{0.50}N_{0.0541}S_{0.0073}$ +	$1.17O_2 \longrightarrow$	$1.52CO + 1.31H_2O + 0.0270N_2 + 0.0073SO_2$
	$CO + 0.5O_2 \longrightarrow CO_2$		
Devoltilsation rate	CPD fitted into Single-step Arrhenius expression [329, 363]		
	Pre-exponential fac. (A_i)	= 237411.4	
	Activation Energy (Ea_i)	= 5.47e+07	J/kmol
Char Combustion	Kinetic/diffusion[201]		
	Diffusion coeff. (C_{diff})	= 5x10^{-12}	$m^3/K^{0.75}$
	Pre-exponential fac. (A_{ichar})	= 0.86	$kg/(m^2s)$
	Activation Energy (E_{ichar})	= 1.13 x 10^8	J/kmol
Radiation	Discrete Ordinates (3 x 3) [205]		
	Absorption coefficient given by WSGG constants [295]		
	Particle emissivity ϵ	= 0.9	
	Particle scattering factor σ_p	= 0.9	
Particles	Eulerian-Lagrangian approach		

As the burner length is sufficiently long to obtain a fully develope velocity profile, the two inlets are modelled as constant velocity profiles across surface and the values of the velocity and temperatures are summarised in Table 6.2. The mean velocity of the particles entering the domain has the same velocity as the carrier gas from the primary inlet. The outlet was set as the pressure outlet condition with zero diffusive flux for species. The inlets and outlet are modelled as black body surfaces to neglect any radiation reflection. The wall temperatures were kept at a constant temperature of 1283 K according to Zhang et al. [187] but it was not measured at the inner wall according to Julien and he states that it was measured two inches behind the inner wall. It is also known from the IFRF case that the wall temperature cannot be constant in the direction of the flame. Michel and Ryan [186] also reported that each flame condition will change the wall temperature in accordance to the flame property. On considering these factors a wall sensitivity analysis is conducted and discussed in the Section 6.3.4. The side walls are treated as adiabatic walls and was given a constant wall emissivity of 0.8 which is the case in

cooled walls [355]. A 3 x 3 angular discretisation is used to solve the radiation heat transfer which is calculated using the discrete ordinates model. The WSGG model is used to calculate the gas absorption coefficient but it was developed mainly for the air fired case, thus a sensitivity analysis is conducted for accurate modelling of the gas absorption coefficient in oxy-fuel conditions. As described in previous chapter in Section 5.2, the benchmark case is set up using standard modelling approach for thermo-chemical conversion where each mass loss process for the particles was set to be a consecutively occurring process.

The visual observations provided the flame stand-off distance which according to Zhang [187] is produced from the luminosity of the flame. The flame luminosity is generally a function of the temperature and the soot produced during combustion. The CFD simulations do not allow direct comparison with the experimental data which are reproduced from image processing using the luminosity of the flame. Hence, the ignition point or flame stand-off distance from the simulations was judged when the flame temperature exceeds 50 K of the maximum input temperature, i.e the maximum wall temperatures. This particular approach was also adopted by Julien [363] and thus this methodology could be used to obtain the stand-off distance. The wall temperature was set at 1283 K for the benchmark cases as reported in the experimental data. According to this definition, when the domain temperature exceeds 1333 K, the minimum axial distance calculated will be the stand-off distance from the model.

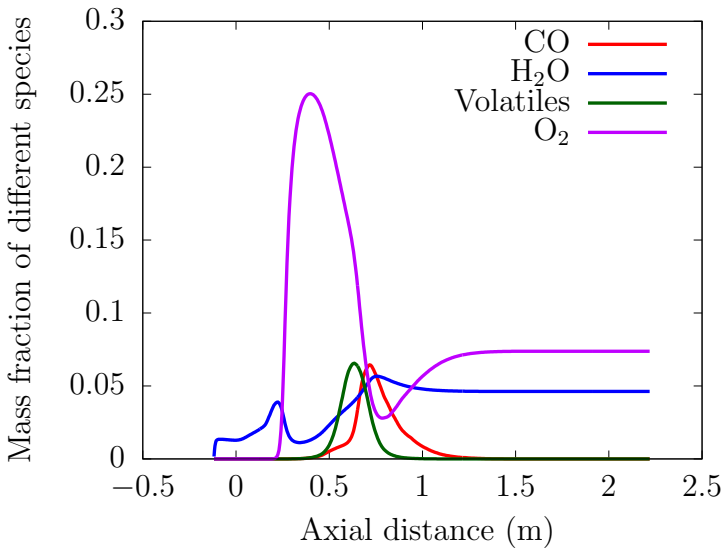

Figure 6.5: Species distribution for benchmark Case 1 along the centreline.

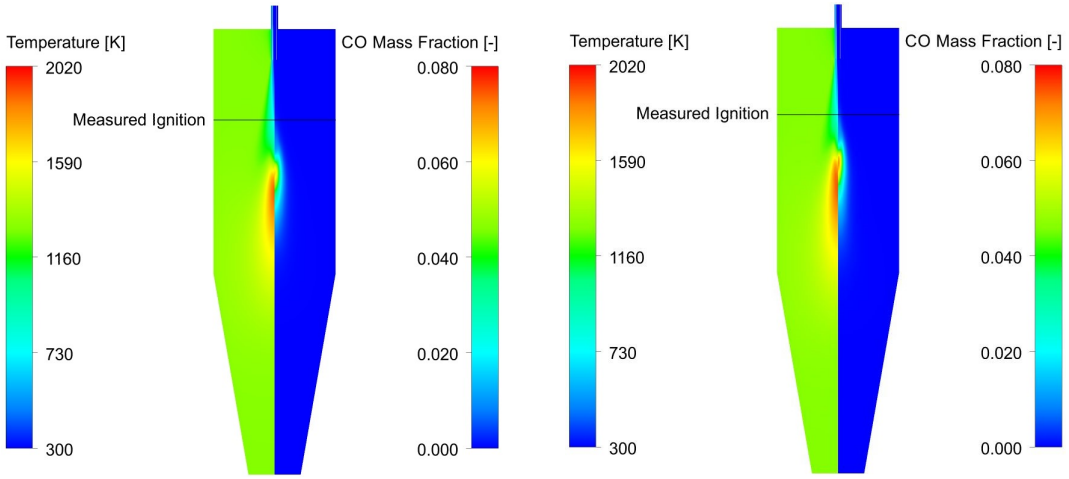

(a) Case 1

(b) Case 2

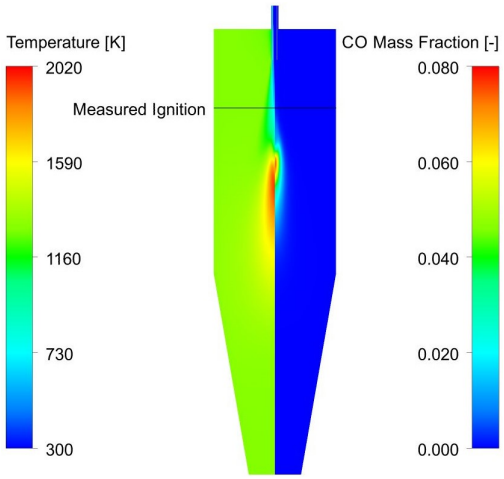

(c) Case 3

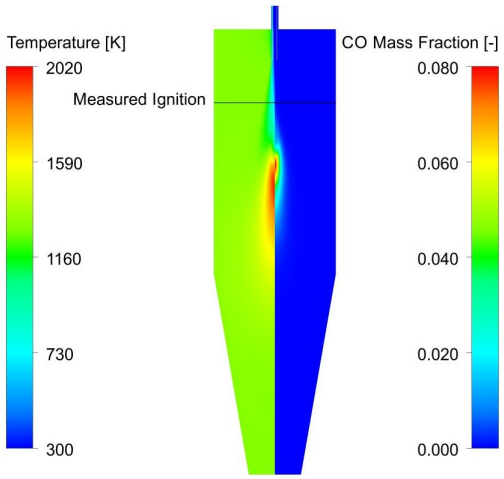

(d) Case 4

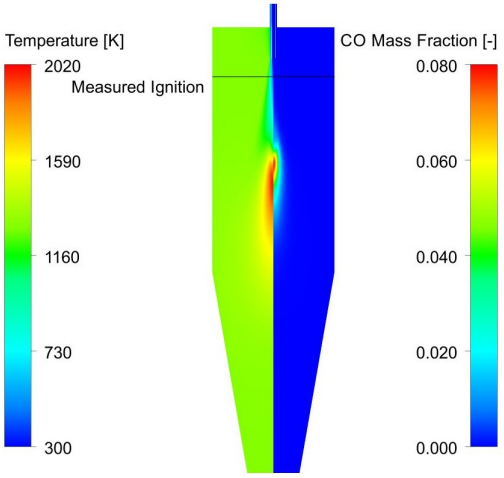

(e) Case 5

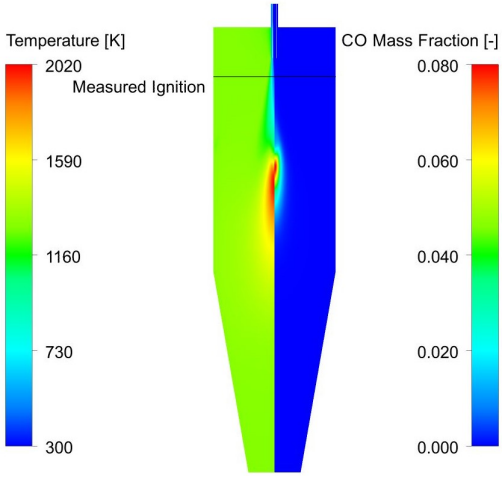

(f) Case 6

Figure 6.6: Distribution of temperature field (left) and CO mass fraction (right) for all the six benchmark CFD cases. Lines indicate the calculated ignition point from experiments using image processing.

The temperature distribution for the six cases is shown in Figure 6.6. The predicted temperature distribution field demonstrates that the flame is lifted and concentrated in the top end of the burner zone. The primary inlet temperature is around 305 K which implied that coal particles did not lose the moisture inside the burner. It lost a majority of the moisture after entering the burner zone which is evident for the first spike of H_2O in Figure 6.5. It delayed the devlolatilisation process. This phenomena delayed the overall ignition of the flame. The CFD benchmark model over predicts the flame stand-off distance when compared to the calculated experimental value.

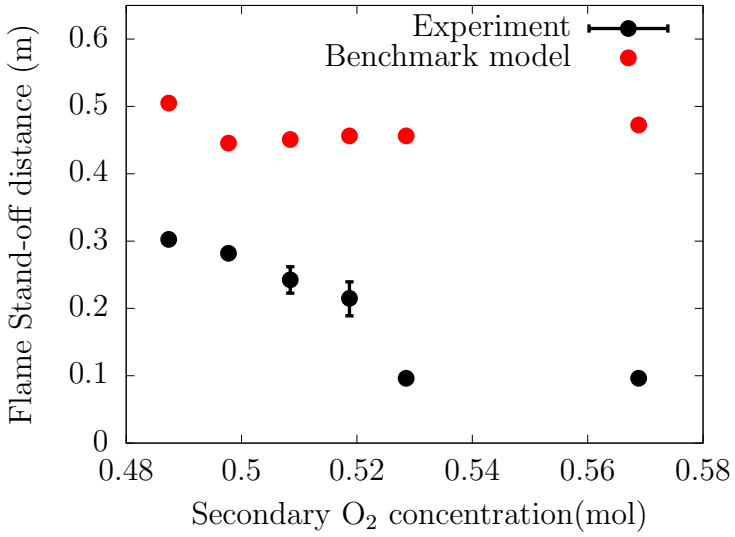

Figure 6.7: Benchmark results for flame stand-off distance against calculated experimental values.

The flame stand-off distance is compared against the experimental values in Figure 6.7. In the current modelling method, in oxy-fuel conditions, the mole fraction of the CO will be a good secondary indicator to suggest where the volatiles and char particles ignite. The results indicate an increase in the peak temperature with an increase in overall volume of O_2 and also a slight increase in the peak CO mole fraction as the O_2 in the secondary stream increased. It is observed that there is little to no difference between the six cases in the overall flame shape.

The measured results in Figure 6.7 show a decrease in the flame stand-off distance with an increase in the O_2 concentration in the secondary stream. The transition from completely lifted flame(Case 1) to attached flame (Case 5 and 6) is observed in the measured results. The results from the benchmark cases do not show a similar trend across all the six cases. The benchmark cases fail to predict the stand-off distance accurately, it over predicts the measured stand-off distance between 1.6 times for the Case 1 to 4.9 times for Case 6.

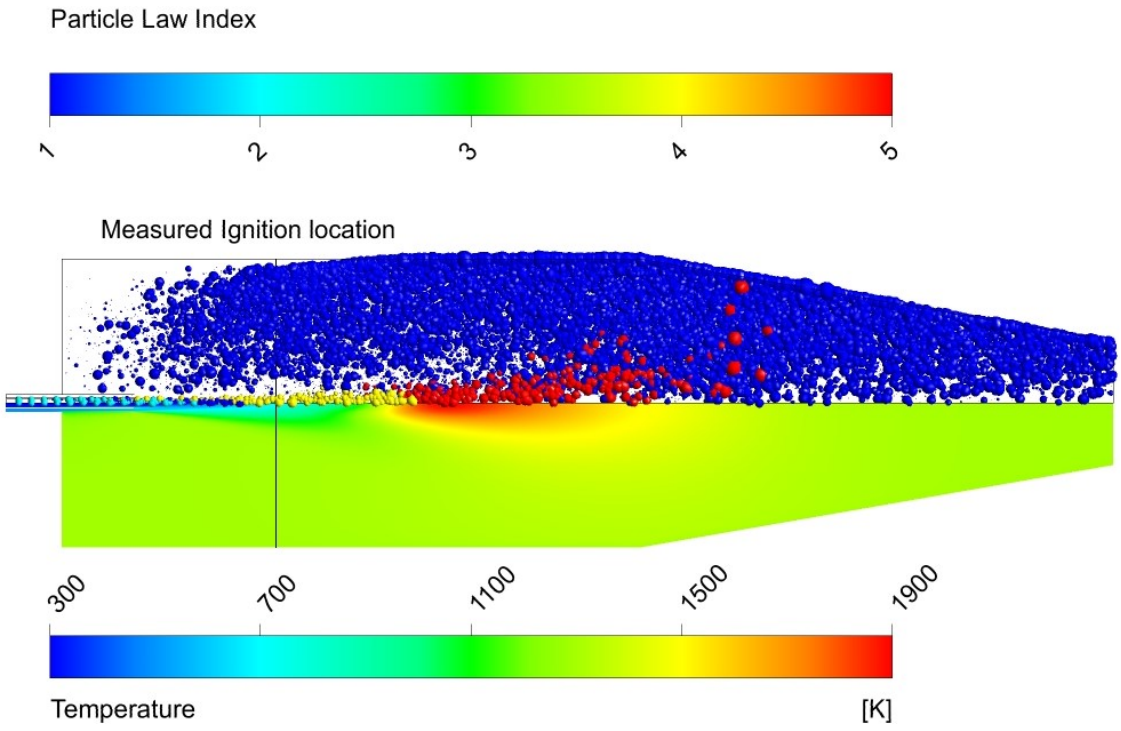

(a) Temperature field

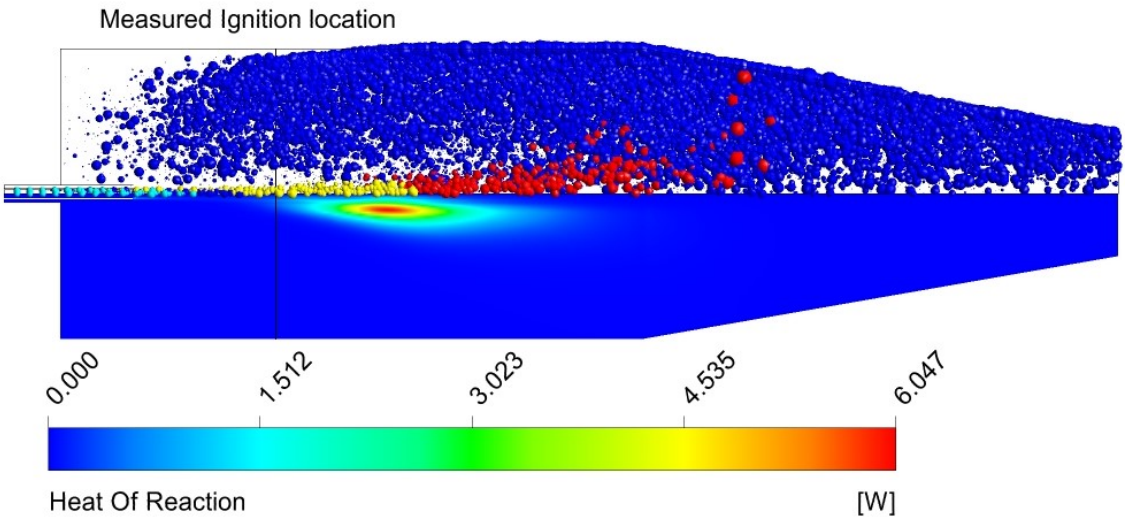

(b) Heat release due to the gas phase reactions.

Figure 6.8: Distribution of particles for benchmark Case 1 highlighting the particle thermo chemistry phase(particle law) along with a)Temperature field and b) Heat release due to gas phase reactions.

Comparing Cases 1 and 2 there is a small decrease in the stand-off distance but the trend does not continue and the flame stand-off distance becomes almost constant for the rest of the benchmark cases and thus the reason for the increase in the overprediction of the stand-off distance. This particular behaviour was also observed by Seidel et al. [201] when using the Eulerian-Lagrangian approach for particle tracking where they obtained no change in the flame stand-off distance even

after increasing the O_2 concentration from 0 to 20.9 % in the primary inlet. This was attributed to the limitations of the consecutively modelled thermo-chemical process in the DPM.

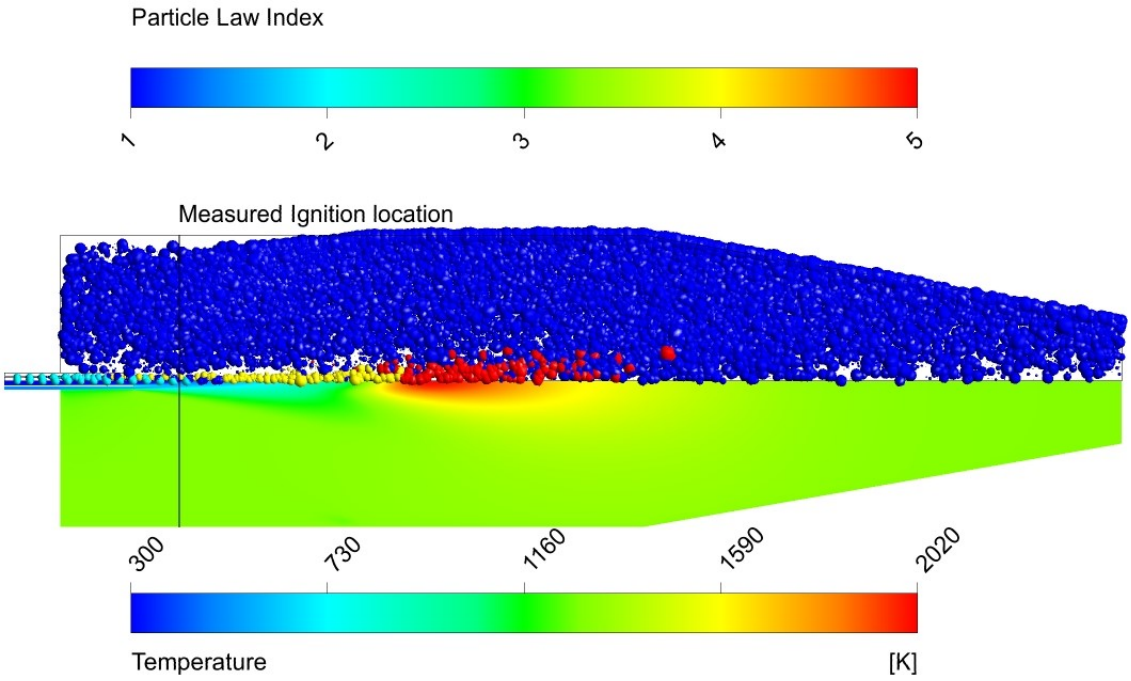

(a) Temperature (K)

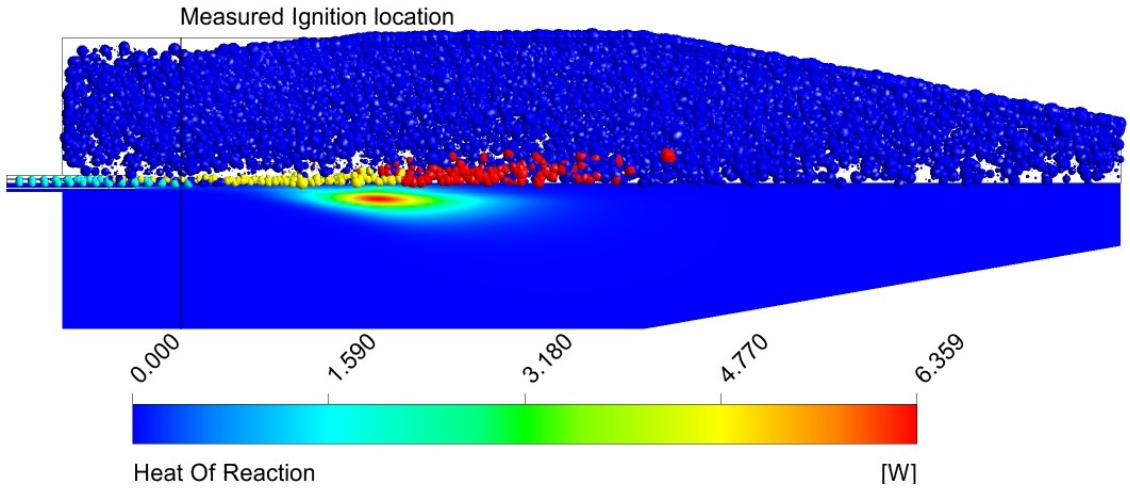

(b) Heat release due to the gas phase reactions

Figure 6.9: Distribution of particles for benchmark Case 6 highlighting the particle thermo chemistry phase(particle law) along with a)Temperature field and b) Heat release due to gas phase reactions.

Experimentally Case 1 and 6 display two extreme behaviours when it comes to flame stand-off distance, hence they were chosen for particle behaviour analysis. As described in previous chapter, that the thermo-chemistry behaviour of the particles is governed by a law, the mean particle thermo-chemistry behaviour for case 1 and case 6 are shown in Figures 6.8 and 6.9. The particle distribution in the furnace are

highlighted by the thermo-chemistry law that it is governed by. As this is a coaxial flame(absence of swirl), the consecutively occurring thermo-chemistry conversion is evident in the Figures 6.8 and 6.9. There is a small overlapping of the different thermo-chemistry phase for different particle sizes in certain regions of the flame. When the smaller particles enter the furnace they are are in devolatilisation phase and the relatively bigger particles are in the moisture evaporation phase which indicates that there is moisture release near the burner which delays the devolatilisation of the bigger particles and this delays the overall ignition process. This phenomena can be confirmed in Figure 6.5 where there is a constant release of inherent moisture inside the burner from the coal particles and this continues in the mixing zone as indicated by the increase in concentration of O_2. This reveals that the smaller particles will tend to ignite earlier but the bigger particles contribute to the delay in the overall ignition phenomena in the current modelling set up.

Figures 6.8 and 6.9 also describe the temperature field, heat released due to the gas phase reaction which shows that the peak temperature of both the flames are due to the combination of the gas phase reactions and char combustion. It illustrates that the early ignition (early temperature rise) is due to the volatiles combustion in gas phase when the particles are in the devolatilisation phase. The measured ignition location suggests that the heat release due to the volatiles combustion should have been initiated closer to the burner when compared with the benchmark simulation for Case 1. This suggests that there is a deficiency in either the submodel's used or the boundary conditions which delays the ignition mechanism.

On comparing the results from the two cases, this indicates that the impact of increase in O_2 is minimal. The increase in O_2 results in an increase in the peak temperature and heat release due to the gas phase reactions but does not impact on the particle behaviour in the flame. It neither increases the reactivity in the ignition phase nor does it impact on the heating rate (which impacts on the devolatilisation rate). The delay due to the moisture release near the burner prevents any increase in the reactivity of O_2 since the volatiles concentration will only increase to the flammability limits once the inherent moisture from the bigger particles is released and the bigger particles start releasing a higher amount of volatiles in the gas phase. This is a major limitation of the consecutively occurring thermo-chemistry model.

The simulation produces unrealistic errors when compared to the calculated results from the experiments. It should be acknowledge that the flame calculations were not only based on the flame temperature but also due to the radiation from the soot and the coal particles. This maybe a source of error in the experimental calculations which is unaccountable purely due to the image methodology used by Zhang et al. The flame also displayed multi-modal ignition behaviour which can be attributed to changes in the furnace conditions after operating for long hours or changes in the ambient conditions. Any changes in the operating conditions are not reported by Zhang et al. The flame stand-off values for the transition flames (Case 2, 3 & 4) are calculated based on mean behaviour of attached and detached flames which does not illustrate the two extreme behaviours of the flames. Hence due to

these reasons the benchmark simulation results should not be entirely criticised for exhibiting such high errors.

In summary the benchmark modelling results are, in general, not in good agreement with the experimental results. The absence of in flame measurements makes it difficult to determine the source of the errors. The mean particle distribution in the furnace suggests that the thermo-chemistry model could be a potential source of error as it prefers homogeneous ignition and the inherent moisture loss close to the burner contributes to the delay in the preferred homogeneous ignition.

6.3 Sensitivity analysis

This section describes the sensitivity analysis conducted on the suspected sub models which could be the source of error's. As there are no inflame measurements or any other parameters to compare against the experimental data, it is difficult to determine any short comings in the sub models used in the numerical simulations. A sensitivity analysis on a few sub models have been already tested by Siedel et al. [201] which included the turbulence model, devolatilisation model and wall temperature. Only the latter had an impact on the flame stand-off distance and the others had no impact on the turbulence prediction or the devolatilisation zone. The other factors which may also influence the flame stand-off distance are the radiation model, the boundary conditions, the turbulence chemistry models and the inability of the current modelling approach of not including heterogeneous ignition. The absorption coefficients for the benchmark cases were given by the WSGG constants. The radiation model needs to be adapted for the oxy fuel condition and thus before testing the ignition model a sensitivity analysis is conducted on the radiation model and the wall temperatures. The eddy dissipation turbulence chemistry models do not account for any CO_2 dissociation reactions and hence an investigation is conducted for different turbulence chemistry models which comprises of the CO_2 dissociation reactions.

6.3.1 Grid independence study

A mesh independence study evaluates whether the solution is dependent on the grid which is done by comparing the solutions between finer and coarser meshes. In this section solutions of three meshes are compared. A coarse mesh with 33342 cells, medium mesh with 68664 cells and a fine mesh with 117216 cells was constructed where the primary refinement was done near the burner. The refinement increased along the furnace with an increase in the number of cells. The CFD simulations were conducted using the benchmark Case 1 for the three meshes.

The comparison of the results for the three meshes are presented in Figure 6.10. The temperature profile along the axis shows no difference to the overall predictions. The velocity field near the burner zone reveals that all the three cases are well meshed to capture the ignition phenomena and the mixing of the two streams.

However the flame stand-off distance is still over predicted when compared to the experimental results. There is a discrepancy in the velocity field downstream which could be attributed to the coarser cells which fail to accurately predict the flow but the results in the coarser grid downstream does not significantly impact on the flow upstream. All the three meshes are adequate enough to provide a consistent mesh independent solution but the fine mesh was chosen for further CFD investigations in order to provide consistency as the benchmark model was simulated using the fine mesh.

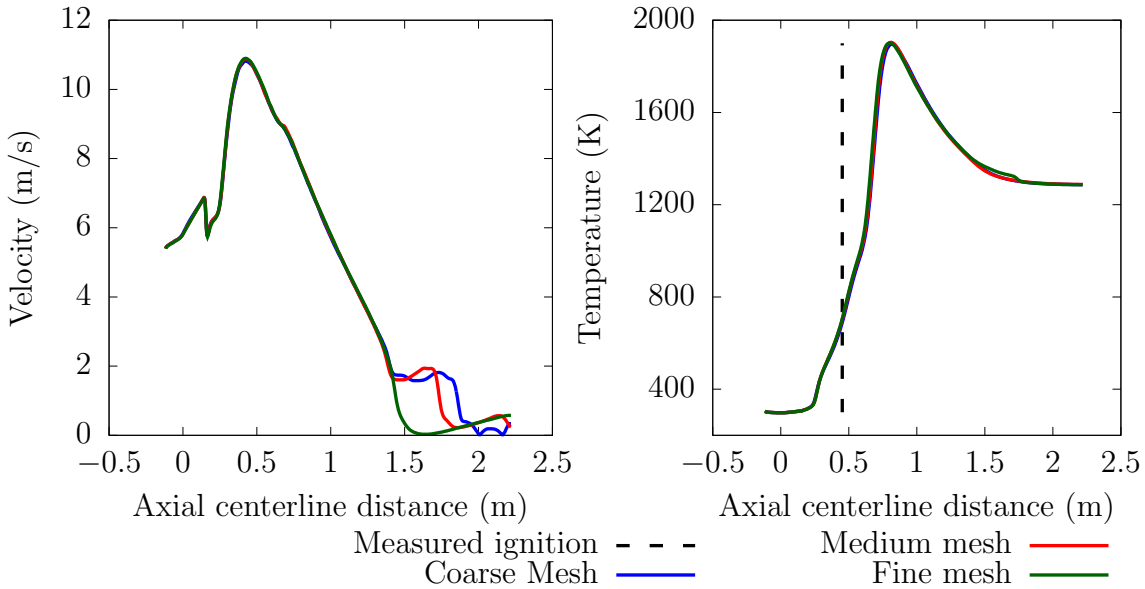

Figure 6.10: The Velocity and Temperature profiles along the axis for the coarse, medium and fine meshes.

6.3.2 Influence of the radiation model

In order to obtain an accurate interaction between the gas, particles and wall, application of a radiation model for the oxy fuel conditions is required. The benchmark Case 1 was tested with two other radiation model which were developed for oxy-fuel conditions, one developed by Johansson et al. [212, 370] and the second by Yin et al. [371]. These models are modifications of the WSGG model in order to account for different H_2O to CO_2 ratios in the oxy-fuel conditions. The radiation model by Johansson et al. has been widely used in the past in oxy coal CFD calculations [372–374]. The constants employed in the modified models are incorporated in the model using user defined functions in Fluent. It was found that the impact of different radiation models had no impact on the flame stand-off distance. This may be due to the radiation being a heat transfer mechanism over a long distance and different radiation models may be more sensitive in a large combustion mechanism. Mathematically it is the beam length which is a function of the area and volume which caps the impact of the different radiation models. Yin et al. [209] investigated the impact of the radiation model proposed in [371] for both large scale and

a small scale oxy-fuel facilities. It was demonstrated that the radiation model by Yin et al. has a significant impact on the overall heat transfer in big furnaces. It also concluded that the influence of the radiation model is negligible for small scale furnaces when compared to the WSGG model which is similar to the findings in the present investigation. Another sensitivity for different radiation models was tested by Yang et al. [195] for oxy coal furnaces and this behaviour was observed where the radiation models for small scale furnaces did not affect the CFD calculations but showed a significant impact in larger combustion systems.

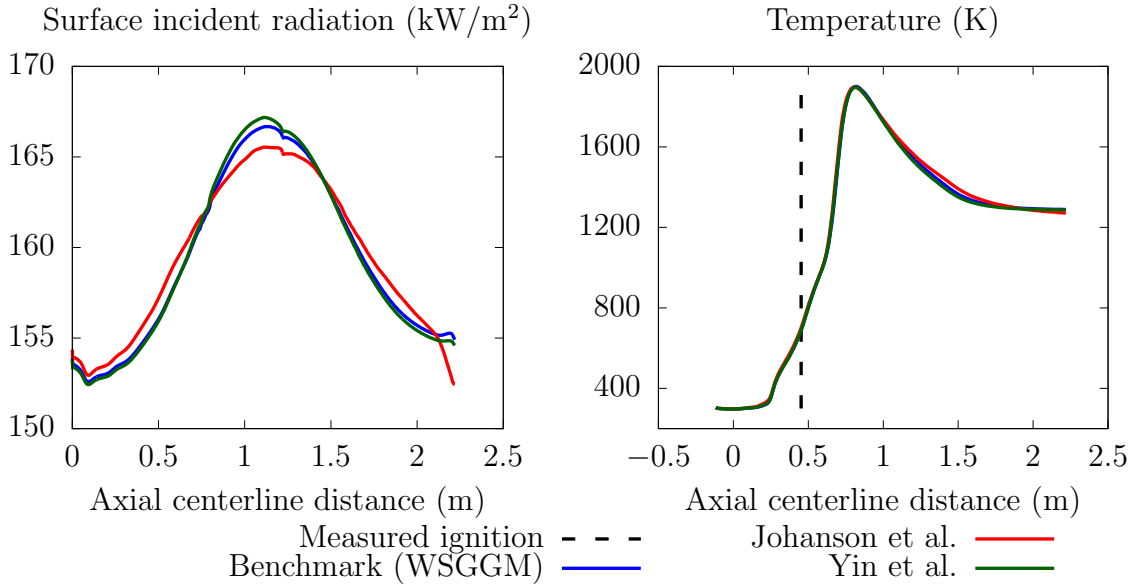

Figure 6.11: Predictions of the different radiation model for the surface incident and centreline temperature profile.

The overall impact of different radiation models on the centreline axial temperature profile and the surface incident radiation is shown in Figure 6.11. There is no difference in the temperature profile predicted by the three radiation models and it can be seen from the surface incident radiation that the flame shape is the same. However, the ignition location which is prior to the peak temperature are the same and over predicted the flame stand-off distance for the benchmark Case 1. Hence, for further investigations any of the three radiation models will suffice well for the CFD calculations. The future investigations are conducted using the WSGG model modified by Johansson et al. in order to secure any improvements in the heat transfer as the model is widely adopted and validated in the past for oxy-fuel conditions.

6.3.3 Impact of different turbulence chemistry interaction models

This section probes into the roles of combustion chemistry and the turbulence chemistry interaction models in oxy fuel flames. The importance of modifying the gas phase chemistry for modelling oxy-fuel flames are detailed in [209, 375–380]. Liu et al. [376] investigated methane + oxy-coal flames using a combination of kinetics from literature which provided good agreement with the experimental data. The mechanism ignored any dissociation reactions of CO_2 and included the reactions which were proposed by Jones et al. [288] for oxy-methane flames, thus it may favour methane combustion in certain conditions in the flame which can generate an error in a pure oxy-coal environment. On the other hand, the same reaction mechanism was also used by Tu et al. [381] for oxy fuel flames and they obtained results which are in excellent agreement with the experimental data which illustrated that this mechanism can be extended to the CFD modelling of oxy-coal flames. Another reaction mechanism used by Kangwanpongpan et al. [375] for oxy-coal flames included the dissociation reaction of CO_2 and its reversible reaction to maintain the equilibrium balance of the CO_2 dissociation which obtained good simulation results when compared to the experimental data. Since these two mechanism's that have been discussed have already provided excellent agreement with experimental data for oxy-coal flames, the two reaction mechanisms are tested for the benchmark Case 1 and monitored for any improvements in the flame stand-off distance. The reaction mechanism and their kinetics are summarised in Table 6.4. 16tn

Table 6.4: Gas phase reaction mechanisms for oxy fuel conditions

No.	Reaction			A	E (J/kmol)
		Liu et al. [376]			
1	Vol $+xO_2$	$\longrightarrow$	$aCO + \frac{b}{2}H_2 + \frac{d}{2}N_2 + \frac{e}{2}SO_2$	3.8e+7	5.55e+7
2	$CO + H_2O$	$\longrightarrow$	$CO_2 + H_2$	2.75e+9	8.37e+7
3	$CO_2 + H_2$	$\longrightarrow$	$CO + H_2O$	6.81e+10	1.14e+8
4	$H_2 + 0.5O_2$	$\longrightarrow$	H_2O	3.9e+17	1.70e+8
		Kangwanpongpan et al. [375]			
1	Vol $+xO_2$	$\longrightarrow$	$aCO + \frac{b}{2}H_2 + \frac{d}{2}N_2 + \frac{e}{2}SO_2$	1.623e+6	5.066e+7
2	$CO + 0.5O_2$	$\longrightarrow$	CO_2	2.238e+6	4.187e+7
3	CO_2	$\longrightarrow$	$CO + 0.5O_2$	1.095e+13	32.820e+7
4	$H_2 + 0.5O_2$	$\longrightarrow$	H_2O	1e+8	0.837e+7
	Vol $= C_aH_bO_cN_dS_e$, $x = \frac{a}{2} - \frac{c}{2} + e$				
	a, b, c ,d, e =1.5211, 2.63076, 0.51994, 0.0542, 0.0148				

The homogeneous reactions described in Table 6.4 can be implemented via turbulence chemistry interaction models which are coupled with the reaction mechanism.

The work performed by Liu et al.[376] tested two turbulence chemistry interaction models with the same mechanism. The two turbulence chemistry interaction models are FRED and EDC which are described in Section 2.8.1. The FRED calculates the finite rate and the two eddy dissipation rates and the net reaction rate is taken as the minimum of the three rates. The ED and FRED models are generally used for simulating the global mechanism for a given condition and the EDC is used for calculating the detail kinetics in a turbulent environment. In this study the reaction mechanism by Liu et al. was tested with the ED, FRED and EDC turbulence chemistry interaction models and the reaction mechanism proposed by Kangwanpongpan et al. is tested with FRED. It should be reminded that there are no inflame measurements of species concentration available and thus it will be difficult to conclude the accuracy of the turbulence chemistry models based on species distribution. The results for investigations will hence be focused on, if any, improvements in the prediction of the flame stand-off distance by the combination of the above turbulence-chemistry models.

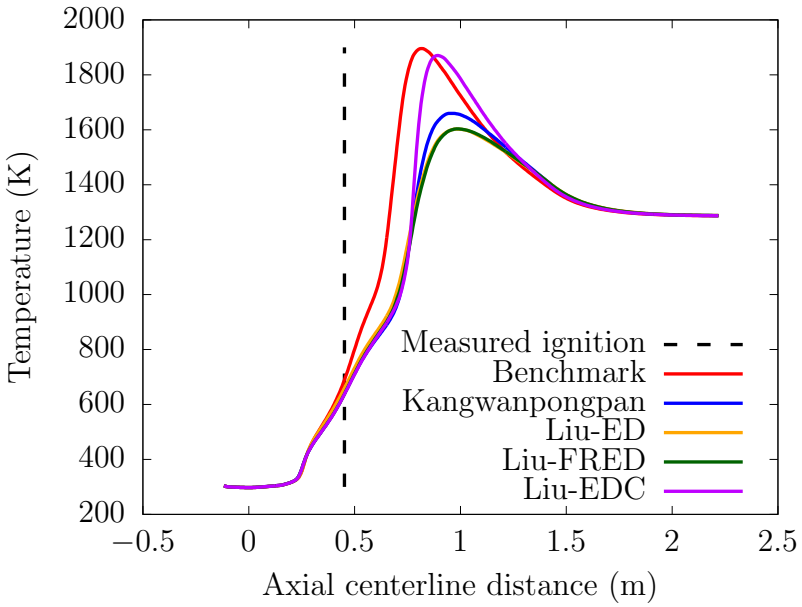

Figure 6.12: Impact of different reaction mechanisms on the centreline temperature profile.

The results of the sensitivity analysis are shown in Figures 6.12–6.14 which describe the species concentration, the temperature profile along the axial centreline and the flame stand-off distance. The temperature profile suggests that the reaction mechanism with the ED model for the benchmark case simulates the stand-off distance with the smallest error. As it assumes only two global reactions and the ED is modelled around the philosophy of "mixed-is-burnt" which enables early ignition. The temperature profile predicted by the Liu-EDC model exhibits a similar flame shape with an increase in the flame stand-off distance, reduction in the overall flame length and a similar flame peak temperature when compared to the bench-

mark case. The reduction in the flame length is evident from the distribution of the CO mass fraction.

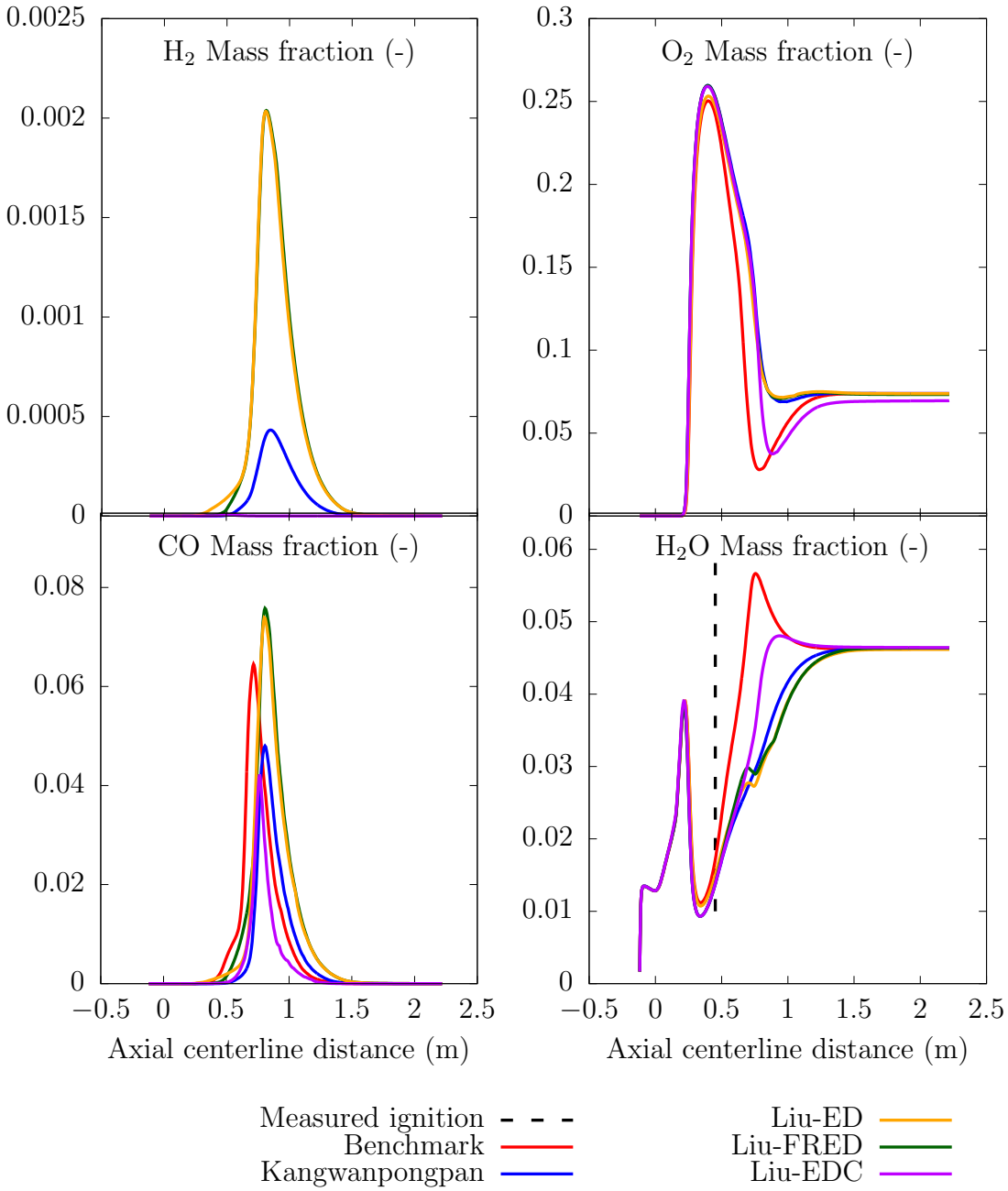

Figure 6.13: Impact of different reaction mechanisms on the centreline species concentration.

The benchmark case converts all the hydrogen in the volatiles to H_2O whereas the reaction H_2 has a delay due to the additional step required for the production of H_2O. Even though there is a reduction in H_2O in the ignition phase, the reaction mechanism favours production of H_2O over CO which is evident in the axial profile of the O_2, CO and H_2O mass fraction and H_2 which is negligible in the flame.

The increase in H_2O in the flame is a result of kinetics of reaction mechanism and increase in the temperature. The delay in the temperature rise of the flame, delay the production of H_2O which is evident from the calculated flame stand-off distance in Figure 6.14.

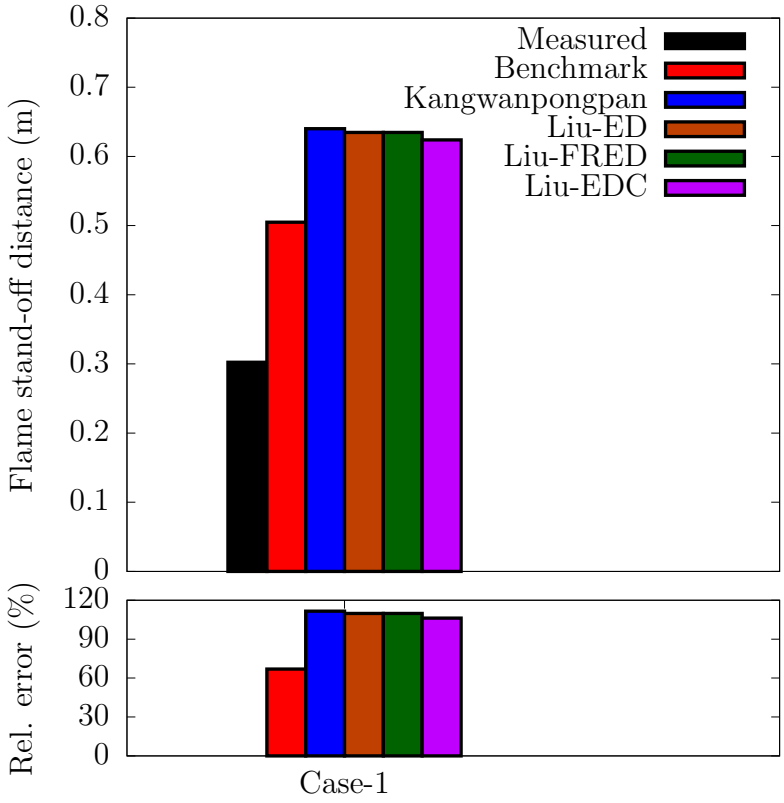

Figure 6.14: Comparison of the flame stand-off distance by different reaction mechanism.

Similar to the Liu-EDC model, the flame stand off distance increases for the Liu-ED model due to the delay caused by the other reactions mixing rate. There is a decrease in the peak temperature as the model favours the production of H_2 in the domain and does not convert all of it to H_2O. This behaviour could be attributed to the eddy dissipation kinetic rate of the reactions involved in the production of H_2O which are a function of the kinetics of the reaction mechanism. This leads to lower H_2O in the flame when compared to the benchmark and the Liu-EDC model which in turn impacts on the reactions of the flame and reduces the peak temperature of the flame. The predictions of the Liu-ED and Liu-FRED models are very similar to each other, and there is negligible difference in the flame stand-off between them. The similarities are because the FRED predicts the behaviour of the flame based on the minimum kinetic rate between the three rates for each reaction mechanism and as observed from the results, the Liu-ED assumes a lower rate for the different reactions compared to the Liu-EDC model. This explains why the predictions of the Liu-FRED model are very similar to the Liu-ED model except for

the early stage combustion or the ignition phase. The differences are exemplified in the early stages whereas the predictions of the CO and H_2 around ≈ 0.5 m along the axial distance where the minimum kinetic rate for the FRED model are taken from the finite-rate reaction rate. In brief there is an increase in the prediction of the flame stand-off distance due to the addition of reactions and the reduction in peak temperature compared to the benchmark case and this can be attributed to the combination of the reaction mechanism and the mathematical operation of the turbulence chemistry interaction models which leads to under prediction of H_2O.

The results for the reaction mechanism used by Kangwanpongan et al. was implemented using the FRED modelled which showed no improvement over the previously discussed cases for the flame stand-off distance. The peak temperatures of the flame is reduced when compared to the benchmark case which is again attributed to the production of H_2 in the flame and the mathematical limitations of the FRED model and the reaction mechanism to convert all the H_2 generated from the combustion of volatiles to H_2O. The peak temperature is higher than the one predicted by the Liu-ED and the Liu-FRED models and this is because this mechanism does not include the competition reaction between CO_2 and O_2 for H_2. This resulted in a reduced production of H_2 and a relatively higher mass fraction of H_2O which is evident in Figure 6.13.

Again, it is difficult to conclude which mechanism is more accurate as there are no available inflame measurements for the species concentration. The sensitivity study suggests that the flame chemistry, accompanied with the turbulence chemistry interaction models, are crucial in modelling the ignition for oxy-coal flames. Each model, when used with a particular mechanism, offers advantages and disadvantages and this study suggests that the prediction of H_2O impacts on the overall temperature field and in turn impacts on the combustion chemistry. As the mechanism and turbulence chemistry interaction model tested in this section provided no improvements in the overall flame stand-off distance, it was decided to use the benchmark reaction mechanism with the ED model for further sensitivity analysis.

6.3.4 Influence of the wall temperature

The sensitivity study in the literature regarding the wall temperatures along the flame length showed the most influence on the flame stand-off distance. Three other wall temperatures were tested for Case 1 and Case 6, i.e. 1450 K, 1600 K and 1800 K constant across the length of the furnace. The analysis of two cases will provide an insight into the impact on flame stand-off distance of extreme cases (Case 1 detached and Case 6 attached). Babak et al. tested Illinois coal on the same furnace and concluded that the flame stand-off distance predictions was in good agreement with the experimental data when the wall temperature is around 1600 K. Siedel et al. showed that when the wall temperatures are changed to 1800 K, the flame stand-off distance predictions are improved. It was important to investigate the influence of the wall temperatures as the studies in the past concluded different wall temperatures which suited their modelling methodologies.

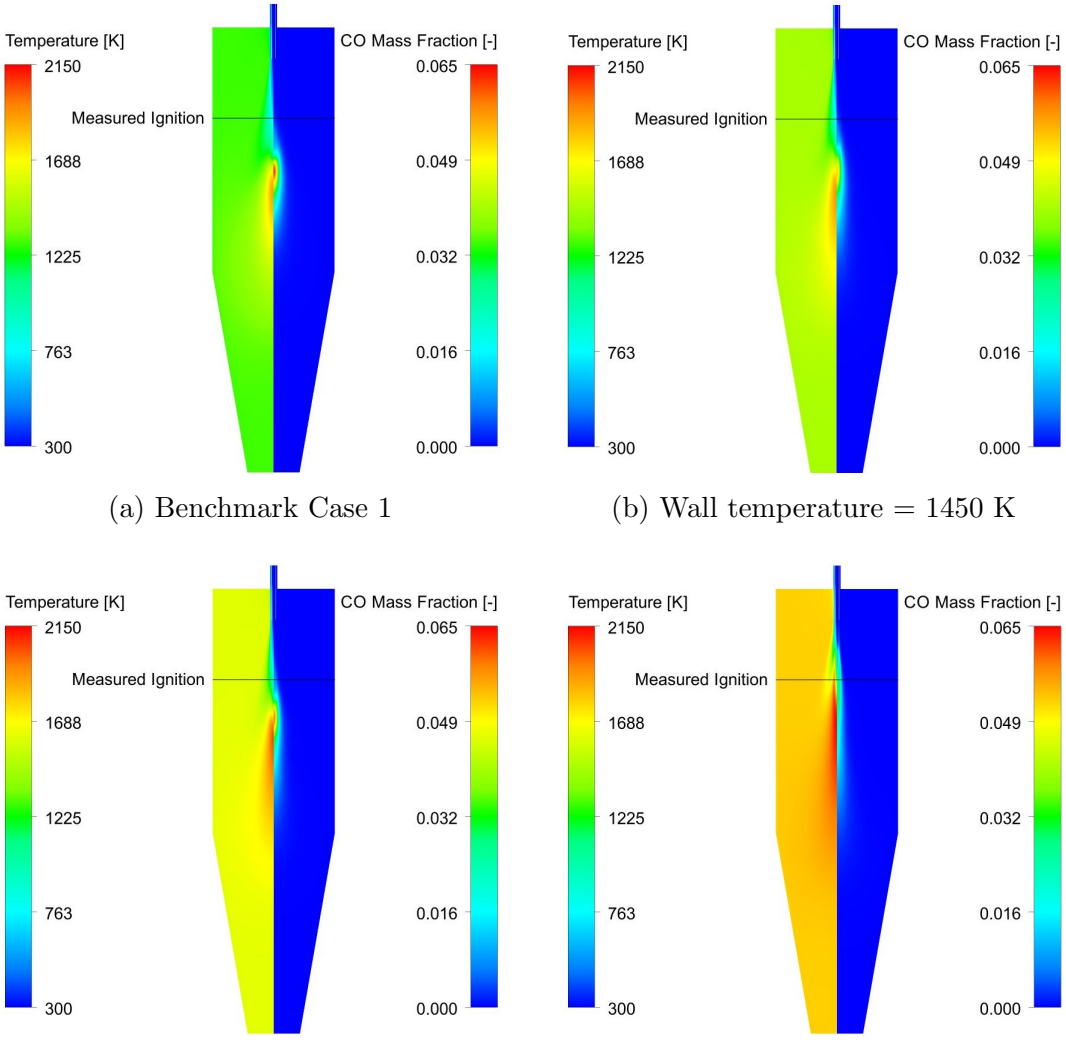

(a) Benchmark Case 1

(b) Wall temperature = 1450 K

(c) Wall temperature = 1600 K

(d) Wall temperature =1800 K

Figure 6.15: Impact of different wall temperatures on flame behaviour of benchmark Case 1.

The results for the wall temperature sensitivity conducted in this study are shown in Figures 6.15–6.17. The criterion for the ignition temperature increases with the increase in wall temperature, i.e. 1500 K, 1650 K and 1850 K for the wall temperatures at 1450 K, 1600 K and 1800 K, respectively. Figure 6.15 shows the changes in the flame shape, temperature field and volatiles combustion with an increase in wall temperature. This is due to the increase in the heat transfer inside the burner which protrudes inside the furnace and to the gas and the particles. This increases the heating rate to the particles and improves the overall devolatilisation rate and char combustion. The small particles experience an increase in thermo-chemical conversion rate and this will ignite the particles close to the tip of the burner. The results show that for the wall temperature at 1800 K the flame stand-off distance is in good agreement with the measured results. The wall temperature shows another important aspect, namely that the peak CO mass fraction decreases with an increase in the wall temperature. This is due to the early combustion of the

char particles which overlaps with the volatiles combustion. The early char burning results in increasing the length of the overall flame compared to the benchmark Case 1 as they burn over different time scales due to their size and O_2 availability. This results in early CO release which is spread across the flame length whereas in the case of the benchmark Case 1 the char particles combust in a concentrated region, thus resulting in a small flame with a higher CO release.

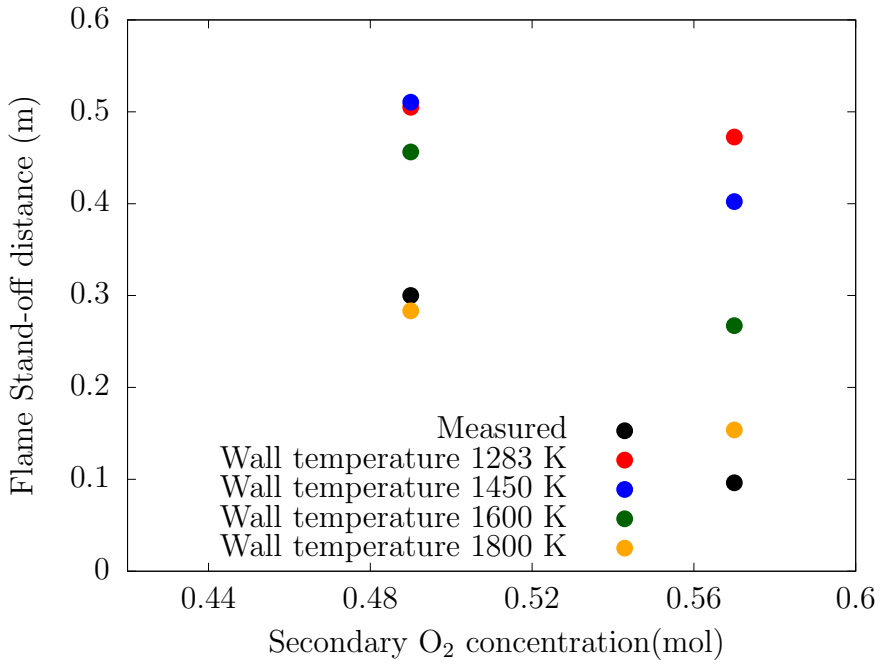

Figure 6.16: Influence of the different wall temperatures on the flame stand-off distance for Case 1 and Case 6.

A quantitative effect of the wall temperature on the flame stand-off distance is illustrated in Figures 6.16 and 6.17. The results for Case 1 are in accordance to the discussion above and if it is assumed that the other sub models have no short comings, 1800 K appears to be an appropriate wall temperature with a small relative error. At the same time, when the sensitivity is conducted on the benchmark Case 6, it reveals that the wall temperature of 1800 K and the others investigated are not enough and they over predict the flame stand-off distance with a high relative error. It follows that there is a gradual decrease in the flame stand-off distance but wall temperature at 1800 K still over predicts the flame stand-off distance by around 1.6 times the experimental value. This indicates that the wall temperature for Case 6 requires even higher wall temperatures which suggests that the wall temperature increased with an increase in flame stability, i.e. in the transition from detached to attached flame due to the higher O_2 concentration in the secondary stream. The overall sensitivity indicates that increasing the wall temperatures improves the predictions of the flame stand-off distance but it could be overcompensating for the other limitations imposed by the other sub models. Hence, it may be concluded that there is a disagreement in the experimental data in the wall temperature and

this could be a contributing factor in inducing errors in the benchmark cases.

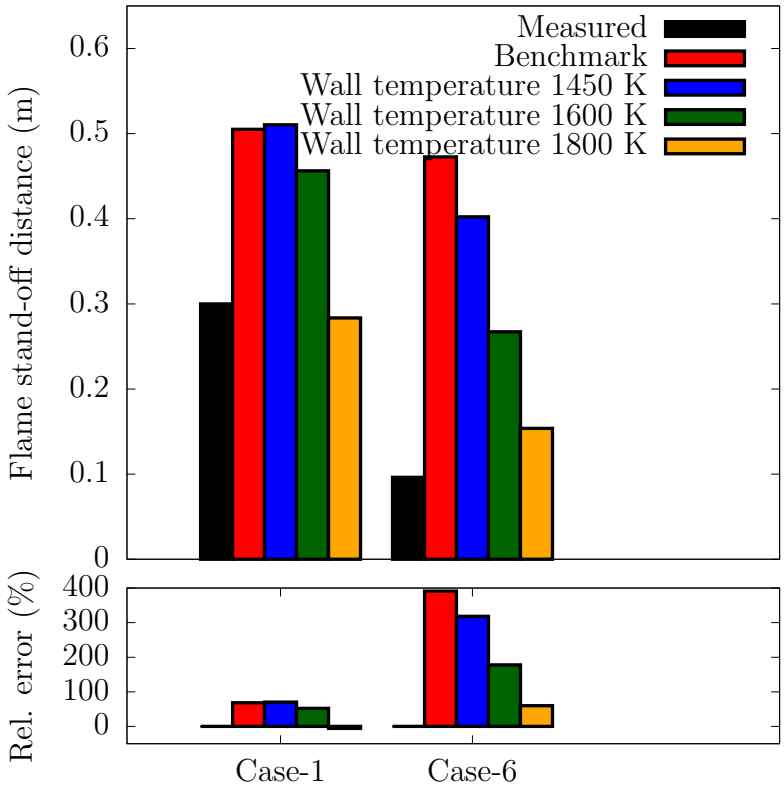

Figure 6.17: Comparison of flame stand-off distance predicted by using different temperatures for the top wall.

6.4 Impact of the ignition model

A single particle ignition study was conducted in oxyfuel conditions for the Utah bituminous coal for a range of diameters and ambient O_2/CO_2 concentration in order to obtain the correlation for the critical particle diameters with respect to O_2 concentration. The correlation is obtained for conditions with higher concentrations and the model was analysed using four particle diameters and O_2 concentrations ranging from 20 - 80 % by volume. As the six cases under investigation were sensitive to the O_2 concentration, and so is the ignition model, the critical diameter correlation was obtained for a wide range of O_2 concentrations. The boundary conditions for the single particle in oxy fuel conditions was kept the same as described in Chapter 4 as the heating rate of $\approx 10^4$ K/s is high enough to simulate the furnace conditions . The simulations were conducted using the FFCM chemical kinetics package and CPD was used for predicting the devolatilisation behaviour which calculated the kinetics at heating rate of 10^4 K/s.

There are two instances where there is transition in ignition mechanism for par-

ticles of 125 and 150 μm. Particle size of 125 and 150 μm ignite heterogeneously (HO-HI) for ambient O_2 concentrations of 50-80% and 70-80% respectively. The particles with diameter 50 μm all ignite heterogeneously. The small quantity of volatiles evolved achieve flammability but with relatively reduced temperatures. The ignition for all the cases with particle size of 90 μm was due to simultaneous combustion of volatiles inside and outside the particle. The cases discussed so far igniting heterogeneously satisfy the inflection condition. The particles with diameter 125 and 150 μm ignite homogeneously for the condition at ambient O_2 30-40% and 30-60% respectively. As the volatile flame was sustained for longer periods of time and the inflection condition is not satisfied. The results from the detailed single particle study is illustrated in Figure 6.18. The correlation for the critical diameter in the oxy-fuel conditions suggests that particles under 90μm ignite heterogeneously. As the mean diameter of the particles size distribution is 63 μm in these simulations, the majority of the particles will experience heterogeneous ignition. The methodology used for the integration of the correlation in the benchmark model is the same as that described in Section 5.4. The combustion behaviour of the particle is changed by modifying the DPM. The devolatilisation law in the DPM is modified by combusting the volatiles inside the particle as soon as they are under the devolatilisation law and critical diameter correlation conditions are satisfied.

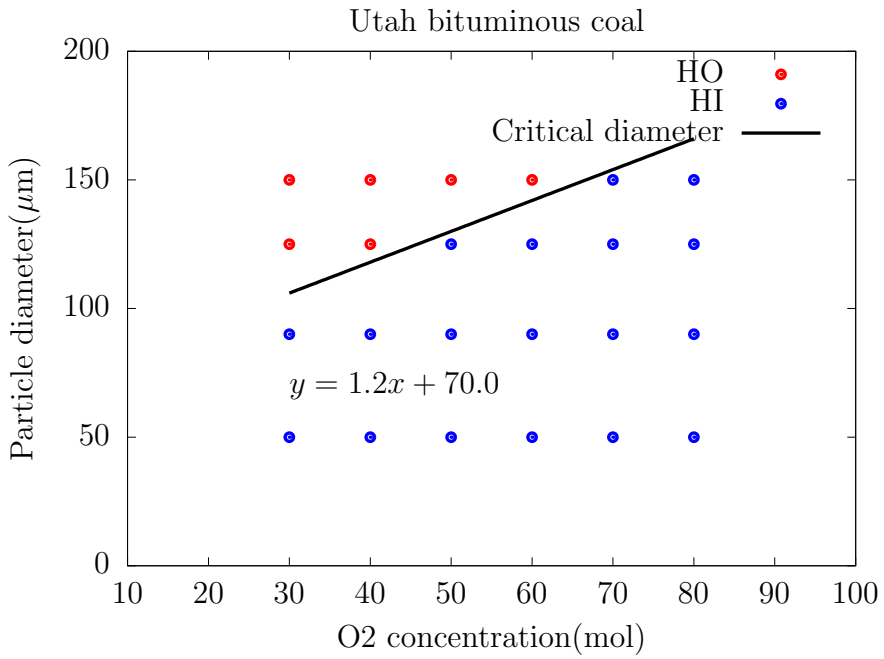

Figure 6.18: Correlation for the critical particle diameters for the Utah bituminous coal.

The results of the ignition model for the temperature and CO mass fraction is shown in Figure 6.19 for all the six cases investigated. The temperature field for all the six cases illustrates that the flame length has increased and the peak temperature of the flame is reduced when compared with each benchmark case. This

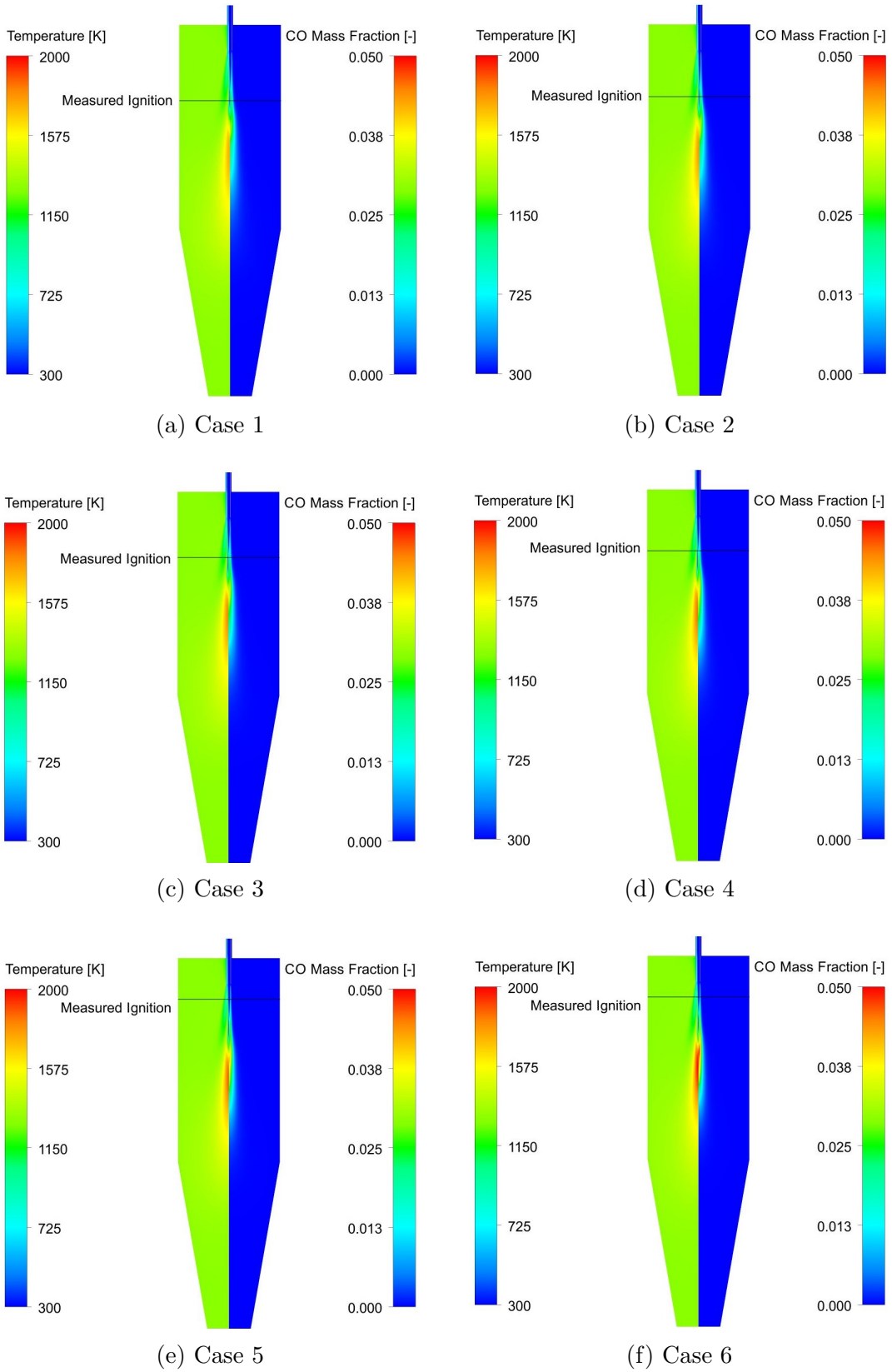

(a) Case 1

(b) Case 2

(c) Case 3

(d) Case 4

(e) Case 5

(f) Case 6

Figure 6.19: Distribution of temperature field (left) and CO mass fraction (right) for all the six CFD cases using ignition model. Lines indicate the calculated ignition point from experiments using image processing.

could be due to the spread of the particles burning in a longer flame compared to more concentrated burning in the benchmark cases, similar to what was observed in the sensitivity of the wall temperatures. Qualitatively defining the flame, the flame shape from the ignition model represents the experimental images as shown in Figure 6.3.The early ignition and increase in the flame length compared to the benchmark cases can be confirmed by the predictions of the CO. The prediction of the CO is a combination of heterogenous volatiles burning, homogenous volatiles combustion and char combustion.

The distribution of particles inside the furnace for a comparison between benchmark cases and the ignition model is shown in Figures 6.20a and 6.20b. The particle distribution are presented by the thermo chemistry law they are governed by. Comparing the two cases, the ignition model results suggest that the particles in the shear layer enter the char combustion phase closer to the burner. This is due to the combustion of the volatiles inside the particle when mixed with the O_2 from the secondary stream. As a result this accelerates the heating rate of the particle and the combustion of the volatiles. The heat generated due to the combustion of the volatiles is shown in Figure 6.21. In addition, it also demonstrates that the early heat release close to the burner also accelerates the devolatilisation rate of the bigger particles downstream. It can be seen from the contour plots and the particles distribution that the ignition takes places in the shear layer of the mixing plane. Also, the initial stages of the flame is very thin, then it grows in width and this is very similar to the situation that occurs in experimental images.

The ignition is quantified by the increase in the temperature of the domain and not primarily on the heat release due to the combustion of volatiles. The contour plots for heat release acts as a secondary indicator of the ignition in the furnace. If the heat released does not result in the exceeding of the maximum temperature of the input temperature(wall temperature in this case) of the furnace, it cannot be quantified as ignition and thus the increase in temperature is used to quantify the ignition. It could be concluded that the increase in the temperature or the ignition in this case is a combination of early heterogeneous ignition of the particles, the gas phase phase combustion of the volatiles and the char combustion. The steady state ignition or the flame stand-off distance predicted by the ignition model is shown in Figure 6.19.

The ignition model is able to predict the lift off with a reduced error when compared to all the benchmark cases considered. It is also able to predict the trend of decreasing flame stand-off distance with the increase in O_2 concentration. The improvements and the percentage error in the ignition model are highlighted in Table 6.5. The flame stand-off distance for Cases 1 - 4 are predicted with reasonable accuracy but it still shows that either the modelling or the boundary conditions induces error. The ignition model is not able to predict the flame stand-off distance for the Cases 5 and 6 with an acceptable error when the wall temperatures is kept at 1283 K. However, on increasing the wall temperature had a positive impact on the predictions of the benchmark cases as it increases the heat transfer to the burner

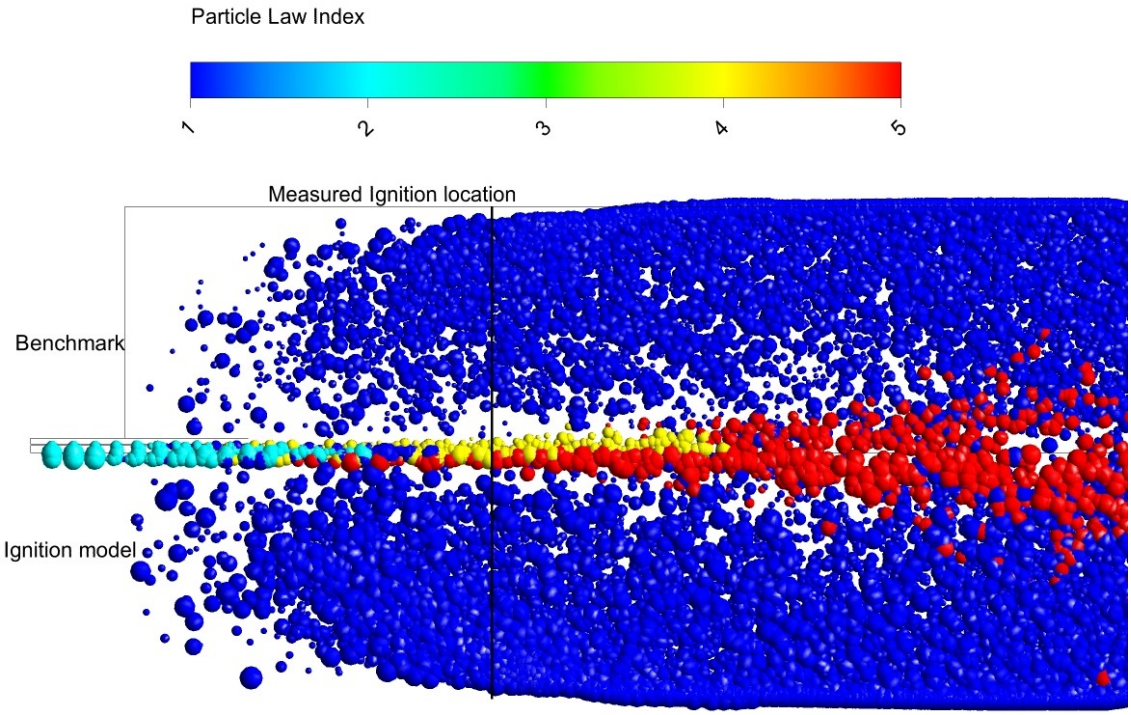

(a) Case 1

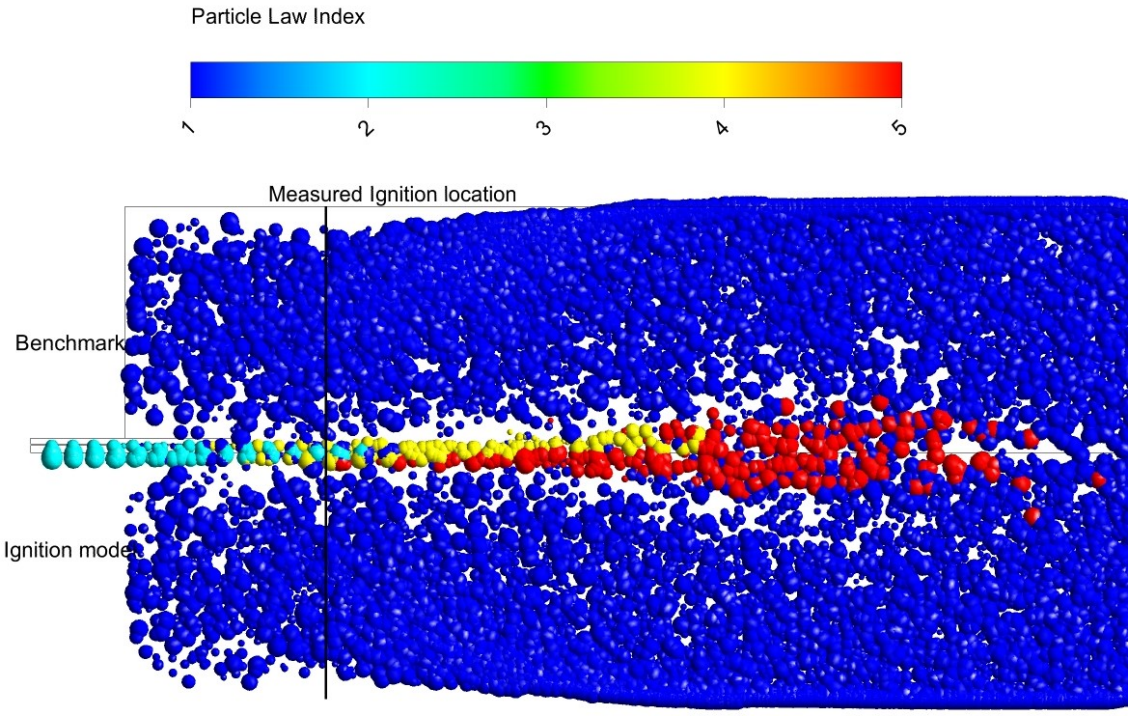

(b) Case 6

Figure 6.20: A comparison between the benchmark case and the ignition model describing the particle distribution field highlighting the thermo chemistry phase of the particles (Particle Law). The particle sizes are not to scale but they are scaled relative to each other.

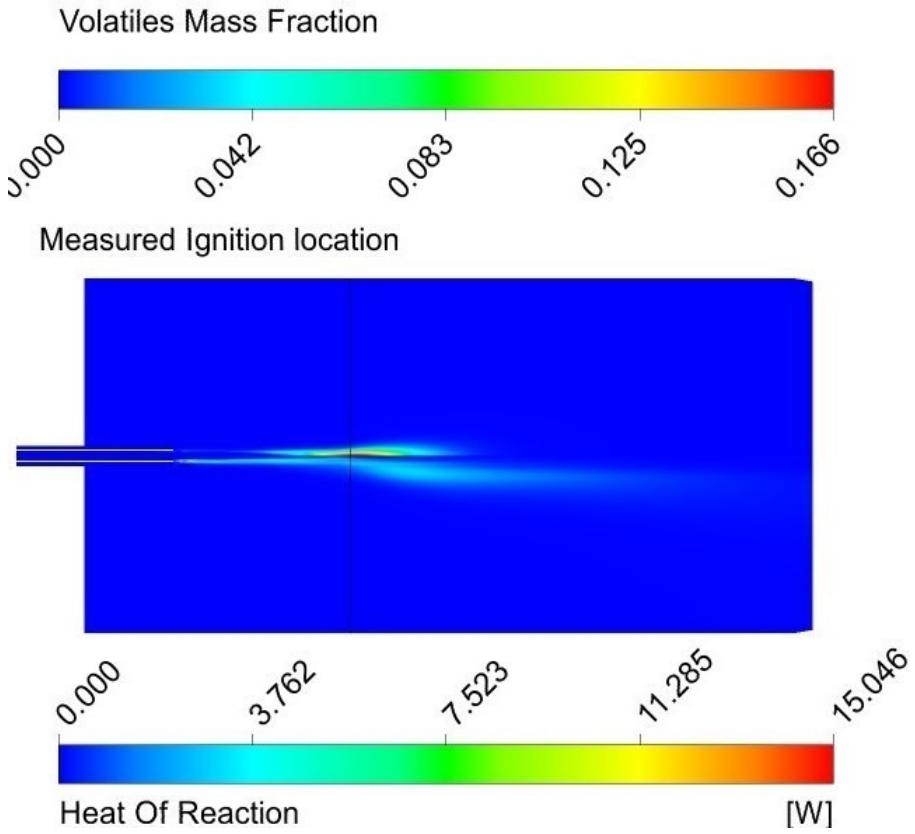

(a) Case 1

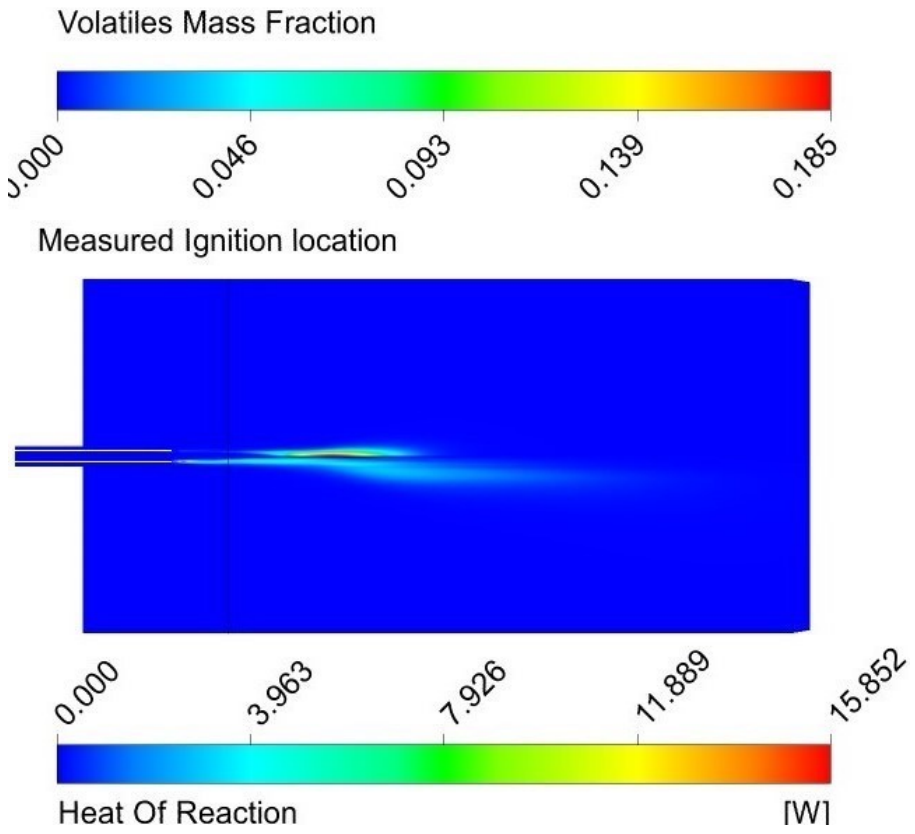

(b) Case 6

Figure 6.21: Distribution of volatiles and heat of volatiles reaction for Case 1 and Case 6 using the ignition model.

protruding into the furnace and the particles. If the wall temperatures are increased in conjunction with the ignition model, it will reduce the error for attached flames. Similar conclusions were also obtained by Julien et al. [363] when investigating the same furnace and the burner. This particular study provides confidence in the application of the new proposed ignition model for the oxy-coal conditions.

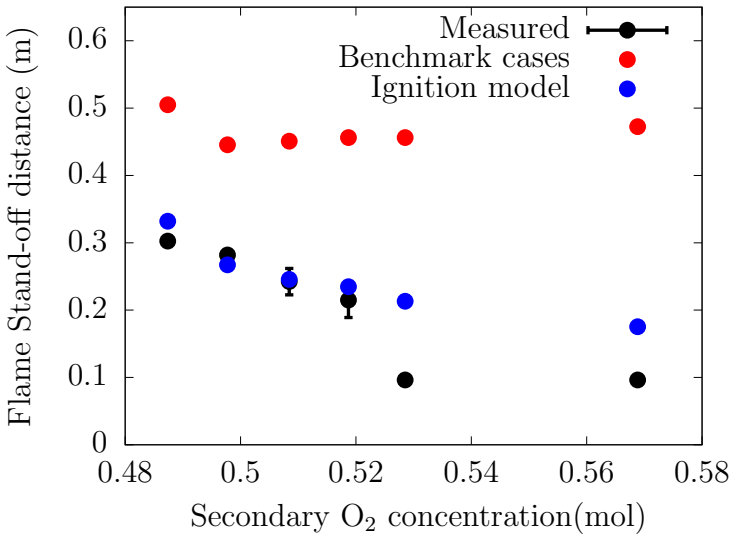

Figure 6.22: Results for the flame stand-off distance against the calculated experimental values for the benchmark cases and the ignition model.

Table 6.5: Improvements in the prediction of the flame stand-off distance due to the ignition model.

Case no	Measured	Benchmark	Rel. Error(%)	Ignition model	Rel. Error(%)
1	0.303	0.505	40.1	0.332	9.8
2	0.282	0.446	36.7	0.267	-5.2
3	0.243	0.451	86.0	0.246	1.3
4	0.215	0.456	112.3	0.235	9.2
5	0.0962	0.456	374.4	0.213	121.6
6	0.0962	0.473	391.2	0.175	82.3

The incorporation of the ignition model is able to improve the predictions of the flame stand-off distance when compared to the benchmark cases. The results show an excellent agreement for the Cases 1 to 4 but there is an increase in error for the Cases 5 and 6. The simulations are much less sensitive to the secondary O_2 concentration but are highly sensitive to the wall temperature. The calculations suggests that the role of O_2 is minor when compared to the wall temperatures for predicting the flame stand-off distance. Due to the lack of appropriate boundary conditions, it may be concluded that the wall temperatures for the attached flames

are higher than 1283 K and this is in line with the conclusion by Julien et al. [363]. The combination of an accurate wall temperature with the ignition model may provide better overall predictions.

6.5 Conclusions

This study investigates the capabilities and limitations of the current existing sub-models used for simulating turbulent coal flames in oxy-fuel conditions. The work also highlights the importance of tuning the current models for oxy-fuel conditions. The novelty of this study was in tuning the thermo-chemistry conversion model for the oxy-fuel conditions which affects the ignition characteristics of the overall flame. The key findings from the study are as follows:

i Six different benchmark cases have been simulated which showed poor agreement with the experimental results. However, there were no inflame measurements available and thus it was difficult to determine any flaws in the specific sub models. The uncertainties in the use of simplified models enforced an investigation into the sensitivity of the different sub models used for oxy-fuel conditions.

ii The sensitivity study of different radiation models showed no impact on the predictions of the flame stand-off distance as the radiation is a heat transfer mechanism over a long distance. The three models analysed were equally good at predicting the radiation for shorter distances in the oxy fuel conditions.

iii The sensitivity analysis on the different reaction mechanisms and the turbulence chemistry interaction model shows no improvement on the flame stand-off distance and reduced the peak temperature of the flame. On the contrary, the other combination of reaction mechanisms and turbulence chemistry interaction model increased the ignition delay compared to the benchmark model. This was primarily due to the combination of reactions, kinetics of the reaction mechanism and the reduction in the overall prediction of H_2O. The ED model with the two step reaction mechanism in the benchmark model is used for further investigation as it showed least relative error for the predictions of flame stand-off distance.

iv The sensitivity study on the wall temperatures suggests that increasing the wall temperatures had a positive impact on the prediction of the flame stand-off distance. The sensitivity study also suggests that increasing the wall temperatures to 1800 K provides excellent agreement with result for the Case 1 but still inherits a significant error for Case 6. Hence, increasing the wall temperatures may be over compensating for the drawbacks in the sub models. The sensitivity indicates that there is a mismatch in the experimental data available for the wall temperatures but it varies on a case by case basis and thus further simulations were conducted using wall temperature at 1283 K.

v The single particle ignition study on the Utah bituminous coal together with the Rosin-Rammler particle distribution suggests that the majority of the

particles in this study ignites heterogeneously. The single particle study thus highlights the limitations of applying the traditional thermo-chemical conversion approach.

vi The application of the ignition model improves the flame stand-off distance predictions for all the cases investigated. The model was able to accurately predict the flame stand-off distance for the Cases 1-4 but fails to predict the flame stand-off distance with good accuracy for the Cases 5 and 6. This was attributed to the uncertainty in the experimental wall temperatures.

vii The impact of increasing the O_2 was minor compared to the wall temperatures which was evident in the benchmark cases as well as in the simulations with the ignition model.

viii The ignition model when accompanied with accurate wall temperatures may provide much better predictions of the flame stand-off distance.

7 Impact of the ignition model in a pilot scale burner at PACT facility

The CFD RANS simulations conducted in this chapter are an extension of the research from the previous Chapter 5. The previous investigation looked into the capabilities and limitations of the ignition model developed by simulating coal flames of coaxial burners as the model predictions are more sensitive for those cases. The validation in previous studies provides confidence in the overall ignition model and can be applied in simulations of swirling burners with confidence. The aim of this chapter is to investigate the impact of ignition model on the pilot scale swirl burner.

The investigation was conducted on the 250 kW_{th} PACT(Pilot scale advance capture technology) facility which is located in Beighton near Sheffield, England. The investigation is focused on the air fired case where the modelling results are validated against measured data such as gas temperature, species concentration and radiative heat flux to the furnace walls. The furnace is modelled as a two-dimensional axis symmetric geometry as well as a complete 3-D geometry, the flame parameters are compared with the previously simulated results which utilised a three-dimensional axis symmetric geometry [195, 302, 382, 383]. The simulations conducted with the model used previously by Yang et.al. [250] is treated as the benchmark simulations. Similar to Chapter 5, the ignition model is integrated in the benchmark case and compared for any improvements in the ignition predictions.

The experimental test facility, boundary conditions and the case set up is described in Section 7.1. The description of the benchmark model is reported in Section 7.2. The investigation for the 2-D benchmark model is discussed in 7.3. The comparison between the literature models and 3-D cases are reported in Section 7.4. The investigation is summarised in Section 7.5.

7.1 Combustion facility

The experimental facility is a downward firing cylindrical furnace with dimensions of 0.9 m inner diameter and 4 m long. The furnace refractory is 0.1 m thick and water-cooled for the first 3 m. The furnace is equipped with preheaters to preheat the oxidising gas of the burner. The test facility is capable of inflame intrusive measurements such as gas species sampling, gas temperature and heat flux. The furnace is also capable of non-intrusive techniques such as 2D and 3D flame imaging

and particle image velocimetry laser measurements. The CAD image of the furnace is shown in 7.1a. The cylindrical walls are made up of eight section where the height of each section is 0.5 m each, the first two sections have many holes for optical and intrusive measurements. The other six sections does not have any flame imaging ports but contain intrusive measuring ports.

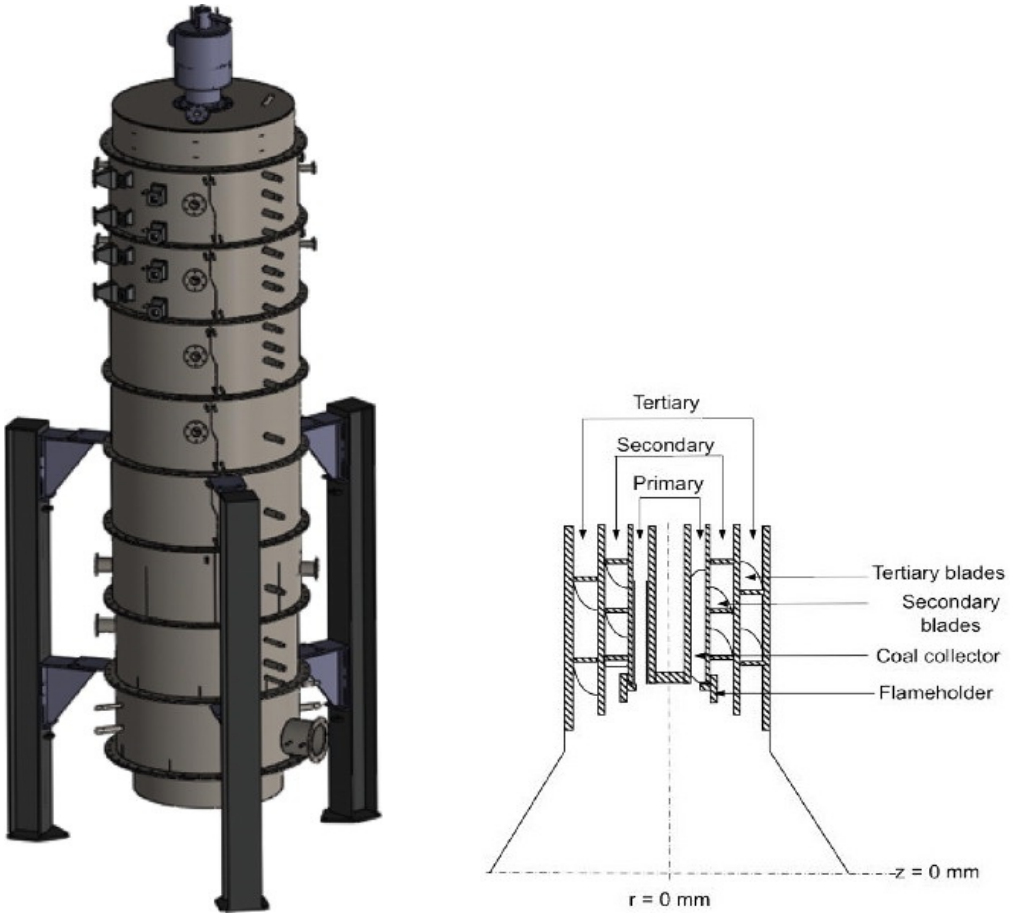

(a) (b)

Figure 7.1: a) CAD image of the furnace [382] and b) Schematic of the Doosan Babcock burner [383].

The burner is low NO_x commercial burner designed by Doosan Babcock which is scaled down to 250 kW_{th}. The schematic of the burner is shown in Figure 7.1b. The burner has three inlets, primary inlet for the fuel and the carrier gas which has coal gutters. The secondary and tertiary registers carries the swirled oxidiser for flame. There flow is swirled with the help of blades and a flame holder is situated at the burner lip for flame stabilisation. The burner is fitted on the top of the furnace which is 0.2 m deep. The quarl region is 0.05 m deep and 0.23 m wide with an angle of 25 degrees. The primary inlet is 0.01059 m wide and 0.303 m long, secondary inlet is 0.01708 m wide and 0.335 m long and the tertiary inlet is 0.01885 m and 0.347 m long. The details of the burner design can be found in [383]. The details of the experimental work chosen for investigation is described in [384].

A range of numerical studies were conducted on this facility on the [195, 302, 382, 383, 385] , however according to author's knowledge there hasn't been a modelling investigation focused on the ignition of the flame. A major emphasis has been given on the radiation modelling in these numerical studies and its impact on different sub-models. The work done by Black et al. simulated the PACT burner using RANS and LES method, they implemented the WSGG model and the FSCK model [302, 383]. They compared the data with the experimental data and concluded that LES simulation with the FSCK model provided the best agreement for the wall radiative heat flux but had no impact on the flame lift off distance and the simulations over predicted the flame lift-off distance and the temperature close to the burner. The numerical investigation done by Yang et al. [195] on the impact of radiation modelling is briefly discussed in Chapter 6. Huynh et al. [382] investigated the impact of particle and flame radiation on the NO_x prediction and compared the results with the experimental in flame and end of the furnace data. The results suggested that the choice of radiation model can vary the NO_x prediction by 10%. Farias et al. examined flame stability for bituminous coal and biomass in oxy-fuel conditions using spectral and digital imaging analysis [385]. The study concluded that oxy-coal flames are more repeatable and more stable compared to coal combusted in air conditions. This Chapter focuses on simulating the air case described in [195, 382] where the experimental measured data is compared with the benchmark case and ignition model. The numerical model used as the benchmark case is the one developed in [195, 382] for the case set up. The results from the 2-D benchmark case and the previously simulated 3-D cases are compared for validation of the methodology.

Table 7.1: Operating conditions for the PACT furnace.

Primary stream	Air combustion	Oxy27	
Coal mass flow	25.71	25.71	kg/hr
Mass flow rate	60.1	60.9	kg/hr
Temperature	297.15	295	K
Blade angle	63	63	Degree
Secondary stream			
Mass flow rate	92.2	87.8	kg/hr
Temperature	524.65	524.65	K
Blade angle	64	64	Degree
Tertiary stream			
Mass flow rate	158.4	150.7	kg/hr
Temperature	524.65	542.65	K
Blade angle	33	33	Degree

The boundary conditions for the combustion cases are described in Table 7.1. In

order to simplify the complex geometry inside the burner, only three registers are considered in the simulation. The value of the blade angles enables the tangential and axial component of the mass flow in each register which is used as boundary input. The calorific value, proximate and ultimate analysis of the El-Cerrejon bituminous coal is presented in the Table 7.2. The particle distribution of the bituminous coal is described using Rossin-Rammler distribution. The measured and the calculated distribution is shown in Figure 7.2 where the minimum diameter is 1 μm, maximum diameter is 600 μm the mean diameter is 120 μm and the spread parameter is 1.1.

Table 7.2: Coal properties of the El-Cerrejon bituminous coal.

Proximate analysis (as received)	[wt%]
Fixed carbon	53.98
Volatiles	35.5
Ash	2.9
Moisture	7.63
Ultimate analysis (dry ash free basis)	**[%wt]**
C	80.92
H	5.12
O	11.79
N	1.65
S	0.52
Gross calorific value (as received)	**29.61 MJ/kg**

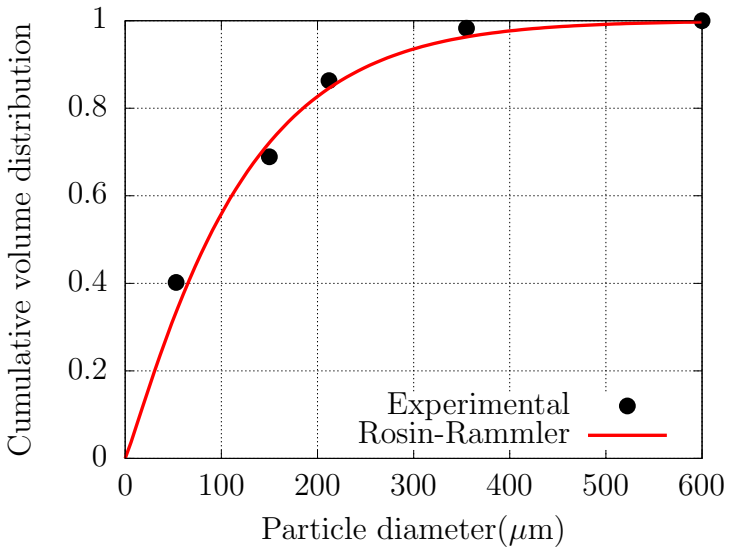

Figure 7.2: Particle size distribution for El-Cerrejon using the Rosin-Rammler correlation where d_e = 120 μm and n = 1.1.

7.2 Benchmark model

The furnace is modelled using two strategy, a two-dimensional axis symmetric geometry and a complete three-dimensional geometry. The aim of simulating two different geometries is to investigate any non uniform profiles in the flow due to difference in the particle distribution. The two-dimensional geometry simplifies the boundary conditions and reduces the computational time required but does not account for the variation in the particle distribution which can sometimes impact the overall ignition and the flame characteristics. The two dimensional geometry simplifies the burner channels by splitting the flow axially and radially based on the blade angle described in Table 7.1.

(a) Burner geometry

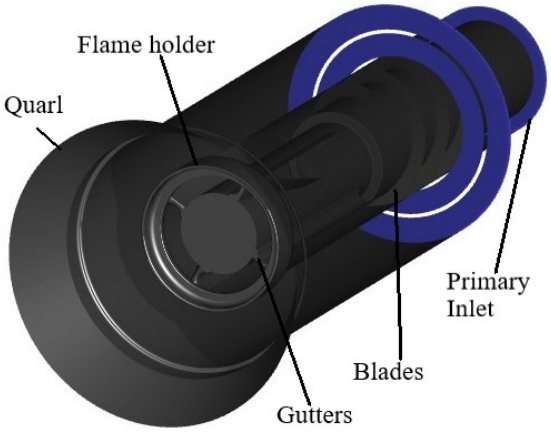

(b) Burner primary air channel

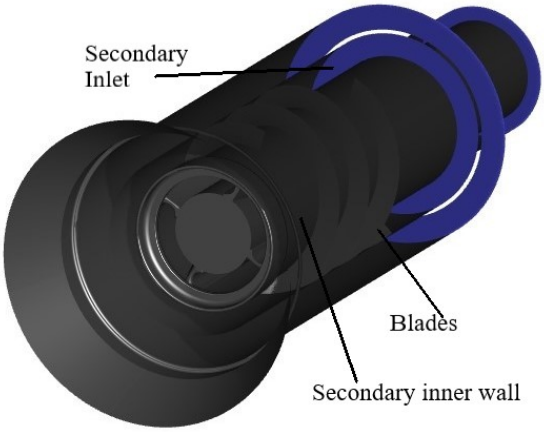

(c) Burner secondary air channel

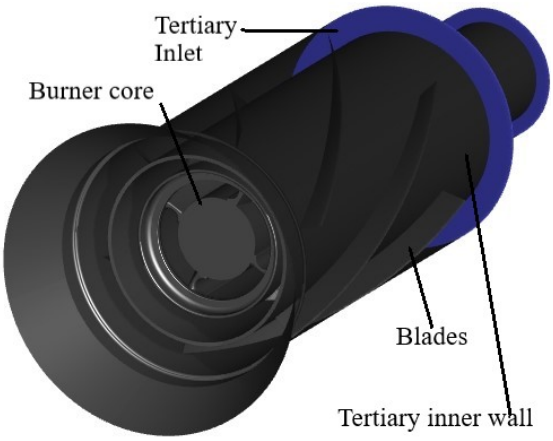

(d) Burner tertiary air channel

Figure 7.3: Burner internal geometry

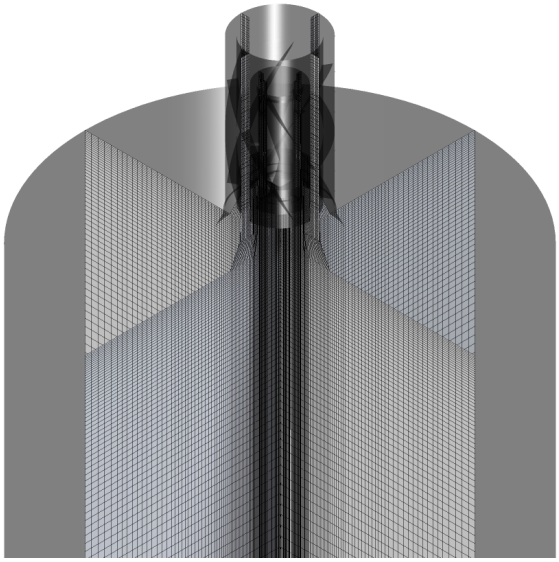

(a) Mesh in X-Y plane

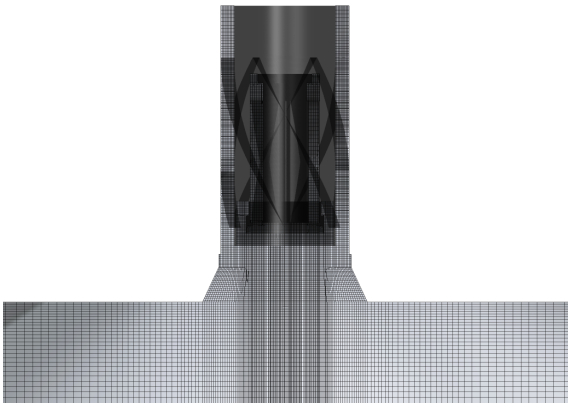

(b) Mesh close to the burner in the Y-axis

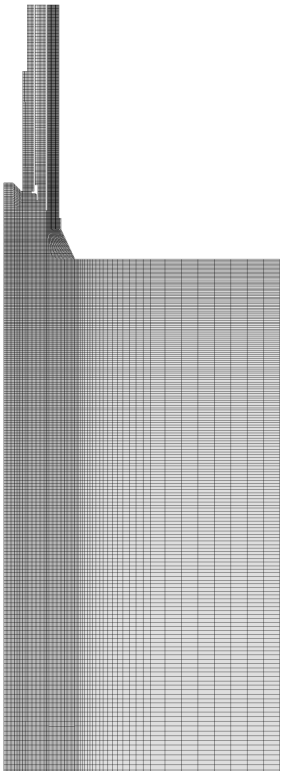

(c) Two-Dimensional axis-symmetric mesh

Figure 7.4: Different meshes generated and used for analysis.

Table 7.3: Models employed for calculating the benchmark case.

Model	Model Parameters		
Turbulence	Reynolds Stress Model [382]		
Gas Phase Chemistry	Eddy dissipation model [195, 280, 302, 382]		
	$C_{1.73}H_{2.45}O_{0.355}N_{0.0567}S_{0.00781}$ +	$1.308O_2 \longrightarrow$	$1.73CO + 1.223H_2O + 0.0284N_2 + 0.00781SO_2$
	$CO + 0.5O_2 \longrightarrow CO_2$		
Devolatisation rate	Single-step Arrhenius expression [382]		
	Pre-exponential fac. (A_i)	= 14841	s^{-1}
	Activation Energy (Ea_i)	= 3.53e+07	J/kmol
Char Combustion Model	Intrinsic model[195, 356, 382]		
	Diffusion coeff. (C_{diff})	= $5.025e^{-12}$	$m^3/K^{0.75}$
	Porosity (θ)	= 0.5	
	Tortuosity (τ)	= $\sqrt{2}$	
	Pore radius (r_p)	= $6e^{-8}$	m
	Int. Surf. A (S_a)	= $1e^5$	m^2/kg
	Stoichiometric coeff. (S_b)	= 1.33	
	Pre-exponential fac. (A_{ichar})	= $4e^{-4}$	$kg/(m^2s)$
	Activation Energy (E_{ichar})	= $6.6e^7$	J/kmol
	Burning Mode (α)	= 0.25	
Radiation	Discrete Ordinates (4 x 4) [205] Absorption coefficient given by WSGG constants [295]		
	Particle emissivity ϵ	= 0.9	
	Particle scattering factor σ_p	= 0.9	
Particles	Eulerian-Lagrangian approach		

The three dimensional geometry accounts for the blade geometry in the CFD simulation which is a ideal for accurate flow predictions. The burner internal channels are shown in Figure 7.3 where the blades and the bluff bodies are detailed.

The holes in the refractory for measurements are assumed to have a negligible impact on the flow and thus they are ignored in the geometry. The refractory wall is modelled as a continuous cylinder. The mesh generated for the two cases are shown in Figure 7.4. The cells are clustered and refined around the burner and coarser near the refractory walls. The full 3-D mesh with burner had around 2.86

million cells where as the 2-D geometry had 40641 cells which significantly reduce the computational time. The computational time for the 2D mesh with 6 cores converged in a day whereas the full 3D case with 18 cores converged in two weeks. A mesh sensitivity analysis is conducted for the 2-D mesh in the section below. The refractory walls are divided into eight sections. This was done to accurately model the heat transfer to and from the wall. It is highlighted in the work by Black et al. in [372] that the thermal conductivity of the walls in section 1 and 2 are different as they are made from different material which has a significant impact on the CFD predictions. The thermal conductivity for section 1 and 2 was set at 0.92 W/m-K and for the rest of the six sections it was set to 0.27 W/m-K. The static wall temperatures of the refractory walls were set at 350 K and the burner internal walls were set as adiabatic. It is acknowledge that there will be a small amount of heat losses due to simplification of the refractory walls and the heat lost through the measuring ports are ignored.

The sub-models for developing the benchmark case are applied from [195, 302, 382, 383] . The Reynolds Stress turbulence model with a linear pressure-strain model excluding wall reflection terms [383] is employed to obtain anisotropic turbulence closure for the reynolds stress which is suitable for predicting highly swirling flows. The velocity and pressure gradient near the wall is calculated using scalable wall functions. The radiation interaction is modelled using Discrete Ordinates (DO) where the discretisation of 4 x 4 is used and the absorption coefficient was represented by WSGG [295]. The particle emissivity and scattering factor of 0.9 were assumed for radiative heat transfer. The single rate devolatilisation kinetics were obtained from [302] where the Q ratio for high temperature volatile yield was calculated to be 1.57. The volatiles were calculated based on the Ultimate analysis of the coal and the gas phase chemistry is modelled using Eddy Dissipation Model where two step global reactions are considered. The relation for the dissipation rate of reactant and products is described in Equations (2.31) and (2.32). The value of empirical constant A in Equation (2.32) is a function of the turbulent scale in the flame region. Visser et al. [386] optimised the value of A in simulations of swirling flows for the volatiles and CO combustion which was used by Yang et al. in [195, 382]. The values of A is set in the model for volatiles and CO was 0.5 and 0.7. The char combustion was represented using the intrinsic model [195].

7.3 Results and discussion for 2D simulations

In order to obtain confidence on the results of the benchmark case, grid independent study was conducted on the two-dimensional geometry. The three dimensional geometry has been tested by Clements et al. [302] for grid independent solution and hence not investigated. The coarse mesh consisted of 40641 cells, medium 85081 cells and the fine mesh had 161528 cells. The cells were primarily refined near the burner and the flame region. The boundary conditions were kept the same as described above with the blended wall thermal conductivity and values of A in the eddy dissipation model set at 0.7 and 0.5 for volatiles and CO.

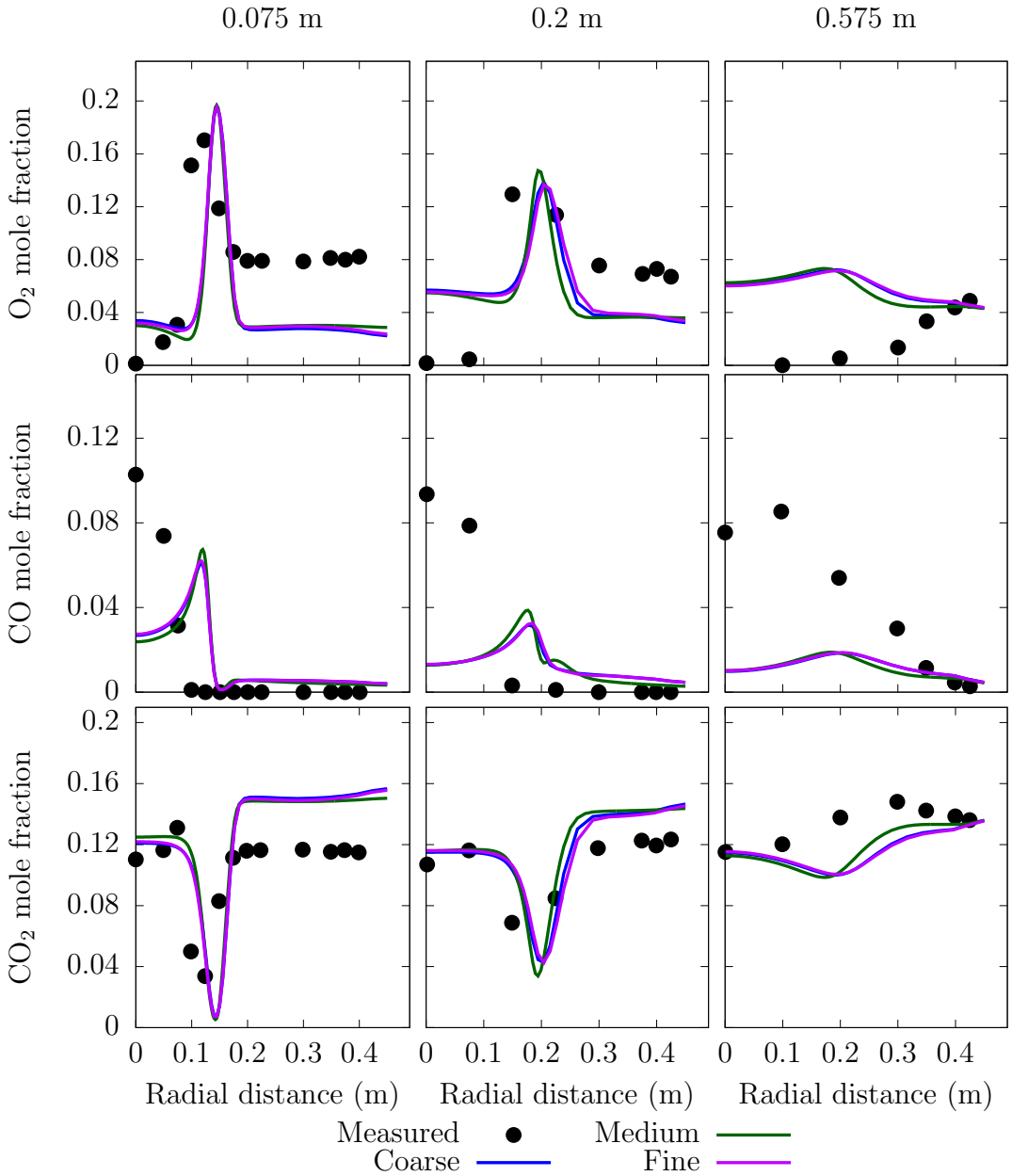

Figure 7.5: Grid independence study comparing the species concentration.

The radial profiles of the species concentration O_2, CO and CO_2 and the temperature field are compared in Figures 7.5 and 7.6 respectively. The radial profiles begin from the burner centerline upto the refractory walls and was compared at three different axial distance i.e 0.075 m, 0.2 m and 0.575 m. The axial distance is measured from the end of the quarl region (show in Figure 7.1b, z=0) where the three streams and the incoming coal mixes. The experimental data for species concentration are available from [195] and hence the results are compared in Figure 7.5. The species and temperature distribution shows that there are two recirculation zones, i.e an outer recirculation zone which is away from the burner (around the refractory walls)

and an inner recirculation zone which is close to the burner centreline. The peak in the O_2 concentration at radial distance of 0.075 m and 0.2 m and the decrease in the CO_2 concentration at the same distance signifies that. The peak in the O_2 is due to the unburnt combustion air from the three inlets. This leads to decrease in the temperature which in that region. The experimental data suggests that the O_2 is completely depleted in the inner circulation region close to the burner (around 0.4 m) but the two-dimensional model fail to predict that. The consumption of O_2 and production of CO_2 are over estimated close to the walls for axial distance of 0.075 m and 0.2 m. There are no significant difference in the results predicted by using the three meshes. It could be fair to say that the solution is mesh independent. The coarse mesh is suffice to obtain an accurate solution. The combustion process in the current model set up fail to accurately predict the species concentration. This could be attributed to inaccurate reaction rate in the recirculation zones. Hence, the model is tested with value of 4 for value of A in Eddy dissipation model which is widely used in combustion applications.

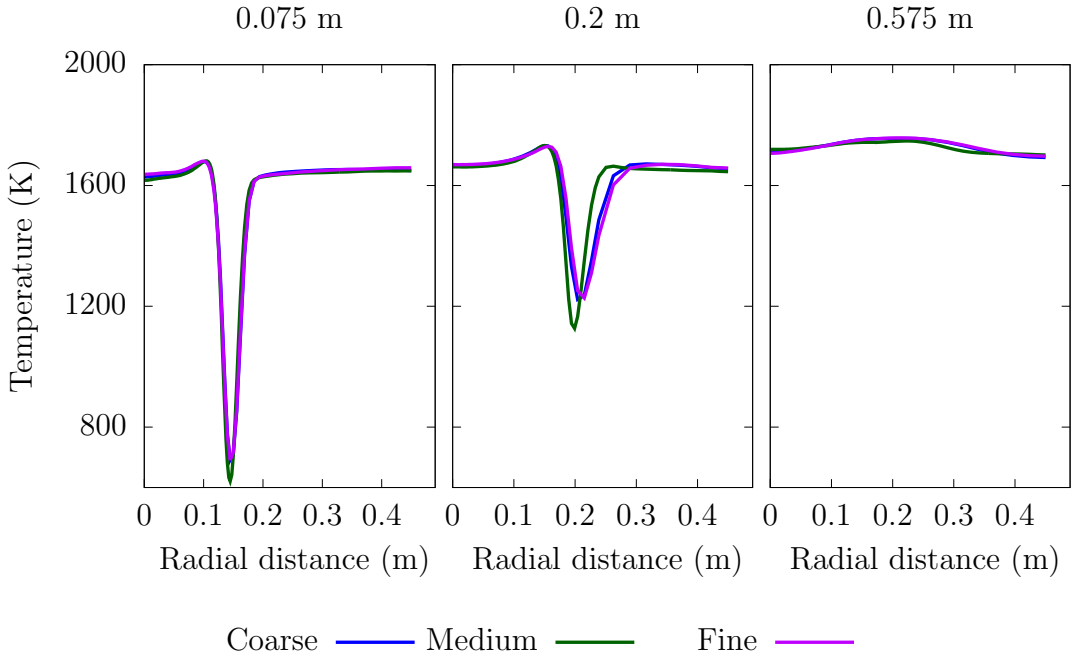

Figure 7.6: Grid independence study comparing the temperature distribution.

The results for the sensitivity analysis for the value of A are shown in Figures 7.7 and 7.8. There is a significant improvement in the species distribution of O_2 and CO_2 close to the burner. The depletion of O_2 is predicted better in the inner recirculation region. The inner recirculation zone is where combustion is intense. Increasing the rate of combustion has a negative impact on the prediction of CO. The conversion of CO to CO_2 is faster for the value of A=4 and the distribution of CO_2 is over predicted at radial distance of 0.2 m and after. The prediction of O_2 and

CO_2 in the outer recirculation region is very similar but not in good agreement with the experiments. The temperature distribution in the corresponding three radial directions shows the subtle differences due to increase in the reaction rate. There is a significant increase in the peak temperature close to the burner (i.e. 0.075 m and 0.2 m).

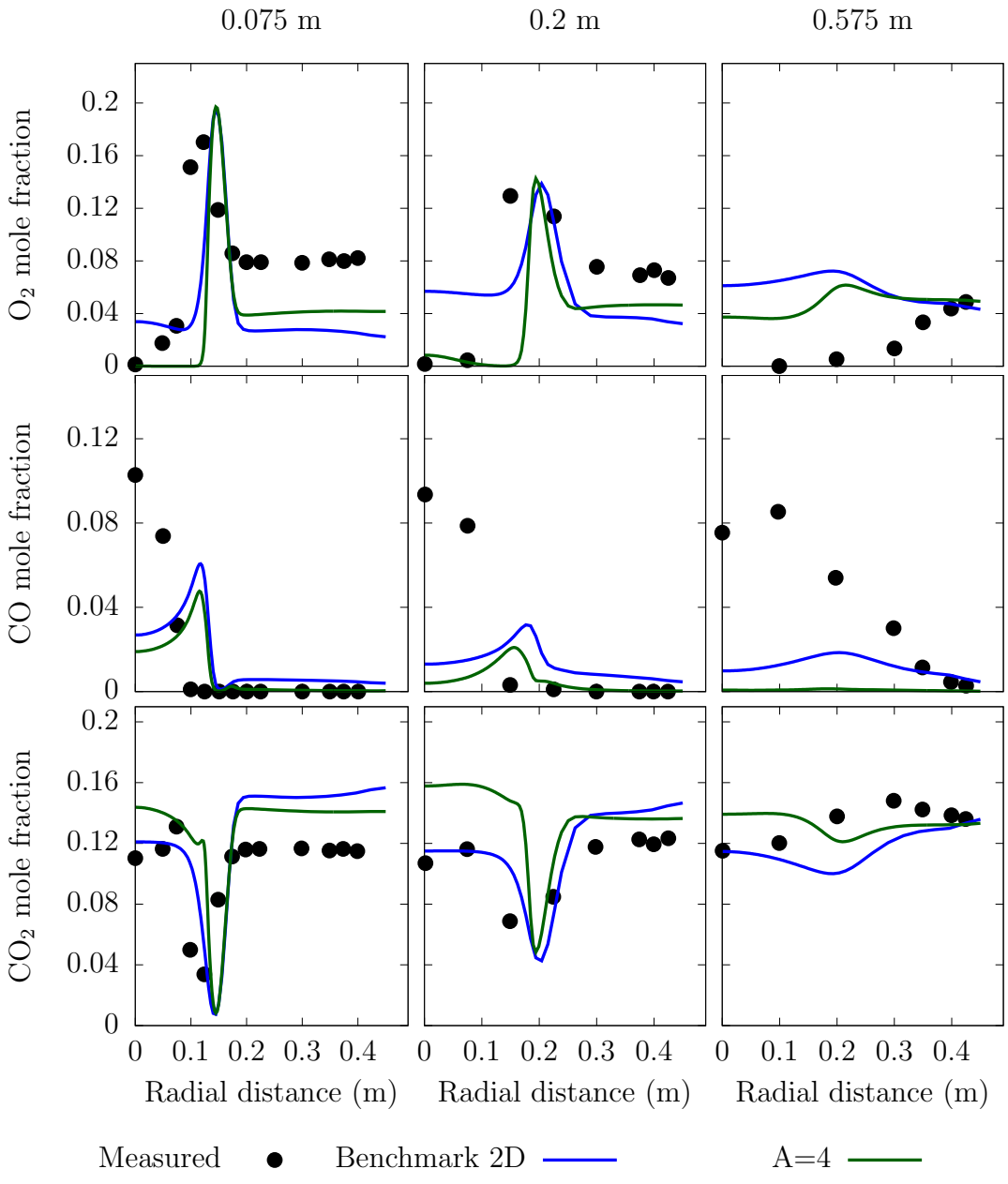

Figure 7.7: Comparison of the species distribution for values of A=4 and A=0.5,0.7 (Benchmark) in the Eddy dissipation model.

The sharp increase in the temperature is evident which is between the inner recirculation region and the shear layer of unburnt cool combustion air from the

inlet. The spike also also indicates that the volatiles in the gas phase burns hotter close to the burner burns and reduces in the temperature away from the burner. The predictions of species by both the models indicate that neither of the case is able to predict the flame combustion appropriately in a two dimensional axis symmetric flow. A factor inducing the error could be the isotropic nature of the two dimensional geometry or the breakdown of the turbulent eddies. In summary, the combustion model proposed by Yang et al. [195] is not suitable for predicting swirling flows using two-dimensional axis symmetric geometry. Hence, it is not used in further investigation in this chapter for predicting accurate ignition of swirled flames.

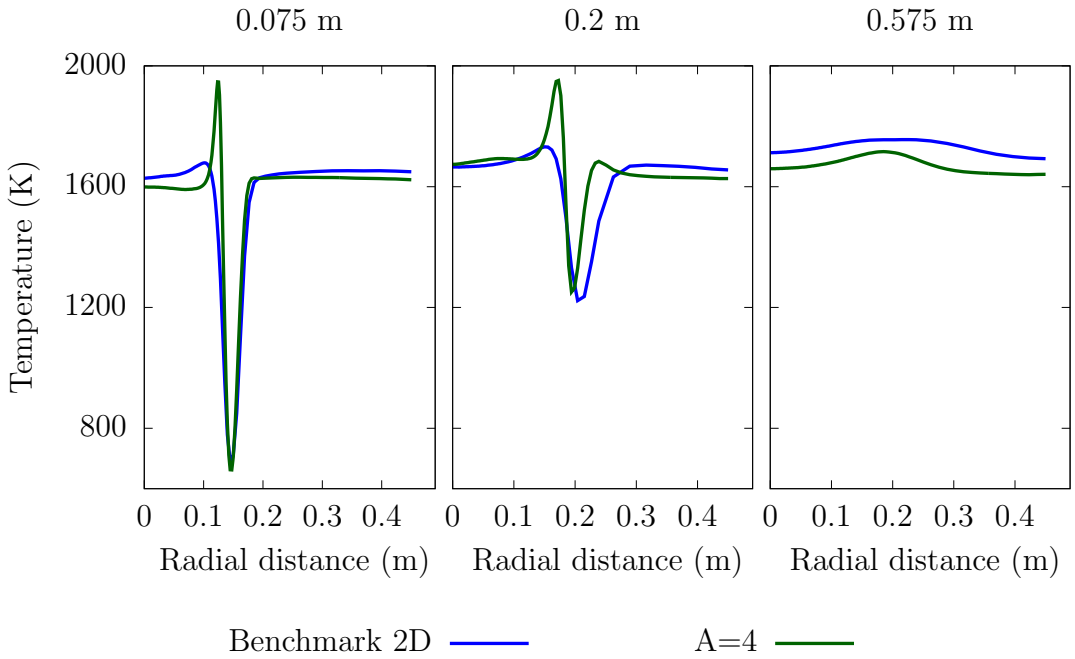

Figure 7.8: Comparison of the temperature field for values of A=4 and A=0.5,0.7(Benchmark) in the Eddy dissipation model.

7.4 Results and discussion for the 3D simulations

The results for the benchmark model with three dimensional geometry is discussed in this section. The experimental data available at the three locations are used for validating the model. The results are also compared with the predictions by Yang et al. [195]. The prediction of the combustion species are shown in Figure 7.9. The species distribution predicted by the benchmark case replicates well, when compared to the predictions by Yang et al. The comparison of the O_2 distribution suggests that the location and the thickness of the swirling jet is in good agreement with the experiments close to the burner. There is a significant over prediction of

the O_2 at the radial distance of 0.575 m which suggest a faster consumption rate of O_2 between 0.2 m and 0.575 m. This indicates that the mixing rate and hence the combustion rate is over predicted at 0.575 m. A similar difference is observed for the other two species as well where the prediction of CO and CO_2 are in good agreement with the experiments close to the burner but a significant difference is observed at a distance of 0.575 m.

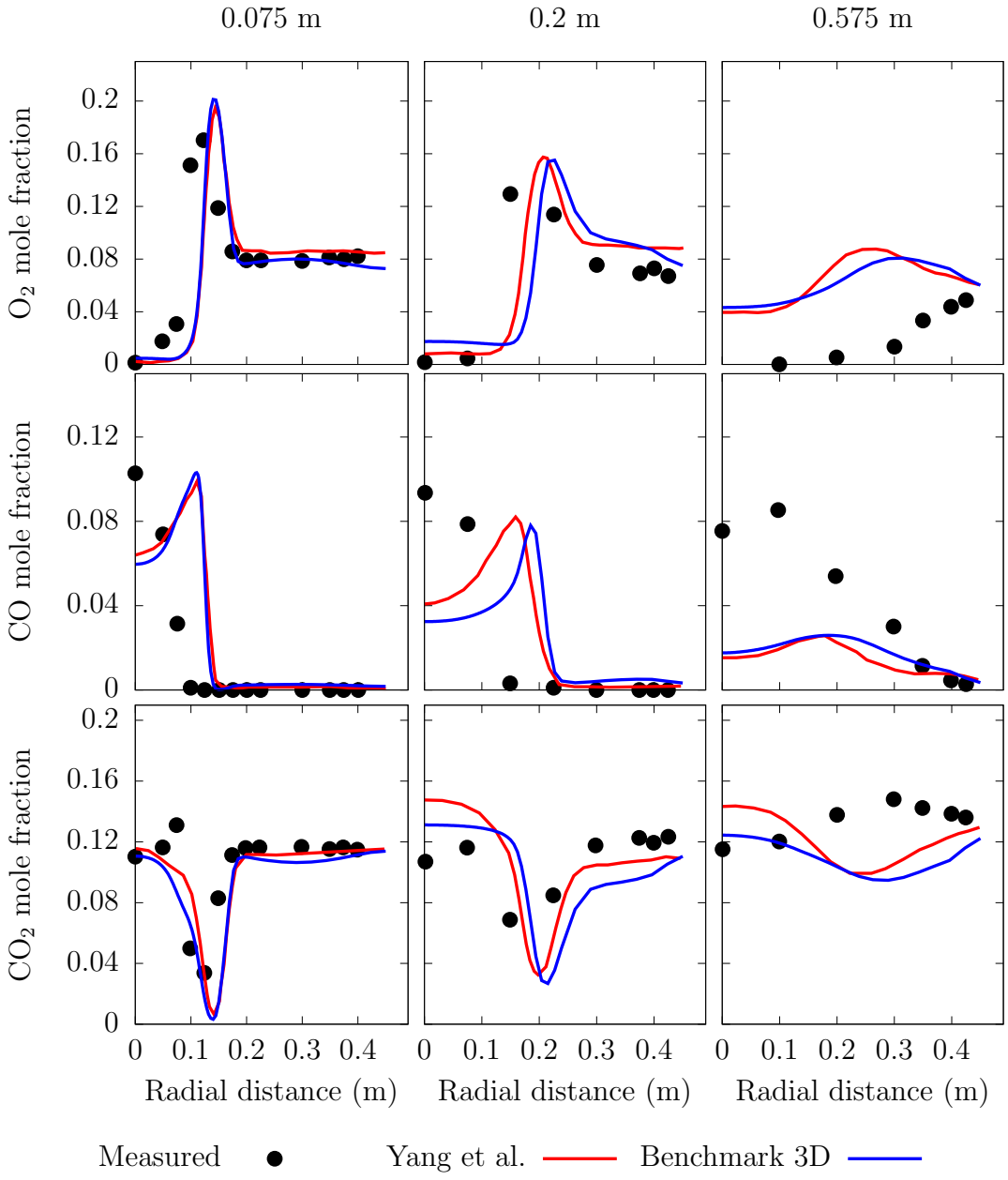

Figure 7.9: Comparison of the species distribution at three radial locations close to the burner between the experimental data, the benchmark model and the predictions from Yang et al.[195].

The distribution of the species at location 0.2 m are offset by a small distance

towards the furnace walls suggesting that the predicted flame main vortex has a wider structure compared to experiments. However, the peak mole fraction of the species and the shape of the flame are in reasonable agreement with the experiments. The distribution of CO is mostly present in the inner recirculation zone close to the burner. This is because the volatiles are released in the inner recirculation and combusted close to the burner. This results in higher concentration of CO near the of the burner. A minor contribution can also be attributed to particles burning in their char phase as the smaller particles enter the char combustion phase early relative to the bigger particles. The distribution increases away from the burner as the inner recirculation expands towards the furnace wall. It is highly unlikely that the Eddy dissipation model is over predicting the rate of combustion of CO as the volatiles are concentrated close to the burner. The under prediction of CO at 0.575 m can be due to inadequate modelling of char combustion. The other contributory factor could be the flame shape which is wider compared to experiments and the species distribution suggests that the mixing of the flow is overpredicted away from the burner [385].

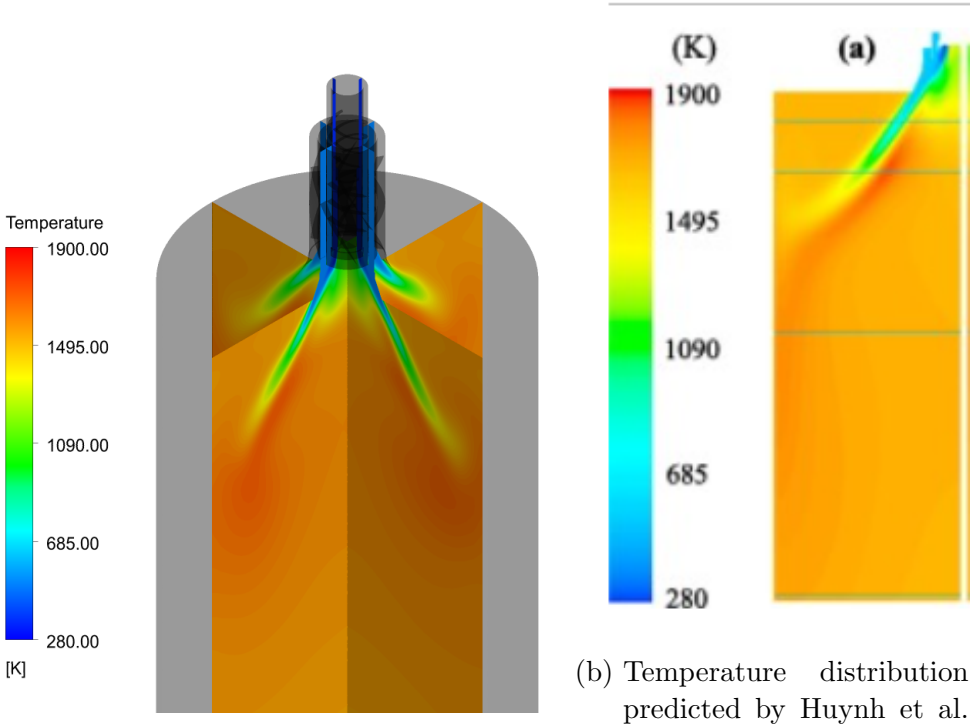

(a) Temperature distribution in X-Y plane for the complete three dimensional case.

(b) Temperature distribution predicted by Huynh et al. using three dimensional axis symmetric flow [382]

Figure 7.10: Comparison of the temperature profiles predicted for different modelling approach.

The temperature distribution, shown in Figure 7.10 describes the two distinct recirculation regions separated by the swirling stream. The temperature prediction are in good agreement with the predictions by Huynh et al. [382]. The temperature distribution suggests that the modelling assumptions for the benchmark model aligns well with the literature model and the CFD simulation is replicated well. The

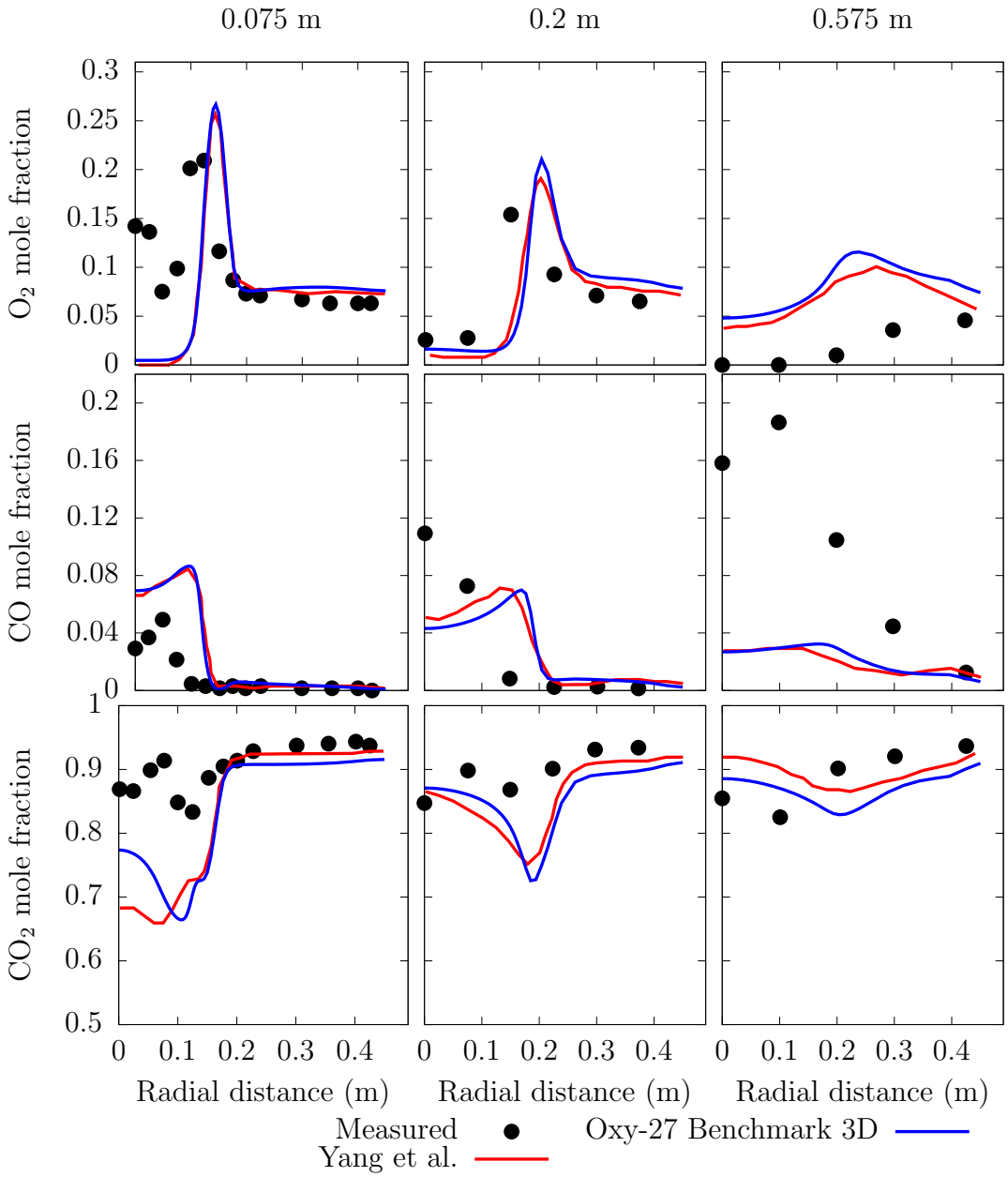

Figure 7.11: Comparison of the species distribution at three radial locations close to the burner between the experimental data, the oxy-27 benchmark case and the predictions from Yang et al.[195].

peak flame temperature is observed between the shear layer of the inner recirculation zone and the swirling stream. According to the CFD results, the CO mole fraction peaks in the similar region. This indicates that in order to predict flame profiles, it is essential to predict the CO accurately. It has been observed in the past that with the current simplified turbulence chemistry models it is difficult to predict the overall distribution of CO in swirling flame as they assume combustion based on mixing [387]. This may over predict the final product species and deplete the intermediate reactants. Even with the limitation of the Eddy dissipation model, the predictions of the CO for the benchmark case are in reasonable agreement with the measured data.

The main aim of this Chapter is to integrate the ignition model developed in previous chapter with the benchmark case and evaluate the impact on the early stage CFD predictions. An investigation on the oxy-27 case was originally planned but due to limitation of the computational resources the research only managed to reach the stage of simulating the benchmark case. The results from the oxy-27 benchmark case are presented in Figure 7.11. The benchmark case align well with the predictions by Yang et al. with the exception of CO_2 at 0.075 m. The CO_2 is overpredicted which can be due to the species error accumulation in CFD. CO_2 for the oxy27 case was set as the last specie in Fluent, the last specie is where the error in the species transport equation is accumulated. Regardless, the required further investigation but due to limitation in the computational resources, it was not investigated further.

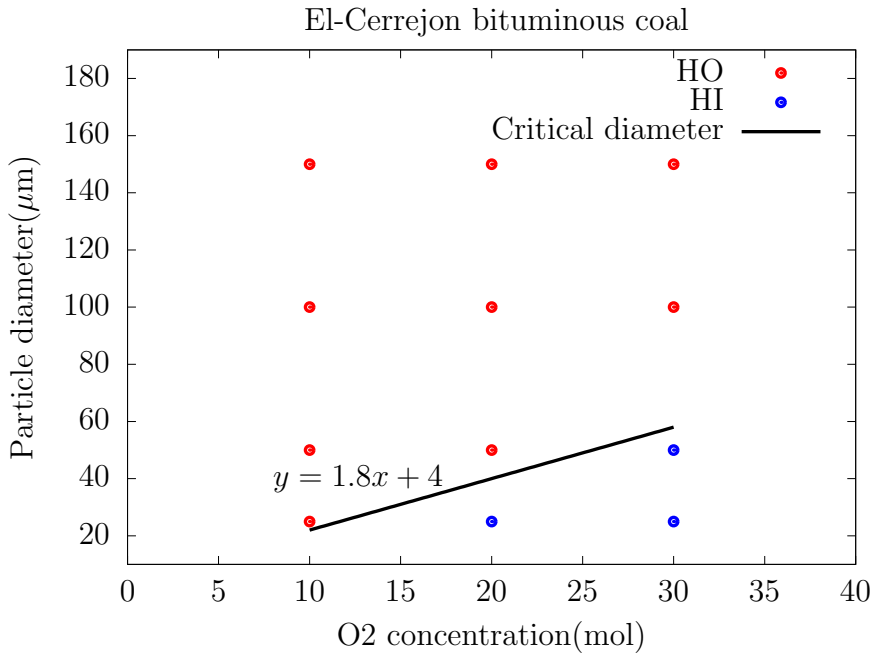

Figure 7.12: Correlation of the critical particle diameters for the El-Cerrejon bituminous coal.

Similar to previous studies, a series of CFD simulation are conducted for quantifying the ignition mechanism for single particles ranging from 25 - 150 μ m. As the particle distribution (Figure 7.2) have a wide spectrum of diameters, four different particle sizes are analysed across three different ambient O_2 mole fractions. The heating in the pilot scale plant may vary significantly, depending on the aerodynamic path the particle experiences. It is impractical to identify and apply the heating rate of all the particles and hence the rate from the entrained flow reactor studies (Chapter 4) is used which is in the range of 5e3 - 1e4 K/s. This heating rate will suffice and will be a reasonable representation of the heating rate in the pilot scale plant. The devolatilisation kinetics were used as described in Table 7.3. The results for the investigation care summarised in Figure 7.12. It shows that particle undergo heterogeneous ignition for three conditions and ignites homogeneously in the rest of the conditions. The correlation of critical particle diameter defines the two ignition mechanism regions. The correlation obtained is used as an input in the ignition model developed in Chapter 5. The correlation indicate that very few particles will ignite heterogeneously and the overall impact of the model will not be significant.

The results for the ignition model are presented in Figure 7.13. The flame profiles and the thickness of the swirling jet for the predictions by the ignition model is very similar to that of the benchmark case. The prediction of O_2 close to the burner in the inner recirculation region stays very similar where it shows that the O_2 is completely consumed. The O_2 predictions close to the refractory walls are reduced by a small fraction. When compared to the experimental data, the results are in better agreement for the ignition model. The predictions suffer downstream at distance of 0.575 m where the consumption of O_2 is under predicted and the overall distribution of O_2 is over predicted. There is a small improvements in the distribution of CO throughout the flame. The peak mole fraction of CO between the shear layer and the inner recirculation zone display better agreement compared to the benchmark case. The overall flame shape still remains the same which can be observed by the sudden decrease in the CO mole fraction. The prediction of the CO_2 improves for radial distance of 0.075 m and 0.2 m which aligns with the prediction of O_2. The improvement in the distribution of CO at 0.575 m has a detrimental impact on the other species which desires for a better combustion chemistry model rather than completely relying on mixing. In summary, the ignition model provides a small improvements in the overall prediction of the flame shape and species prediction. The improvements for a high volatile bituminous coal will generally be minimal as they generally undergo three stage sequential combustion. The small improvements in the predictions of CO suggest that the heterogeneous ignition of smaller particles play a key role in the early stage of combustion for swirling flows. It could be concluded that the heat release in the shear layer is improved over benchmark model. It appears that the small improvements in the overall combustion behaviour have an impact downstream and requires an investigation into other turbulence chemistry models.

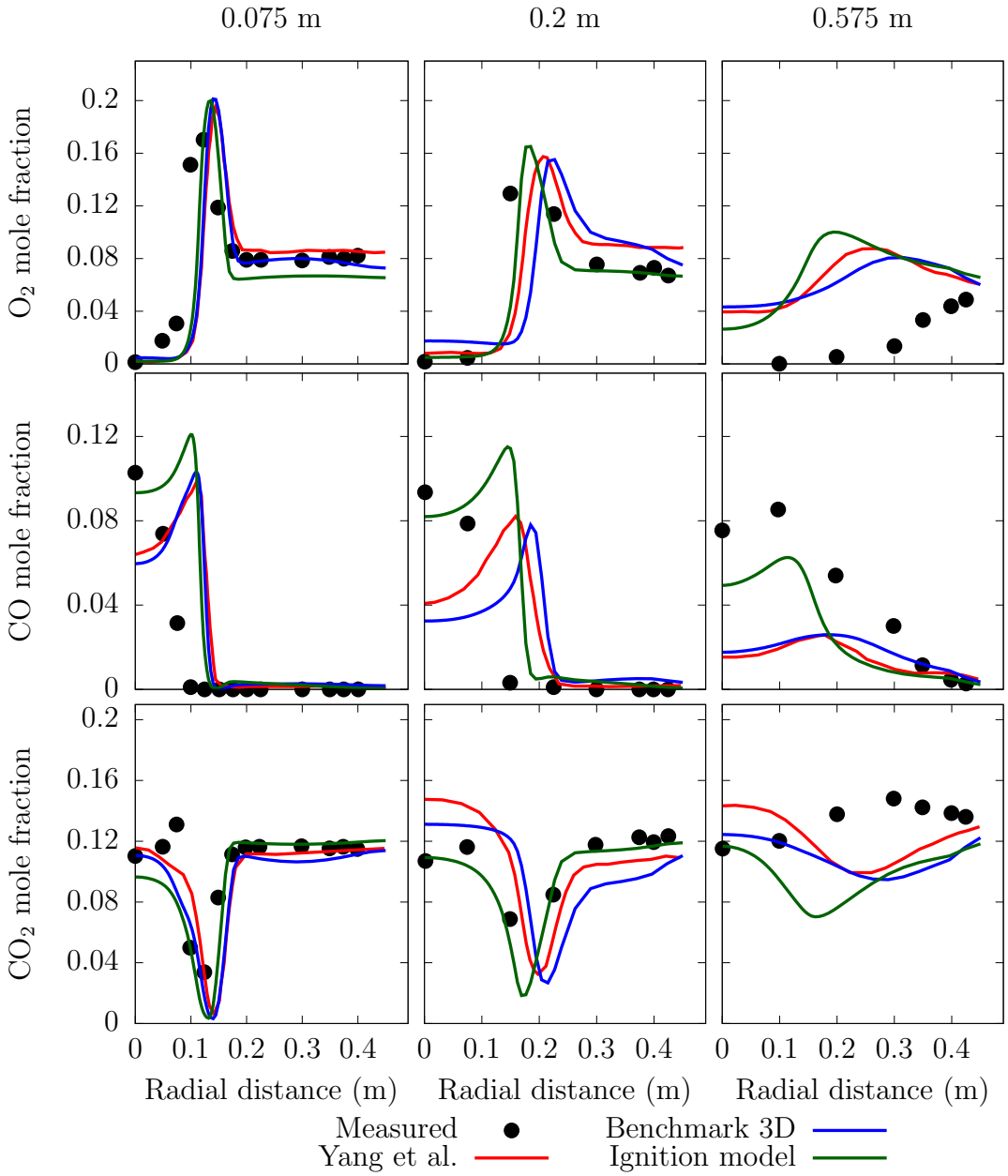

Figure 7.13: Comparison of the species distribution at three radial locations close to the burner between the experimental data, the benchmark model, the ignition model and the predictions from Yang et al.[195].

7.5 Conclusions

In this chapter, the ignition model developed in previous studied was tested for a pilot scale burner with swirling jet. The benchmark case was tested for two types of geometries, a two dimensional axis-symmetric and a complete three dimensional geometry which includes internal blades for a more accurate representation of the

burner internals. The benchmark case was modelled based on the literature and the predictions are compared at three radial locations close to the burner. The major outcome from this research are as follows:

i The two dimensional geometry is able to replicate the thickness of the swirling jet but falls short in predicting the combustion behaviour. This was indicated by the comparison of the species distribution at the three radial location.

ii The predictions of the benchmark model with three dimensional geometry align with the predictions from the CFD model in the literature [195] which shows that the assumptions and the submodels used are accurate.

iii The results from benchmark case suggest that the prediction of the CO can be further improved downstream at 0.575 m. The overall mixing is overestimated which results in poor prediction of the species at radial distance of 0.575 m. The peak mole of CO close to the burner can be improved which increases the accuracy of the peak temperatures of the flame.

iv The prediction from the ignition model shows an improvement in the overall flame shape, thickness and the predictions of the species. The distribution and the overall flame shape is similar as few particles ignite heterogeneously but has a significant improvement in the overall distribution of CO close to the burner.

v The improvement in the CO predictions has a detrimental impact on the prediction of O_2 and CO_2 which indicate that improvement in the char and the gas chemistry models can improve the overall combustion behaviour

8 Conclusions and future work

This research project developed a mathematical model which is focused on ignition characteristics of coal in industrial burners. Ignition quantification for a single solid fuel particle has been researched extensively but still it has been a question of debate over the past few decades mainly due to its heterogeneity and fuel properties. The ignition modelling for an industrial scale burner is relatively unexplored topic in the field of computational fluid dynamics and there is limited framework dedicated around it.

The main aim of this thesis was to develop an ignition model which can accurately predict the ignition delay or the lift off in pulverised fuel flames. The ignition model was developed in stages where the model is validated against experiments at every stage. The research comprised of four major studies which ranged from quantifying ignition mechanism for a single particle and extending the learnings in simulations of pilot scale burners.

8.1 Individual chapter summaries

8.1.1 Investigation of different devolatilisation network models

The aim of the this research chapter was to investigate different network models for devolatilisation and propose the model suitable for further investigation. The key findings are as follows:

i Three network models are tested for predicting the high temperature volatile yield of 36 coals. The 36 coals were experimentally tested on hot wire mesh for replicating high heating rate environment. The predictions from the three network models namely CPD, FG-DVC and PC-Coal Lab were compared against the measured data.

ii The PC-Coal Lab covers a wider range of coals for the correlation compared to the other two models. FG-DVC accommodates the least number of coals as it covers smaller region on the Van-Kervelen diagram. This made FG-DVC least effective for investigating the devolatilisation behaviour of coals.

iii CPD and PC-Coal Lab have a good agreement with the measured data set. The predictions by the CPD model is restricted to the data range of the library coals, anything outside the bounds result in poor prediction. As the PC-Coal

Lab entails a licence cost, the CPD proves to be a better and less demanding model of the three models investigated.

8.1.2 Mathematical model for ignition of a single particle

The aim of this study was to develop a model which can quantify ignition mechanism of a single particle. The model reveals that volatiles are ignited in the continuous phase(outside the particle) but transits towards the particle surface and into the core. The time taken for this transition defines whether the volatiles dominantly burn homogeneously in the domain or simultaneously(heterogeneously) burn inside and outside the particle. The model investigated two different ranks of coal under varying ambient O_2 conditions. The model is extended for different particle sizes and a correlation for critical particle diameter is obtained between particle size and ambient O_2 concentration. This differentiates the ignition mechanism of the particle. The key findings are as follows:

O_2/N_2 conditions for bituminous coal

i The modelling predictions for the peak flame temperatures and the ignition time delay for 90 μm particle diameter across varying ambient O_2 concentration are in excellent agreement with the measured data which are used as validating parameters for the model.

ii There is little to no impact on the ignition time delay of the particle with increase in ambient O_2. This increases the tendency of the particle to ignite heterogeneously with increase in O_2.

iii The transition in the ignition mechanism for the 90 μm particle is predicted between 50-60% ambient O_2 molar concentration. The predictions are in good agreement with the experimental data.

iv The modelling results using CH_4 as the only hydrocarbon specie released as volatiles, accompanied with application of Westbrook-Dryer mechanism for accounting gas phase reactions, over predicts the ignition phenomena. It is thus not recommended for future investigation. On the contrary the results produced using FFCM mechanism are in excellent agreement with the measured data.

v The model extension to other particle sizes reveal that there is an increase in the ignition delay time with an increase in particle size. The particle tend to ignite homogeneously with increase in particle size. The investigation led to development of a correlation for critical particle diameter which can be integrated in simulating pulverised fuel flames.

O_2/N_2 conditions for lignite

i The higher inherent moisture content of the lignite increases the ignition delay time when compared to bituminous coal. The higher moisture content also increases the porosity of the particle during the devolatilisation phase.

This enhances diffusion of O_2 inside the particle and promotes heterogeneous ignition.

ii The overall modelling parameters such as ignition delay time and ignition mechanism for particle size of 90 μm are in good agreement with the experimental data. The peak flame temperatures are under predicted by the model which was attributed to the fragmentation of the particle.

iii Similar to the bituminous coal, the ignition mechanism transits from HO to HO-HI with increase in ambient O_2 concentration.

iv The FFCM mechanism is suitable for simulating ignition mechanism for lignites across various conditions and is recommended for future investigations.

v Compared to bituminous coal, the correlation of critical particle diameter for lignite suggest that there are greater number of particles which ignite heterogeneously.

O_2/CO_2 conditions for bituminous coal

i The modelling predictions for the ignition time delay and peak flame temperatures are in excellent agreement with the experimental data which suggests that the model can be used for further investigation.

ii The ignition delay times are much longer for the oxyfuel cases when compared to O_2/N_2 cases because of the lower temperatures around the particle injector and heating capacity of CO_2. However, the ignition delay time reduces with increase in ambient O_2 concentration.

iii The longer ignition delay enhances the O_2 diffusion in and around the particle which leads to particle igniting heterogeneously.

iv The sensitivity to ambient temperature suggests that there will be a decrease in particle ignition temperature and ignition time delay with increase in ambient temperature but it has no impact on the ignition mechanism for the temperatures tested.

8.1.3 Modelling investigation of ignition in IFRF co-axial burner

A coaxial burner was chosen for investigation of coal flames because it is easy to visualise and identify different thermo-chemistry phase of the particles (i.e. the process of moisture loss, devolatilisation and char combustion) in the post processing. The aim of this study was to integrate a correlation of critical particle diameter in the existing sub models used for simulating coal combustion flames. The measurements of the inflame parameters are used for validating the ignition model. The key findings from the investigations are as follows:

i The benchmark simulations suggested that the ignition is primarily due to the combustion of volatiles in the gas phase. The peak flame temperatures of the flame at around 1.9 m is due to the combination of volatiles and char combustion.

ii The predictions by the benchmark case are in reasonable agreement with the experimental values which provides confidence in the sub-models used for simulations. The rise in axial temperature lagged with an error of 10% (between 1.25 m and 1.5 m) which indicated that the flame lift off distance is not accurately predicted by the benchmark case.

iii The correlation for critical particle diameter and the particle size distribution suggest that a small amount of particles are ignited heterogeneously. It is one of the reasons why the benchmark case is able predict flame parameters with a small error.

iv The ignition model developed in this study improves the predictions of the flame parameters and hence the modelling methodology can be used for future combustion calculations in air conditions. The model illustrated that ignition is due to combination of the volatiles combustion in both phases and char combustion of small particles in the early stages of the flame.

8.1.4 Modelling investigation for a Utah coaxial oxy-fuel burner

The Utah coaxial burner was chosen to investigate pulverised fuel flames in oxyfuel conditions as it enables to qualitatively visualise the impact of the ignition model on the particle behaviour (similar to the IFRF burner investigation). Six different benchmark cases were simulated which showed poor agreement with the experimental data. However, there were no inflame measurement which made it difficult to determine any flaws in the specific sub-models. This enforced an investigation into the sensitivity of different sub-models used for oxy-fuel conditions. The key findings from the investigation are as follows:

i The modified radiation model had no impact on the predictions of the flame stand-off distance due to scale of the furnace. The models analysed have proven to be equally good for simulating oxy-fuel coal combustion.

ii The combination of different reaction mechanisms and the turbulence chemistry interaction model shows no improvement on the flame stand off distance. The other combinations tested increased the flame stand-off and hence it was decided that ED model with two step reaction is used for further investigation.

iii The sensitivity study on the wall temperatures showed that there is a decrease in flame stand off distance with increase in wall temperatures. The best agreement was achieved for Case 1 when the wall temperature is as high as 1800 K but it still displayed a significant error for Case 6. This indicated that the increased wall temperature may be overcompensating for the other sub-models. The sensitivity suggests that there is a mismatch in the experimental data for the wall temperatures and it varies on a case by case basis.

iv The particle distribution and the correlation for the critical particle diameter suggests that there will be a greater amount of particles igniting heterogeneously.

v The ignition model improves the flame stand off distance predictions for Cases 1-4 but still presented significant errors for Cases 5 and 6. The results indicate that the ignition model may be over predicting the heterogeneous ignition of particles and it requires small tuning for oxy-fuel conditions (i.e. changing the ignition temperature of the particles). The model shows that it is better equipped in predicting flame stand off distance compared to the traditional thermo-chemistry models. The overall modelling results can be improved if the uncertainty of wall temperature is eliminated.

8.1.5 Impact of ignition in a pilot scale burner at PACT facility

The downward firing solid fuel furnace at PACT facility in Beighton, UK was chosen for investigating the influence of the ignition model in a low NOx swirled burner. The experimental work was conducted by the research team at the University of Sheffield. This provided a comprehensive knowledge of the furnace operating conditions, reducing any errors in the CFD input. The numerical investigation done by Yang et al and Huynh et al was chosen for benchmark cases. A comparison is made for the benchmark case between experimental results, a complete 3D case and a 2D axissymmetric geometry and the literature predictions. The key findings are as follows:

i The CFD simulation results for the benchmark 2D case has few shortcomings and are not in agreement with the results obtained by Yang et al.

ii The overall CFD results from the 3D benchmark case are in good agreement with the predictions by Yang et al. confirming the literature model is replicated well.

iii The overall 3D benchmark case are in reasonable agreement with the experimental data. The distribution of CO are under predicted in the inner recirculation zone close to the burner, which suggest that there is scope for improving the predictions in the ignition zone.

iv The ignition model is able to improve the overall distribution of CO close to the burner suggesting the heterogeneous ignition of the small particles have a small impact on the overall flame characteristics.

v The mixing is over predicted downstream which is observed in species prediction at 0.575 m. The over prediction of the swirling jet mixing, results in impacting the species distribution as Eddy dissipation model is dominated by the mixing phenomena. An investigation with different turbulence chemistry model is suggested for improving the flame predictions.

8.2 Proposals for future work

The investigation of the devolatilisation models in Chapter 3 can be extended to study the impact of the devolatilisation kinetics on the overall combustion system.

As CPD is inbuilt in Fluent, it would be desirable to test the computational and scientific efficiency of the sub-model vs the single rate fitted kinetics. It will improve the combustion prediction in the early stages of the flame.

Investigating the ignition mechanism of a single particle in Chapter 4 shows that the results are in good agreement with the experimental data. The particle size tested in this research were all assumed to have uniform spherical shape, the logical step would be to validate the model for non-spherical shapes and different sizes. The model capability can be improved once different ranks of coal and a variety of biomass are validated. The application of detail chemistry showed a significant improvement in the overall results when compared to reduced mechanism. The predictions of the volatiles species evolved can be tuned with other reduced mechanism (e.g. Jones-Lindsted) for an improvement in the gas phase chemistry. The model predictions can also be further improved if the gas phase chemistry is tuned or validated for oxyfuel conditions.

The application of the ignition model in the coaxial burners showed a significant improvement over the benchmark cases. It would have been ideal to validate the ignition model for particle to particle interaction in a laminar flow environment. Due to the lack of experimental studies providing inflame validating data the research was propelled into the next phase. If there are future experiments conducted in literature which analyse multi particle ignition in laminar flow environment, it would be ideal to test the ignition model and fine tune it for future application. The minimum ignition temperature of the particle in the ignition model was set at 800 K for all the simulations tested which provided excellent improvements over the benchmark case. In order to fine tune the model for oxyfuel conditions a sensitivity analysis can be conducted on the particle ignition temperature.

In Chapter 7, the first improvement would be to extend the investigation of the ignition model to oxyfuel conditions. A future study can be the application of the ignition model in a boiler and compare the CFD predictions against the experimental data to validate the model. The results for the benchmark case are sensitive to the turbulence mixing as the Eddy dissipation model is directly coupled with the mixing parameters of the flame. It would be ideal to test the CFD simulations with the Flamelet models or detail chemistry model. In order to achieve that a reasonable amount of computational resources are required and it could be conducted in the future as the computational resources gets cheaper. The model can be extended to investigate the overall impact on NOx formation inside the hot zone of the flame. Finally, it would be ideal to see the impact of the ignition model on different fuels which can provide fuel flexibility to different power plant operators. .

Bibliography

[1] World Energy Council. *World energy resources*. World Energy Council, 2016.

[2] C. R. Warren and M. McFadyen. Does community ownership affect public attitudes to wind energy? a case study from south-west scotland. *Land use Policy*, 27(2):204–213, 2010.

[3] R. H. Lasseter. Microgrids. In *Power Engineering Society Winter Meeting, 2002. IEEE*, volume 1, pages 305–308. IEEE, 2002.

[4] S. Chowdhury, S. P. Chowdhury, and P. Crossley. *Microgrids and active distribution networks*. Stevanage, UK, 1st edition, 2009.

[5] O. Hafez and K. Bhattacharya. Optimal planning and design of a renewable energy based supply system for microgrids. *Renewable Energy*, 45:7–15, 2012.

[6] BP British Petroleum. Statistical review of world energy, 2016.

[7] C. S. Thomas. Petroleum and coal proven reserves: The case for coal and the demise of opec. In *Stopping Climate Change: the Case for Hydrogen and Coal*, pages 35–40. Springer, 2017.

[8] British Petroleum. Bp energy outlook 2030. *London, BP*, page 40, 2013.

[9] International Energy Agency. World energy outlook. 2012.

[10] A. Franco and A. R. Diaz. The future challenges for "clean coal technologies": joining efficiency increase and pollutant emission control. *Energy*, 34(3):348–354, 2009.

[11] M. J. Miller. Retrofit SO_2 and NOx control technologies for coal-fired power plants. *Environmental Progress*, 5(3):171–177, 1986.

[12] D. Popp. Exploring links between innovation and diffusion: adoption of no x control technologies at us coal-fired power plants. *Environmental and Resource Economics*, 45(3):319–352, 2010.

[13] R. K. Srivastava, N. Hutson, B. Martin, F. Princiotta, and J. Staudt. Control of mercury emissions from coal-fired electric utility boilers. 2006.

[14] Y. Zhao, S. Wang, L. Duan, Y. Lei, P. Cao, and J. Hao. Primary air pollutant emissions of coal-fired power plants in china: Current status and future prediction. *Atmospheric Environment*, 42(36):8442–8452, 2008.

[15] J. Barrett. Greenhouse molecules, their spectra and function in the atmosphere. *Energy & Environment*, 16(6):1037–1045, 2005.

[16] International Energy Agency. Global energy review 2020. *India.[Online] https://www.iea.org/countries/ [Accessed: 15th May 2021]*, 2021.

[17] N. Zamani. The relationship between crude oil and coal markets: A new approach. *International Journal of Energy Economics and Policy*, 6(4):801–805, 2016.

[18] Tracking Clean Energy Progress. IEA input to the clean energy ministerial. *IEA Report*, 2013.

[19] A. Komaki, T. Gotou, T. Uchida, T. Yamada, T. Kiga, and C. Spero. Operation experiences of oxyfuel power plant in Callide oxyfuel project. *Energy Procedia*, 63:490–496, 2014.

[20] M. M. Halmann and M. Steinberg. *Greenhouse gas carbon dioxide mitigation: science and technology*. CRC press, 1998.

[21] World Resources Institute. Climate watch 2020, 2020.

[22] European Comission. Regulation of the european parliament and of the council on enhancing ship and port facility security. *Assessment*, 39:14, 2003.

[23] J. Rogelj, Michel Den E., N. Höhne, T. Fransen, H. Fekete, H. Winkler, R. Schaeffer, F. Sha, K. Riahi, and M. Meinshausen. Paris agreement climate proposals need a boost to keep warming well below 2°C. *Nature*, 534(7609):631–639, 2016.

[24] Parliament of the United Kingdom. Climate Change Act 2008. *HM Government*, pages 1–103, 2008.

[25] M. Lockwood. The political sustainability of climate policy: The case of the UK Climate Change Act. *Global Environmental Change*, 23(5):1339–1348, 2013.

[26] P. Tans and R. Keeling. Trends in atmospheric carbon dioxide. *NOAA/ESRL. https://www.esrl.noaa.gov/gmd/ccgg/trends/ [4th November 2021]*, 2021.

[27] K. Haustein, M. R. Allen, P. M. Forster, F. E. L. Otto, D. M. Mitchell, H. D. Matthews, and D. J. Frame. A real-time global warming index. *Scientific reports*, 7(1):1–6, 2017.

[28] P. Denholm, E. Ela, B. Kirby, and M. Milligan. Role of energy storage with renewable electricity generation. *National Renewable Energy Lab.(NREL)*, 1(10):1–100, 2010.

[29] S. Bruno and G. Jürgen. Lithium batteries: Status, prospects and future. *Journal of Power Sources*, 195(9):2419 – 2430, 2010.

[30] J. Conti, P. Holtberg, J. Diefenderfer, A. LaRose, J. T. Turnure, and L. Westfall. International energy outlook 2016 with projections to 2040.

[31] M. Aitken. Why we still don't understand the social aspects of wind power: A critique of key assumptions within the literature. *Energy Policy*, 38(4):1834–1841, 2010.

[32] G. Walker, P. Devine-Wright, S. Hunter, H. High, and B. Evans. Trust and community: Exploring the meanings, contexts and dynamics of community renewable energy. *Energy Policy*, 38(6):2655–2663, 2010.

[33] R. Bolton and T. J. Foxon. A socio-technical perspective on low carbon investment challenges–insights for UK energy policy. *Environmental innovation and societal transitions*, 14:165–181, 2015.

[34] R. Steve. Trust and the transformation of energy systems. *Energy Policy*, 38(6):2617 – 2623, 2010. The Role of Trust in Managing Uncertainties in the Transition to a Sustainable Energy Economy, Special Section with Regular Papers.

[35] J. Koppejan and S. Van Loo. *The handbook of biomass combustion and co-firing*. Routledge, 2012.

[36] K. Tokimatsu, R. Yasuoka, and M. Nishio. Global zero emissions scenarios: The role of biomass energy with carbon capture and storage by forested land use. *Applied Energy*, 185:1899–1906, 2017.

[37] C. B. Field, J. E. Campbell, and D. B. Lobell. Biomass energy: the scale of the potential resource. *Trends in Ecology & Evolution*, 23(2):65–72, 2008.

[38] L. Reijnders. Conditions for the sustainability of biomass based fuel use. *Energy Policy*, 34(7):863–876, 2006.

[39] K. C. Pavanan, R. A. Bosch, R. Cornelissen, and J. C. Philp. Biomass sustainability and certification. *Trends in Biotechnology*, 31(7):385–387, 2013.

[40] A. Evans, V. Strezov, and T. J. Evans. Sustainability considerations for electricity generation from biomass. *Renewable and Sustainable Energy Reviews*, 14(5):1419–1427, 2010.

[41] S. Wheatley, B. Sovacool, and D. Sornette. Of disasters and dragon kings: a statistical analysis of nuclear power incidents and accidents. *Risk Analysis*, 37(1):99–115, 2017.

[42] M. B. Roth and P. Jaramillo. Going nuclear for climate mitigation: An analysis of the cost effectiveness of preserving existing US nuclear power plants as a carbon avoidance strategy. *Energy*, 131:67–77, 2017.

[43] A. Rosen. Why nuclear energy is not an answer to global warming. International Physicians for the Prevention of Nuclear War, Germany, London Medact Conference submission, December http://www. nuclear-policy. info/wp/wp-content/uploads/2017/01/Why-nuclear-energyis-not-an-answer-to-global-warming. pdf, 2016.

[44] D. Abbott et al. Is nuclear power globally scalable? *Proc. IEEE*, 99(10):1611–1617, 2011.

[45] D. Abbott. Limits to growth: Can nuclear power supply the world's needs? *Bulletin of the Atomic Scientists*, 68(5):23–32, 2012.

[46] D. Zhang. *Ultra-supercritical Coal Power Plant: Materials, Technologies and Optimisation*. Woodhead Publishing, 2013.

[47] D. M. D'Alessandro, B. Smit, and J. R. Long. Carbon dioxide capture: prospects for new materials. *Angewandte Chemie International Edition*, 49(35):6058–6082, 2010.

[48] B. Metz, O. Davidson, H. De Coninck, M. Loos, and L. Meyer. Ipcc special report on carbon dioxide capture and storage. Technical report, Intergovernmental Panel on Climate Change, Geneva (Switzerland). Working Group III, 2005.

[49] J. C. Bergstrom and D. Ty. Economics of carbon capture and storage. *Carbon Capture and Storage*, page 241, 2017.

[50] J. M. Deutch. Retrofitting of Coal-Fired Power Plants for CO_2 Emissions Reductions An MIT Energy Initiative Symposium. March,2009.

[51] M. Mitrović and A. Malone. Carbon capture and storage (ccs) demonstration projects in canada. *Energy Procedia*, 4:5685–5691, 2011.

[52] VGB PowerTech e.V. CO_2 Capture and Storage VGB Report on the State of the Art. Technical report, VGB PowerTech Service GmbH, 2004.

[53] H. Baron. *The oil and gas engineering guide*. Editions Technip, 2010.

[54] M. Kanniche, R. Gros-Bonnivard, P. Jaud, J. Valle-Marcos, J. Amann, and C. Bouallou. Pre-combustion, post-combustion and oxy-combustion in thermal power plant for co 2 capture. *Applied Thermal Engineering*, 30(1):53–62, 2010.

[55] F. L. Horn and M. Steinberg. Control of carbon dioxide emissions from a power plant (and use in enhanced oil recovery). *Fuel*, 61(5):415–422, 1982.

[56] N. Florin and P. Fennell. Carbon capture technology: future fossil fuel use and mitigating climate change. *Grantham institute for climate change briefing paper*, (3), 2010.

[57] T. C. Merkel, H. Lin, X. Wei, and R. Baker. Power plant post-combustion carbon dioxide capture: an opportunity for membranes. *Journal of Membrane Science*, 359(1):126–139, 2010.

[58] B. J. P. Buhre, L. K. Elliott, C. D. Sheng, R. P. Gupta, and T. F. Wall. Oxy-fuel combustion technology for coal-fired power generation. *Progress in Energy and Combustion Science*, 31(4):283–307, 2005.

[59] M. B. Toftegaard, J. Brix, P. A. Jensen, P. Glarborg, and A. D. Jensen. Oxy-fuel combustion of solid fuels. *Progress in energy and combustion science*, 36(5):581–625, 2010.

[60] R. M. Davidson and S. O. Santos. *Oxyfuel combustion of pulverised coal*. IEA Clean Coal Centre London, UK, 2010.

[61] IEA GHG. Impact of impurities on CO_2 capture, transport & storage. *Cheltenham: International Energy Agency Greenhouse Gas R&D Programme*, 2004.

[62] X. Li, Y. Liu, R. Stanger, L. Belo, T. Ting, and T. Wall. Gas quality control in oxy-pf technology for carbon capture and storage. *Fuel*, pages 241–249, 2012.

[63] M. Bilio, S. Brown, M. Fairweather, H. Mahgerefteh, et al. CO_2 pipelines material and safety considerations. In *Hazards XXI: Process Safety and Environmental Protection in a Changing World*, volume 155, pages 423–429. Institution of Chemical Engineers, 2009.

[64] K. Abdulla. Peak energy & resources, climate change, and the preservation of knowledge. *Renewable and Sustainable Energy Reviews*, 12(1):200–217, 2013.

[65] E. K. Halland, F. Riis, C. Magnus, W. T. Johansen, I. M. Tappel, I. T. Gjeldvik, T. Solbakk, and V. T. H. Pham. CO_2 Storage Atlas of the Norwegian part of the North Sea. *Energy Procedia*, 37:4919–4926, 2013.

[66] H. C. Mantripragada, H. Zhai, and E. S. Rubin. Boundary Dam or Petra Nova–Which is a better model for CCS energy supply? *International Journal of Greenhouse Gas Control*, 82:59–68, 2019.

[67] B. R. Pease, A. A. Levasseur, and O. K. Chow. Fuel switching. A pilot-scale approach to boiler performance predictions. *Energy & Fuels*, 7(6):768–773, 1993.

[68] A. M. Carpenter. *Switching to cheaper coals for power generation*. IEA Coal Research London, 1998.

[69] M. Cloke, E. Lester, and W. Gibb. Characterization of coal with respect to carbon burnout in pf-fired boilers. *Fuel*, 76(13):1257–1267, 1997.

[70] C. Penterson. The Effects of Coal Quality and Fuel Switching on Low NOx Burner Performance. 2008.

[71] A. R. Jones. Flame failure detection and modern boilers. *Journal of Physics E: Scientific Instruments*, 21(10):921, 1988.

[72] J. Towell, T. Martinez, D. Hightower, R. Maxey, P. E. Gerry Snow, H. Gonzalez, and R. Rians. Improvements in Fuel Flexibility and Operating Cost Reduction at CSU Drake Station with Targeted In-Furnace Injection™ Technology. *Carbon*, 100(66.29):53–03, 2010.

[73] L. Bartoňová. Unburned carbon from coal combustion ash: an overview. *Fuel Processing Technology*, 134:136–158, 2015.

[74] V. Llinares Jr and A. A. Levasseur. Fuel switching and the state-of-the-art of coal and boiler performance analyses. In *International Power Generation Conference, Atlanta, GA, USA, 10/18-22/92*, pages 1–7, 1992.

[75] A. Arenillas, F. Rubiera, B. Arias, J. J. Pis, J. M. Faundez, A. L. Gordon, and X. A. Garcia. A TG/DTA study on the effect of coal blending on ignition behaviour. *Journal of Thermal Analysis and Calorimetry*, 76(2):603–614, 2004.

[76] S. Su, J. H. Pohl, D. Holcombe, and J. A. Hart. Techniques to determine ignition, flame stability and burnout of blended coals in pf power station boilers. *Progress in Energy and Combustion Science*, 27(1):75–98, 2001.

[77] J. Faúndez, B. Arias, F. Rubiera, A. Arenillas, X. García, A. L. Gordon, and J. J. Pis. Ignition characteristics of coal blends in an entrained flow furnace. *Fuel*, 86(14):2076–2080, 2007.

[78] A. M. Carpenter. *Coal blending for power stations*. IEA Coal Research UK, 1995.

[79] H. Schuster and C. Peterson. Experience with various coals in power plants in the united states and europe. In *Coal-Gen 2002 Conference and Exhibition*, 2002.

[80] E. J. Anthony and F. Preto. Pressurized combustion in FBC systems. In *Pressurized Fluidized Bed Combustion*, pages 80–120. Springer, 1995.

[81] D. Tillman. *The combustion of solid fuels and wastes*. Academic Press, 2012.

[82] J. F. Unsworth, C. S. Fowler, and L. F. Jones. Moisture in coal: 2. Maceral effects on pore structure. *Fuel*, 68(1):18–26, 1989.

[83] J. Yu, J. A. Lucas, and T. F. Wall. Formation of the structure of chars during devolatilization of pulverized coal and its thermoproperties: A review. *Progress in Energy and Combustion Science*, 33(2):135–170, 2007.

[84] N. Oka, T. Murayama, H. Matsuoka, S. Yamada, T. Yamada, S. Shinozaki, M. Shibaoka, and C. G. Thomas. The influence of rank and maceral composition on ignition and char burnout of pulverized coal. *Fuel Processing Technology*, 15:213–224, 1987.

[85] D. Rezaei, Y. Zhou, J. Zhang, K. E. Kelly, E. G. Eddings, R. J. Pugmire, M. S. Solum, and J. O. Wendt. The effect of coal composition on ignition and flame stability in coaxial oxy-fuel turbulent diffusion flames. *Energy & Fuels*, 27(8):4935–4945, 2013.

[86] V. Strezov, J. A. Lucas, and L. Strezov. Quantifying the heats of coal devolatilization. *Metallurgical and Materials Transactions B*, 31(5):1125–1131, 2000.

[87] K. Zygourakis. Mechanisms and optimization of coal combustion. Technical report, National Energy Technology Lab., Pittsburgh, PA (US); National Energy Technology Lab., Morgantown, WV (US), 2000.

[88] T. F. Wall, G. Liu, H. Wu, D. G. Roberts, K. E. Benfell, S. Gupta, J. A. Lucas, and D. J. Harris. The effects of pressure on coal reactions during pulverised coal combustion and gasification. *Progress in Energy and Combustion Science*, 28(5):405–433, 2002.

[89] J. Yu, V. Strezov, J. Lucas, and T. Wall. Swelling behaviour of individual coal particles in the single particle reactor. *Fuel*, 82(15):1977–1987, 2003.

[90] M. Sami, K. Annamalai, and M. Wooldridge. Co-firing of coal and biomass fuel blends. *Progress in Energy and Combustion Science*, 27(2):171–214, 2001.

[91] N. M. Laurendeau. Heterogeneous kinetics of coal char gasification and combustion. *Progress in Energy and Combustion Science*, 4(4):221–270, 1978.

[92] I. W. Smith. The combustion rates of coal chars: a review. In *Symposium (International) on combustion*, volume 19, pages 1045–1065. Elsevier, 1982.

[93] R. Jovanovic, A. Milewska, B. Swiatkowski, A. Goanta, and H. Spliethoff. Sensitivity analysis of different devolatilisation models on predicting ignition point position during pulverized coal combustion in O_2/N_2 and O_2/CO_2 atmospheres. *Fuel*, 101:23–37, 2012.

[94] G. Miessen, F. Behrendt, O. Deutschmann, and J. Warnatz. Numerical studies of the heterogeneous combustion of char using detailed chemistry. *Chemosphere*, 42(5):609–613, 2001.

[95] L. Tognotti, J. P. Longwell, and A. F. Sarofim. The products of the high temperature oxidation of a single char particle in an electrodynamic balance. In *Symposium (International) on Combustion*, volume 23, pages 1207–1213. Elsevier, 1991.

[96] J. F. Griffiths and J. A. Barnard. *Flame and combustion*. CRC Press, 1995.

[97] M. Taniguchi, H. Okazaki, H. Kobayashi, S. Azuhata, H. Miyadera, H. Muto, T. Tsumura, et al. Pyrolysis and ignition characteristics of pulverized coal particles. *Journal of Energy Resources Technology-Transactions of The ASME*, 123(1):32–38, 2001.

[98] R. H. Essenhigh, Mahendra K Misra, and David W Shaw. Ignition of coal particles: a review. *Combustion and Flame*, 77(1):3–30, 1989.

[99] H. Jüntgen and K. H. Van Heek. An update of german non-isothermal coal pyrolysis work. *Fuel Processing Technology*, 2(4):261–293, 1979.

[100] C. T. Chitsora, H. Mühlen, K. H. Van Heek, and H. Jüntgen. The influence of pyrolysis conditions on the reactivity of char in H_2O. *Fuel Processing Technology*, 15:17–29, 1987.

[101] T. H. Fletcher. Swelling properties of coal chars during rapid pyrolysis and combustion. *Fuel*, 72(11):1485–1495, 1993.

[102] N. N. Semenov. On the theory of combustion processes. *Z. phys. Chem*, 48:571–582, 1928.

[103] M. Chen, L. Fan, and R. H. Essenhigh. Prediction and measurement of ignition temperatures of coal particles. In *Symposium (International) on Combustion*, volume 20, pages 1513–1521. Elsevier, 1985.

[104] J. Pedro, S. Seixas, and R. H. Essenhigh. Ignition temperatures of a high-ash portuguese anthracite: Comparison with a low-ash pennsylvania anthracite. *Combustion and Flame*, 66(2):215–218, 1986.

[105] P. J. Brooks and R. H. Essenhigh. Variation of ignition temperatures of fuel particles in vitiated oxygen atmospheres: Determination of reaction mechanism. In *Symposium (International) on Combustion*, volume 21, pages 293–302. Elsevier, 1988.

[106] M. Chen, L. Fan, and R. H. Essenhigh. Prediction and measurement of ignition temperatures of coal particles. In *Symposium (International) on Combustion*, volume 20, pages 1513–1521. Elsevier, 1985.

[107] L. D. Smoot and P. J. Smith. Heterogeneous char reaction processes. In *Coal Combustion and Gasification*, pages 77–110. Springer, 1985.

[108] R. W. Arms. The ignition temperature of coal. Technical report, University of Illinois at Urbana Champaign, College of Engineering. Engineering Experiment Station, 1922.

[109] S. Bandyopadhyay and D. Bhaduri. Prediction of ignition temperature of a single coal particle. *Combustion and Flame*, 18(3):411–415, 1972.

[110] X. Du and K. Annamalai. The transient ignition of isolated coal particle. *Combustion and Flame*, 97(3-4):339–354, 1994.

[111] S. R. Gubba, L. Ma, M. Pourkashanian, and A. Williams. Influence of particle shape and internal thermal gradients of biomass particles on pulverised coal/biomass co-fired flames. *Fuel processing technology*, 92(11):2185–2195, 2011.

[112] N. Gat. On internal temperature gradients in a pyrolysing coal particle. *Combustion Science and Technology*, 49(5-6):297–303, 1986.

[113] A. Rocha and C. G. Veras. Numerical study on the transient ignitition of single particle with the cmvc-cpdnlg model. *17th International Congress of Mechanical Engineering*, 2003.

[114] M. Zhu, H. Zhang, Z. Zhang, and D. Zhang. A numerical modeling study of ignition of single coal particles under microgravity conditions. *Combustion Science and Technology*, 183(11):1221–1235, 2011.

[115] B. Liu, Z. Zhang, H. Zhang, and D. Zhang. Volatile release and ignition behaviors of single coal particles at different oxygen concentrations under microgravity. *Microgravity Science and Technology*, 28(2):101–108, 2016.

[116] D. O. Glushkov, P. A. Strizhak, and O. V. Vysokomornaya. Numerical research of heat and mass transfer during low-temperature ignition of a coal particle. *Thermal Science*, 19(1):285–294, 2015.

[117] C. Wendt, C. Eigenbrod, O. Moriue, and H. J. Rath. A model for devolatilization and ignition of an axisymmetric coal particle. *Proceedings of the Combustion Institute*, 29(1):449–457, 2002.

[118] B. Goshayeshi and J. C. Sutherland. A comparison of various models in predicting ignition delay in single-particle coal combustion. *Combustion and Flame*, 161(7):1900–1910, 2014.

[119] C. A. G. Veras, J. Saastamoinen, J. A. Carvalho Jr, and M. Aho. Overlapping of the devolatilization and char combustion stages in the burning of coal particles. *Combustion and Flame*, 116(4):567–579, 1999.

[120] M. Vascellari, H. Xu, and C. Hasse. Flamelet modeling of coal particle ignition. *Proceedings of the Combustion Institute*, 34(2):2445–2452, 2013.

[121] A. Kazakov and M. Frenklach. Reduced reaction sets based on gri-mech 1.2. *University of California at Berkeley, Berkeley, CA, http://www. me. berkeley. edu/drm*, 1994.

[122] C. D. Pierce and P. Moin. Progress-variable approach for large-eddy simulation of non-premixed turbulent combustion. *Journal of fluid Mechanics*, 504:73–97, 2004.

[123] J. Watanabe and K. Yamamoto. Flamelet model for pulverized coal combustion. *Proceedings of the Combustion Institute*, 35(2):2315–2322, 2015.

[124] S. Jiménez and C. Gonzalo-Tirado. Properties and relevance of the volatile flame of an isolated coal particle in conventional and oxy-fuel combustion conditions. *Combustion and Flame*, 176:94–103, 2017.

[125] G. L. Tufano, O. T. Stein, A. Kronenburg, A. Frassoldati, T. Faravelli, L. Deng, A. M. Kempf, M. Vascellari, and C. Hasse. Resolved flow simulation of pulverized coal particle devolatilization and ignition in air-and O_2/CO_2-atmospheres. *Fuel*, 186:285–292, 2016.

[126] G. L. Tufano, O. T. Stein, A. Kronenburg, G. Gentile, A. Stagni, A. Frassoldati, T. Faravelli, A. M. Kempf, M. Vascellari, and C. Hasse. Fully-resolved simulations of coal particle combustion using a detailed multi-step approach for heterogeneous kinetics. *Fuel*, 240:75–83, 2019.

[127] G. L. Tufano, O. T. Stein, B. Wang, A. Kronenburg, M. Rieth, and A. M. Kempf. Coal particle volatile combustion and flame interaction. part ii: Effects of particle reynolds number and turbulence. *Fuel*, 234:723–731, 2018.

[128] G. Gentile, P. E. A. Debiagi, A. Cuoci, A. Frassoldati, E. Ranzi, and T. Faravelli. A computational framework for the pyrolysis of anisotropic biomass particles. *Chemical Engineering Journal*, 321:458–473, 2017.

[129] T. Maffei. Kinetic model of coal combustion. 2013.

[130] T. Maffei, G. Gentile, S. Rebughini, M. Bracconi, F. Manelli, S. Lipp, A. Cuoci, and M. Maestri. A multiregion operator-splitting cfd approach for coupling microkinetic modeling with internal porous transport in heterogeneous catalytic reactors. *Chemical Engineering Journal*, 283:1392–1404, 2016.

[131] M. Momeni, C. Yin, S. Knudsen Kær, and S. L. Hvid. Comprehensive study of ignition and combustion of single wooden particles. *Energy & Fuels*, 27(2):1061–1072, 2013.

[132] A. B. Fuertes, E. Hampartsoumian, and A. Williams. Direct measurement of ignition temperatures of pulverized coal particles. *Fuel*, 72(9):1287–1291, 1993.

[133] R. G. Kim, D. Li, and C. H. Jeon. Experimental investigation of ignition behavior for coal rank using a flat flame burner at a high heating rate. *Experimental Thermal and Fluid Science*, 54:212–218, 2014.

[134] R. Khatami, C. Stivers, and Y. A. Levendis. Ignition characteristics of single coal particles from three different ranks in o_2/n_2 and o_2/co_2 atmospheres. *Combustion and Flame*, 159(12):3554–3568, 2012.

[135] J. Köser, L. G. Becker, A. K. Goßmann, B. Böhm, and A. Dreizler. Investigation of ignition and volatile combustion of single coal particles within oxygen-enriched atmospheres using high-speed oh-plif. *Proceedings of the Combustion Institute*, 36(2):2103–2111, 2017.

[136] Y. Yuan, S. Li, G. Li, N. Wu, and Q. Yao. The transition of heterogeneous-homogeneous ignitions of dispersed coal particle streams. *Combustion and Flame*, 161(9):2458–2468, 2014.

[137] E. Marek and K. Stańczyk. Case studies investigating single coal particle ignition and combustion. *Journal of Sustainable Mining*, 12(3):17–31, 2013.

[138] M. Ottaway. Use of thermogravimetry for proximate analysis of coals and cokes. *Fuel*, 61(8):713–716, 1982.

[139] J. Faúndez, A. Arenillas, F. Rubiera, X. García, A. L. Gordon, and J. J. Pis. Ignition behaviour of different rank coals in an entrained flow reactor. *Fuel*, 84(17):2172–2177, 2005.

[140] D. Magalhães, F. Kazanç, A. Ferreira, M. Rabaçal, and M. Costa. Ignition behavior of Turkish biomass and lignite fuels at low and high heating rates. *Fuel*, 207:154–164, 2017.

[141] G. Simões, D. Magalhães, M. Rabaçal, and M. Costa. Effect of gas temperature and oxygen concentration on single particle ignition behavior of biomass fuels. *Proceedings of the Combustion Institute*, 36(2):2235–2242, 2017.

[142] Y. Fan, Z. Zou, Z. Cao, Y. Xu, and X. Jiang. Ignition characteristics of pulverized coal under high oxygen concentrations. *Energy & Fuels*, 22(2):892–897, 2008.

[143] Y. Fan, Z. Zhou, Z. Cao, X. Jiang, and Y. Xu. The influence of high oxygen concentration on ignition characteristics of pulverized bituminous coal. *Challenges of Power Engineering and Environment*, pages 174–179, 2007.

[144] A. Ponzio, S. Senthoorselvan, W. Yang, W. Blasiak, and O. Eriksson. Ignition of single coal particles in high-temperature oxidizers with various oxygen concentrations. *Fuel*, 87(6):974–987, 2008.

[145] R. Jovanovic, A. Milewska, B. Swiatkowski, A. Goanta, and H. Spliethoff. Numerical investigation of influence of homogeneous/heterogeneous ignition/combustion mechanisms on ignition point position during pulverized coal combustion in oxygen enriched and recycled flue gases atmosphere. *International Journal of Heat and Mass Transfer*, 54(4):921–931, 2011.

[146] C. Zou, L. Cai, and C. Zheng. Numerical research on the homogeneous/heterogeneous ignition process of pulverized coal in oxy-fuel combustion. *International Journal of Heat and Mass Transfer*, 73:207–216, 2014.

[147] E. Kharbat, K. Annamalai, and C. Gopalakrishnan. Ignition and combustion of isolated and binary array of coal particles. *Combustion and Flame*, 100(3):413–421, 1995.

[148] J. B. Howard and R. H. Essenhigh. Mechanism of solid-partical combustion with simultaneous gas-phase volatiles combustion. In *Symposium (International) on Combustion*, volume 11, pages 399–408. Elsevier, 1967.

[149] C. L. Sun and M. Y. Zhang. Ignition of coal particles at high pressure in a thermogravimetric analyzer. *Combustion and Flame*, 115(1):267–274, 1998.

[150] Y. Chen, S. Mori, and W. Pan. Studying the mechanisms of ignition of coal particles by tg-dta. *Thermochimica Acta*, 275(1):149–158, 1996.

[151] R. S. Conti and M. Hertzberg. Thermal autoignition temperatures from the 1.2-l furnace and their use in evaluating the explosion potential of dusts. In *Industrial Dust Explosions*. ASTM International, 1987.

[152] R. Khatami, C. Stivers, K. Joshi, Y. A. Levendis, and A. F. Sarofim. Combustion behavior of single particles from three different coal ranks and from sugar cane bagasse in O_2/N_2 and O_2/CO_2 atmospheres. *Combustion and Flame*, 159(3):1253–1271, 2012.

[153] T. Kiga, S. Takano, N. Kimura, K. Omata, M. Okawa, T. Mori, and M. Kato. Characteristics of pulverized-coal combustion in the system of oxygen/recycled flue gas combustion. *Energy Conversion and Management*, 38:S129–S134, 1997.

[154] A. Molina, E. S. Hecht, and C. R. Shaddix. Ignition of a group of coal particles in oxyfuel combustion with CO_2 recirculation. In *AIChE annual meeting, conference proceedings*, 2009.

[155] C. R. Shaddix and A. Molina. Particle imaging of ignition and devolatilization of pulverized coal during oxy-fuel combustion. *Proceedings of the Combustion Institute*, 32(2):2091–2098, 2009.

[156] B. Arias, C. Pevida, F. Rubiera, and J. J. Pis. Effect of biomass blending on coal ignition and burnout during oxy-fuel combustion. *Fuel*, 87(12):2753–2759, 2008.

[157] J. Riaza, R. Khatami, Y. A. Levendis, L. Álvarez, M. V. Gil, C. Pevida, F. Rubiera, and J. J. Pis. Single particle ignition and combustion of anthracite, semi-anthracite and bituminous coals in air and simulated oxy-fuel conditions. *Combustion and Flame*, 161(4):1096–1108, 2014.

[158] J. Riaza, R. Khatami, Y. A. Levendis, L. Álvarez, M. V. Gil, C. Pevida, F. Rubiera, and J. J. Pis. Combustion of single biomass particles in air and in oxy-fuel conditions. *Biomass and Bioenergy*, 64:162–174, 2014.

[159] R. K. Rathnam, L. K. Elliott, T. F. Wall, Y. Liu, and B. Moghtaderi. Differences in reactivity of pulverised coal in air (O_2/N_2) and oxy-fuel (O_2/CO_2) conditions. *Fuel Processing Technology*, 90(6):797–802, 2009.

[160] G. Scheffknecht, L. Al-Makhadmeh, U. Schnell, and J. Maier. Oxy-fuel coal combustion—a review of the current state-of-the-art. *International Journal of Greenhouse Gas Control*, 5:S16–S35, 2011.

[161] L. Al-Makhadmeh. *Coal pyrolysis and char combustion under oxy-fuel conditions*. Shaker Verlag, 2009.

[162] J. Brix, P. A. Jensen, and A. D. Jensen. Coal devolatilization and char conversion under suspension fired conditions in O_2/N_2 and O_2/CO_2 atmospheres. *Fuel*, 89(11):3373–3380, 2010.

[163] A. G. Borrego and D. Alvarez. Comparison of chars obtained under oxy-fuel and conventional pulverized coal combustion atmospheres. *Energy & Fuels*, 21(6):3171–3179, 2007.

[164] T. Wall, Y. Liu, C. Spero, L. Elliott, S. Khare, R. Rathnam, F. Zeenathal, B. Moghtaderi, B. Buhre, C. Sheng, et al. An overview on oxyfuel coal combustion—state of the art research and technology development. *Chemical engineering research and design*, 87(8):1003–1016, 2009.

[165] J. Dwyer Jr, J. G. Hansel, and T. Philips. Temperature influence on the flammability limits of heat treating atmospheres. In *Proceedings of the 22nd heat treating society conference and the 2nd international surface engineering congress. Indianapolis*, pages 24–28, 2003.

[166] M. Sheldon. A study of the flammability limits of gases and vapors. *Fire Prevention*, 174:23–31, 1984.

[167] G. Kim, Y. Kim, and Y. Joo. Conditional moment closure for modeling combustion processes and structure of oxy-natural gas flame. *Energy & Fuels*, 23(9):4370–4377, 2009.

[168] R. J. Kee, F. M. Rupley, E. Meeks, and J. A. Miller. Chemkin-iii: A fortran chemical kinetics package for the analysis of gas-phase chemical and plasma kinetics. Technical report, Sandia National Labs., Livermore, CA (United States), 1996.

[169] A. E. Lutz, R. J. Kee, and J. A. Miller. Senkin: A fortran program for predicting homogeneous gas phase chemical kinetics with sensitivity analysis. Technical report, Sandia National Labs., Livermore, CA (USA), 1988.

[170] K. J. Hughes, T. Turanyi, A. R. Clague, and M. J. Pilling. Development and testing of a comprehensive chemical mechanism for the oxidation of methane. *International Journal of Chemical Kinetics*, 33(9):513–538, 2001.

[171] C. Zou, L. Cai, D. Wu, Y. Liu, S. Liu, and C. Zheng. Ignition behaviors of pulverized coal particles in O_2/N_2 and O_2/H_2O mixtures in a drop tube furnace using flame monitoring techniques. *Proceedings of the Combustion Institute*, 35(3):3629–3636, 2015.

[172] H. M. Cassel and I. Liebman. The cooperative mechanism in the ignition of dust dispersions. *Combustion and Flame*, 3:467–475, 1959.

[173] X. Du, C. Gopalakrishnan, and K. Annamalai. Ignition and combustion of coal particle streams. *Fuel*, 74(4):487–494, 1995.

[174] S. Wang, H. Lu, Y. Zhao, R. Mostofi, H. Y. Kim, and L. Yin. Numerical study of coal particle cluster combustion under quiescent conditions. *Chemical Engineering Science*, 62(16):4336–4347, 2007.

[175] Y. Yuan, S. Li, F. Zhao, Q. Yao, and M. B. Long. Characterization on hetero-homogeneous ignition of pulverized coal particle streams using ch chemiluminescence and 3 color pyrometry. *Fuel*, 184:1000–1006, 2016.

[176] Y. Yuan, S. Li, Y. Xu, and Q. Yao. Experimental and theoretical analyses on ignition and surface temperature of dispersed coal particles in o_2/n_2 and o_2/co_2 ambients. *Fuel*, 201:93–98, 2017.

[177] K. Xu, Y. Wu, Z. Wang, Y. Yang, and H. Zhang. Experimental study on ignition behavior of pulverized coal particle clouds in a turbulent jet. *Fuel*, 167:218–225, 2016.

[178] F. Zhao, S. Li, Y. Ren, Q. Yao, and Y. Yuan. Investigation of mechanisms in plasma-assisted ignition of dispersed coal particle streams. *Fuel*, 186:518–524, 2016.

[179] K. L. Cashdollar. Overview of dust explosibility characteristics. *Journal of Loss Prevention in the Process Industries*, 13(3):183–199, 2000.

[180] C. K. Man and J. R. Gibbins. Factors affecting coal particle ignition under oxyfuel combustion atmospheres. *Fuel*, 90(1):294–304, 2011.

[181] M. Taniguchi, T. Shibata, K. Yamamoto, C. Kuhr, and O. Ito. Lean flammability limit for oxy-fuel fired pulverized coal combustion systems. *Energy Procedia*, 4:892–899, 2011.

[182] K. Yamamoto, T. Murota, T. Okazaki, and M. Taniguchi. Large eddy simulation of a pulverized coal jet flame ignited by a preheated gas flow. *Proceedings of the Combustion Institute*, 33(2):1771–1778, 2011.

[183] K. Yamamoto, D. Kina, T. Okazaki, M. Taniguchi, H. Okazaki, and K. Ochi. Les of pulverized coal combustion furnaces. In *Proceedings of the ASME 2011 Power Conference*, 2011.

[184] M. Muto, K. Yuasa, and R. Kurose. Numerical simulation of ignition in pulverized coal combustion with detailed chemical reaction mechanism. *Fuel*, 190:136–144, 2017.

[185] M. Rieth, A. M. Kempf, A. Kronenburg, and O. T. Stein. Carrier-phase dns of pulverized coal particle ignition and volatile burning in a turbulent mixing layer. *Fuel*, 212:364–374, 2018.

[186] J. B. Michel and R. Payne. *Detailed measurement of long pulverized coal flames for the characterization of pollutant formation*. International Flame Research Foundation, 1980.

[187] J. Zhang. *Oxy-coal Compustion: Stability of Coaxial Pulverized Coal Flames in O_2/CO_2 Environments*. PhD thesis, Department of Chemical Engineering, University of Utah, 2010.

[188] J. Zhang, K. E. Kelly, E. G. Eddings, and J. O. L. Wendt. Ignition in 40 kw co-axial turbulent diffusion oxy-coal jet flames. *Proceedings of the Combustion Institute*, 33(2):3375–3382, 2011.

[189] J. Zhang, K. E. Kelly, E. G Eddings, and J. O. L. Wendt. CO_2 effects on near field aerodynamic phenomena in 40 kW, co-axial, oxy-coal, turbulent diffusion flames. *International Journal of Greenhouse Gas Control*, 5:S47–S57, 2011.

[190] D. M. Woycenko, W. L. Van De Kamp, and P. A. Roberts. Combustion of pulverized coal in a mixture of oxygen and recycled flue gas. *IFRF Document No. F*, 98, 1995.

[191] C. Ndibe, S. Grathwohl, M. Paneru, J. Maier, and G. Scheffknecht. Emissions reduction and deposits characteristics during cofiring of high shares of torrefied biomass in a 500 kw pulverized coal furnace. *Fuel*, 156:177–189, 2015.

[192] R. Spörl, J. Maier, and G. Scheffknecht. Sulphur oxide emissions from dust-fired oxy-fuel combustion of coal. *Energy Procedia*, 37:1435–1447, 2013.

[193] R. Spörl, M. Paneru, S. Babat, G. Stein-Brzozowska, J. Maier, and G. Scheffknecht. The influence of air and oxy-fuel combustion on fly ash and deposits. *Fuel Processing Technology*, 141:258–265, 2016.

[194] J. Szuhánszki, O. F. Moguel, K. Finney, M. Akram, and M. Pourkashanian. Biomass combustion under oxy-fuel and post combustion capture conditions at the pact 250 kw air/oxy-fuel ctf. *UKCCSRC, presentation*, 2017.

[195] X. Yang, A. Clements, J. Szuhánszki, X. Huang, O. F. Moguel, J. Li, J. Gibbins, Z. Liu, C. Zheng, D. Ingham, et al. Prediction of the radiative heat transfer in small and large scale oxy-coal furnaces. *Applied Energy*, 211:523–537, 2018.

[196] J. Guo, F. Hu, X. Jiang, P. Li, and Z. Liu. Effects of gas and particle radiation on ifrf 2.5 mw swirling flame under oxy-fuel combustion. *Fuel*, 263:116634, 2020.

[197] T. Asotani, T. Yamashita, H. Tominaga, Y. Uesugi, Y. Itaya, and S. Mori. Prediction of ignition behavior in a tangentially fired pulverized coal boiler using cfd. *Fuel*, 87(4):482–490, 2008.

[198] T. Asotani, T. Yamashita, H. Tominaga, Y. Uesugi, Y. Itaya, and S. Mori. Effect of radiative heat transfer properties on combustion simulation for pulverized coal experimental furnace. In *International Heat Transfer Conference 13*. Begel House Inc., 2006.

[199] A. H. Al-Abbas, J. Naser, and D. Dodds. Cfd modelling of air-fired and oxy-fuel combustion of lignite in a 100kw furnace. *Fuel*, 90(5):1778–1795, 2011.

[200] S. P. Khare, T. F. Wall, A. Z. Farida, Y. Liu, B. Moghtaderi, and R. P. Gupta. Factors influencing the ignition of flames from air-fired swirl pf burners retrofitted to oxy-fuel. *Fuel*, 87(7):1042–1049, 2008.

[201] T. Seidel, G. Krishnamoorthy, and W. S. Seames. Characterizing flame stability and radiative heat transfer in non-swirling oxy-coal flames using different multiphase modeling frameworks. *Fuel*, 256:115948, 2019.

[202] J. D. Anderson Jr. Computational fluid dynamics- The basics with applications. 27(6):1661–71, 1995.

[203] W. E. Ranz and W. R. Marshall. Evaporation from drops, parts i & ii. *Chem Eng Prog.*, 48:141–146, 1952.

[204] F. C. Lockwood and N. G. Shah. A new radiation solution method for incorporation in general combustion prediction procedures. In *Symposium (international) on combustion*, volume 18, pages 1405–1414. Elsevier, 1981.

[205] J. Y. Murthy and S. R. Mathur. Finite volume method for radiative heat transfer using unstructured meshes. *Journal of thermophysics and heat transfer*, 12(3):313–321, 1998.

[206] P. Edge, M. Gharebaghi, R. Irons, R. Porter, R. T. J. Porter, M. Pourkashanian, D. Smith, P. Stephenson, and A. Williams. Combustion modelling opportunities and challenges for oxy-coal carbon capture technology. *Chemical Engineering Research and Design*, 89(9):1470–1493, 2011.

[207] W. L. Grosshandler. Radiative heat transfer in nonhomogeneous gases: a simplified approach. *International Journal of Heat and Mass Transfer*, 23(11):1447–1459, 1980.

[208] M. F. Modest. *Radiative heat transfer*. Academic press, 2013.

[209] C. Yin, L. A. Rosendahl, and S. K. Kær. Chemistry and radiation in oxy-fuel combustion: a computational fluid dynamics modeling study. *Fuel*, 90(7):2519–2529, 2011.

[210] P. J. Edge, P. J. Heggs, M. Pourkashanian, and P. L. Stephenson. Integrated fluid dynamics-process modelling of a coal-fired power plant with carbon capture. *Applied thermal engineering*, 60(1-2):242–250, 2013.

[211] C. Galletti, G. Coraggio, and L. Tognotti. Numerical investigation of oxy-natural-gas combustion in a semi-industrial furnace: validation of cfd submodels. *Fuel*, 109:445–460, 2013.

[212] R. Johansson, B. Leckner, K. Andersson, and F. Johnsson. Account for variations in the H_2O to CO_2 molar ratio when modelling gaseous radiative heat transfer with the weighted-sum-of-grey-gases model. *Combustion and Flame*, 158(5):893–901, 2011.

[213] V. Kez, F. Liu, J. L. Consalvi, J. Ströhle, and B. Epple. A comprehensive evaluation of different radiation models in a gas turbine combustor under conditions of oxy-fuel combustion with dry recycle. *Journal of Quantitative Spectroscopy and Radiative Transfer*, 172:121–133, 2016.

[214] D. J. Acheson. *Elementary Fluid Dynamics*. Oxford University Press, 1990.

[215] A. N. Kolmogorov. The local structure of turbulence in incompressible viscous fluid for very large reynolds numbers. In *Dokl. Akad. Nauk SSSR*, volume 30, pages 299–303, 1941.

[216] B. E. Launder and D. B. Spalding. The numerical computation of turbulent flows. *Computer Methods in Applied Mechanics and Engineering*, 3(2):269–289, 1974.

[217] V. Yakhot and S. A. Orszag. Renormalization group analysis of turbulence. i. basic theory. *Journal of Scientific Computing*, 1(1):3–51, 1986.

[218] V. Yakhot and L. M. Smith. The renormalization group, the ε-expansion and derivation of turbulence models. *Journal of Scientific Computing*, 7(1):35–61, 1992.

[219] T. H. Shih, W. W. Liou, A. Shabbir, Z. Yang, and J. Zhu. A new k-ε eddy viscosity model for high reynolds number turbulent flows. *Computers & Fluids*, 24(3):227–238, 1995.

[220] D. C. Wilcox et al. *Turbulence modeling for CFD*, volume 2. DCW industries La Canada, CA, 1993.

[221] F. R. Menter. Improved two-equation k-omega turbulence models for aerodynamic flows. 1992.

[222] B. E. Launder. Second-moment closure: present... and future? *International Journal of Heat and Fluid Flow*, 10(4):282–300, 1989.

[223] B. E. Launder, G. Reece, and W. Rodi. Progress in the development of a reynolds-stress turbulence closure. *Journal of Fluid Mechanics*, 68(3):537–566, 1975.

[224] M. M. Gibson and B. E. Launder. Ground effects on pressure fluctuations in the atmospheric boundary layer. *Journal of Fluid Mechanics*, 86(3):491–511, 1978.

[225] I. R. Gran and B. F. Magnussen. A numerical study of a bluff-body stabilized diffusion flame. part 2. influence of combustion modeling and finite-rate chemistry. *Combustion Science and Technology*, 119(1-6):191–217, 1996.

[226] F. Breussin, F. Pigari, and R. Weber. Predicting the near-burner-one flow field and chemistry of swirl-stabilied low-Nox flames of pulveried coal using the RNG-k-ε, RSM and k-ε turbulence models. In *Symposium (International) on Combustion*, volume 26, pages 211–217. Elsevier, 1996.

[227] A. E. German and T. Mahmud. Modelling of non-premixed swirl burner flows using a reynolds-stress turbulence closure. *Fuel*, 84(5):583–594, 2005.

[228] N. Stockwell, C. Zhang, T. Ishii, and Y. Hino. Numerical simulations of turbulent non-premixed combustion in a regenerative furnace. *ISIJ international*, 41(10):1272–1281, 2001.

[229] J. M. Tsao and C. A. Lin. Reynolds stress modelling of jet and swirl interaction inside a gas turbine combustor. *International journal for numerical methods in fluids*, 29(4):451–464, 1999.

[230] K. L. Smith, L. D. Smoot, T. H. Fletcher, and R. J. Pugmire. *The Structure and Reaction Processes of Coal*. Springer Science & Business Media, 2013.

[231] M. R. Khan and R. G. Jenkins. Swelling and plastic properties of coal devolatilized at elevated pressures: an examination of the influences of coal type. *Fuel*, 65(5):725–731, 1986.

[232] L. Chen, S. Z. Yong, and A. F. Ghoniem. Oxy-fuel combustion of pulverized coal: characterization, fundamentals, stabilization and cfd modeling. *Progress in Energy and Combustion Science*, 38(2):156–214, 2012.

[233] M. M. Baum and P. J. Street. Predicting the combustion behaviour of coal particles. *Combustion Science and Technology*, 3(5):231–243, 1971.

[234] D. B. Anthony, J. B. Howard, H. C. Hottel, and H. P. Meissner. Rapid devolatilization of pulverized coal. In *Symposium (international) on Combustion*, volume 15, pages 1303–1317. Elsevier, 1975.

[235] D. B. Anthony, J. B. Howard, H. C. Hottel, and H. P. Meissner. Rapid devolatilization and hydrogasification of bituminous coal. *Fuel*, 55(2):121–128, 1976.

[236] H. Kobayashi, J. B. Howard, and A. F. Sarofim. Coal devolatilization at high temperatures. In *Symposium (international) on Combustion*, volume 16, pages 411–425. Elsevier, 1977.

[237] G. M. Kimber and M. D. Gray. Rapid devolatilization of small coal particles. *Combustion and Flame*, 11(4):360–362, 1967.

[238] S. Badzioch and P. G. Hawksley. Kinetics of thermal decomposition of pulverized coal particles. *Industrial & Engineering Chemistry Process Design and Development*, 9(4):521–530, 1970.

[239] M. Vascellari and G. Cau. Influence of turbulence–chemical interaction on cfd pulverized coal mild combustion modeling. *Fuel*, 101:90–101, 2012.

[240] M. Vascellari, R. Arora, M. Pollack, and C. Hasse. Simulation of entrained flow gasification with advanced coal conversion submodels. part 1: Pyrolysis. *Fuel*, 113:654–669, 2013.

[241] A. Arenillas, F. Rubiera, C. Pevida, and J. J. Pis. A comparison of different methods for predicting coal devolatilisation kinetics. *Journal of Analytical and Applied Pyrolysis*, 58:685–701, 2001.

[242] S. Niksa, L. E. Heyd, W. B. Russel, and D. A. Saville. On the role of heating rate in rapid coal devolatilization. In *Symposium (international) on Combustion*, volume 20, pages 1445–1453. Elsevier, 1985.

[243] S. K. Ubhayakar, D. B. Stickler, C. W. Von Rosenberg, and R. E. Gannon. Rapid devolatilization of pulverized coal in hot combustion gases. In *Symposium (International) on Combustion*, volume 16, pages 427–436. Elsevier, 1977.

[244] T. H. Fletcher and D. R. Hardesty. Compilation of sandia coal devolatilization data: Milestone report. milestone report. Technical report, Sandia National Labs., Livermore, CA (United States), 1992.

[245] D. M. Grant, R. J. Pugmire, T. H. Fletcher, and A. R. Kerstein. Chemical model of coal devolatilization using percolation lattice statistics. *Energy & Fuels*, 3(2):175–186, 1989.

[246] D. B. Genetti. *An advanced model of coal devolatilization based on chemical structure*. PhD thesis, Brigham Young University. Department of Chemical Engineering, 1999.

[247] M. Rieth, A. G. Clements, M. Rabaçal, F. Proch, O. T. Stein, and A. M. Kempf. Flamelet les modeling of coal combustion with detailed devolatilization by directly coupled cpd. *Proceedings of the Combustion Institute*, 36(2):2181–2189, 2017.

[248] M. Saha, A. Chinnici, B. B. Dally, and P. R. Medwell. Numerical study of pulverized coal mild combustion in a self-recuperative furnace. *Energy & Fuels*, 29(11):7650–7669, 2015.

[249] K. Wan, Z. Wang, Y. He, J. Xia, Z. Zhou, J. Zhou, and K. Cen. Experimental and modeling study of pyrolysis of coal, biomass and blended coal–biomass particles. *Fuel*, 139:356–364, 2015.

[250] B. Yan, Y. Cheng, P. Xu, C. Cao, and Y. Cheng. Generalized model of heat transfer and volatiles evolution inside particles for coal devolatilization. *AIChE Journal*, 60(8):2893–2906, 2014.

[251] T. H. Fletcher, A. R. Kerstein, R. J. Pugmire, M. S. Solum, and D. M. Grant. Chemical percolation model for devolatilization. 3. direct use of carbon-13 nmr data to predict effects of coal type. *Energy & Fuels*, 6(4):414–431, 1992.

[252] R. G. Kim, B. H. Lee, C. H. Jeon, J. H. Song, Y. J. Chang, and T. H. Fletcher. An experimental and numerical study on the characteristics of devolatilization process for coals utilized in korea using cpd model. *Transactions of the Korean Society of Mechanical Engineers B*, 33(8):613–621, 2009.

[253] Y. Tian, K. Xie, S. Zhu, and T. H. Fletcher. Simulation of coal pyrolysis in plasma jet by CPD model. *Energy & Fuels*, 15(6):1354–1358, 2001.

[254] R. S. Jupudi, V. Zamansky, and T. H. Fletcher. Prediction of light gas composition in coal devolatilization. *Energy & Fuels*, 23(6):3063–3067, 2009.

[255] R. C. Shurtz, K. K. Kolste, and T. H. Fletcher. Coal swelling model for high heating rate pyrolysis applications. *Energy & Fuels*, 25(5):2163–2173, 2011.

[256] D. Genetti, T. H. Fletcher, and R. J. Pugmire. Development and application of a correlation of 13c nmr chemical structural analyses of coal based on elemental composition and volatile matter content. *Energy & Fuels*, 13(1):60–68, 1999.

[257] A. D. Carr and J. E. Williamson. The relationship between aromaticity, vitrinite reflectance and maceral composition of coals: implications for the use of vitrinite reflectance as a maturation parameter. *Organic Geochemistry*, 16(1):313–323, 1990.

[258] A. P. Richards and T. H. Fletcher. A comparison of simple global kinetic models for coal devolatilization with the cpd model. *Fuel*, 185:171–180, 2016.

[259] Inc Advanced Fuel Research. Functional-group, depolymerization, vaporization, cross-linking model.

[260] P. R. Solomon, D. G. Hamblen, R. M. Carangelo, M. A. Serio, and G. V. Deshpande. General model of coal devolatilization. *Energy & Fuels*, 2(4):405–422, 1988.

[261] P. R. Solomon, M. A. Serio, R. M. Carangelo, R. Bassilakis, Z. Z. Yu, S. Charpenay, and J. Whelan. Analysis of coal by thermogravimetry—fourier transform infrared spectroscopy and pyrolysis modeling. *Journal of Analytical and Applied Pyrolysis*, 19:1–14, 1991.

[262] Y. Zhao, M. A. Serio, R. Bassilakis, and P. R. Solomon. A method of predicting coal devolatilization behavior based on the elemental composition. In *Symposium (international) on combustion*, volume 25, pages 553–560. Elsevier, 1994.

[263] S. Niksa and A. R. Kerstein. Flashchain theory for rapid coal devolatilization kinetics. 1. formulation. *Energy & Fuels*, 5(5):647–665, 1991.

[264] S. Niksa. Flashchain theory for rapid coal devolatilization kinetics. 2. impact of operating conditions. *Energy & Fuels*, 5(5):665–673, 1991.

[265] S. Niksa. Flashchain theory for rapid coal devolatilization kinetics. 3. modeling the behavior of various coals. *Energy & Fuels*, 5(5):673–683, 1991.

[266] S. Niksa. Flashchain theory for rapid coal devolatilization kinetics. 4. predicting ultimate yields from ultimate analyses alone. *Energy & Fuels*, 8(3):659–670, 1994.

[267] S. Niksa. Flashchain theory for rapid coal devolatilization kinetics. 5. interpreting rates of devolatilization for various coal types and operating conditions. *Energy & Fuels*, 8(3):671–679, 1994.

[268] S. Niksa. Flashchain theory for rapid coal devolatilization kinetics. 6. predicting the evolution of fuel nitrogen from various coals. *Energy & Fuels*, 9(3):467–478, 1995.

[269] S. Niksa. Flashchain theory for rapid coal devolatilization kinetics. 7. predicting the release of oxygen species from various coals. *Energy & Fuels*, 10(1):173–187, 1996.

[270] S. Niksa. Flashchain theory for rapid coal devolatilization kinetics. 8. modeling the release of sulfur species from various coals. *Energy & Fuels*, 31(5):4925–4938, 2017.

[271] S. Niksa. Predicting the devolatilization behavior of any coal from its ultimate analysis. *Combustion and Flame*, 100(3):384–394, 1995.

[272] E. Biagini and L. Tognotti. A generalized correlation for coal devolatilization kinetics at high temperature. *Fuel Processing Technology*, 126:513–520, 2014.

[273] A. Grucelski and J. Pozorski. Application of lattice boltzmann method to meso-scale modelling of coal devolatilisation. *Chemical Engineering Science*, 172:503–512, 2017.

[274] B. H. Yan, C. X. Cao, Y. Cheng, Y. Jin, and Y. Cheng. Experimental investigation on coal devolatilization at high temperatures with different heating rates. *Fuel*, 117:1215–1222, 2014.

[275] G. P. Smith, D. M. Golden, M. Frenklach, N. W. Moriarty, B. Eiteener, M. Goldenberg, C. T. Bowman, R. K. Hanson, S. Song, W. C. Gardiner, V. V. Lissiankski, and Z. Qin. http://combustion.berkeley.edu/gri-mech/.

[276] G. P. Smith, Y. Tao, and H. Wang. Foundational fuel chemistry model version 1.0 (ffcm-1). *epub, accessed July*, 26:2018, 2016.

[277] C. W. Zhou, Y. Li, U. Burke, C. Banyon, K. P. Somers, S. Ding, S. Khan, J. W. Hargis, T. Sikes, O. Mathieu, et al. An experimental and chemical kinetic modeling study of 1, 3-butadiene combustion: Ignition delay time and laminar flame speed measurements. *Combustion and Flame*, 197:423–438, 2018.

[278] A. M. Eaton, L. D. Smoot, S. C. Hill, and C. N. Eatough. Components, formulations, solutions, evaluation, and application of comprehensive combustion models. *Progress in Energy and Combustion Science*, 25(4):387–436, 1999.

[279] L. D. Smoot and P. J. Smith. *Coal Combustion and Gasification*. Springer Science & Business Media, 2013.

[280] B. F. Magnussen and B. H. Hjertager. On mathematical modeling of turbulent combustion with special emphasis on soot formation and combustion. In *Symposium (international) on Combustion*, volume 16, pages 719–729. Elsevier, 1977.

[281] D. B. Spalding. Mixing and chemical reaction in steady confined turbulent flames. In *Symposium (International) on Combustion*, volume 13, pages 649–657. Elsevier, 1971.

[282] B. F. Magnussen and B. W. Hjertager. On the structure of turbulence and a generalized eddy dissipation concept for chemical reaction in turbulent flow. In *19th AIAA aerospace Meeting, St. Louis, USA*, volume 198, 1981.

[283] C. K. Westbrook and F. L. Dryer. Simplified reaction mechanisms for the oxidation of hydrocarbon fuels in flames. *Combustion Science and Technology*, 27(1-2):31–43, 1981.

[284] F. L. Dryer and I. Glassman. High-temperature oxidation of co and ch4. In *Symposium (International) on combustion*, volume 14, pages 987–1003. Elsevier, 1973.

[285] A. A. F. Peters and R. Weber. Mathematical modeling of a 2.4 mw swirling pulverized coal flame. *Combustion Science and Technology*, 122(1-6):131–182, 1997.

[286] D. J. Hautman, F. L. Dryer, K. P. Schug, and I. Glassman. A multiple-step overall kinetic mechanism for the oxidation of hydrocarbons. pages 219–235, 1981.

[287] F. U. Ruckert, T. Sabel, U. Schnell, K. R. G. Hein, and B. Risio. Comparison of different global reaction mechanisms for coal-fired utility boilers. *Progress in Computational Fluid Dynamics, an International Journal*, 3(2-4):130–139, 2003.

[288] W. P. Jones and R. P. Lindstedt. Global reaction schemes for hydrocarbon combustion. *Combustion and Flame*, 73(3):233–249, 1988.

[289] P. L. Walker, F. Rusinko, and L. G. Austin. Gas reactions of carbon. *Advances in Catalysis*, 11:133–221, 1959.

[290] T. L. Bergman and F. P. Incropera. *Fundamentals of heat and mass transfer*. John Wiley & Sons, 2011.

[291] R. E. Mitchell, R. J. Kee, P. Glarborg, and M. E. Coltrin. The effect of co conversion in the boundary layers surrounding pulverized-coal char particles. In *Symposium (International) on Combustion*, volume 23, pages 1169–1176. Elsevier, 1991.

[292] K. Zygourakis and C. W. Sandmann. Discrete structural models and their application to gas-solid reacting systems. *AIChE journal*, 34(12):2030–2040, 1988.

[293] O. Levenspiel. Chemical reaction engineering. *Industrial & Engineering Chemistry Research*, 38(11):4140–4143, 1999.

[294] M. A. Field. Rate of combustion of size-graded fractions of char from a low-rank coal between 1 200 k and 2 000 k. *Combustion and Flame*, 13(3):237–252, 1969.

[295] T. F. Smith, Z. F. Shen, and J. N. Friedman. Evaluation of coefficients for the weighted sum of gray gases model. *Journal of Heat Transfer*, 104(4):602–608, 1982.

[296] E. W. Thiele. Relation between catalytic activity and size of particle. *Industrial & Engineering Chemistry*, 31(7):916–920, 1939.

[297] Y. Liu, M. Geier, A. Molina, and C. R. Shaddix. Pulverized coal stream ignition delay under conventional and oxy-fuel combustion conditions. *International Journal of Greenhouse Gas Control*, 5:S36–S46, 2011.

[298] A. Molina and C. R. Shaddix. Ignition and devolatilization of pulverized bituminous coal particles during oxygen/carbon dioxide coal combustion. *Proceedings of the Combustion Institute*, 31(2):1905–1912, 2007.

[299] E. S. Hecht, J. S. Lighty, and C. R. Shaddix. Kinetic rates of oxidation and gasification reactions of coal chars reacting in oxy-combustion environments. In *8th US National Combustion Meeting, Park City, UT*, 2013.

[300] M. Weidmann, D. Honoré, V. Verbaere, G. Boutin, S. Grathwohl, G. Godard, C. Gobin, R. Kneer, and G. Scheffknecht. Experimental characterization of pulverized coal mild flameless combustion from detailed measurements in a pilot-scale facility. *Combustion and Flame*, 168:365–377, 2016.

[301] J. S. Truelove and D. Holcombe. Measurement and modelling of coal flame stability in a pilot-scale combustor. In *Symposium (International) on Combustion*, volume 23, pages 963–971. Elsevier, 1991.

[302] A. G. Clements, S. Black, J. Szuhanszki, A. Pranzitelli, W. Nimmo, and M. Pourkashanian. Les and rans of air and oxy-coal combustion in a pilot-scale facility: predictions of radiative heat transfer. *Fuel*, 151:146–155, 2015.

[303] A. Sadiki, S. Agrebi, M. Chrigui, A. S. Doost, R. Knappstein, F. Di Mare, J. Janicka, A. Massmeyer, D. Zabrodiec, J. Hees, et al. Analyzing the effects of turbulence and multiphase treatments on oxy-coal combustion process predictions using les and rans. *Chemical Engineering Science*, 166:283–302, 2017.

[304] S. Yadav and S. S. Mondal. Numerical modelling of oxy-coal combustion to access the influence of swirl strength, combustion environment and gasification reactions on the flow and combustion behaviour. *Combustion Theory and Modelling*, 25(3):488–513, 2021.

[305] C. K. Man, J. R. Gibbins, J. G. Witkamp, and J. Zhang. Coal characterisation for nox prediction in air-staged combustion of pulverised coals. *Fuel*, 84(17):2190–2195, 2005.

[306] N. Berkowitz. *An introduction to coal technology*. Elsevier, 2012.

[307] H. Fatehi and X. S. Bai. A comprehensive mathematical model for biomass combustion. *Combustion Science and Technology*, 186(4-5):574–593, 2014.

[308] K. M. Bryden and M. J. Hagge. Modeling the combined impact of moisture and char shrinkage on the pyrolysis of a biomass particle. *Fuel*, 82(13):1633–1644, 2003.

[309] Y. Xu, S. Zhai, M.and Jin, X. Zou, S. Liu, and P. Dong. Numerical simulation of high-temperature fusion combustion characteristics for a single biomass particle. *Fuel Processing Technology*, 183:27–34, 2019.

[310] H. Lu, W. Robert, G. Peirce, B. Ripa, and L. L. Baxter. Comprehensive study of biomass particle combustion. *Energy & Fuels*, 22(4):2826–2839, 2008.

[311] Y. B. Yang, V. N. Sharifi, J. Swithenbank, L. Ma, L. I. Darvell, J. M. Jones, M. Pourkashanian, and A. Williams. Combustion of a single particle of biomass. *Energy & Fuels*, 22(1):306–316, 2007.

[312] Y. A. Levendis, K. Joshi, R. Khatami, and A. F. Sarofim. Combustion behavior in air of single particles from three different coal ranks and from sugarcane bagasse. *Combustion and Flame*, 158(3):452–465, 2011.

[313] R. Khatami and Y. A. Levendis. An overview of coal rank influence on ignition and combustion phenomena at the particle level. *Combustion and Flame*, 164:22–34, 2016.

[314] R. Khatami. Ignition and combustion of pulverized coal and biomass under different oxy-fuel O_2/N_2 and O_2/CO_2 environments. 2014.

[315] A. M. Beckmann, J. Bibrzycki, M. Mancini, A. Szl, and R. Weber. Mathematical modeling of reactants' transport and chemistry during oxidation of a millimeter-sized coal-char particle in a hot air stream. *Combustion and Flame*, 180:2–9, 2017.

[316] L. Li, A. Tahmasebi, J. Dou, S. Khoshk Rish, L. Tian, and J. Yu. Mechanistic Investigations of Particle Ignition of Pulverized Coals: An Enhanced Numerical Model and Experimental Observations. *Energy & Fuels*, 34(12):16666–16678, 2020.

[317] Y. B. Yang, V. N. Sharifi, J. Swithenbank, L. Ma, L. I. Darvell, J. M. Jones, M. Pourkashanian, and A. Williams. Combustion of a single particle of biomass. *Energy & Fuels*, 22(1):306–316, 2008.

[318] ANSYS Fluent. 19.0 ansys fluent udf manual. *ANSYS, Inc. Canonsburg, PA, USA*, 2019.

[319] M. L. Hobbs, P. T. Radulovic, and L. D. Smoot. Modeling fixed-bed coal gasifiers. *AIChE Journal*, 38(5):681–702, 1992.

[320] C. N. Satterfield. *Mass transfer in heterogeneous catalysis*. MIT press, 1969.

[321] R. B. Bird, W. E. Stewart, and E. N. Lightfoot. *Transport phenomena*, volume 1. John Wiley & Sons, 2006.

[322] H. A. McGee. *Molecular engineering*. McGraw-Hill, 1991.

[323] J. G. Speight. *Environmental analysis and technology for the refining industry*, volume 167. John Wiley & Sons, 2005.

[324] B. A. Adesanya and H. N. Pham. Mathematical modelling of devolatilization of large coal particles in a convective environment. *Fuel*, 74(6):896–902, 1995.

[325] I. Petersen and J. Werther. Experimental investigation and modeling of gasification of sewage sludge in the circulating fluidized bed. *Chemical Engineering and Processing: Process Intensification*, 44(7):717–736, 2005.

[326] P. H. Given, D. Weldon, and J. H. Zoeller. Calculation of calorific values of coals from ultimate analyses: theoretical basis and geochemical implications. *Fuel*, 65(6):849–854, 1986.

[327] T. Li, C. Geschwindner, J. Köser, M. Schiemann, A. Dreizler, and B. Böhm. Investigation of the transition from single to group coal particle combustion using high-speed scanning oh-lif and diffuse backlight-illumination. *Proceedings of the Combustion Institute*, 2020.

[328] W. Zhu, X. Li, J. Peng, Z. Wang, R. Sun, L. Zhang, X. Yu, and Y. Yu. Study on the combustion behaviours of two high-volatile coal particle streams with high-speed oh-plif. *Fuel*, 265:116956, 2020.

[329] B. Goshayeshi and J. C. Sutherland. A comparative study of thermochemistry models for oxy-coal combustion simulation. *Combustion and Flame*, 162(10):4016–4024, 2015.

[330] H. Fatehi, W. Weng, M. Costa, Z. Li, M. Rabaçal, M. Aldén, and X. Bai. Numerical simulation of ignition mode and ignition delay time of pulverized biomass particles. *Combustion and Flame*, 206:400–410, 2019.

[331] W. Yang, B. Liu, H. Zhang, Y. Zhang, W. Yuxin, and J. Lyu. Prediction improvements of ignition characteristics of isolated coal particles with a one-dimensional transient model. *Proceedings of the Combustion Institute*, 2020.

[332] V. S. Gururajan, T. F. Wall, R. P. Gupta, and J. S. Truelove. Mechanisms for the ignition of pulverized coal particles. *Combustion and flame*, 81(2):119–132, 1990.

[333] Y. Qi, M. Wang, R. Ma, P. Ge, J. Wu, M. Gu, and S. Ji. Numerical simulation investigation of ignition and combustion process for single pulverized particle of anthracite. *Fuel*, 239:330–337, 2019.

[334] P. A. Bejarano and Y. A. Levendis. Single-coal-particle combustion inO_2/N_2 and O_2/CO_2 environments. *Combustion and flame*, 153(1-2):270–287, 2008.

[335] A. Brink et al. Eddy break-up based models for industrial diffusion flames with complex gas phase chemistry. 1998.

[336] M. Saito, M. Sadakata, M. Sato, T. Soutome, H. Murata, and Y. I. Ohno. Combustion rates of pulverized coal particles in high-temperature/high-oxygen concentration atmosphere. *Combustion and flame*, 87(1):1–12, 1991.

[337] X. Shang, C. Si, J. Wu, Z. Miao, Y. Zhang, Y. Wang, B. Wang, and K. Hou. Comparison of drying methods on physical and chemical properties of shengli lignite. *Drying Technology*, 34(4):454–461, 2016.

[338] D. Magalhães, A. Panahi, F. Kazanç, and Y. A. Levendis. Comparison of single particle combustion behaviours of raw and torrefied biomass with turkish lignites. *Fuel*, 241:1085–1094, 2019.

[339] A. Minotti. O_2/CH_4 kinetic mechanisms for aerospace applications at low pressure and temperature, validity ranges and comparison. *Aeronautics and Astronautics*, page 369, 2011.

[340] S. Farazi, J. Hinrichs, M. Davidovic, T. Falkenstein, M. Bode, S. Kang, A. Attili, and H. Pitsch. Numerical investigation of coal particle stream ignition in oxy-atmosphere. *Fuel*, 241:477–487, 2019.

[341] C. P. Zemtsop, M. K. Stöllinger, S. Heinz, and D. Stanescu. Large-eddy simulation of swirling turbulent jet flows in absence of vortex breakdown. *AIAA journal*, 47(12):3011–3021, 2009.

[342] K. J. Knill, T. Nakamura, and M. E. Morgan. The effect of mixing on no x reduction by coal fuel staging. *Report on the AP19 investigation. IFRF Doc. No. F*, 37, 1990.

[343] R. Weber, J. Dugue, and A. Sayre. *Measurements and Computations of Quarl Zone Flow Field and Chemistry ina a Swirling Pulverized Coal Flame*. IFRF, 1992.

[344] R. Weber, J. P. Smart, and W. vd Kamp. On the (mild) combustion of gaseous, liquid, and solid fuels in high temperature preheated air. *Proceedings of the Combustion Institute*, 30(2):2623–2629, 2005.

[345] R. Weber, J. Dugue, A. Sayre, and B. M. Visser. Quarl zone flow field and chemistry of swirling pulverized coal flames: Measurements and computation. In *Symposium (International) on Combustion*, volume 24, pages 1373–1380. Elsevier, 1992.

[346] S. Orsino, M. Tamura, P. Stabat, S. Constantini, O. Prado, and R. Weber. Excess enthalpy combustion of coal (results of high temperature air combustion trials). Technical report, Tech. Rep. IFRF Doc, 2000.

[347] J. Smart, G. Nathan, N. Smith, G. Newbold, D. Nobes, and D. Morgan. On the development of a coal fired precessing jet burner. 1999.

[348] F. C. Lockwood and A. P. Salooja. The prediction of some pulverized bituminous coal flames in a furnace. *Combustion and flame*, 54(1-3):23–32, 1983.

[349] M. Mancini, R. Weber, and U. Bollettini. Predicting nox emissions of a burner operated in flameless oxidation mode. *Proceedings of the combustion institute*, 29(1):1155–1163, 2002.

[350] M. K. Stöllinger. *Probability density function modeling of turbulent premixed combustion and pulverized coal combustion*. University of Wyoming, 2010.

[351] M. Stöllinger, B. Naud, D. Roekaerts, N. Beishuizen, and S. Heinz. Pdf modeling and simulations of pulverized coal combustion–part 1: Theory and modeling. *Combustion and Flame*, 160(2):384–395, 2013.

[352] M. Stöllinger, B. Naud, D. Roekaerts, N. Beishuizen, and S. Heinz. Pdf modeling and simulations of pulverized coal combustion–part 2: Application. *Combustion and flame*, 160(2):396–410, 2013.

[353] Z. F. Tian, P. J. Witt, M. P. Schwarz, and W. Yang. Comparison of two-equation turbulence models in simulation of a non-swirl coal flame in a pilot-scale furnace. *Combustion Science and Technology*, 181(7):954–983, 2009.

[354] P. Rosin. Laws governing the fineness of powdered coal. *Journal of Institute of Fuel*, 7:29–36, 1933.

[355] F. C. Marincola. *Large eddy simulation of coal combustion*. PhD thesis, Imperial College London, 2013.

[356] I. W. Smith. The intrinsic reactivity of carbons to oxygen. *Fuel*, 57(7):409–414, 1978.

[357] M. Muto, K. Tanno, and R. Kurose. A dns study on effect of coal particle swelling due to devolatilization on pulverized coal jet flame. *Fuel*, 184:749–752, 2016.

[358] A. Williams. *Combustion and gasification of coal*. Routledge, 2018.

[359] K. A. Kemenov and W. H. Calhoon. A study of strain rate effects for turbulent premixed flames with application to les of a gas turbine combustor model. *Flow, Turbulence and Combustion*, 94(4):731–765, 2015.

[360] B. Coriton, J. H. Frank, and A. Gomez. Effects of strain rate, turbulence, reactant stoichiometry and heat losses on the interaction of turbulent premixed flames with stoichiometric counterflowing combustion products. *Combustion and flame*, 160(11):2442–2456, 2013.

[361] L. W. Kostiuk, K. N. C. Bray, and R. K. Cheng. Experimental study of premixed turbulent combustion in opposed streams. part ii—reacting flow field and extinction. *Combustion and flame*, 92(4):396–409, 1993.

[362] D. Rezaei. *Co-axial turbulent diffusion flames with directed oxygen injection*. The University of Utah, 2013.

[363] J. Pedel, J. N. Thornock, and P. J. Smith. Ignition of co-axial turbulent diffusion oxy-coal jet flames: Experiments and simulations collaboration. *Combustion and flame*, 160(6):1112–1128, 2013.

[364] B. Goshayeshi. *Coal combustion simulation using one-dimensional turbulence model*. PhD thesis, Department of Chemical Engineering, University of Utah, 2014.

[365] J. Pedel, J. N. Thornock, and P. J. Smith. Large eddy simulation of pulverized coal jet flame ignition using the direct quadrature method of moments. *Energy & fuels*, 26(11):6686–6694, 2012.

[366] J. Pedel. *Large eddy simulations of coal jet flame ignition using the direct quadrature method of moments*, volume 74. 2012.

[367] J. L. P Chen and S. W. Churchill. A theoretical model for stable combustion inside a refractory tube. *Combustion and Flame*, 18(1):27–36, 1972.

[368] L. Chen and A. F. Ghoniem. Simulation of oxy-coal combustion in a 100 kwth test facility using rans and les: a validation study. *Energy & Fuels*, 26(8):4783–4798, 2012.

[369] S. Park, J. A. Kim, C. Ryu, T. Chae, W. Yang, Y. J. Kim, H. Park, and H. C. Lim. Combustion and heat transfer characteristics of oxy-coal combustion in a 100 mwe front-wall-fired furnace. *Fuel*, 106:718–729, 2013.

[370] R. Johansson, K. Andersson, B. Leckner, and H. Thunman. Models for gaseous radiative heat transfer applied to oxy-fuel conditions in boilers. *International Journal of Heat and Mass Transfer*, 53(1-3):220–230, 2010.

[371] C. Yin, L. C. R. Johansen, L. A. Rosendahl, and S. K. Kær. New weighted sum of gray gases model applicable to computational fluid dynamics (cfd) modeling of oxy- fuel combustion: derivation, validation, and implementation. *Energy & Fuels*, 24(12):6275–6282, 2010.

[372] S. Black, J. Szuhánszki, A. Pranzitelli, L. Ma, P. J. Stanger, D. B. Ingham, and M. Pourkashanian. Effects of firing coal and biomass under oxy-fuel conditions in a power plant boiler using cfd modelling. *Fuel*, 113:780–786, 2013.

[373] L. Chen et al. *Computational fluid dynamics simulations of oxy-coal combustion for carbon capture at atmospheric and elevated pressures*. PhD thesis, Massachusetts Institute of Technology, 2013.

[374] P. Nakod, G. Krishnamoorthy, M. Sami, and S. Orsino. A comparative evaluation of gray and non-gray radiation modeling strategies in oxy-coal combustion simulations. *Applied Thermal Engineering*, 54(2):422–432, 2013.

[375] T. Kangwanpongpan, R. C. da Silva, and H. J. Krautz. Prediction of oxy-coal combustion through an optimized weighted sum of gray gases model. *Energy*, 41(1):244–251, 2012.

[376] J. Liu, S. Chen, Z. Liu, K. Peng, N. Zhou, X. Huang, T. Zhang, and C. Zheng. Mathematical modeling of air and oxy-coal confined swirling flames on two extended eddy-dissipation models. *Industrial & engineering chemistry research*, 51(2):691–703, 2012.

[377] F. Hu, P. Li, J. Guo, Z. Liu, L. Wang, J. Mi, B. Dally, and C. Zheng. Global reaction mechanisms for mild oxy-combustion of methane. *Energy*, 147:839–857, 2018.

[378] Y. Kuang, B. He, W. Tong, C. Wang, J. Song, and Z. Ying. Numerical simulation of pulverized coal mild-oxy combustion under different oxygen concentrations. *Journal of the Energy Institute*, 2020.

[379] J. Andersen, C. L. Rasmussen, T. Giselsson, and P. Glarborg. Global combustion mechanisms for use in cfd modeling under oxy-fuel conditions. *Energy & Fuels*, 23(3):1379–1389, 2009.

[380] A. Frassoldati, A. Cuoci, T. Faravelli, E. Ranzi, C. Candusso, and D. Tolazzi. Simplified kinetic schemes for oxy-fuel combustion. In *1st International conference on sustainable fossil fuels for future energy*, pages 6–10, 2009.

[381] Y. Tu, H. Liu, K. Su, S. Chen, Z. Liu, C. Zheng, and W. Li. Numerical study of h2o addition effects on pulverized coal oxy-mild combustion. *Fuel Processing Technology*, 138:252–262, 2015.

[382] H. Huynh, A. G. Clements, J. Szuhánszki, W. F. Gale, L. Ma, D. B. Ingham, and M. Pourkashanian. Investigation of particle radiation and its effect on no prediction in a pilot-scale facility for both air and oxy-coal combustion. *Fuel*, 250:254–264, 2019.

[383] A. J. Black. *Oxy-fuel combustion for carbon capture using computational fluid dynamics*. PhD thesis, University of Leeds, 2014.

[384] J. Szuhánszki. *Advanced oxy-fuel combustion for carbon capture and sequestration*. PhD thesis, University of Leeds, 2014.

[385] O. F. Moguel, J. Szuhánszki, A. G. Clements, D. B. Ingham, L. Ma, and M. Pourkashanian. Oscillating coal and biomass flames: A spectral and digital imaging approach for air and oxyfuel conditions. *Fuel Processing Technology*, 173:243–252, 2018.

[386] B. M. Visser, J. P. Smart, W. L. Van de Kamp, and R. Weber. Measurements and predictions of quarl zone properties of swirling pulverised coal flames. In *Symposium (International) on Combustion*, volume 23, pages 949–955. Elsevier, 1991.

[387] C. Hasse, P. Debiagi, X. Wen, K. Hildebrandt, M. Vascellari, and T. Faravelli. Advanced modeling approaches for cfd simulations of coal combustion and gasification. *Progress in Energy and Combustion Science*, 86:100938, 2021.